Republic of Iraq
Ministry of Higher Education
and Scientific Research
University of Babylon
College of Science
Department of Chemistry

Synthesis and Biological Applications of New Biopolymers Based on *N*-substituted Maleimide

A Thesis

Submitted to the Council of the College of Science, University of Babylon, in Partial Fulfillment of the Requirements for the Degree of Doctor of Philosophy of Science / Chemistry

By

Ammar Abdul-Hussein Awad Abd

B.Sc. Chemistry 2011 –University of Karbala

M.Sc. Chemistry 2014 –University of Karbala

Supervised by

Prof. Dr. Mohanad Mousa Kareem

2021 A.D 1443 A.H

بِسْمِ اللَّـهِ الرَّحْمَـٰنِ الرَّحِيمِ

((وَأَنْزَلَ اللَّهُ عَلَيْكَ الْكِتَابَ وَالْحِكْمَةَ وَعَلَّمَكَ مَا لَمْ

تَكُنْ تَعْلَمُ ۚ وَكَانَ فَضْلُ اللَّهِ عَلَيْكَ عَظِيمًا))

صدق الله العلي العظيم

سورة النساء : الآية (١١٣)

CERTIFICATION

I certify that this thesis was prepared under my supervision at the Department of Chemistry, College of Science, Babylon University, in partial requirements for the Degree of Ph.D Doctorate in Organic Chemistry and this work has never been published anywhere.

Signature:

Name: **Dr. Mohanad Mousa Kareem**

Title: Professor

Address: Department of Chemistry-College of Science-Babylon University

Date: / /

In the view of the available recommendation, I forward this thesis for debate by the examining committee.

Signature:

Name: **Dr. Saadon Abdulla Aowda**

Title: Professor

Address: Head of Department of Chemistry-College of Science-Babylon University

Date: / /

Dedication

To .....

The promised absent

Awaited justice

Al-Imam Al-Mahdi "aj"

ACKNOWLEDGEMENTS

First, I thank Almighty Allah, The Creator, for Mercy and Guidance in my whole life and giving me the ability to conduct this research work.

Many thanks to my supervisor, prof. Dr. Mohanad Mousa Kareem, for the supervision, his support and encouragements throughout the course of this presented research work.

Thanks are due to the head of the Chemistry Department Prof. Dr. Saadon Abdulla Aowda, Prof. Dr. Faris Hammoud Muhammad Al-Amshawi, and all the staff for their assistance during this research work.

Also my grateful thanks go to prof. Dr. Mohammad Nadhum Bahjat, who assists me in carrying out the viscosity and density measurements.

I would like to express my genuine gratitude to Dr. Noor Salman Kadhim Al-Khafaji for assistance in screening of anti-bacterial activity.

I would like to express my sincerest gratitude to the following people for moral support during this study:

My friends: Ayad Ali Disher, Salah Hashem Shaheed, and all my colleagues in the department of chemistry for their supporting and helping me during the work period.

I would like to thank my wife and my family for their encouragement and supportment.

Amaar

Summary

In this study, four lines were included to prepare and characterize thirty-three compounds of maleimide derivatives carrying a drug group, and to study some of their applications.

The first line was the preparation of a number of maleimide monomers (M1-M11) by the addition of the drug containing an amine group to Maleimide benzoyl chloride solution in a dimethyl sulfoxide solvent in the presence of triethylamine (Scheme A).

The second line involved the polymerization of the monomers prepared from the first line in toluene solvent in the presence of benzoyl peroxide at a temperature of 90 °C to produce 11 homopolymer (PM1-PM11) and again, with acrylic acid to produce 11 heterogeneous polymers (PM12-PM22) (Schemes B and C).

The third line included the study of some biological applications such as studying the antibacterial activity against Gram-positive bacteria (*Staphylococcus aurous*) and Gram-negative bacteria (*Escherichia coli*) for all compounds.

A number of monomers and polymers showed higher inhibition zones than the free drugs towards (Staphylococcus bacteria), and the monomer (M5) loaded with cephalexin gave the highest inhibition zone, while most of the monomers showed higher activity against gram-negative bacteria, the monomer (M6) and homopolymer (PM6) loaded with ciprofloxacin had the highest inhibitory diameters than ciprofloxacin alone against both types.

The two Heteropolymer; (PM15) loaded with amoxicillin showed higher inhibition against (*E.coli*) than amoxicillin alone and (PM20) loaded with isoniazid drug showed higher activity against both types of bacteria .

The fourth line included the study of drug release (in acidic and alkaline medium), swelling percentages and relative molecular weights by viscosity method of the prepared polymers. In addition, the cytotoxicity and anticancer activity of some homogeneous and heterogeneous polymers were studied towards breast cancer cell line (MCF7). The Homopolymer (PM5) showed a high inhibition of the growth of breast cancer cells and little cytotoxicity, while the Hetropolymer (PM16) had the highest inhibition of

cancer cell growth and less cytotoxicity, which may make it a promising drug for the treatment of breast cancer.

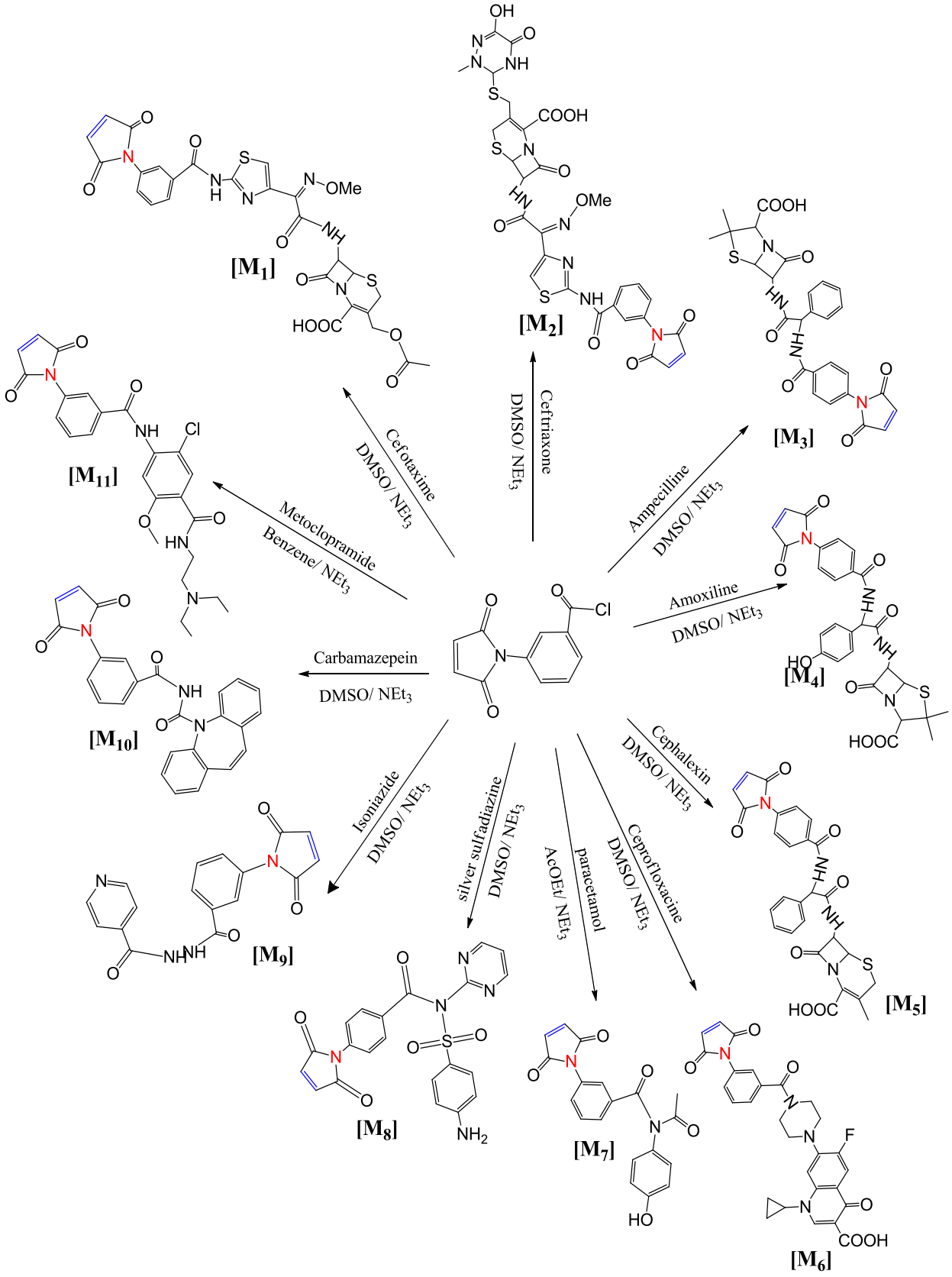

Scheme A: Synthesis of monomers (M_1-M_{11})

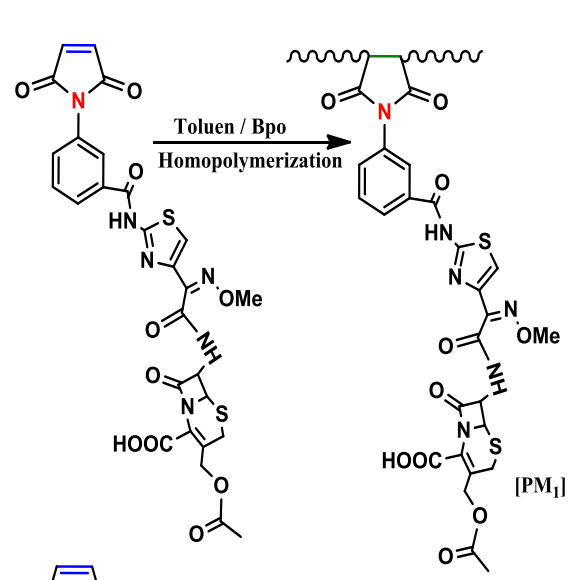
Toluen / Bpo
Homopolymerization
[PM1]

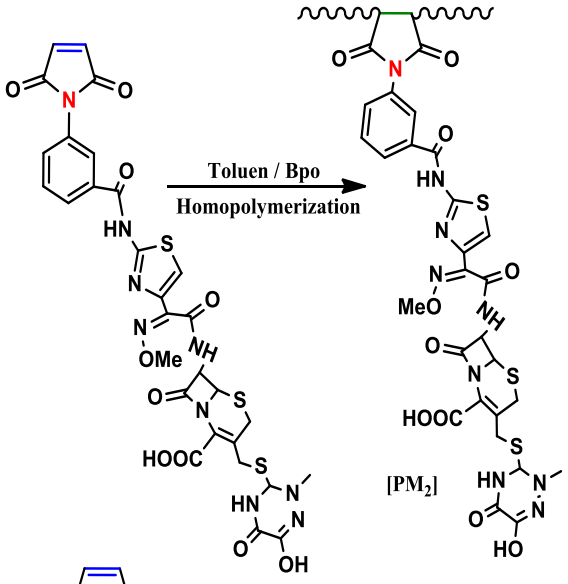
Toluen / Bpo
Homopolymerization
[PM2]

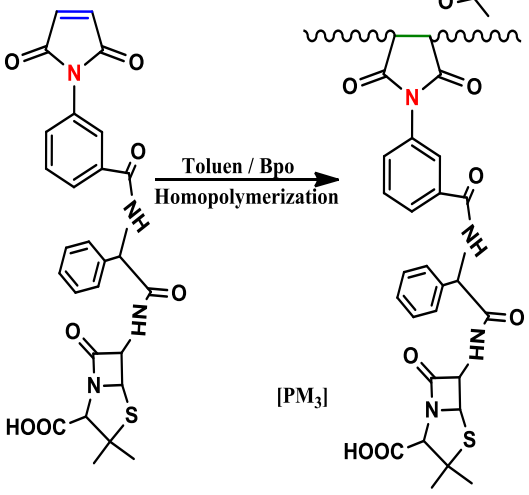
Toluen / Bpo
Homopolymerization
[PM3]

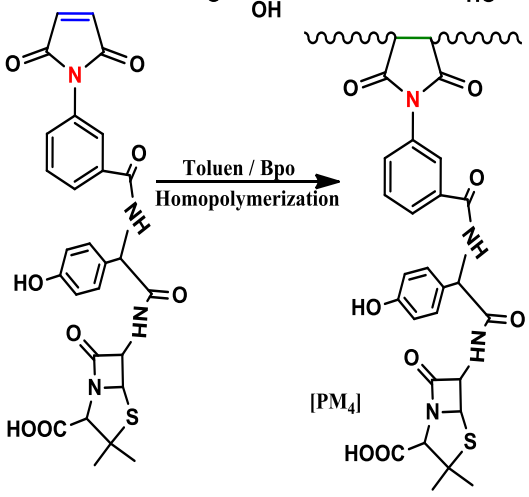
Toluen / Bpo
Homopolymerization
[PM4]

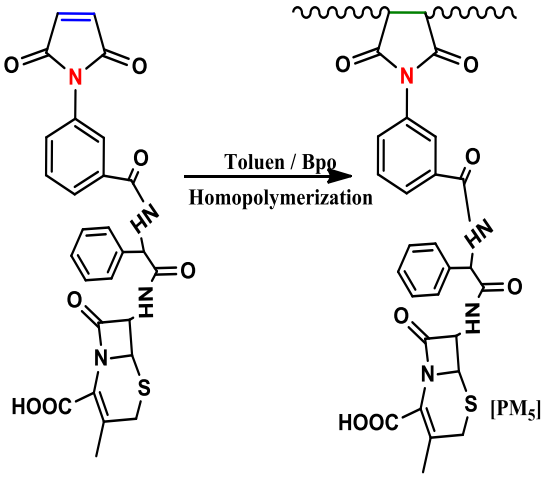
Toluen / Bpo
Homopolymerization
[PM5]

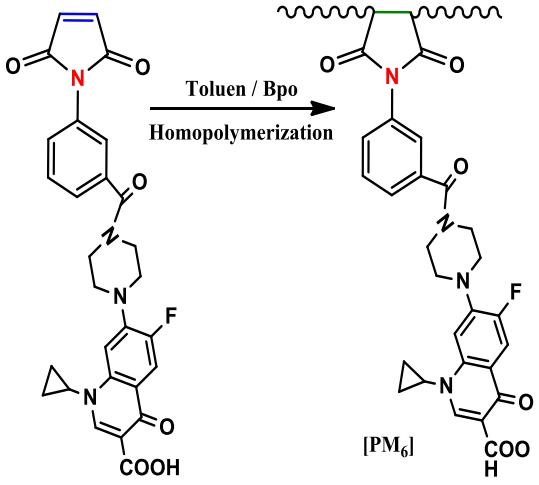
Toluen / Bpo
Homopolymerization
[PM6]

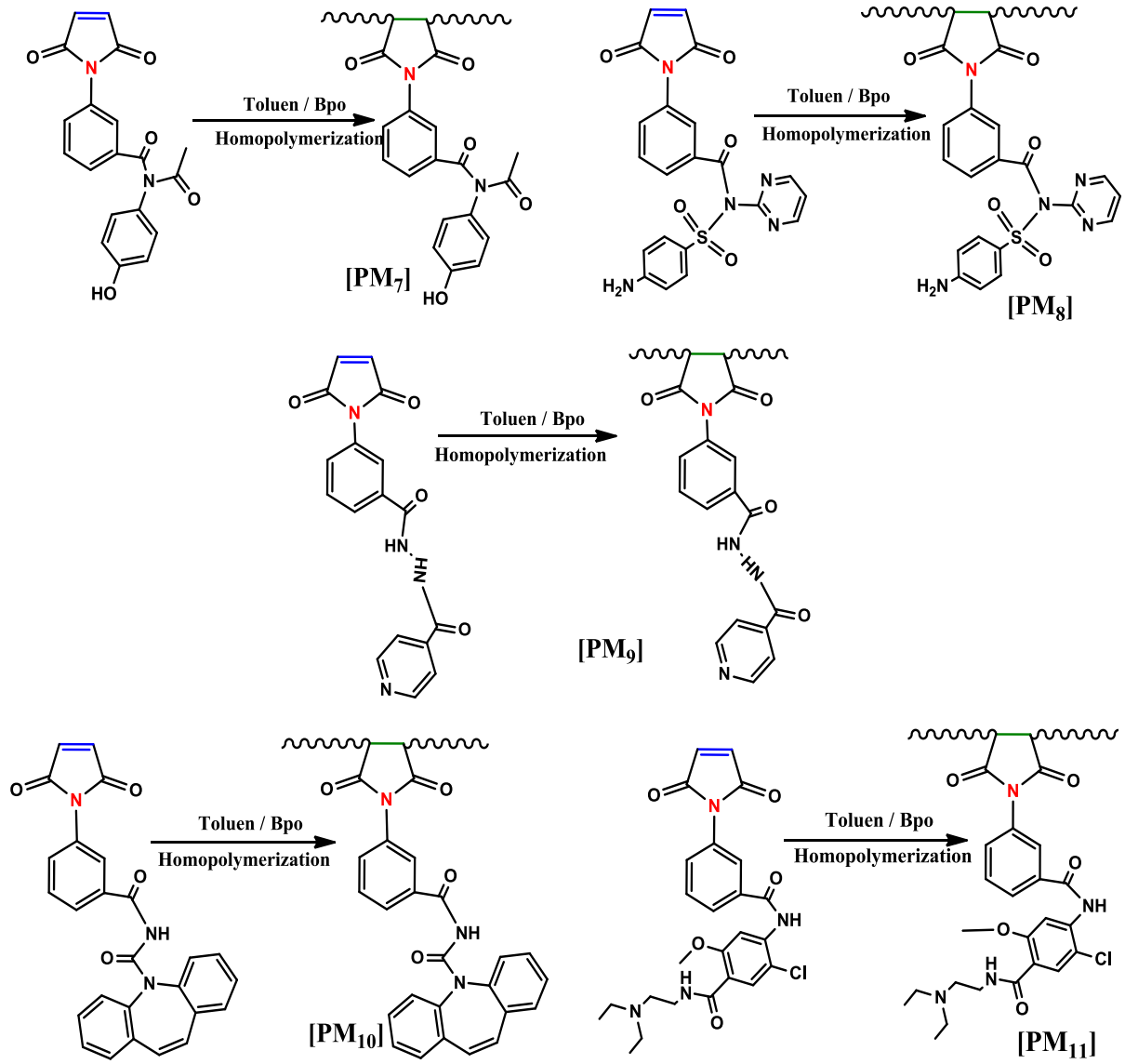

Scheme B: Synthesis of Homopolymers (PM1-PM11)

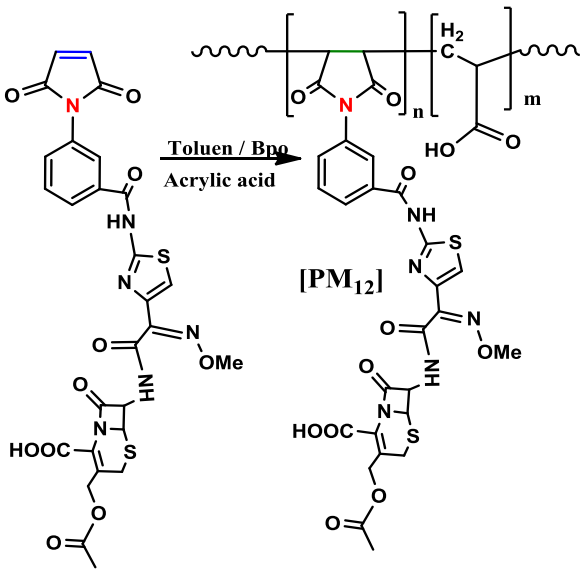

[PM12]

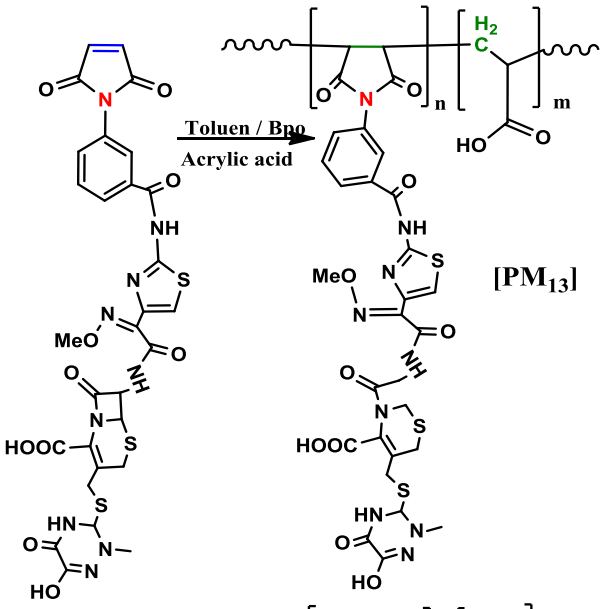

[PM13]

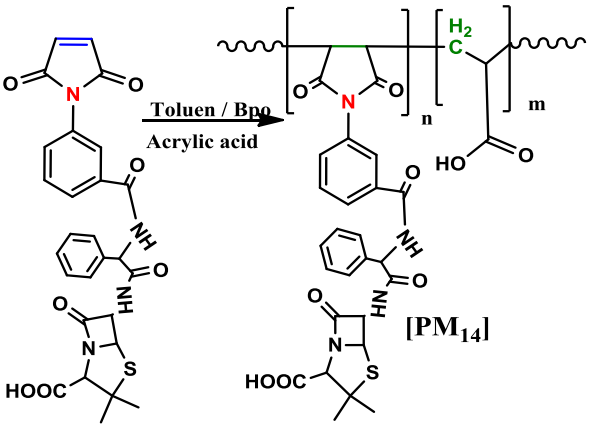

[PM14]

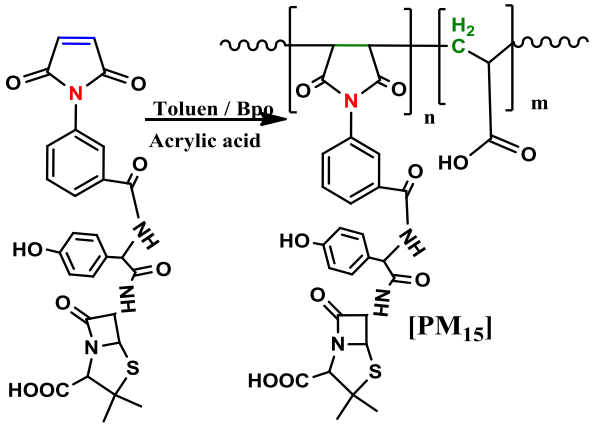

[PM15]

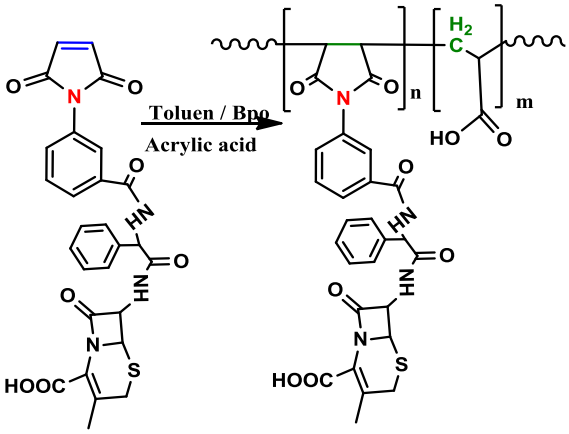

[PM16]

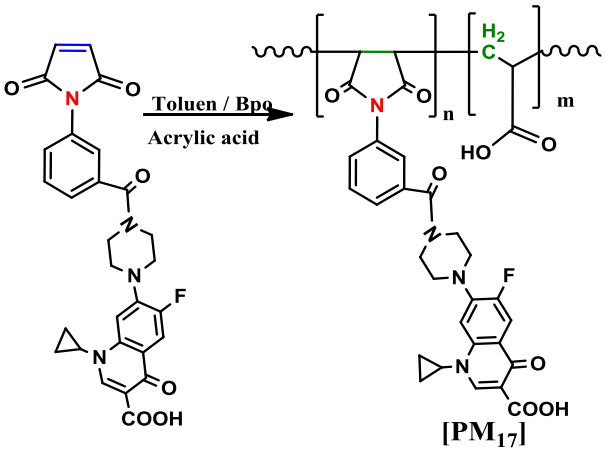

[PM17]

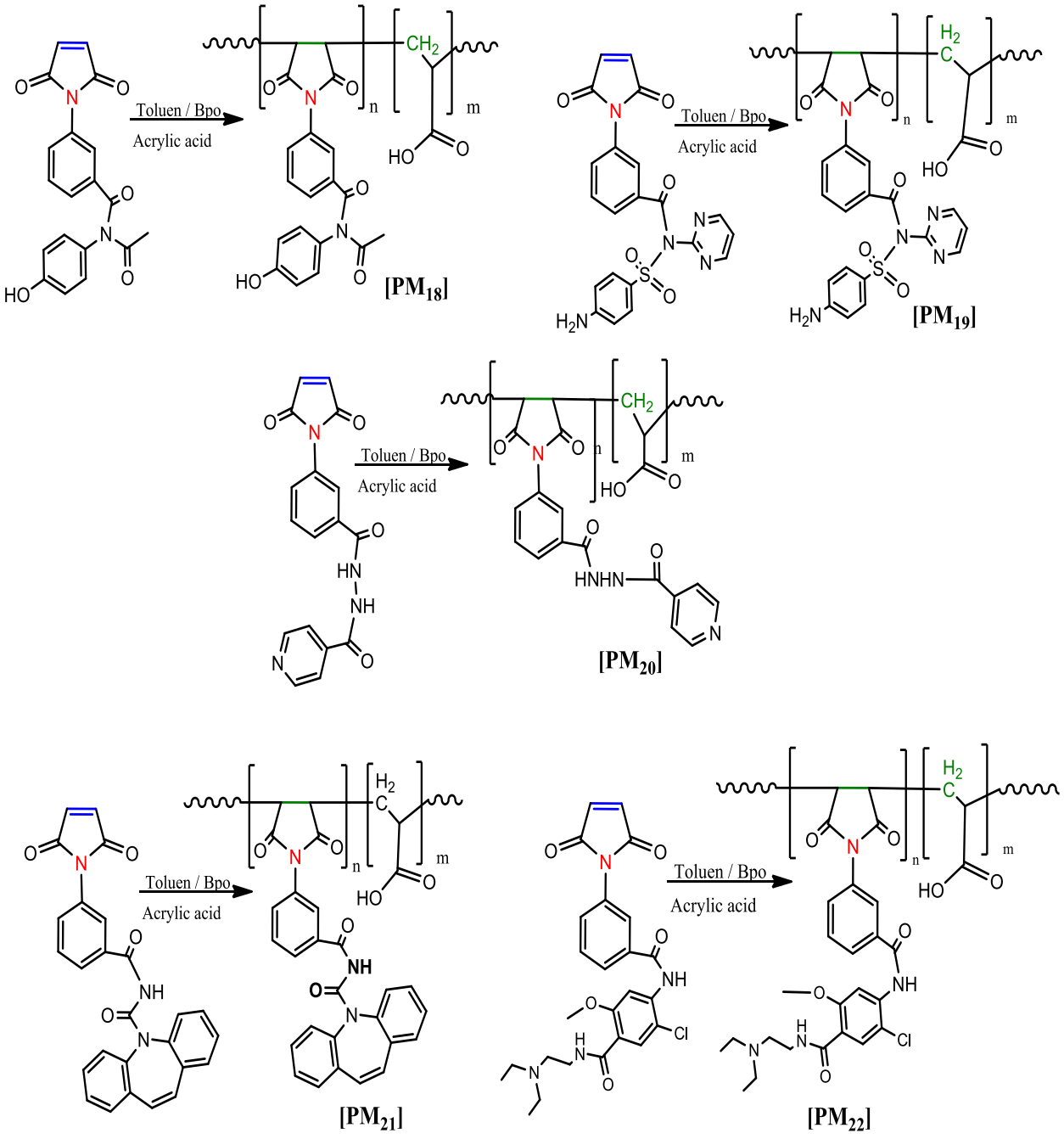

Scheme C: Synthesis of Homopolymers (PM_{12}-PM_{22})

List of Contents

Directory of Tables

	List of Abbreviations	
Symbol	**Description**	
DMP	2-dodecylsulfanylthiocarbonylsulfanyl-2-methylpropionic acid	
AA	Acrylic acid	
alt	Alternative	
AIBN	Azobisisobutyronitrile	
Bpo	Benzoyl peroxide	
Bu	Butyl-	
DMSO	Dimethyl sulfoxide	
DMF	Dimethylformamide	
EGFR	Epidermal growth factor receptor	
EtOH	Ethanol absolute	
FT-IR	Fourier Transform Infrared	
IC_{50}	Half maximal inhibitory concentration	
[η]	Intrinsic viscosity	
MalVE	Maltose-substituted vinyl ethers	
M.P	Melting points	
EtMI	N-ethyl Maleimide	
OD	Optical density (Absorption)	
PEG	Poly ethylene glycol	
PLLA	Poly lactic acid	
PGA	poly(glycolic acid)	
PLGA	poly(lactide-co-glycolide)	
PPMI	Poly(*N*-phenyl maleimide)	
^{1}HNMR	Proton nuclear magnetic resonance	
η_{red}	Reduced viscosity	
η_{rel}	Relative viscosity	
RMSD	Root Mean Square Deviation	
η_{sp}	Specific viscosity,	
T	Temperature	
Ph-CH_3	Toluene	
Et_3N/ TEA	Triethyl amine	
UV-Vis	Ultraviolet-visible	
VAc	Vinyl acetate	
η	viscosity	

Chapter One

INTRODUCTION

1. Introduction

It makes sense to start with an antibacterial agent that can be chemically changed into a polymerizable derivative while still retaining bioactive functional groups following polymerization. The modification can also be carried out on a premade polymer that contains reactive moieties. By connecting a complementary reactive antimicrobial agent containing hydroxyl, carboxyl, or amino groups to the polymer backbone or its pendent groups, functional moieties can be chemically changed.

1.1. Polymeric Macromolecules

A macromolecule is a molecule that consists of a large number of atoms [(1)]. The term macromolecule is often used for molecules that contain more than 100 atoms, especially for polymers. Many examples exist in biology, especially in biochemistry. This includes proteins, starch, lipids, and nucleic acids (such as DNA), which are sometimes called biomolecules or biopolymers. Manufactured examples include plastics. It is also the origin of crystals and minerals, while substances that consist of a large number of atoms bonded together by bonds similar to molecular bonds, are rarely called "macro molecules" [(2)].

Substances that consist of large particles often have unusual physical properties. The properties of liquid crystals and elastic units such as rubber are an example of these unusual properties [(3)].

Another characteristic that distinguishes large units that is not found in smaller molecules is their need for help to dissolve in solutions. It takes certain salts or ions to dissolve in water. Evolution of proteins may occur when there is a high or low concentration of solutions. Polysaccharides can form linear polymers (cellulose) or complex structures because monosaccharides have several functional groups (glycogen).

Polysaccharides play a variety of functions in living species, including energy storage (e.g., starch) and structural elements (chitin in arthropods and fungi).

Fats are hydrocarbons that do not form polymers. Fats consist of glycerol and fatty acids. Phospholipids are commonly found in the phospholipid bilayer. They have a hydrophilic head and hydrophobic tail. Protein is another type of macromolecule [(4)]. Amino acids are the monomers of proteins. There are proteins that are used for structural support, storage, transportation, cellular connectivity, locomotion, defense against foreign matter, and more [(5)].

1.2. Naturally accruing Macromolecules:

Many biological molecules are macromolecules, which are high-molecular-weight polymers constructed from basic precursors [(4)]. Polymerization of comparatively small molecules with molecular weights of 500 g/mole or less results in the formation of proteins, nucleic acids, and polysaccharides. The number of polymerized units will vary between tens of thousands and millions [(6)].

The synthesis of macromolecules is a significant energy-consuming activity in cells. Macromolecules can be further assembled into supramolecular complexes, which can then be used to form functional units such as ribosomes**.** Cellulose, proteins, polypeptides, and polynucleotides are examples of naturally occurring macromolecules (e.g. DNA, deoxyribonucleic acid). Intermolecular forces may also shape macromolecules from smaller molecular groups as molecular clusters or inclusion compounds. Molecular functional units are unique supermolecules in biological structures that perform a particular purpose[(7)]. One of the most important natural macromolecule is rubber or polyisoprene, refers to a group of polymers made from the polymerization of cis-1,4-Polyisoprene (figure 1.1), also known as

isoprene rubber, is a key component of natural rubber used in engineering applications like, adhesives, rubber bands, vibration dampers, springs, bearings, and other synthetic applications such as high-performance tires for race cars, hoses, buses, automotive parts and aircraft thanks to its strength and heat resistance [8].

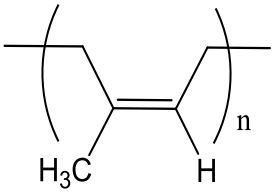

Figure 1.1: Structure of Polyisoprene (natural rubber).

Isoprene polymer chains are long and loosely bound in natural rubber. When the chains are ripped apart, they reattach, giving rubber its elasticity. Natural rubber is made from the latex sap of rubber trees, as opposed to synthetic rubbers, which are made from petrochemicals (although other plants also produce latex, rubber trees are the most efficient at producing rubber, making them the suppliers of latex for 99 percent of natural rubber) [9].

In addition to above, there are many other examples for natural macromolecules such as chitin and keratin [10]. Chitin, like cellulose, is a structural polymer made up of smaller monomers (monosaccharides) that bind to form solid fibers. The fibers form fragile bonds between themselves when secreted in an ordered manner within or outside of cells. Chitin and cellulose are also carbohydrates, while keratin is a fibrous protein. Since structural polymers are only found in such groups, they appeared early in the evolution of life [11]. Plants have cellulose, mammals have keratin, and mollusks, fungi cell walls, arthropod exoskeletons such as crustaceans and spiders, cephalopod beaks, and lissamphibian flesh all contain this polysaccharide [12]. Paraphrase that has been formalized Chitin is similar to another polysaccharide called cellulose in that it forms crystalline nanofibrils or Bristles. It acts exactly the same way as the

protein keratin does. Chitin has been shown to be useful in a variety of medical, industrial, and biotechnological applications [13]. Chitin is considered a good source for another semi natural chitosan polymer where this polymer produced via deacetylation of chitin t by hydrolysis of the acetamide groups either enzymatically or by chemical hydrolysis with concentrated NaOH or KOH (40–50%) at temperatures above 100 °C [14, 15]. Chitosan is a heterogeneous polymer made up of N-acetyl-d-glucosamine and d-glucosamine monomers that come in a variety of units based on the degree of acetylation [16, 17]. The carbohydrate backbone is very similar to cellulose, which is made up of 1,4-linked d-glucosamine with differing degrees of N-acetylation, only that the acetylamino group on the C2 position replaces the hydroxyl group[11] (Scheme 1.1) .

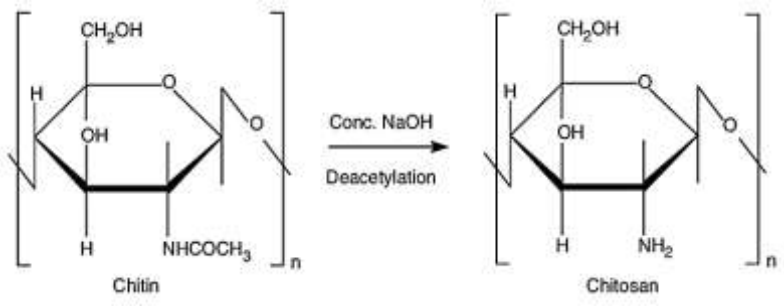

Scheme 1.1: Chitin hydrolysis

1.3. Synthetic macromolecules

Macromolecule is a more common concept than polymer. Macromolecules are organic compounds with at least 1,000 atoms bound together by covalent bonds [18,19]. Natural substances such as cellulose, proteins, lignin, and others are abundant, as are synthetic compounds such as plastics, fabrics, elastomers, coatings, and adhesives.

Homopolymers are polymers made up of similar repeated groups, and the term "polymer" is often applied to no repetitive macromolecules including organic geopolymers, lignin, and proteins. The degree of polymerization is measured by the number of repeated units [20].

Polymer scientists are now searching for more precision chemistry methods to create synthetic uniform macromolecules with previously unheard of properties, as a result of this , the field of sequence defined polymers was born [21, 22]. This intense request of precise, discrete synthetic macromolecules resulted in the emergence of modern experimental methods or the repurposing of previously developed chemistry tools for their preparation [20].

1.4. Classification of polymers

Polymers unclassified under one category because of their complex structures, different behaviors and vast applications. polymers Classification depends on different facts like the source (natural, synthetic and semi synthetic), structure (linear, ramified and cross-linked), polymerization process (step growth and chain polymers), and molecular forces (elastomers, fibers, thermoplastic and heat-resistant polymers). Various forms of classification may be used such as the field of applications, or based on monomers (Homopolymers and Heteropolymer or co-polymer) [23].

1.5. Polymers for different applications

1.5.1. Bioactive Polymers

Biomolecules including oligopeptides and oligosaccharides have low structural integrity and are very hygroscopic, making them difficult to handle and process. They also have a hard time blending with hydrophobic synthetic polymers including polycaprolactone, polylactic acid, polyamide, poly (methyl methacrylate), and poly (lactic-co-glycolic acid). These synthetic polymers are often non-bioactive and, to differing degrees, cause foreign body reactions in patients. As a result, the ability to convert a conventional polymer into a bioactive one while maintaining mechanical and physical properties will be extremely beneficial to the medical technology industry. As a result, developing novel composite

products with biological and mechanical properties is crucial for bettering healthcare results [24].

Bioactivity refers to a material's ability to influence its biological environment [25]. In the 1990s the term tissue engineering was first identified by Langer and Vacanti [26]. Three-dimensional structured, biomaterial-based polymeric scaffolds have been used to establish a bioactive environment in which cells bind and propagate since that time. Antonio J. Salgado and his coauthors [27] reviewed that Synthetic biodegradable polymers are the most widely used in the field of biomedical engineering such as Poly(α-hydroxy acids), poly(Ɛ-caprolactone), poly(propylene fumarates), poly(carbonates), poly-(phosphazenes), poly (anhydrides), poly(L-lactic acid) (PLLA) and poly(lactide-co-glycolide) (PLGA). These may use as components needed for making bone regeneration or tissue engineering a successful therapy so, their chemical versatility and processability differ depending on their composition and design, so a direct analogy with natural polymers is impossible [28].

The polyester polymers poly (lactic acid), (PLA) and poly (glycolic acid) (PGA) are combined to form poly (lactic-co-glycolic) acid (PLGA), which is one of the most widely used biodegradable synthetic polymers for tissue engineering applications. The higher the PGA ratio in a PLGA scaffold, the sooner the PLGA can degrade. Lactic acid and glycolic acid are nontoxic byproducts of its degradation. Biodegradability, adaptability and customization for various forms of formulations, and surface modulation for selective drug delivery are just a few of the benefits of PLGA [29].

Polymer materials are extremely important; various polymers have a wide range of applications based on their physical, chemical, and structural properties. Polymers are also used in the implant of artificial

skin for the deceased; these polymers are mainly silicone, PTFE, and polyurethane-based [30]. Scientists successfully tested and implanted synthetic polysiloxane polymer (Silastic) artificial skin [31] (figure 1.2). These polymers can also withstand chemical attacks [32].

Figure 1.2: Some of bioactive polymer applications [25]

Rutnakornpituk M. and his coworkers [33] have prepared polydimethylsiloxane-modified chitosan via cationic ring-opening polymerization of octamethylcyclotetrasiloxane (D4). The siloxane prepolymers will be then functionalized with epoxy groups at both terminals. Consequently, the epoxy-difunctionalized polysiloxanes will be readily reacted with amine groups in chitosan and essentially form siloxane-chitosan networks (Scheme 1.2). The mechanical, thermal, and physical properties of bioactive polymer were extensively studied and polymer suggested to be used as artificial skin or wound dressing, in the future.

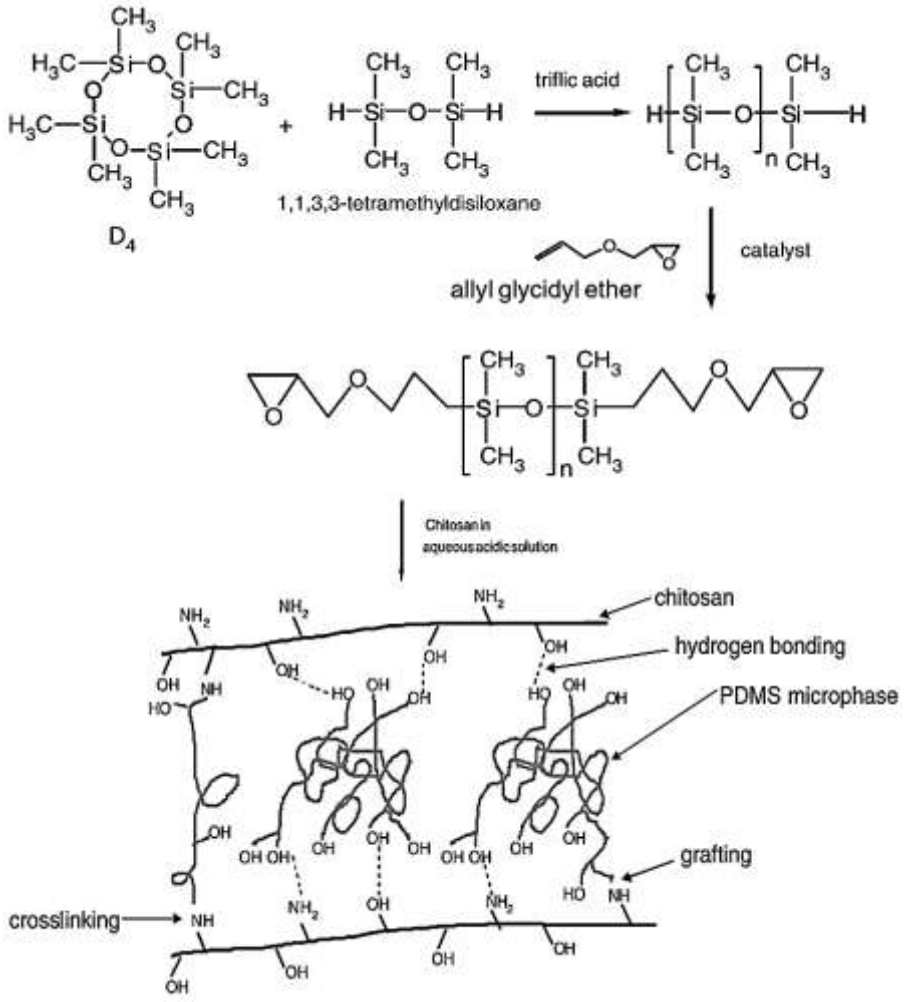

Scheme 1.2: Synthetic route of crosslinking bio active polymer

1.5.2. Antimicrobial polymers

Since potentially toxic compounds are not embedded and therefore cannot leach out, self-sterilizing antimicrobial polymers are environmentally safe [(34)]. They can also be quickly absorbed into fibers, extruded into fibers, and they avoid microorganisms from adhering to their surface [(35,36)]. Antimicrobial polymers are made by covalently binding biocidal functional groups to the polymers, giving them antimicrobial or antiseptic properties [(37)]. The bulk polymer is modified, or the surface is selectively modified, using accessible reactive moieties.

Chemical transformation of a biocidal molecule into a polymerizable compound that can then be polymerized or co-polymerized with another monomer is another type of synthesis [(38, 39)].

Both of these methods have been useful in proving the viability of non-leaching antimicrobial polymeric products. Polymers are a big scientific field that has significantly improved our culture. Polymers have a range of attractive properties, including high strength or modulus to weight ratios (light weight but comparatively rigid and strong), hardness, durability, corrosion resistance, and lack of conductivity (heat and electrical), to name a few [40].

Many of these properties make them ideal candidates for use in a variety of fields, including medicinal equipment, health care, food, irrigation, catalysis, electronics, environmental, green energy, and textiles[41]. Antimicrobial polymeric materials can be used in the areas just described, avoiding the resistance issues that come with using antibiotics. An antimicrobial agent is a substance that prevents the development of microorganisms. In addition, the toxicity of such antimicrobial agents is strictly proportional to their efficacy. As a result, the synthesis of effective yet non-toxic antimicrobial polymers is urgently needed [35].

Antimicrobial polymers can be categorized into two classes. Polymers loaded with antimicrobial agents that are released over time [42-44], or polymers containing metal ions (such as Ag+) that eventually disperse from the matrix fall into the first group [45, 46].

The use of stimuli-responsive polymeric materials is well-known in the field of controlled drug delivery systems [47]. This is due to the fact that they can alter their drug release rates drastically in response to stimulation such as the local pH or body temperature [48].

Many other antimicrobial polymers were synthesized and their biological activity studied. Moon et al [39] have synthesized bio active polymer by loading norfloxacin drug on Glycidylmethylacrylate, and polymerization the produced acrylic monomer and then blended with low

density polyethylene. The resultant blended polymer possessed a strong antibacterial activity even though the content of polymer in the blend was as limited as 1% wt/wt, (Scheme 1.3).

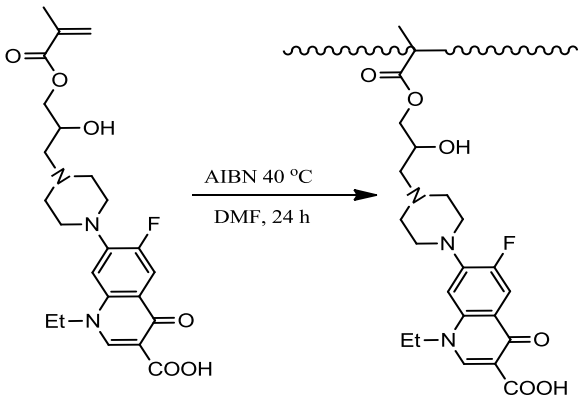

Scheme 1.3: Norfloxacin drug loaded on Glycidylmethylacrylate polymer.

The synthesis of poly (4-[(2,4-dichloro-5-fluorophhenyl)-3-oxoprop-1, en-1-yl] phenyl acrylate (figure 1.3) was performed and its antimicrobial activity was examined against microorganisms such as *E. coli*, P. aeruginosa, and Salmonella typhi. A photometry assay showed the ability to destroy bacteria was used to estimate the minimum concentration of that compound [49].

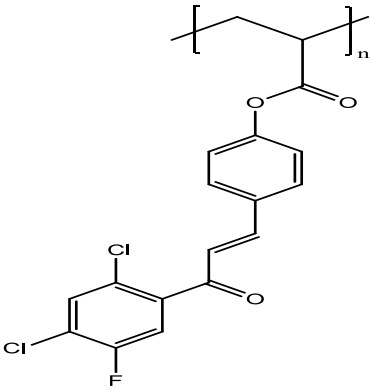

Figure 1.3: Structure of poly (4-[(2,4-dichloro-5-fluorophhenyl)-3-oxoprop-1, en-1-yl] phenyl acrylate.

Maleimide derives its name from the combination of maleic acid and imide. Maleimides are maleimide derivatives in which the NH groups have been substituted with alkyl or aryl groups. $H_2C_2(CO)2NH$ is the general formula for maleimide compounds. Maleimides were

polymerized either by heating or catalysis, either alone or in combination with other monomers. Maleimides are polymerized by free radical polymerization into polyimides and resins. Polyimides and resins are thermally stable, long-lasting, and resistant to water and radiation.

A bio-active poly(*N*-tri-n-butyl tine-maleimide) co-polystyrene polymer was synthesized by Al-muaikel NS and coworker [50] based on organo-tin maleimide (figure 1.4), this copolymer showed good antibacterial activity toward 13 types i.e., *S. aureus, S. epidermidis, S. faecalis, Bacillus megaterium, Bacillus cereus, Shigella dysenteriae, Shigella sonnei, S. typhimurium, S. typhi, E. coli, Yersinia enterocolitica and Yersinia pseudotuberculosis*. The results demonstrated that the copolymer is more sensitive to Gram-positive bacteria.

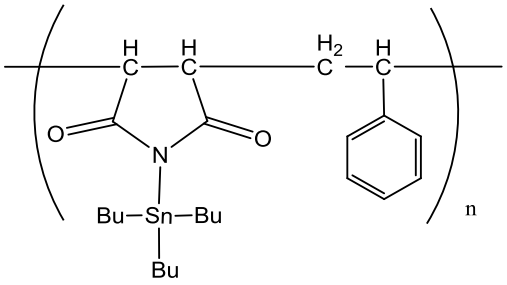

Figure 1.4: Structure of poly (N-tri-n-butyl tine-maleimide) co-polystyrene.

In the chemistry of metal complexes, polymers complexes were studied by Muhammad NA and his co-authors [51]. A number of polymer metal complexes (Co II, Mn II, Ni II, Cu II, and Cd II) were prepared and their antimicrobial activity against *Bacillus subtilis*, *Streptococcus pneumonia*, *Pseudomonas aeruginosa* and *Escherichia coli* bacteria and against *Aspergillus fumigatus*, *Syncephalastrum racemosum*, *Geotricum candidum* and *Candida albicans* fungi were investigated. The results showed the ability of these complexes, especially for polymer-Co(II) and the polymer-Cd(II) complexes to inhibit the growth of these microbes was better than that of the parent polymer (figure 1.5).

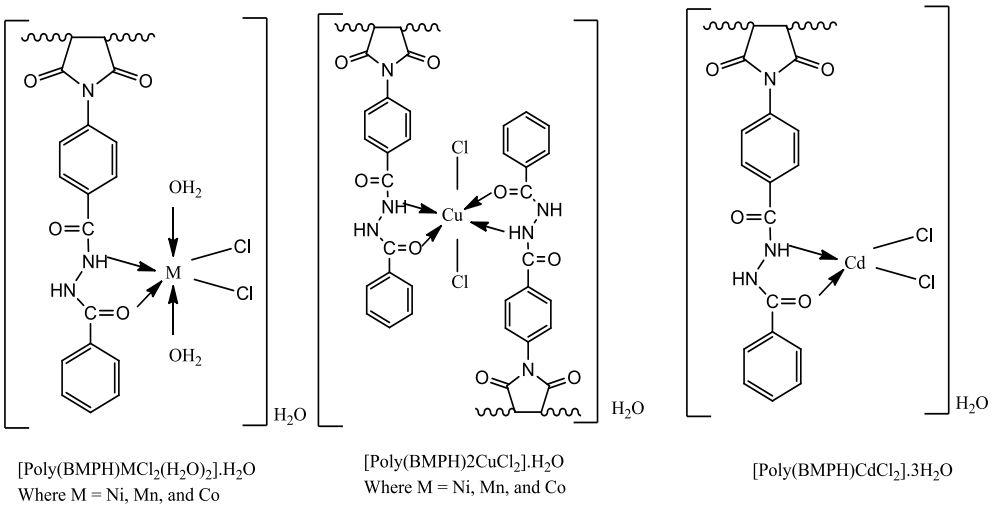

Figure 1.5: Maleimide-Polymer-metal complexes

Loaded group studied maleimide and isobutylene alternating co-polymers to explain the effect of hydrogen bonding and hydrophobicity in conjunction with a steady cationic charge on antibacterial polymer selectivity. This is the first research to look at hydrogen bonding as a method for increasing bacterial selectivity. They intended to provide a degradable polymer with tunable side chain hydrophobicity by developing polymers containing ester- and amide-groups, with various length side chains varying from ethyl to hexyl to research the effects of hydrophobicity while retaining cationic charge density constant. The amide sequence has been demonstrated to be effective antibacterial agents [52] (Figure 1.6).

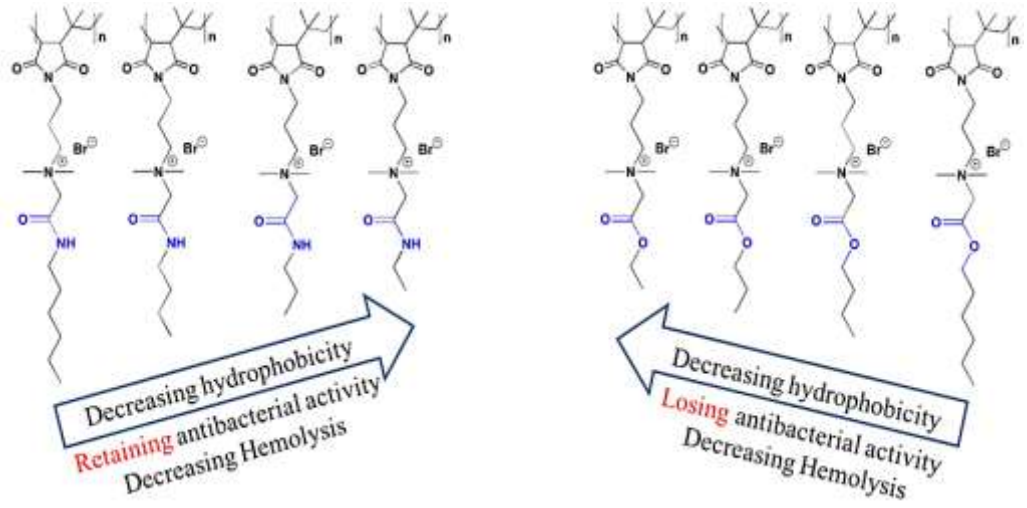

Figure 1.6: Poly (maleimide-alt-isobutylene) derivatives.

Minoda M and co-authors [53] investigated the copolymerization of lactose or maltose-substituted vinyl ethers (LacVE) and maltose-substituted maleimide (MalMI) or N-ethyl maleimide to produce glycopolymers with two types of disaccharide residues in the pendants as glycosaminoglycan-mimetic glycopolymers, based (Figure 1.7). A lectin binding assay was used to investigate the resulting periodic glycopolymers' complex associations with lectins. A cytotoxicity test was conducted to validate the glycopolymers in this study's possible applicability as promising products in the biomedical and pharmaceutical fields.

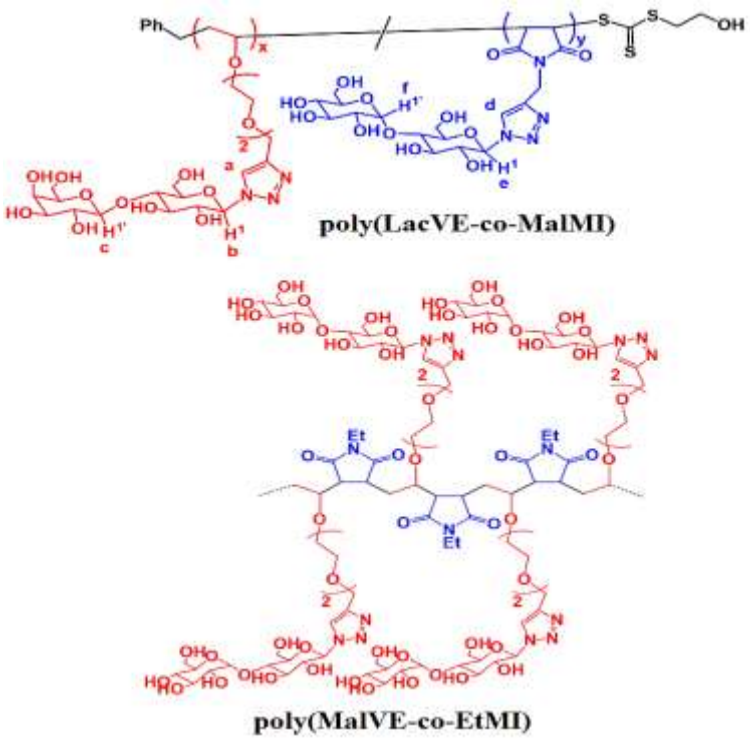

Figure 1.7: The polymers used in the study.

1.5.3. Luminescent and bio-imaging polymers

Polymers with broad -aromatic building blocks are known as luminescent polymers. These materials have attracted a lot of interest for a number of applications in bio-imaging and other fieldsdue to their high emission properties [54]. Despite their strong usefulness, the complicated synthesis and toxicity of wide conjugated systems, low miscibility in aquatic media, and low photobleaching resistance of such luminogens

limit their further development and applications [55]. Note that the photochemical modification of a pigment or fluorophore molecule so that it is permanently unable to fluoresce is known as photobleaching (or fading). This is caused by the fluorophore and adjacent molecules breaking covalent bonds or reacting in non-specific ways.

Goswami KG and co-authors [56] studied a new co-polymers with pH-responsive solubility variation in aqueous solution based on styrene monomer and maleimide (MA), which possess two different small peptide units (glycyl-glycine and alanyl-alanine) in the polymer side chains in a predominately alternating fashion. These co-polymers show unusual luminescence characteristics in different organic solvents under UV light irradiation, whereas in the solid state they emit blue, green and red fluorescence as witnessed from the corresponding fluorescence microscopy micrographs. The alternating distribution of the two monomers throughout the polymer backbone, these polymers have various possible usefulnesses in sensing and bio-imaging fields (Scheme 1.4).

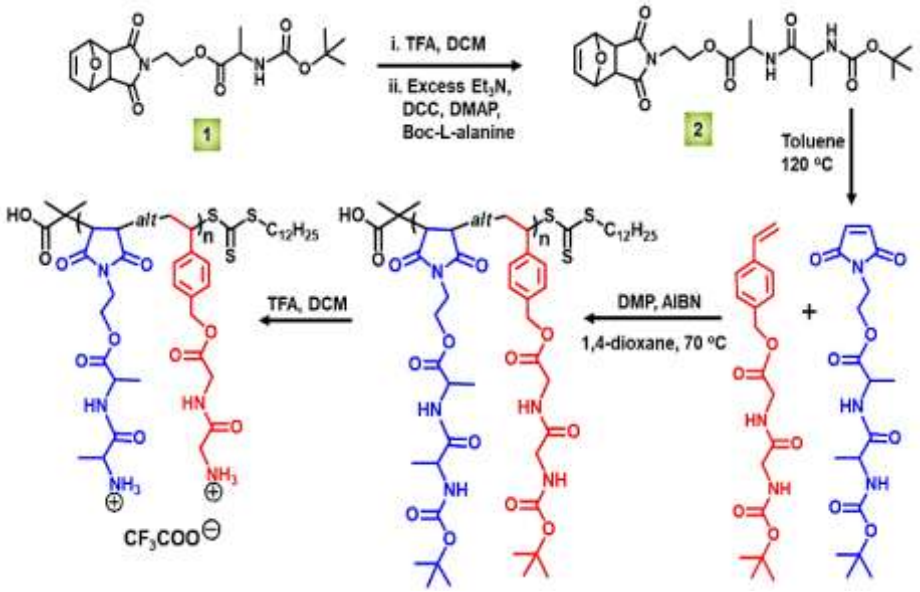

Scheme 1.4: Synthetic pathway of the copolymers with glycyl-glycine and alanyl-alanine side-chain pendants

Depending on theoretical calculations, Bauri K and his coworkers [57] mentioned that the fluorescence characteristics due to the keto-Enol tautomerism played an important role in the observed multicolor fluorescence, since the tautomeric balance is affected significantly by pH and polarity of the solution. Tautomeric structures of PPMI, responsible for pH-tunable emission and solvatochromism phenomena, (figure 1.8, D).

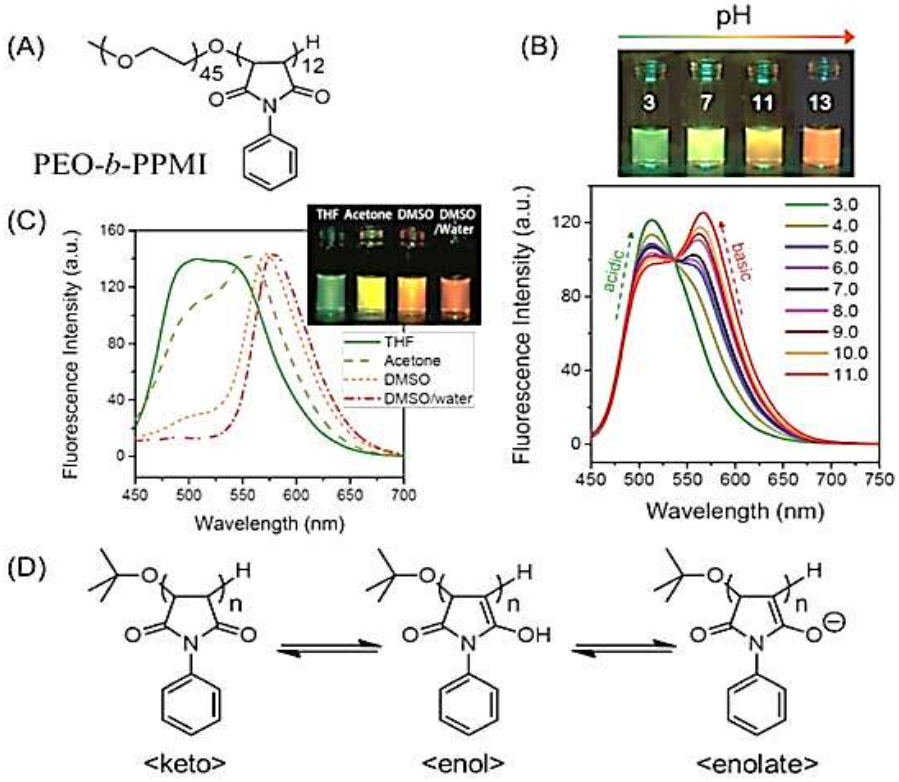

Figure 1.8: Tautomeric structures of PPMI

1.6. Polymeric Prodrugs and drug delivery system

The end purpose of drug treatment is site-specific drug delivery [58]. Passive drug enrichment in the organ, transporter-mediated delivery, selective metabolic activation by enzymes, and antigen targeting are all ways to achieve site selectivity [59].

It is possible to develop drug delivery systems that directly administer anti-cancer drugs to tumors because of the unique properties of the tumor microenvironment and tumor angiogenesis [60]. Many

conventional therapeutic agents, on the other hand, have poor pharmacokinetic profiles and are administered nonspecifically throughout the body, resulting in systemic toxicity and serious side effects.

Polymeric delivery systems have been extensively used for a variety of biomedical and medicinal uses in recent decades [61]. Yolles and coworkers introduced the idea of a polymeric delivery mechanism in the early 1970s, with the aim of delivering the right volume of active agent to the right site at the right time [58].

Polymeric delivery systems have had a lot of coverage since then. Targeted delivery systems should discharge or release drugs at or close the targeted site, while controlled release systems should inject the drug into the systemic circulation at a fixed pace. Targeted delivery has the benefit of achieving elevated local opioid concentrations. Instead of being spread across the body, the medication is mostly administered to the tumor [62, 63].

Indeed, most medications have an optimal dose range within which they have the most value. Concentrations outside of this spectrum are harmful or have no medicinal value. For medications that are quickly metabolized and eliminated from the body following administration, controlled release over a long period of time is extremely helpful. The concentration of medication at the site of action after traditional administration (4 injections at 6 hourly intervals) is opposed to that after release from a controlled release procedure, as seen in (Figure 1.9) [61].

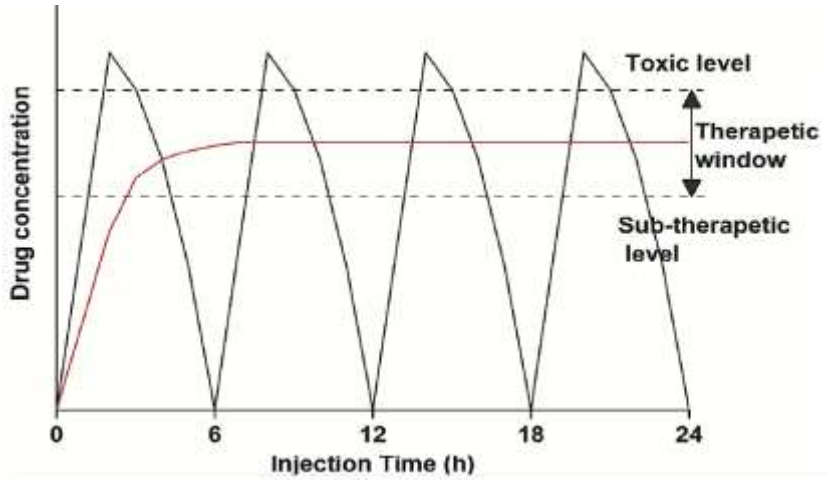

Figure 1.9: Controlled Drug release (red curve) and 4 injections levels diagram

From clear and easily accessible materials to state-of-the-art optimized formulations that take advantage of the variety of linear, branched, and hyper branched architectures, as well as combinations thereof, macromolecule-based drug delivery has come a long way [64,65].

Polymer chemist's ingenuity has resulted in an avalanche of new polymers with extraordinary properties that are now common place in our world. Material engineering has been used to improve the general composition and properties of these polymers [66].

Cancer gene therapy through systemic gene delivery will be a very appealing method of cancer treatment. Approaching the tumor via the bloodstream may have some benefits over local intratumoral infusion, including the ability to enter several distant metastases [67]. Regrettably, the required tumor-targeted gene delivery mechanism does not yet exist.

To gain access to tumor tissue, an optimal gene delivery scheme must meet criteria such as:

(1) The gene delivery system must have ligands capable of mediating cell specific identification and internalization into target cells.

(2) The gene delivery system must be immune to nonspecific interactions with the biological environment, such as blood components and non-target cells [68].

Saha B, and coworkers created a leucine-based purely alternating polyampholyte luminogen with an oppositely charged functional moiety that was synthesized in an alternative manner in the poly(styrene-alt-maleimide) skeleton Scheme 1.5 [(69)]. In addition to its high selectivity against traces of CS_2 liquid and vapor, the synthesized polymer can endow the material with low cytotoxicity and strong protein-resistant capability. Furthermore, it has the ability to be used as a nonviral vector for gene delivery.

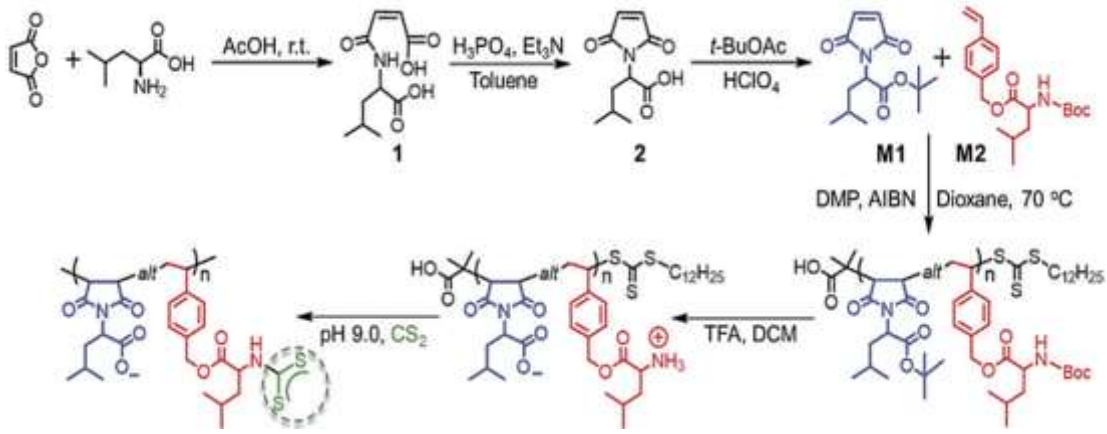

Scheme 1.5: Synthetic scheme of leucine-based poly(styrene-alt-maleimide).

Over the last few years, there has been an increase in the development of biomaterials therapeutic methods, including multiple functional drug delivery systems or diagnostics, to improve the treatment or detection of different diseases. Since cancer is one of the leading causes of death worldwide, improving anticancer treatment has been a major driving force behind nanomedicine growth. Nonetheless, chronic inflammatory disorders (CID), such as rheumatoid arthritis, multiple sclerosis, systemic lupus erythematosus, and inflammatory bowel disease, have a significant social effect due to their high prevalence [(70)].

Jung E and coworkers synthesized maleimide polymer based on 5-fluorouracil (5-FU) which is used in cancer chemotherapy for the treatment of breast cancer and adenocarcinomas of the gastrointestinal tract.

MIEFU (Maleimidoglycylyl-5-fluorouracil) was generated by combining Maleimidoglycloyl chloride and 5-fluorouracil. Photopolymerizations with 2,2-dimethoxy-phenylacetophenone as an initiator at 25 °C for 48 hours yielded the homopolymer of MIEFU and its copolymers with acrylic acid or vinyl acetate (Scheme 1.6) [71].

The in vitro cytotoxicities test of the samples show inhibition of cancer cell lines against mouse mammary carcinoma (FM3A), mouse leukemia (P388), and human histiocytic lymphoma (U937) cancer cell lines: with the order of MIEFU ≥ poly(MIEFU) > poly(MIEFU-co-AA) > poly(MIEFU-co-VAc).

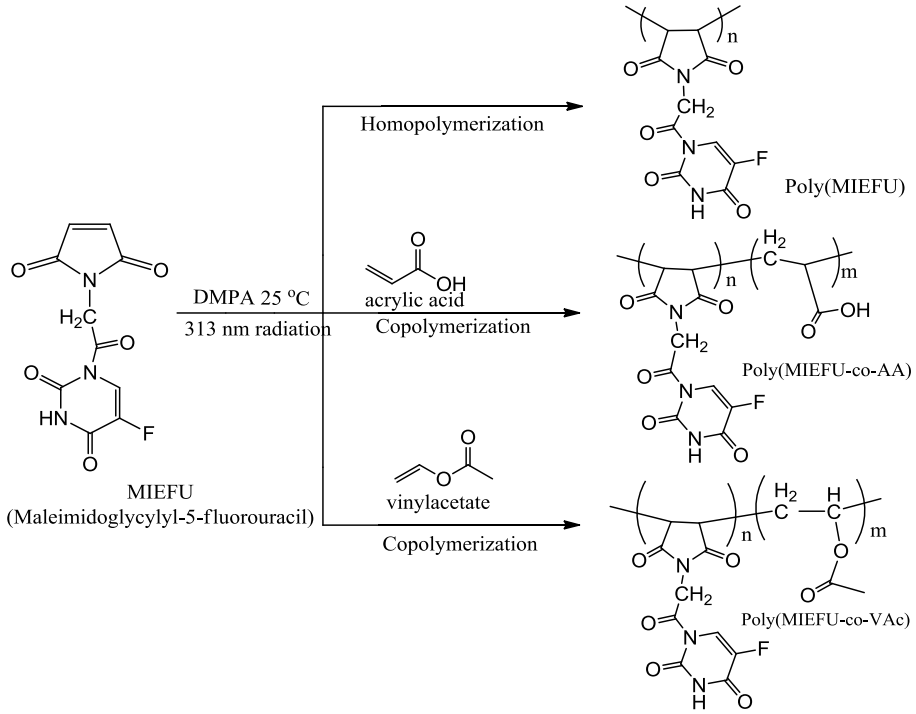

Scheme 1.6: Synthetic scheme of homo and co-MIEFU polymer

To avoid the problems associated with nonspecific drug delivery, several approaches have been developed. A large number of drugs with macromolecular properties have been discovered as a result of recent advances in biotechnology combined with novel technologies such as combinatorial chemistry and high-throughput screening. Endogenous macromolecules are now widely used as therapeutic modalities, in

contrast to traditional drug therapy, which only uses xenobiotics as medicines [72].

However, because of their hydrophilic nature, charged structure, and large molecular mass, these drugs are poorly absorbed in the gastrointestinal tract, presenting a major challenge for safe and effective delivery [62]. In vivo delivery of macromolecules involves transport of the drug from the site of administration through various physiological barriers to the target site. First, drugs have to survive through the hostile extracellular conditions such as extreme pH, immune defense, enzymatic degradation, and scavenger systems. All living cells are protected by a double-layered plasma membrane that selectively allows the uptake of smaller molecules. Similarly, the nucleus is guarded by a double-layered nuclear membrane as it contains important genetic material [72].

Liposomes are small artificial spherical vesicles which can be made of natural phospholipids and cholesterol. Liposomes are promising drug delivery mechanisms due to their size, hydrophobic and hydrophilic properties (along with biocompatibility) [73, 74].

For drug delivery to the brain, Liposomes were functionalized with maleimide PEG-ylate and then conjugated to thiol groups from protein such as holo-transferrin (Tf) (containing two iron atoms Fe^{3+}) without sacrificing Fe^{3+} from Tf in the presence of tris(2-carboxyethyl) phosphine (TCEP) hydrochloride as sulfhydryl reductant. Using a small amount (0.3 mol percent) of maleimide-PEG to change the liposome surface resulted in pH sensitive liposomes that use thiol-conjugation to improve cellular uptake [75] (Scheme 1.7).

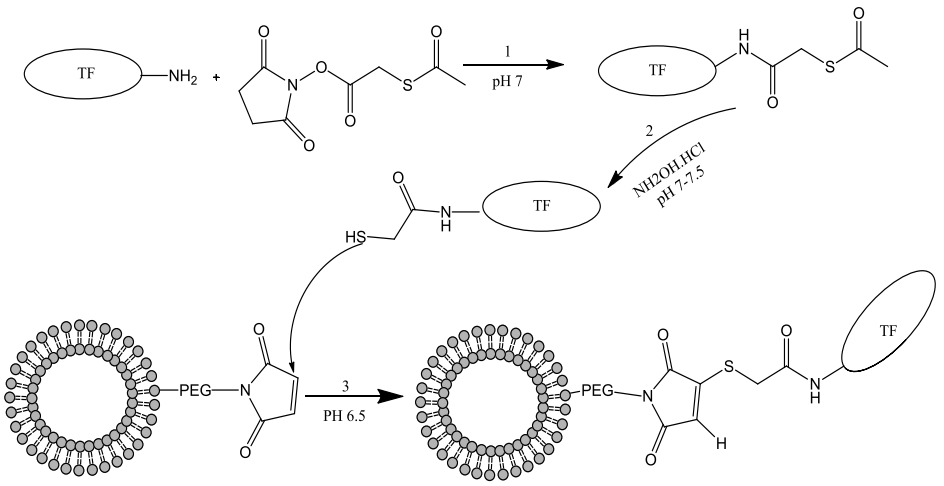

Scheme 1.7: step 1: reaction scheme of Tf thiolation with N-succinimidyl-S-acetylthioacetate, step 2: the activation of thiolated Tf, step 3: conjugation of Tf to liposomes, bearing maleimide-PEG-DSPE.

1.7. Polymer drug Conjugates

Polymer conjugates, are defined as macromolecular prodrugs, are high-molecular-weight conjugates that usually contain many molecules of low-molecular-weight drugs or a mixture of drugs attached to a polymer chain to improve drug pharmacokinetics (Figure 1.10) [(76)]. Polymer conjugates have a molecular weight that is markedly larger than that of the conjugated drug, and their larger hydrodynamic radius slows PCs' renal excretion, prolonging the drug's circulation in the bloodstream.

Furthermore, PCs are unable to reach healthy endothelium, limiting conjugated drug delivery to non-targeted tissues and organs.

Inflamed tissues' endothelium, on the other hand, is more permeable to macromolecules than healthy tissues' endothelium, allowing PCs to accumulate passively [(70)]. As the drug is conjugated to the polymer backbone, it is normally inert. Regulated drug release in the target tissue or cells is allowed by a biodegradable spacer between the drug and the polymer chain based on enzymatically or reductively cleavable linkers or hydrolysable bonds. PC with anti-inflammatory drugs are attractive candidates for troublesome of Combined Immunodeficiency (CID)

therapy due to passive aggregation, regulated drug release, and the possible delivery of targeting moieties to individual cells or imaging agents.

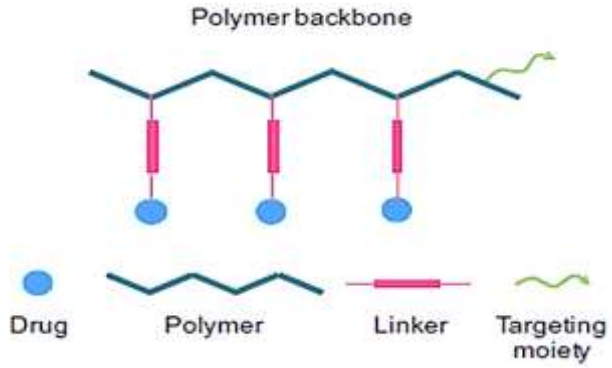

Figure 1.10: The scheme of the polymer drug conjugates

A long course of nonsteroidal anti-inflammatory drugs (NSAIDs) is often used in the treatment of osteoarthritis [(77)]. Long-term use of NSAIDs, on the other hand, may result in serious systemic side effects such as gastrointestinal ulceration or hemorrhage, an elevated risk of heart disease, kidney failure, and depression [(78)]. Because of the localized nature of osteoarthritis, a site specific intra-articular drug injection has become an appealing alternative to administering therapeutic agents directly into the infected region because it allows for local therapeutic doses to be obtained at a much lower administered dosage thus minimizing total systemic exposure to the drug [(48)].

Mageed F A R. and co-authors [(42)] have synthesized new homogenous and heterogeneous maleimide polymers conjugated with Sulfadiazine and Chlorodizepoxide drugs and study of their Controlled drug release and swelling % in different pH values at 37 ºC (Scheme 1.8).

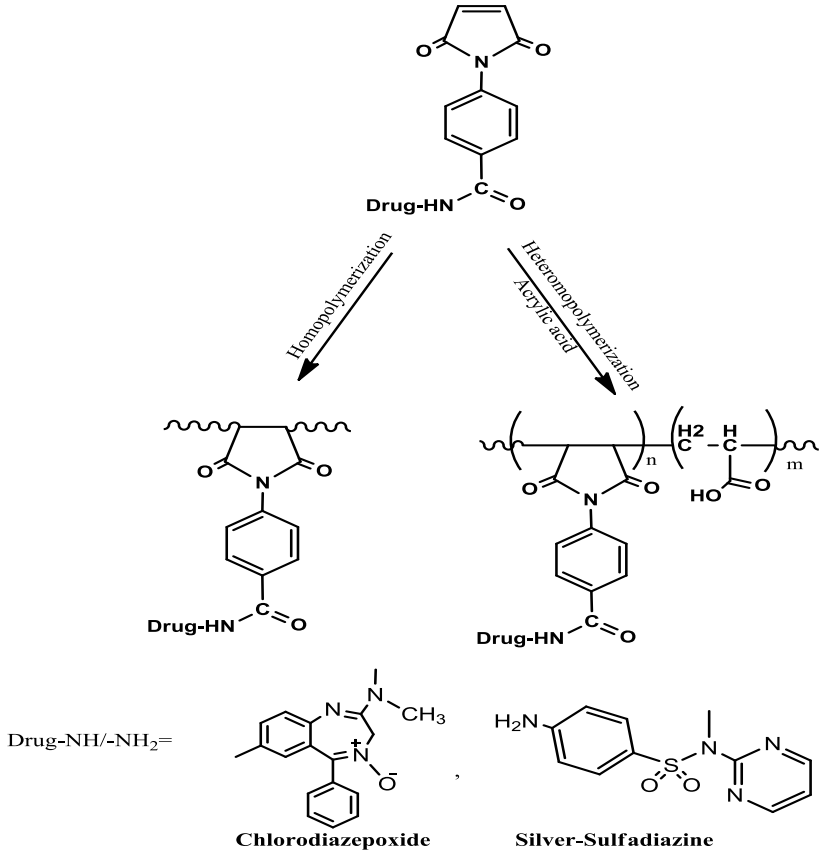

Scheme 1.8: The structure of N-*p*-Benzoic maleimide Prodrug polymers

N-[5-salicylic maleimide] Prodrug monomer and its polymerization and co-polymerization with acrylic acid as promising candidate for drug delivery applications were reported by Kareem M M. and Abbas L A. [79]. These compounds are loaded with some pendent drugs molecules, and showing good drug release behavior and swelling ratio in basic and neutral media (figure 1.11).

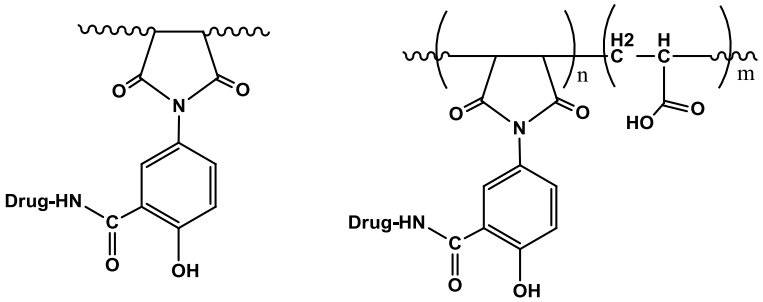

Drug-NH/-NH$_2$= Theophylline , Pseudoephederine , 4-Aminoantipyrine

Figure 1.11: The structure of N-[5-salicylic maleimide] Prodrug polymer

1.8.Swelling

1.8.1. limited swelling

Hydrogels are hydrophilic cross-linked polymeric networks that can capture large quantities of water or biological fluids but are insoluble. The inclusion of hydrophilic groups such as carboxyls, alcohols, and sulphonic acid contributes to the hydrophilicity. Hydrogels are well adapted biomaterials for applications such as contact lenses, tissue substitutes, artificial organs, bone substitutes, hemodialysis membranes, absorbent covering for blood perfusion, soft tissue replacements, and plastic surgery due to their low interfacial tension and greater permeability to small molecules, as well as their soft and rubbery design[(80)].

The swelling ratio is the fractional rise in the hydrogel's weight due to water absorption. The sol fraction is the portion of the polymer that is not part of a cross-linked network after a crosslinking reaction. The degree of hydrogel degradation is determined by a reduction in sol fraction over time, which represents polymer degradation [(81)] (figure 1.12).

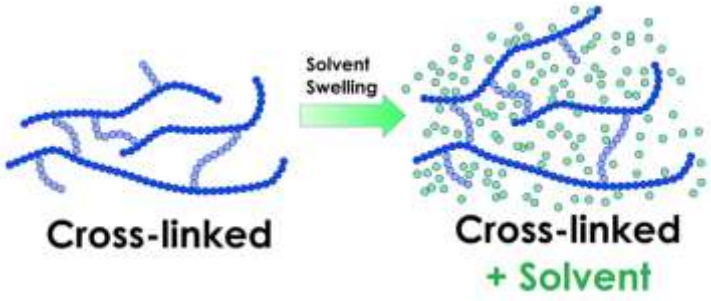

Figure 1.12: Swelling of cross-linked polymeric networks

1.8.2. Unlimited swelling

It is the swelling that led finally to polymeric dissolution. That mechanism is what causes spontaneous breakdown. It's comparable to the full mixture of various liquids such as water and alcohol. As a low molecular weight liquid comes into close contact with a polymer, the molecular of the latter may attempt to transfer rapidly into the polymer

chains, filling the spaces between the structure components until dissolution of the polymer [82], (figure 1.13).

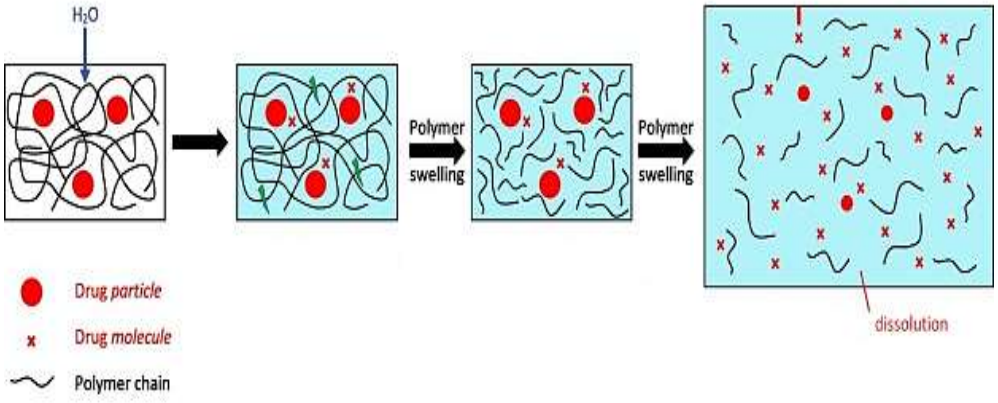

Figure 1.13: Continuous swelling until dissolution

From a scientific standpoint, it is important to understand the polymer's tendency to swell in various liquids. A volumetric or gravimetric approach is used to assess the degree of swelling. The second method involves weighing the polymer sample before and after swelling, and then using equation (1:1) to calculate the swelling degree (%) is determined from the following equation:

$$\text{Swelling ratio (\%)} = (Ws - Wd)/Wd \times 100 \quad \ldots\ldots(1{:}1)$$

[Wd= Weight of polymer; Ws= weight of swollen polymer]

We can only assess the degree of swelling in small swelling polymers; we can't do it for unlimited swelling since the sample weight is continuously decreasing due to dissolution. In the figure (1.14) it is apparent that the swelling increases over time to the point where a horizontal track is located at the slope, a point where the swelling ends, a limit or swelling balance.

In Figure 1.14, the maximal floatation of a first sample is larger than that of the second sample, such that different polymers require different times to achieve equilibrium. This property is very important.

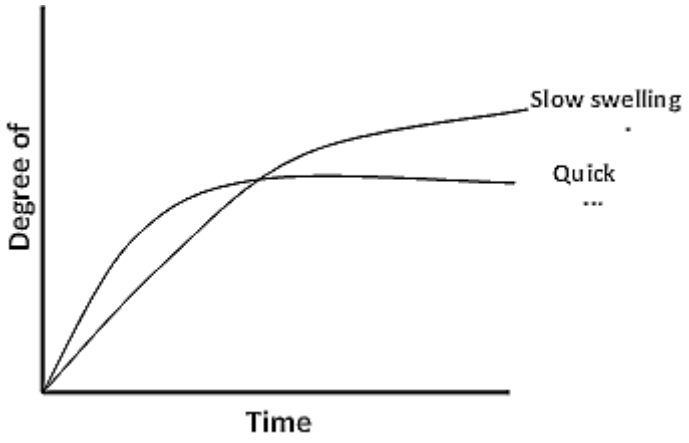

Figure 1.14: Kinetic of swelling

Therefore, when we place both samples in a certain solvent for a long time, the second swelling would be much higher than the first sample, but if the degrees of swelling are measured within a brief amount of time, we should note the reverse, meaning that, in the first sample, the swelling quantity is greater than the second. We should therefore assess the strength of the polymers to swell from the highest level [83, 84].

1.9. Biological activity Concept

Biological activity is characterized as a molecular entity's and ability to produce a particular biological impact on a subject. It is calculated in terms of potency, or the amount of a molecular entity that is needed to achieve the desired result. A biological assay is used to determine a biological activity.

Chemical compounds can have poisonous and negative side effects that make them unsuitable for medicinal use. In most cases, activity is dose-dependent. Meeting ADME (Absorption, Distribution, Metabolism, and Excretion) expectations is vital to the activity's success [85]. The compound must not only be successful against the target but also have the ADME properties that make it ideal for use as a medication in order to be safe. The substance is chemically active whether it stimulates or interferes with any cellular tissue in the human body, and the drug action

is used to characterize the substance's beneficial effects, toxicity, and the candidate's effects on the substances.

Finding new effects on a target receptor is a crucial first step in the lengthy phase of drug development. Despite the fact that biochemical assays are becoming more high-throughput, an experiment-only technique that aims to scan the chemical space exhaustively remains unsolvable. Over the last few decades, researchers have evolved computer-aided virtual screening techniques to speed up drug development [(86)]. Structure-based methods include knowledge of the receptor structure and binding site, and they model protein–ligand interactions to predict binding free energy [(87)].

1.10. MTT Tetrazolium Assay Concept

The MTT tetrazolium reduction assay (3-(4,5-dimethylthiazol-2-yl)-2,5-diphenyltetrazolium bromide) was the first homogeneous cell viability assay designed for a 96-well format suitable for high throughput screening (HTS) [(88, 89)]. As demonstrated by thousands of published publications, the MTT tetrazolium assay technology has been broadly embraced and remains widespread in academic laboratories. The MTT substrate is prepared in a physiologically controlled solution, applied to cells in culture, and incubated for 1 to 4 hours at a final concentration of 0.2 - 0.5 mg/ml. Using a plate reading spectrophotometer, variations in absorbance at 570 nm are reported to determine the amount of formazan (which is potentially directly proportional to the number of viable cells). A 630 nm reference wavelength is often used, but it is not needed for most assay conditions [(90)].

MTT is converted into a purple-colored formazan substance with a maximum absorbance near 570 nm by viable cells with active metabolism (Scheme 1.9). Since cells lose their capacity to translate MTT into formazan when they die, color formation serves as a useful and handy

indicator of only viable cells [91]. Although the precise cellular mechanism of MTT reduction into formazan is unknown, it is thought to entail a reaction with NADH or other reducing molecules that pass electrons to MTT [92].

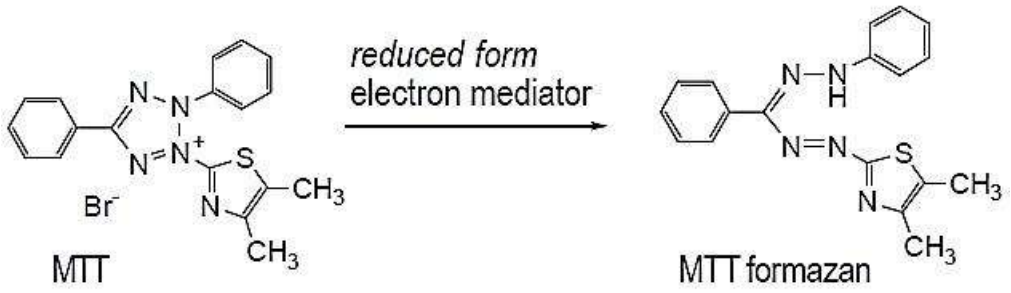

Scheme 1.9: Transformation of MTT to formazan product

The MTT tetrazolium formazan product accumulates within cells as an insoluble precipitate, as well as at the cell surface and in the culture medium. Prior to taking absorbance samples, the formazan must be solubilized [93, 94]. To solubilize the formazan element, stabilize the colour, prevent evaporation, and minimize interference from phenol red and other culture medium components, a number of methods have been used [94]. Solubilization approaches include acidified isopropanol, DMSO, dimethylformamide, SDS, and detergent-organic solvent hybrids.

Longer incubation times result in color aggregation and improved exposure to a point; nevertheless, the incubation period is reduced due to the cytotoxic existence of the detection reagents, which depend on the cell's energy (reducing alternatives such as NADH) to produce a signal. The amount of formazan product generated by cell populations in log phase growth is typically proportional to the number of metabolically active viable cells, as shown by the linearity of response in Figure 1.15 [95]. The rate of MTT reduction into formazan would most likely be affected by culture conditions that change the cells' metabolism.

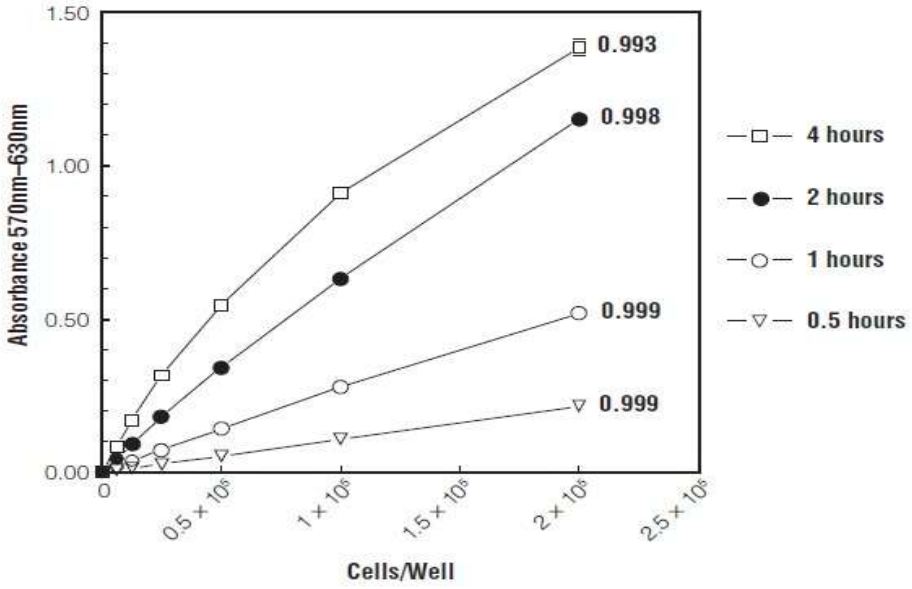

Figure 1.15: Direct association between formazan absorption and the number of hybridoma cells B9 and a time dependent increase in absorption

1.11. The MCF7 cancer cell line

MCF-7 (Michigan Cancer Foundation-7) is a human breast adenocarcinoma cell line that has been used as a model for in vitro cancer research as well as estrogen and progesterone receptor science for over 40 years and is one of the most important cancer cell lines used as a model for investigating mechanisms that affect patient care [(96)].

MCF-7 cells were isolated from the pleural effusion of a 69-year-old woman with metastatic disease in 1973 by Dr. Soule and colleagues at the Michigan Cancer Foundation, from which their name comes [(97)]. The woman had undergone a mastectomy of her right breast for a benign tumor 7 years prior to the start of primary cell culture, as well as a subsequent radical mastectomy of her left breast for a malignant adenocarcinoma four years later [(98)]. Breast cancer is the most common malignant neoplasm in women and is expected to be among the most common cancers. Metastasis is the most common cause of death from

breast cancer, accounting for 90 percent of all deaths. While advances have been made in cancer prevention and detection methods, breast cancer still has a high mortality rate among women. To monitor tumor formation, radiation, chemotherapy, and surgery may be used, but these options must be sufficient to treat breast cancer metastases [(99)].

1.12. Molecular Docking

Molecular docking is a kind of computational modeling, which facilitates the prediction of preferred binding orientation of one molecule (eg. ligand) to another (eg. receptor), when both interact each other in order to form a stable complex [(100)]. Because of its uses in medicine, the protein ligand interaction is the most interesting instance. A ligand is a tiny molecule that interacts with the binding sites of proteins. Binding can take place in a number of different mutual conformations [(101)].

Molecular docking is commonly utilized in current drug design to investigate drug-receptor interactions. Molecular docking is widely used to anticipate the binding orientation of small molecule therapeutic candidates to their protein targets in order to predict the small molecule's affinity and activity [(102)].

Aim of the work

Synthesis and characterization of new Maleimide drug bearing monomers and study their biological activity. These compounds may modify and improve the therapeutic efficiency and safety of drugs.

1. The new N-substituted maleimide monomers were synthesized by condensation of 3-maleimido benzoyl chloride with 11 different drugs including (Cefotaxime, Ciprofloxacin, Ceftriaxone, Ampicillin, Amoxicillin, Paracetamol, Silver-Sulfadiazine, Metoclopramide hydrochloride, Cephalexin, Isoniazid and carbamazepine).
2. Polymerization the prepared monomers by free radical polymerization to produce homo and hetero polymers.
3. Identification of prepared monomers and (homo and hetero) polymers by FT-IR, ^{1}HNMR, and ^{13}CNMR techniques for some of monomers.
4. Studying the anti-bacterial activity of all prepared compounds. Antibacterial activity against two pathogenic strains of *Escherichia coli* and *Staphylococcus aurous* using corresponding drugs as standards by disk-diffusion method.
5. Study the solubility and viscosity average molecular weight of the prepared polymers, and measuring the drug release of polymers.
6. Study of the drug release behavior in acidic and basic media as well as studying the swelling ratio.
7. Studying the in vitro MTT reduction assay in human breast cancer cell line (MCF7) for some of prepared polymers [PM_1, PM_2, PM_5, PM_6, PM_8, PM_{12}, PM_{13}, PM_{16}, PM_{17}, and PM_{19}].

Chapter Two

2

EXPERIMENTAL PART

2. Experimental and Methods

2.1. Chemical and Techniques:

2.1.1. Chemicals

Table (2-1), show the chemical and materials which are used in this study.

Table 2.1: The chemical and materials

Materials	Company	Purities %
3-amino benzoic acid	CDH	**98**
Acetone	Sigma Aldrich	**99.8**
Acid acrylic	BDH	**99.8**
Amoxicillin	Samarra Company	**99.9**
Ampicillin	Samarra Company	**99.9**
Benzoyl peroxide	Fluka	**98.9**
Borax	BDH	**99**
Carbamazepine	Samarra Company	**99.9**
Ceftriaxone	Samarra Company	**99.9**
Cephalexin	Samarra Company	**99.9**
Ciprofloxacin	Samarra Company	**99.9**
Clafuran	Samarra Company	**99.9**
Dimethyl sulphoxide	BDH	**98.9**
Dimethylformamide	Sigma Aldrich	**99**
Dry Benzene	Sigma Aldrich	**99**
Ethanol absolute	Riedel-de Haen	**99.9**
Ethyl acetate	Sigma Aldrich	**99.8**
HCl	Sigma Aldrich	**37%**
Hexane	BDH	**99.7**
Isoniazid	Samarra Company	**99.9**
KCl	BDH	**99**
Maleic anhydride	Fluka	**95.5**
Metoclopramide	Samarra Company	**99.9**
Paracetamol	Samarra Company	**99.9**
Sulfadiazine	Samarra Company	**99.9**
Thionylchloride	CDH	**99.9**
Toluene	Riedel-de Haen	**99**
Triethylamine	Fluka	**99.5**

2.1.2. (Techniques) Instruments Analysis and Equipments:

1- Melting points were determined using SMP30 melting point at University of Babylon, college of science.

2- The IR spectra measurements were recorded using a Fourier Transformation Infrared Spector Promoter AT-FT-IR Bruker Tensor II within range (400-4000) cm^{-1} at College of Science, University of Babylon.

3- The ^{1}HNMR spectra were carried out on a Varian INOVA 500 MHz NMR spectrometer and 125.59 MHz for C-NMR in dimethyl sulfoxide (DMSO-d^6), chemical shifts are in δ units (ppm), Center Tehran Laboratory College, university of Tehran.

4. Microelemental analysis was used to estimate the content of C, H, N, and S, using (Euro EA3000 Elemental Analyzes, Italy), at Tehran University Central lab and Nan Physics Research lab (NPR) lab.

5- UV-absorptivities were recorded with double beam PG CECIL-CE7200 Spectrophotometer, using quartz cells with a light path of (1cm) in two pre-prepared puffer solutions (pH= 2 and 8), at University of Babylon, College of Science.

6-Viscosity Measurement, Viscosity of polymers was recorded on Capillary Viscosity type Ostwald, 0.54 mm diameter, at University of Babylon, College of Science.

7- Ultrasonic Bath (Sonicator) IKON INDUTRIES Brand was used to dissolve and purify some prepared compounds.

8- Molecular Docking study was carried out by using Molecular Operating Environment (MOE 2019.0102).

9- Crystallographic structures of EGFR with its Ligand (6D8E, A1 chain with FZP ligand for Comparison) were obtained from Protein Data Bank (PDB).

2.2. Preparation Methods:

2.2.1 Synthesis of Compound [A_1]: N- (m-Carboxyphenyl) maleiamic Acid (m-CPMA)

A solution of *m*-aminobenzoic acid (13.71 g, 0.1 mol) in acetone gradually added to a solution of maleic anhydride (9.8 g, 0.1 mol) in acetone with continuous stirring for 5 hrs. at ambient temperature. Then the solution was filtered and the precipitate of crude *m*-CPMA was dried and then recrystallized from ethanol to obtain pure *m*-CPMA in 90% Yield, mp 223-224 °C.

2.2.2. Synthesis of compound [A_2]: N-(3-Carboxyphenyl) maleimide (m-CPMI)

A solution of (2.35 g, 0.01mol) *m*-CPMA in 120 mL acetic acid were heated in oil bath for refluxing and it became a clear, homogenous brown liquid upon refluxing at 140 °C for 4 hrs.

The solvent was evaporated from the mixture by using rotary evaporator to give a yellow powdery precipitate. The obtained precipitate was recrystallized from ethyl acetate obtaining the product in a 70% Yield with mp 238-240 °C (Lit. mp. 239-241 °C) [(103)].

2.2.3. Synthesis of compound [A_3]: *N*-[3-(Chlorocarbonyl) phenyl] maleimide *(m-CPMI)*

A solution of (8.5715 gm, 0.0395 mol) *m*-CPMI in thionyl chloride (30 mL) was refluxed at 80°C for 2 hrs. The unreacted thionyl chloride was evaporated off and residual product was recrystallized from DCM to obtained pure light yellow crystals of acid chloride. It was obtained in 90% yield, mp 125-127 °C (Lit. mp = 126-128 ^{o}C) [(103)].

2.2.4. General Procedure for the Synthesis of Maleimide-Drug Monomer Derivatives [M_1-M_{11}]

3-Maleimide benzoyl Chloride (16 mmol, 4 g) was added with stirring to solution of (16 mmol) of deferent Drugs in 60 mL of ethyl acetate for (Paracetemol), benzene for (Metoclopramide) and 30 mL DMSO for (Silver-Sulfadiazine, Clafuran, Ceftriaxone, Ciprofloxacin, Amoxicillin, Cephalexin and Ampicillin, Carbamazepine and Isoniazid), then (16 mmol) of triethylamine (Et_3N) was added dropwise at room temperature and then heated for (1-2.5) at 60 °C according to TLC Technique; the colored formed precipitate in the first and second groups was filtered, dried and recrystallized with Acetone: Ethyl acetate (1:1). Whereas, the solution in the third group was poured crushed ice, left for (30min), was filtered of solution with further crystallized from Ethanol: water (1: 3).

2.2.5. General Procedure for the Synthesis of homopolymers [PM_1-PM_{11}]

Monomer [$\mathbf{M_1}$-$\mathbf{M_{11}}$] (5.3 mmol) was suspended in 50 mL of toluene in a 100 mL two neck round bottom flask, which was tightly sealed and placed in an oil bath at 90 ºC and (0.1 g) of Benzoyl peroxide (Bpo) was added to the reaction mixture as initiator. The reaction mixture was heated for (10-12 hrs.) under nitrogen flow and at the end of polymerization; the mixture was cooling in ice path, precipitate was filtered, recrystallized with suitable solvent and finally dried in an oven at 50 ºC.

2.2.6. General Procedure for the Synthesis of Heteropolymer [PM_{12}-PM_{22}]

In a dry tow neck round bottom flask, (3.77 mmol), from each prepared monomer and acrylic acid in 50 mL of dry toluene and (0. 1 g) of the initiator Benzoyl peroxide (Bpo) was added under nitrogen gas

flow, the flask was tightly sealed and heated on oil bath at 90 °C for 10 hours. When the polymerization period is finished, precipitate was filtered, washed with ether and then dried in oven at 50 °C.

2.3. Measurement of Swelling of polymers [PM_1-PM_{22}]

Gravimetric measurements were used to determine dynamic swelling. The polymeric samples were suspended in 100 mL of water at 25°C in a beaker. At five consecutive hours and days, the hydrogel sample was withdrawn, rapidly wiped free of surface water using filter paper, weighed on an analytical scale balance (accuracy 0.0002), and reintroduced to the swelling solution. The equation was used to compute the swelling ratio [84].

$$\text{Swelling ratio (\%)} = (Ws - Wd)/Wd \times 100 \quad \ldots\ldots(2.1)$$

[Wd= Weight of polymer; Ws= weight of swollen polymer][85]

2.4. Release of drugs

By using UV-visible spectrophotometer (the different wave lengths of drugs are inserted within the tables), the drug release from the prepared polymers was determined in two different buffer solutions (pH= 2 and 8.0) at five consecutive hours and seven days at 24 ˚C. Table 3.8 represents the drug release from the prepared polymers.

The polymeric solutions were prepared by dissolving (0.005 g) from each polymer in 100 mL of different buffer solutions at constant temperature 24 ^{o}C [43]. After each hour (five consecutive hours) and consequently each day (six consecutive days) 5mL from each solution were drawn and measured for the absorbance at the wave length of the free drugs dissolving in same buffer solution.

Buffer solutions:

1. pH=2 : This solution was prepared, by mixing 500 ml of 0.2 M of KCl and 0.86 ml of 0.2 M of HCl.

2. pH=8.0: This solution was prepared, by mixing 500 ml of 0.025 M of Borax[$Na_2B_4O_7.10H_2O$] and 0.43 ml of 0.1 M of HCl.

2.5. Cytotoxic assay [112]

To determine the cytotoxic effect of some of prepared polymers (PM_1, PM_2, PM_5, PM_6, PM_8, PM_{12}, PM_{13}, PM_{16}, PM_{17} and PM_{19}) the MTT assay was done using 96-well plates [97]. Cell lines were seeded at 1×10^4 cells/well. After 24 hrs. or a confluent monolayer was achieved, cells were treated with tested compounds at different concentration. Cell viability was measured after 72 hrs. of treatment by removing the medium, adding 28 µL of 2 mg/mL solution of MTT and incubating the cells for 2.5 h at 37 °C. After removing the MTT solution, the crystals remaining in the wells were solubilized by the addition of 130 µL of DMSO (Dimethyl Sulfoxide) followed by 37 °C incubation for 15 min with shaking [95]. The absorbency was determined on a microplate reader at 492 nm; the assay was performed in triplicate. The inhibition rate of cell growth (the percentage of cytotoxicity) was calculated as the following equation:-

Cytotoxicity = A-B/A *100 …… (2.2)

Where A is the optical density of control, and B is the optical density of the samples [98]. On the other hand, the percent of cell viability was determined using the equation given below [99]:

Percentage (%) of cell viability = $\frac{A570\ of\ treated\ cell}{A570\ of\ control\ cell}\ x\ 100$…….. (2.3)

2.5.1. Statistical analysis:

The obtained data were statically analyzed using an unpaired t-test with GraphPad Prism 6 [(94)]. The values were presented as the mean ± SD of triplicate measurements.

2.5.2. Chemicals and reagents

Table 2.2: Chemicals and reagents used determine the cytotoxic effect

No.	Items	Company	Country
1	Trypsin/EDTA	Capricorn	Germany
2	DMSO	Santacruz Biotechnology	USA
3	RPMI 1640	Capricorn	Germany
4	MTT stain	Bio-World	USA
5	Fetal bovine serum	Capricorn	Germany

2.5.3. Instruments

Table 2.3: Instruments used determine the cytotoxic effect

No.	Item	Company	Country
1	CO_2 incubator	Cypress Diagnostics	Belgium
2	Microtiter reader	Gennex Lab	USA
3	Laminar flow hood	K & K Scientific Supplier	Korea
4	Micropipette	Cypress Diagnostics	Belgium
5	Cell culture plates	Santa Cruz Biotechnology	USA

2.5.4. Maintenance of cell cultures

MCF-7 Cells were maintained in RPMI-1640 supplemented with 10% fetal bovine serum, 100 units/mL penicillin, and 100 (µg/ml) streptomycin. Cells were passaged using Trypsin-EDTA reseeded at 80% confluence twice a week, and incubated at 37 °C [(94)].

2.6: Molecular weights of prepared polymers

The Ostwald technique is a straightforward method for determining viscosity, which involves comparing the flow times of two liquids of similar volume using the same viscometer. The molecular weight of the polymer is determined using a viscometer, and the molecular weight acquired using this method is referred to as viscosity average molecular weight. Because the polymer solution has a relatively high molecular weight, it has a very high viscosity when compared to pure solvent [(113)].

2.6.1: Preparation of the Polymers Stock Solution

(10 mg/ml) of polymers in Dimethylformamide by weighing out 1.25 g of each polymer, transferring it to a Erlenmeyer Flask 125 ml and dissolving in 125 mL Dimethylformamide. Prepare from this solutions of concentration 8, 6, 4 and 2 mg/ml by transferring 40, 30, 20 or 10 ml respectively of the stock solution to a 50 mL volumetric flask and diluting with dimethylformamide up to the mark.

After charging with polymer solution the viscometer was immersed vertically in the constant-temperature water bath (30 °C) for ten minutes for thermal equilibration.

By calibrating the viscometer under identical experimental conditions with a liquid of known viscosity and density, the viscosity of the polymer samples could be determined directly from the equation [(97)]:

$$\frac{\eta}{\eta_o} = \frac{\rho\, t}{\rho_o\, t_o} \quad \text{..... (2.4)}$$

Where η the viscosity of the polymer solution, η_o the viscosity of the solvent, ρ and ρ_o, are the densities of the polymer solution and solvent respectively. With the concentrations used here the densities of the dilute polymer solutions and the pure solvent taken to be the same and the equation become [115]:

$$\frac{\eta}{\eta_o} = \frac{t}{t_o} \quad \ldots\ldots\ldots\ldots \quad (2.5)$$

To determine the molecular weight of the polymers conventional plots of η_{sp} /c vs. c, were extrapolated to obtain the intrinsic viscosity [η] from the intercept [114].

$$\eta_{sp} = \frac{\eta}{\eta_o} - 1 \quad \ldots\ldots\ldots\ldots \quad (2.6)$$

The reduced viscosity η_{red} is given by the relation:

$$\eta red_d = \frac{\frac{\eta}{\eta_o} - 1}{c} \; or \; \eta sp/c \quad \ldots \quad (2.7)$$

The molecular weight of the polymers was obtained by substitution [η] value in the equation [112]:

$$\mathbf{[\eta] = K \cdot M^a} \quad \ldots\ldots\ldots\ldots \quad (2.8)$$

Were [η] is intrinsic viscosity, M is molecular weight of the polymer, K and a are constant for a particular polymer/solvent/temperature system Values of K and a are available for poly(N-phenylmaleimide) (PNPI) give no clear linear proportionality of the intrinsic viscosity to molar mas where K = 1.34 x 10^{-4} and a = 0.71 similar to the Mark-Houwink constants of methyl methacrylate/*N*-phenylmaleimide copolymers, K = 1.34 x 10^{-4} and a = 0.73 [115]. In the same manner, a Mark-Houwink constant was calculated for poly [*N*-(4-acetyl) phenyl amino] maleimide-co-acrylic acid (APAMI-co-AA) using the plots of viscosities of the polymer fractions in DMF against the molecular weight [117].

Table 2.4: Data used to determine the intrinsic viscosity and M.Wt of [PM_1]

pm 1 polymer concentration mg/ml	time flow t/s	$\eta/\eta_o = t/t_o$	$\eta_{red}=\eta_{sp}/c$
DMF	65	1	0
10	137.8	2.12	0.112
8	122.9	1.890769231	0.111346
6	107.7	1.656923077	0.109487
4	92.6	1.424615385	0.106154
2	78.1	1.201538462	0.100769
[η]=0.0997 L/g	M= 12655.28 D		

Table 2.5: Data used to determine the intrinsic viscosity and M.Wt of [PM_2]

pm 2 polymer concentration mg/ml	time flow t/s	$\eta/\eta_o = t/t_o$	$\eta_{red} = \eta_{sp}/c$
DMF	65	1	0
10	143.2	2.203076923	0.120308
8	128.1	1.970769231	0.121346
6	111.4	1.713846154	0.118974
4	95.2	1.464615385	0.116154
2	79.7	1.226153846	0.113077
[η]=0.1121 L/g	M= 13067.7 D		

Table 2.6: Data used to determine the intrinsic viscosity and M.Wt of [PM_3]

pm 3 polymer concentration mg/ml	time flow t/s	$\eta/\eta_o = t/t_o$	η_{red}=ηsp/c
DMF	65	1	0
10	130.8	2.012307692	0.101231
8	120.2	1.849230769	0.106154
6	103.4	1.590769231	0.098462
4	90.6	1.393846154	0.098462
2	78	1.2	0.1
[η]=0.0978 L/g	M= 10782.6 D		

Table 2.7: Data used to determine the intrinsic viscosity and M.Wt of [PM_4]

pm 4 polymer concentration mg/ml	time flow t/s	$\eta/\eta_o = t/t_o$	η_{red}=ηsp/c
DMF	65	1	0
10	129.8	1.996923077	0.099692
8	116.7	1.795384615	0.099423
6	100.3	1.543076923	0.090513
4	89.4	1.375384615	0.093846
2	76.8	1.181538462	0.090769
[η]=0.0878 L/g	M= 9262.9 D		

Table 2.8: Data used to determine the intrinsic viscosity and M.Wt of [PM_5]

pm 5 polymer concentration mg/ml	time flow t/s	$\eta/\eta_o = t/t_o$	$\eta_{red}=\eta_{sp}/c$
DMF	65	1	0
10	128.7	1.98	0.098
8	115.2	1.772307692	0.096538
6	99.3	1.527692308	0.087949
4	87.4	1.344615385	0.086154
2	76.3	1.173846154	0.086923
[η]=0.0814 L/g	M= 8326.3 D		

Table 2.9: Data used to determine the intrinsic viscosity and M.Wt of [PM_6]

pm 6 polymer concentration mg/ml	time flow t/s	$\eta/\eta_o = t/t_o$	$\eta_{red}=\eta_{sp}/c$
DMF	65	1	0
10	124.9	1.921538462	0.092154
8	112.6	1.732307692	0.091538
6	99.8	1.535384615	0.089231
4	86.7	1.333846154	0.083462
2	75.8	1.166153846	0.083077
[η]=0.080 L/g	M= 8125.3 D		

Table 2.10: Data used to determine the intrinsic viscosity and M.Wt of [PM_7]

pm7 polymer concentration mg/ml	time flow t/s	$\eta/\eta_o = t/t_o$	$\eta_{red}=\eta_{sp}/c$
DMF	65	1	0
10	129.8	1.996923077	0.099692
8	118.9	1.829230769	0.103654
6	102.1	1.570769231	0.095128
4	88.6	1.363076923	0.090769
2	76.2	1.172307692	0.086154
[η]=0.0833 L/g	M= 8601.3 D		

Table 2.11: Data used to determine the intrinsic viscosity and M.Wt of [PM_8]

pm 8 polymer concentration mg/ml	time flow t/s	$\eta/\eta_o = t/t_o$	$\eta_{red}=\eta_{sp}/c$
DMF	65	1	0
10	131.8	2.027692308	0.102769
8	117.9	1.813846154	0.101731
6	104.7	1.610769231	0.101795
4	90.3	1.389230769	0.097308
2	77.4	1.190769231	0.095385
[η]=0.094 L/g	M= 10197.25 D		

Table 2.12: Data used to determine the intrinsic viscosity and M.Wt of [PM_9]

pm 9 polymer concentration mg/ml	time flow t/s	$\eta/\eta_o = t/t_o$	$\eta_{red}=\eta_{sp}/c$
DMF	65	1	0
10	131.1	2.016923077	0.101692
8	117.7	1.810769231	0.101346
6	102.4	1.575384615	0.095897
4	90.3	1.389230769	0.097308
2	76.7	1.18	0.09
[η]=0.0890 L/g	M= 9441.7 D		

Table 2.13: Data used to determine the intrinsic viscosity and M.Wt of [PM_{10}]

pm 10 polymer concentration mg/ml	time flow t/s	$\eta/\eta_o = t/t_o$	$\eta_{red}=\eta_{sp}/c$
DMF	65	1	0
10	148.6	2.286153846	0.128615
8	131.6	2.024615385	0.128077
6	114.9	1.767692308	0.127949
4	98.1	1.509230769	0.127308
2	81.4	1.252307692	0.126154
[η]=0.1259 L/g	M= 15389.1 D		

Table 2.14: Data used to determine the intrinsic viscosity and M.Wt of [PM_{11}]

pm 11 polymer concentration mg/ml	time flow t/s	$\eta/\eta_o = t/t_o$	$\eta_{red}=\eta_{sp}/c$
DMF	65	1	0
10	123.8	1.904615385	0.090462
8	113.2	1.741538462	0.092692
6	100.6	1.547692308	0.091282
4	87.3	1.343076923	0.085769
2	75.7	1.164615385	0.082308
[η]=0.0815 L/g	M= 7610.9 D		

Table 2.15: Data used to determine the intrinsic viscosity and M.Wt of [PM_{12}]

pm 12 polymer concentration mg/ml	time flow t/s	$\eta/\eta_o = t/t_o$	$\eta_{red}=\eta_{sp}/c$
DMF	65	1	0
10	137.3	2.112307692	0.111231
8	124.4	1.913846154	0.114231
6	108.2	1.664615385	0.110769
4	92.2	1.418461538	0.104615
2	78.7	1.210769231	0.105385
[η]=0.1029 L/g	M= 11582.9 D		

Table 2.16: Data used to determine the intrinsic viscosity and M.Wt of [PM_{13}]

pm 13 polymer concentration mg/ml	time flow t/s	$\eta/\eta_o = t/t_o$	$\eta_{red}=\eta_{sp}/c$
DMF	65	1	0
10	134.1	2.063076923	0.106308
8	122.8	1.889230769	0.111154
6	104.9	1.613846154	0.102308
4	91.3	1.404615385	0.101154
2	76.8	1.181538462	0.090769
[η]=0.09 L/g	M= 9591.4D		

Table 2.17: Data used to determine the intrinsic viscosity and M.Wt of [PM_{14}]

pm 14 polymer concentration mg/ml	time flow t/s	$\eta/\eta_o = t/t_o$	$\eta_{red}=\eta_{sp}/c$
DMF	65	1	0
10	148.8	2.289230769	0.128923
8	131.4	2.021538462	0.127692
6	114.1	1.755384615	0.125897
4	97.9	1.506153846	0.126538
2	81.5	1.253846154	0.126923
[η]=0.1256 L/g	M= 15337.45 D		

Table 2.18: Data used to determine the intrinsic viscosity and M.Wt of [PM_{15}]

pm 15 polymer concentration mg/ml	time flow t/s	$\eta/\eta_o = t/t_o$	$\eta_{red}=\eta_{sp}/c$
DMF	65	1	0
10	148.3	2.281538462	0.128154
8	130.5	2.007692308	0.125962
6	113.7	1.749230769	0.124872
4	97.1	1.493846154	0.123462
2	81.2	1.249230769	0.124615
[η]=0.1225 L/g	M= 14806.98 D		

Table 2.19: Data used to determine the intrinsic viscosity and M.Wt of [PM_{16}]

pm 16 polymer concentration mg/ml	time flow t/s	$\eta/\eta_o = t/t_o$	$\eta_{red}=\eta_{sp}/c$
DMF	65	1	0
10	146.2	2.249230769	0.124923
8	130.6	2.009230769	0.126154
6	113.9	1.752307692	0.125385
4	97.2	1.495384615	0.123846
2	80.5	1.238461538	0.119231
[η]=0.1198 L/g	M= 14349.4 D		

Table 2.20: Data used to determine the intrinsic viscosity and M.Wt of [PM_{17}]

pm 17 polymer concentration mg/ml	time flow t/s	$\eta/\eta_o = t/t_o$	$\eta_{red}=\eta_{sp}/c$
DMF	65	1	0
10	121.6	1.870769231	0.087077
8	113.1	1.74	0.0925
6	99.5	1.530769231	0.088462
4	86.3	1.327692308	0.081923
2	75.4	1.16	0.08
[η]=0.0786 L/g	M= 7925.7 D		

Table 2.21: Data used to determine the intrinsic viscosity and M.Wt of [PM_{18}]

pm 18 polymer concentration mg/ml	time flow t/s	$\eta/\eta_o = t/t_o$	$\eta_{red}=\eta_{sp}/c$
DMF	65	1	0
10	129.6	1.993846154	0.099385
8	118.1	1.816923077	0.102115
6	105.9	1.629230769	0.104872
4	91.1	1.401538462	0.100385
2	77.3	1.189230769	0.094615
[η]=0.0969 L/g	M= 10643.1 D		

Table 2.22: Data used to determine the intrinsic viscosity and M.Wt of [PM_{19}]

pm 19 polymer concentration mg/ml	time flow t/s	$\eta/\eta_o = t/t_o$	$\eta_{red}=\eta_{sp}/c$
DMF	65	1	0
10	131.6	2.024615385	0.102462
8	115.2	1.772307692	0.096538
6	101.5	1.561538462	0.09359
4	89.4	1.375384615	0.093846
2	77.9	1.198461538	0.099231
[η]=0.0944 L/g	M= 10258.4 D		

Table 2.23: Data used to determine the intrinsic viscosity and M.Wt of [PM_{20}]

pm 20 polymer concentration mg/ml	time flow t/s	$\eta/\eta_o = t/t_o$	$\eta_{red}=\eta_{sp}/c$
DMF	65	1	0
10	139.1	2.14	0.114
8	126.4	1.944615385	0.118077
6	107.5	1.653846154	0.108974
4	94.8	1.458461538	0.114615
2	79.2	1.218461538	0.109231
[η]=0.1091 L/g	M= 12561.6 D		

Table 2.24: Data used to determine the intrinsic viscosity and M.Wt of [PM_{21}]

pm 21 polymer concentration mg/ml	time flow t/s	$\eta/\eta_o = t/t_o$	$\eta_{red}=\eta_{sp}/c$
DMF	65	1	0
10	141.9	2.183076923	0.118308
8	124.7	1.918461538	0.114808
6	107.3	1.650769231	0.108462
4	91.8	1.412307692	0.103077
2	79.2	1.218461538	0.109231
[η]=0.1018 L/g	M= 11408.9 D		

Table 2.25: Data used to determine the intrinsic viscosity and M.Wt of [PM_{22}]

pm 22 polymer concentration mg/ml	time flow t/s	$\eta/\eta_o = t/t_o$	$\eta_{red}=\eta_{sp}/c$
DMF	65	1	0
10	148.2	2.310769231	0.131077
8	130.5	2.038461538	0.129808
6	115.5	1.776923077	0.129487
4	98.7	1.518461538	0.129615
2	81.9	1.26	0.13
[η]=0.1293 L/g	M= 15977.63 D		

Chapter Three

3

RESULTS & DISCUSSION

3. Results and Discussion

3.1. Synthesis and characterization of [A_1], [A_2] and [A_3]

When maleic anhydride reacts with *m*-amino-benzoic acid in the presence of dried acetone, N-(3-carboxyphenyl) maleamic acid [A_1] was obtained in 90% yield, mp 223-224 °C.

Compound [A_2] was cyclodehydrated by using glacial acetic acid at high temperature, Equation 3-1, the mechanism of this reaction shown in Scheme 3-1. The percentage of obtained m-CPMI was 70% and m.p. was observed between 238-240 ˚C.

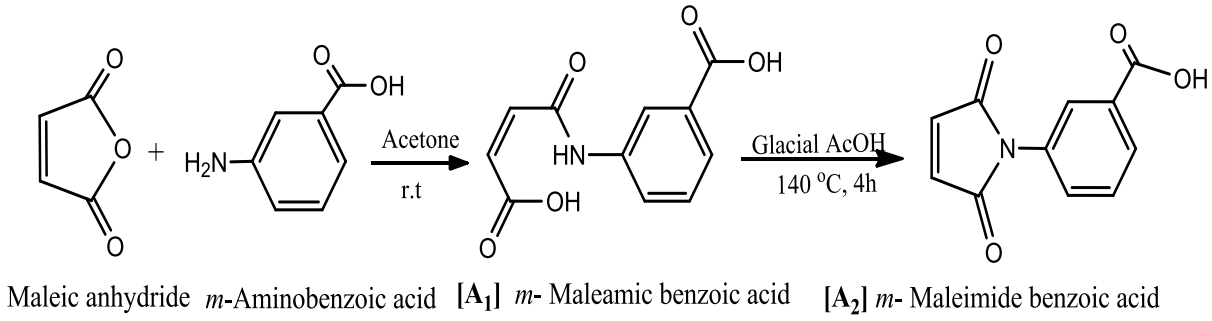

Equation 3-1: Synthesis of compound [A_1] and [A2]

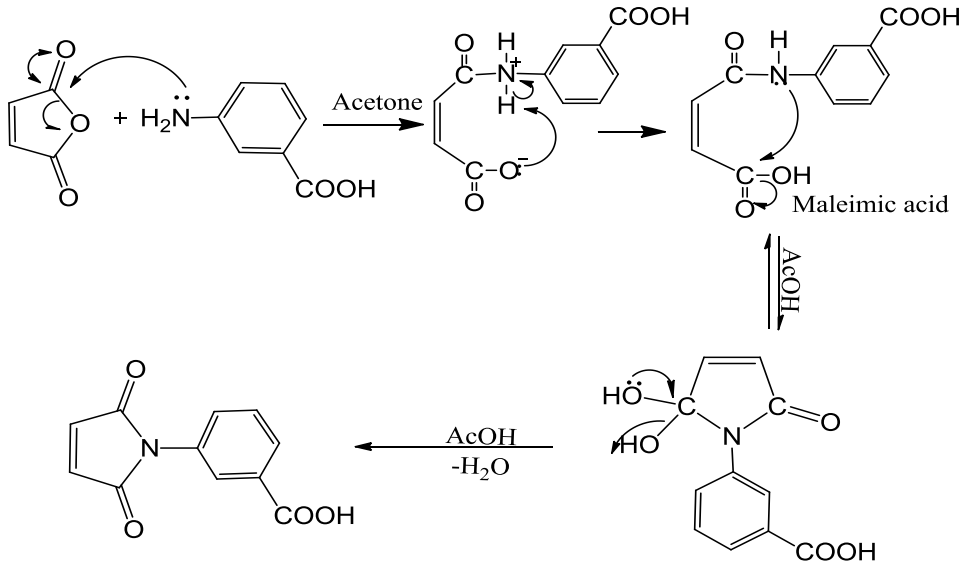

Scheme 3.1: Addition-elimination (cyclization-dehydration) mechanism for the formation of *N*-benzoic maleimide from maleamic acid in the presence of glacial acetic acid

Characterization of Compound [A_1]: FT-IR (cm^{-1}): compound [A_1] show a board band between 3400-2500 for carboxylic acid O-H of and 3220 (amide N-H) for acyclic maleamic derivative, 3101 (olefinic =C-H), 3015 (aromatic =C-H), 1609 -1453 (C=C aromatic ring), 1723, 1699 (C=O, two carboxylic acid groups coupled with amide), 1382 (C-N), (Figure 3.1).

Characterization of Compound [A_2], FT- IR (cm^{-1}): various absorption bands were observed at 3500-2500 (Carboxylic acid O-H), 3097, 3074 (=C-H of maleimide and aromatic), 1709 and 1693 (C=O stretch, 5-membered imide ring and carboxyl groups), 1609-1423 (Aromatic C=C), 1383 (C-N), 835 (*Cis*-CH=CH bending) [(119)]. Disappearing of amide absorption at 3220 cm^{-1}, carboxylic acid carbonyl at 1723 cm^{-1} and showing new characteristic band for maleimide carbonyl at 1709 cm^{-1} ensure the success of cyclodehydration reaction of maleamic acid[(120)] (Figure 3.2).

Because of the double bond and sp2- hybridized carbons in Maleimide this molecule is even more likely to be planar and tend to be symmetric and the dipole moment derivate associated with the C=C stretching intensity is located perpendicularly to C=C bond similarly to what is also observed in cis-$C_2H_2X_2$, so the double bond stretching vibration of maleimide ring is hard to observed in the FT-IR spectrum [(121,122)].

^{1}HNMR spectrum of compound [A_2] (Figure 3.3), The singlet signal 6.875 ppm belong to maleimide protons (a), the aromatic protons (b) signals appeared between 7.268-8.393 ppm and the carboxylic acid proton (c) appeared as brad signal at 11.804 ppm.

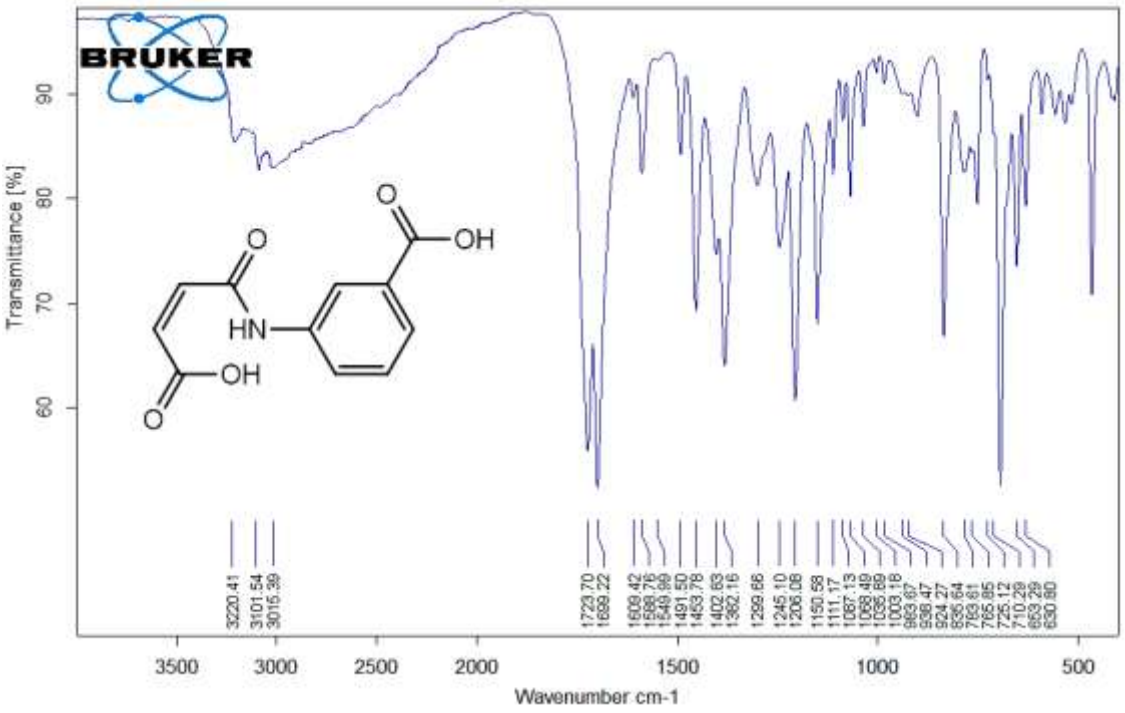

Figure 3.1: FT-IR spectrum of compound [A_1]

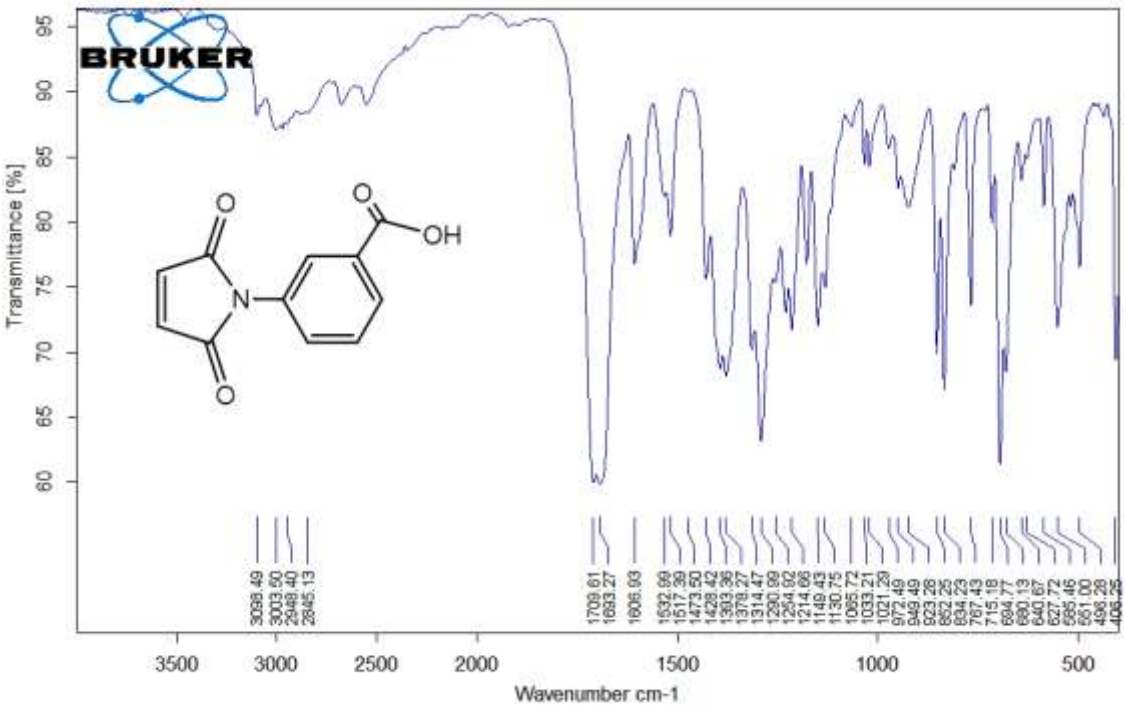

Figure 3.2: FT-IR spectrum of compound [A_2]

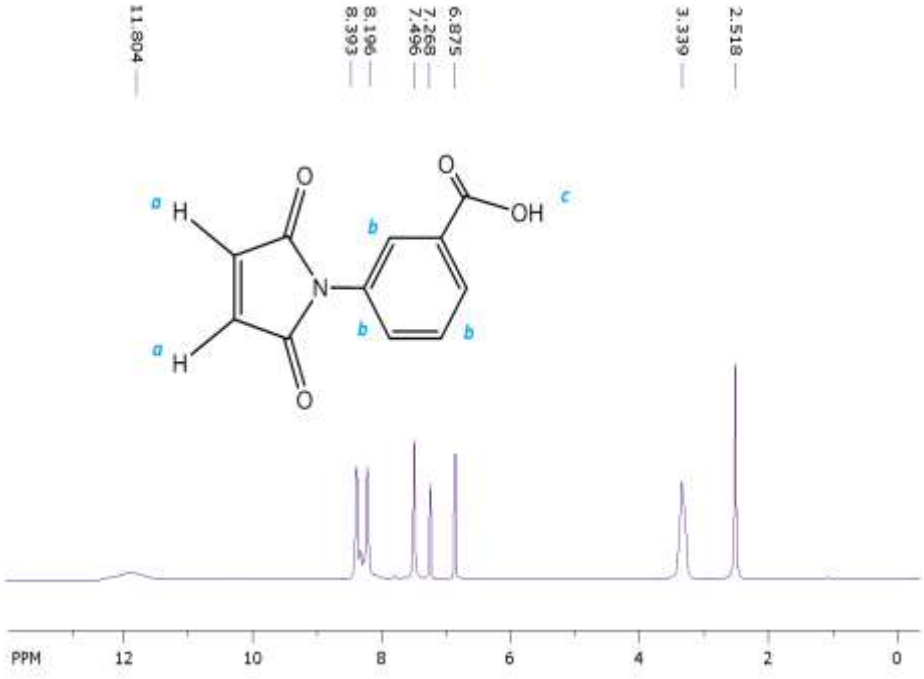

Figure 3.3: ^{1}H-NMR spectrum of compound [A_2]

m-CPMI [A_2] reacted with thionyl chloride and *m*-Maleimido-benzoyl chloride (*m*-CPMIC) [A_3] was obtained. The yield percentage of obtained *m*-CPMIC was 90% and mp 125-127 °C (Lit. mp = 126-128^{o}C) [99, 100].

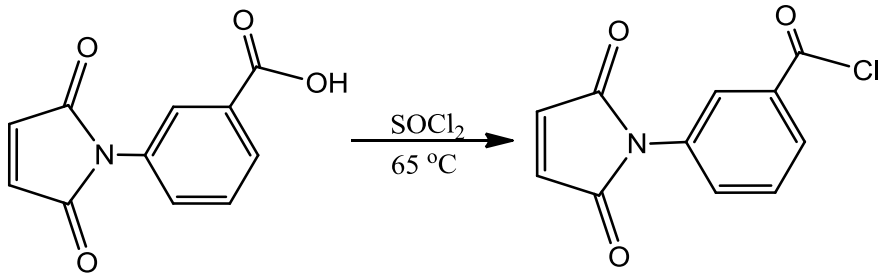

N-(3-Carboxyphenyl) maleimide N-[3-(Chlorocarbonyl) phenyl] maleimide

Equation 3-2: Synthesis of compound [A_3] *(m-CPMIC)*

Characterization of compound [A_3], IR (cm^{-1}): shows no absorption band for Carboxylic acid O-H in the range of 3500-2500 and the characteristic stretching vibration of carbonyl group of acid chloride (COCl) occur at high wave number (1769 cm^{-1}) give evidence for the success of the synthesis of (*m*-CPMIC).

The (=C-H) of maleimide and aromatic appeared at 3108 and 3081 and strong absorption 1718 for CONCO of maleimide carbonyl groups 1597 and 1581 (Aromatic C=C), (Figure 3.3).

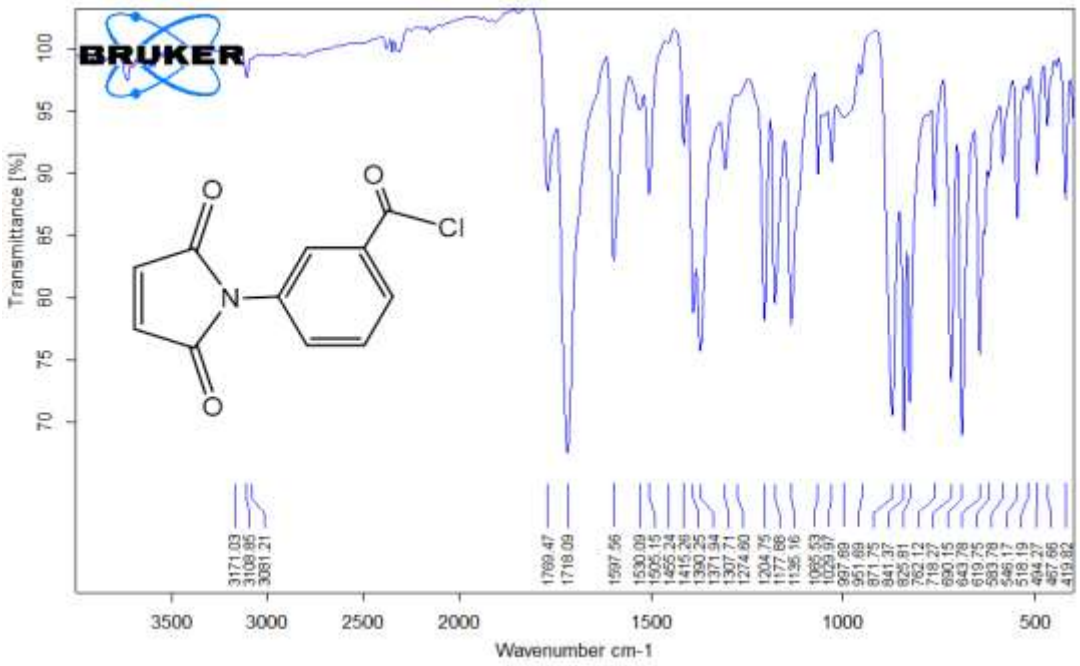

Figure 3.4: FT-IR spectrum of compound [A_3]

3.3. Synthesis of Maleimide-Drug Monomers [M_1-M_{11}]

3-Maleimide benzoyl Chloride [A3], (16 mmol) was added with stirred to solution of 16 mmol of different Drugs (Clafuran, Ciprofloxacin, Ceftriaxone, Ampicillin, Amoxicillin, Paracetemol, Silver-Sulfadiazine, Metoclopramide, Cephalexin, Isoniazid, and Carbamazepine, respectively) in suitable solvent as follow : 60 mL of ethyl acetate for (Paracetemol), (60 mL) of dry Benzene for (Metoclopramide) and (30 mL) DMSO for the other drugs. The mechanism of this reaction shown in (Scheme 3-2).

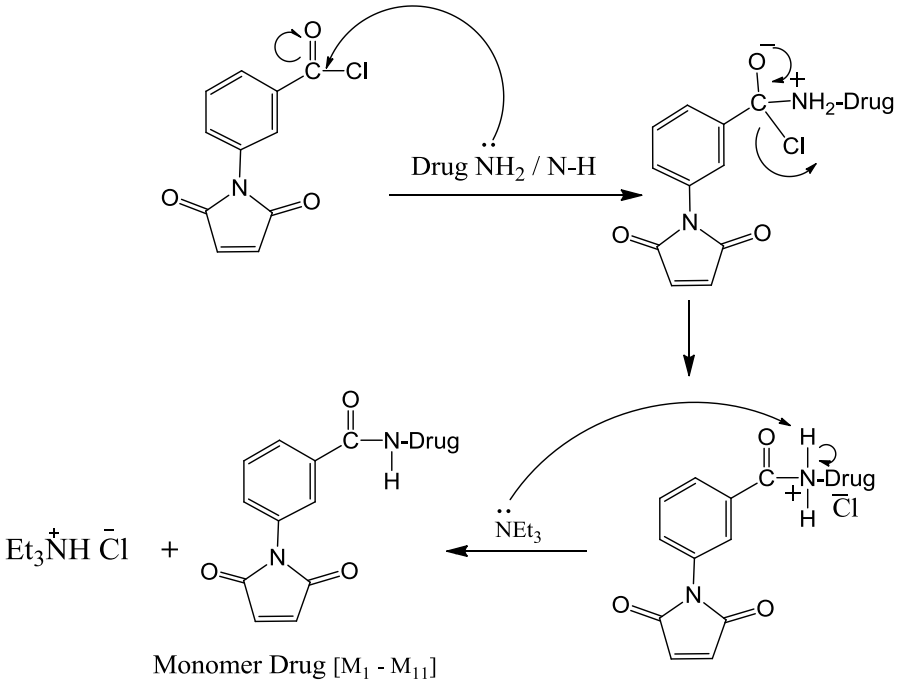

Scheme 3.2: Mechanism of Synthesized Compound [M_1-M_{11}]

The chemical structures of all prepared compound were characterized by FTIR and 1H-NMR, and CHNS spectroscopies, beside to 13C-NMR for 5 monomers.

Table 3.1: (C.H.N.S) Elementary Analysis of the Monomers

Com. no .	Calculated %				Found %			
	C	H	N	S	C	H	N	S
M_1	49.54	3.39	12.84	9.80	48.22	3.11	11.35	9.20
M_2	46.09	3.33	16.68	12.73	44.95	3.50	16.14	12.44
M_3	59.12	4.41	10.21	5.85	58.10	4.25	9.59	5.32
M_4	57.44	4.28	9.92	5.68	57.15	4.20	9.66	5.27
M_5	59.33	4.06	10.25	5.87	58.01	3.88	9.78	5.15
M_6	63.39	4.37	10.56	-	61.67	4.07	10.20	-
M_7	65.66	4.51	13.92	-	64.44	4.22	12.98	-
M_8	56.12	3.36	15.58	7.13	55.95	3.30	15.07	6.85
M_9	60.71	3.60	16.66	-	60.10	3.42	9.13	-
M_{10}	71.72	3.94	9.65	-	70.22	4.10	6.13	-
M_{11}	60.18	5.45	11.23	-	60.06	5.12	11.08	-

Synthesis of beta-lactam drug-maleimide: maleimide compounds [M_1, M_2, M_3, M_4, and M_5] was synthesized by reaction of (3.75g, 16 mmol) of 3-maleimide benzoyl Chloride (A_3) with stirred solution of 16 mmol of each one of (Clafuran, ceftriaxone, ampicillin, amoxicillin, and cephalexin, respectively) in 30 mL of dimethyl sulfoxide and 16 mmol of triethylamine (NEt_3) was added dropwise as catalyst at room temperature, and then heated for (2 h.) at 60 ˚C, as shown in equation 3.3.

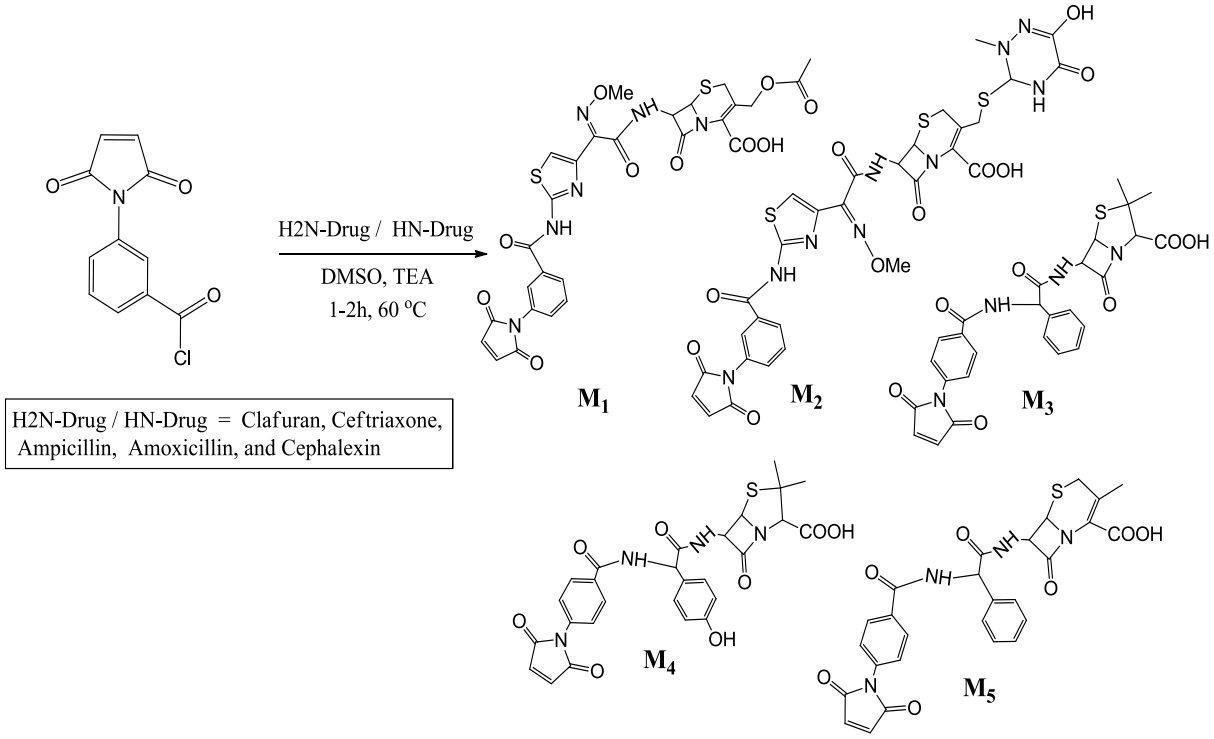

Equation 3-3: Synthesis of compounds [M_1-M_5]

Characterization: FT-IR spectra (Figures 3.5, 3.7, 3.9, 3.11, 3.13) of the synthesized compounds (M_1-M_5) shows strong stretching frequencies for the Maleimide carbonyl groups at 1714-1709 cm^{-1}, disappearing of (-COCl) band and showing a characteristic stretching bands at the range 1764-1788 cm^{-1} due to beta lactam carbonyl and broad absorption band of carboxyl groups in drug structures around ~3500-2500 cm^{-1} [(123)].

The ^{1}HNMR spectra (Figures 3.6, 3.8, 3.10, 3.12, 3.14) for (M_1- M_5) show characteristic signals for maleimide (CH=CH) protons at 6.718-7.182 ppm and for beta lactam protons at 4.063-5.146 ppm, broad and weak signal at 12.488-13.117 ppm for carboxylic acid group of (drugs).

There are some characteristic bands for compound [M_1], Figure 3.5 such as 1752 cm^{-1} due to stretching vibration of carbonyl ester group of the drug and the ketoxime ether group C=N-OMe and C=N of thiazole ring in [M_1] and [M_2] appeared at 1621-1553 cm^{-1} [103].

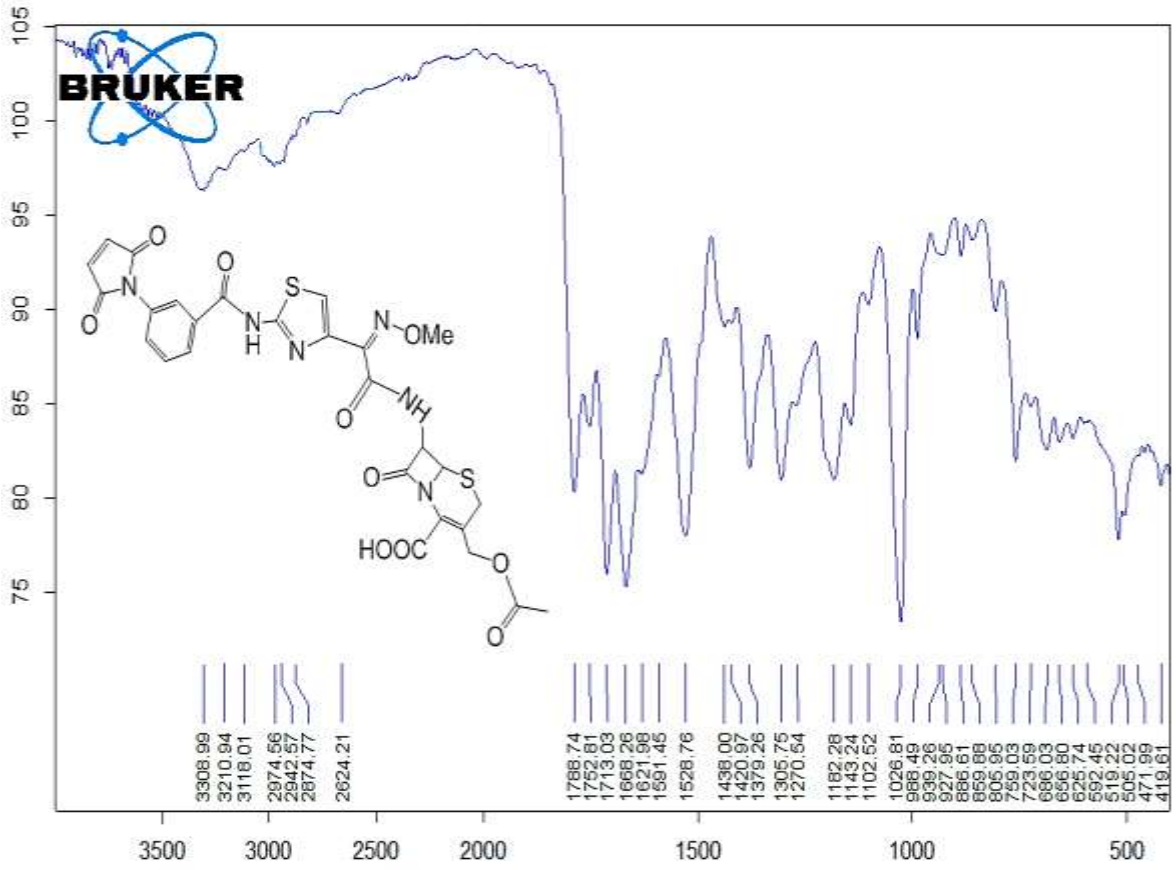

Figure 3.5: FT-IR spectrum of compound [M_1]

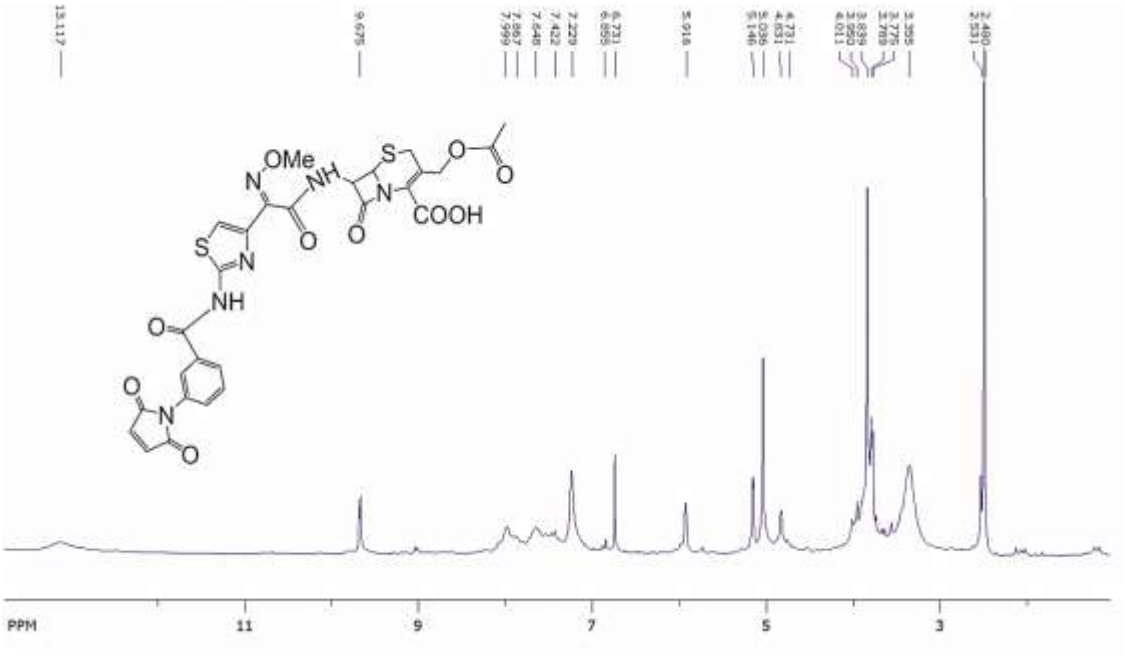

Figure 3.6: ^{1}H-NMR spectrum of compound [M_1]

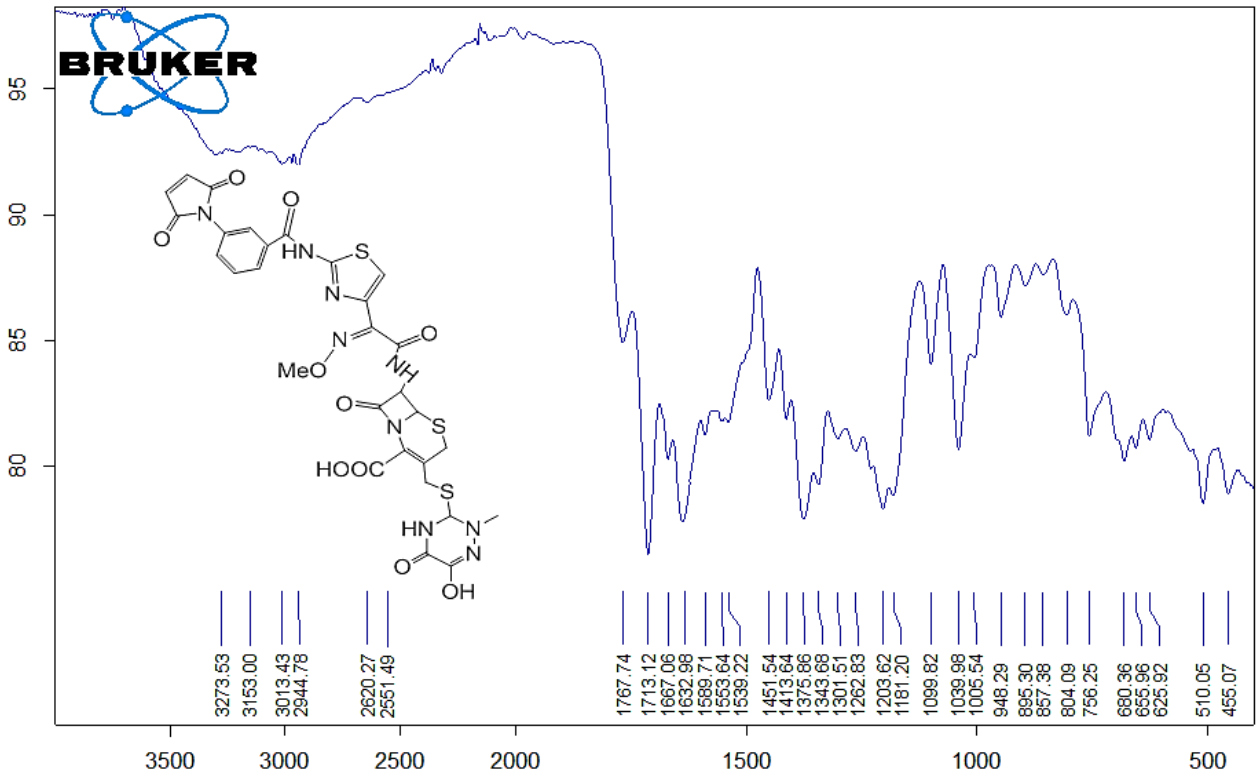

Figure 3.7: FT-IR spectrum of compound [M_2]

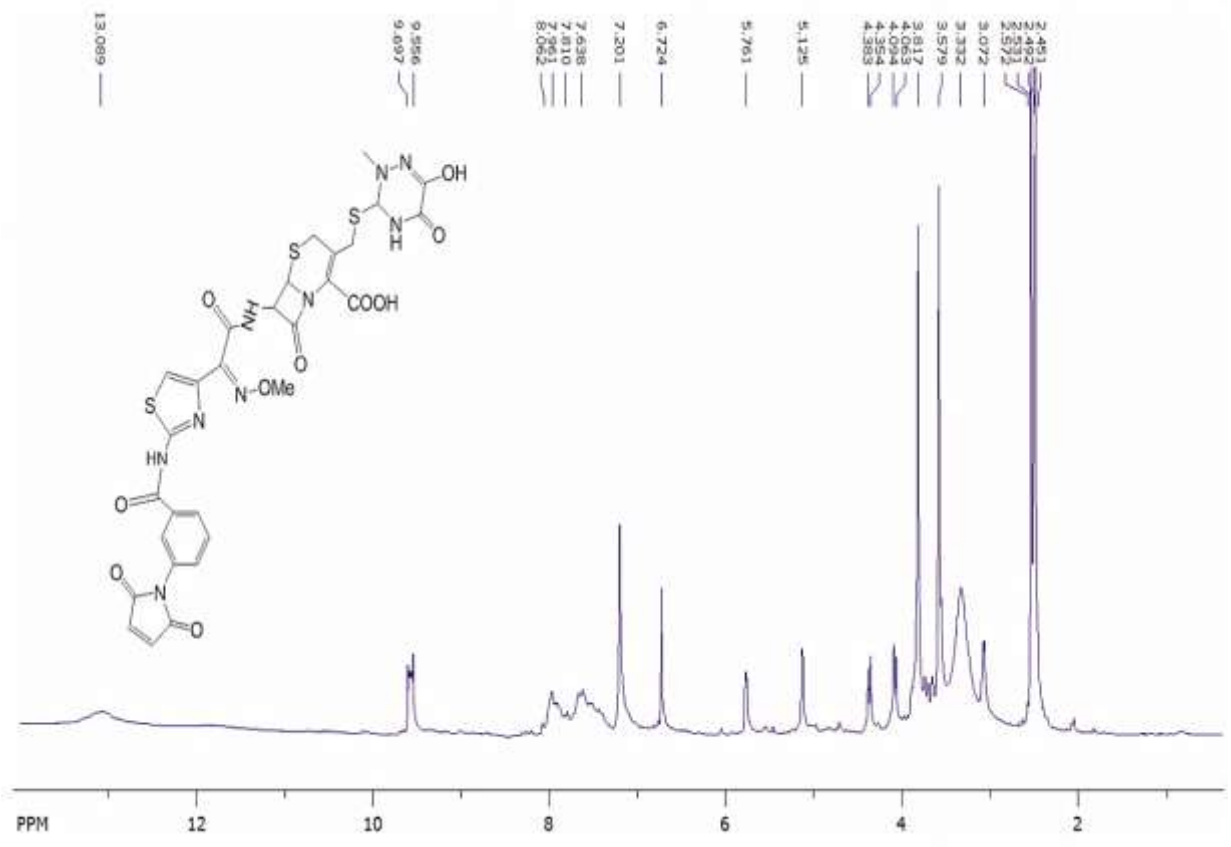

Figure 3.8: ^{1}H-NMR spectrum of compound [M_2]

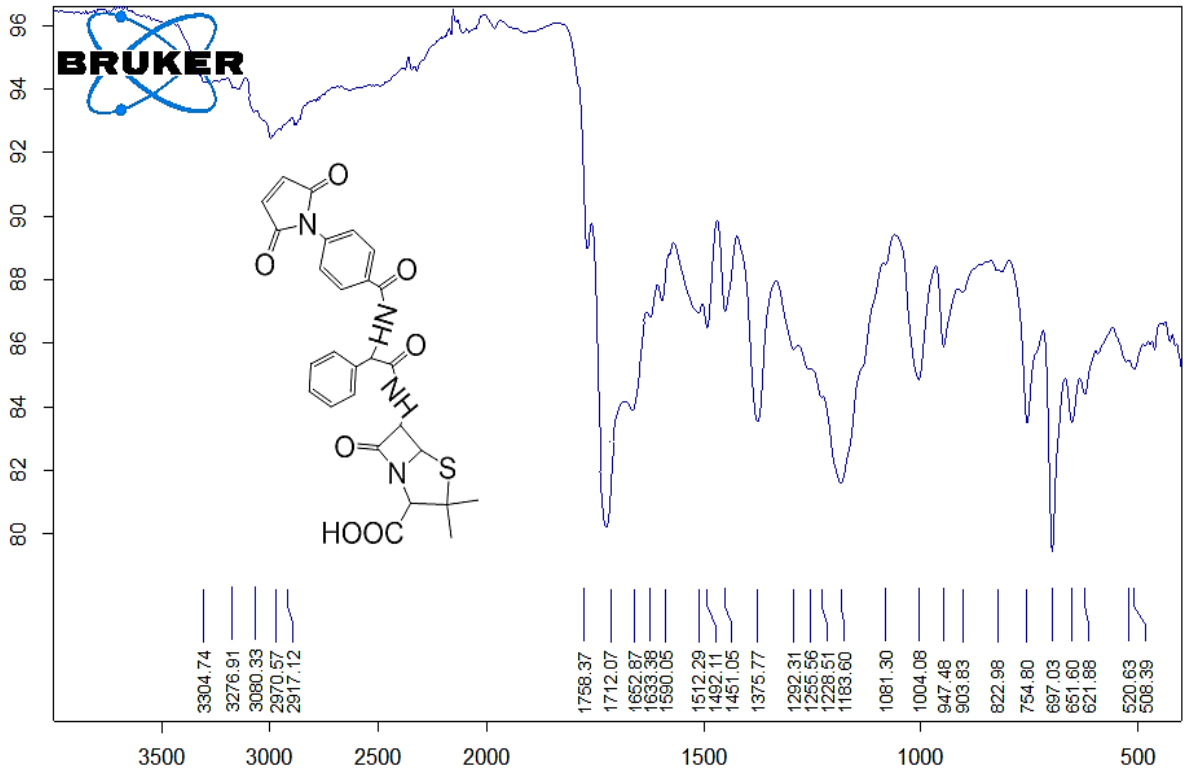

Figure 3.9: FT-IR spectrum of compound [M_3]

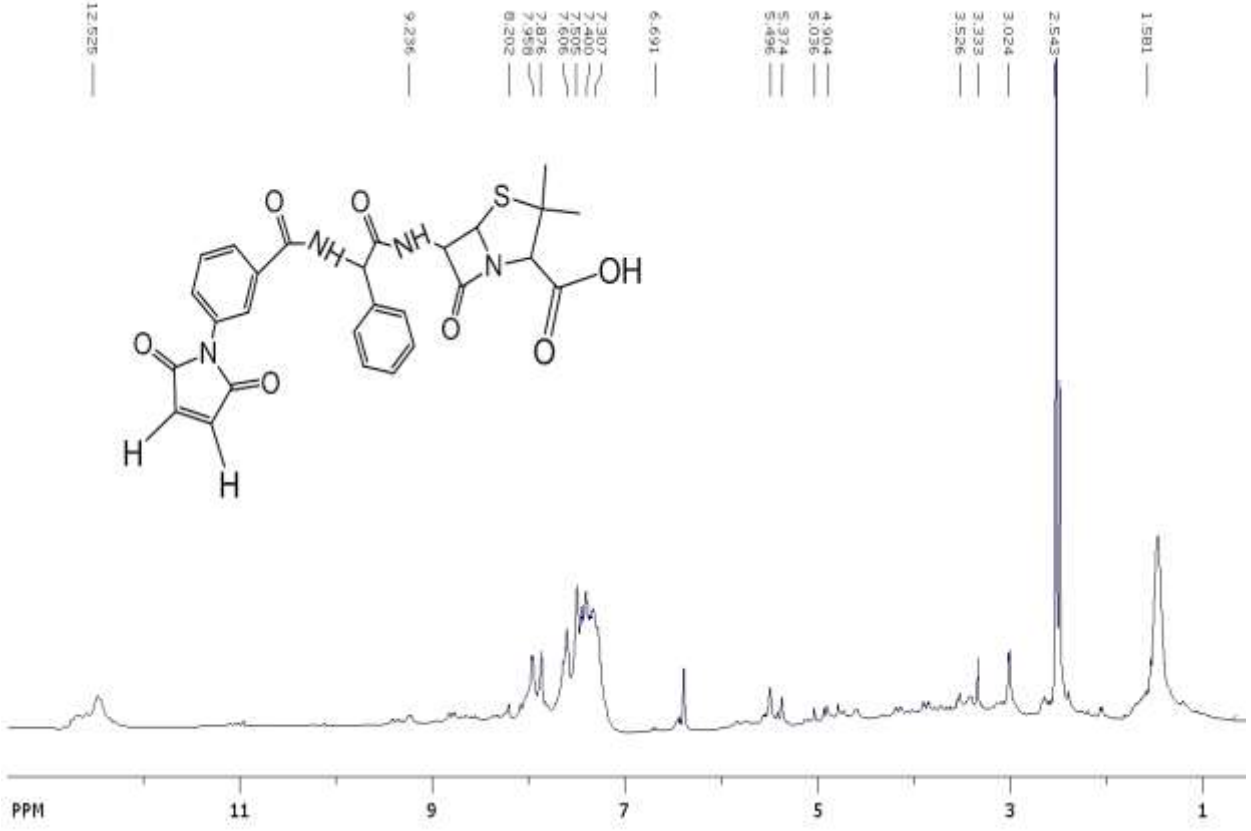

Figure 3.10: ^{1}H-NMR spectrum of compound [M_3]

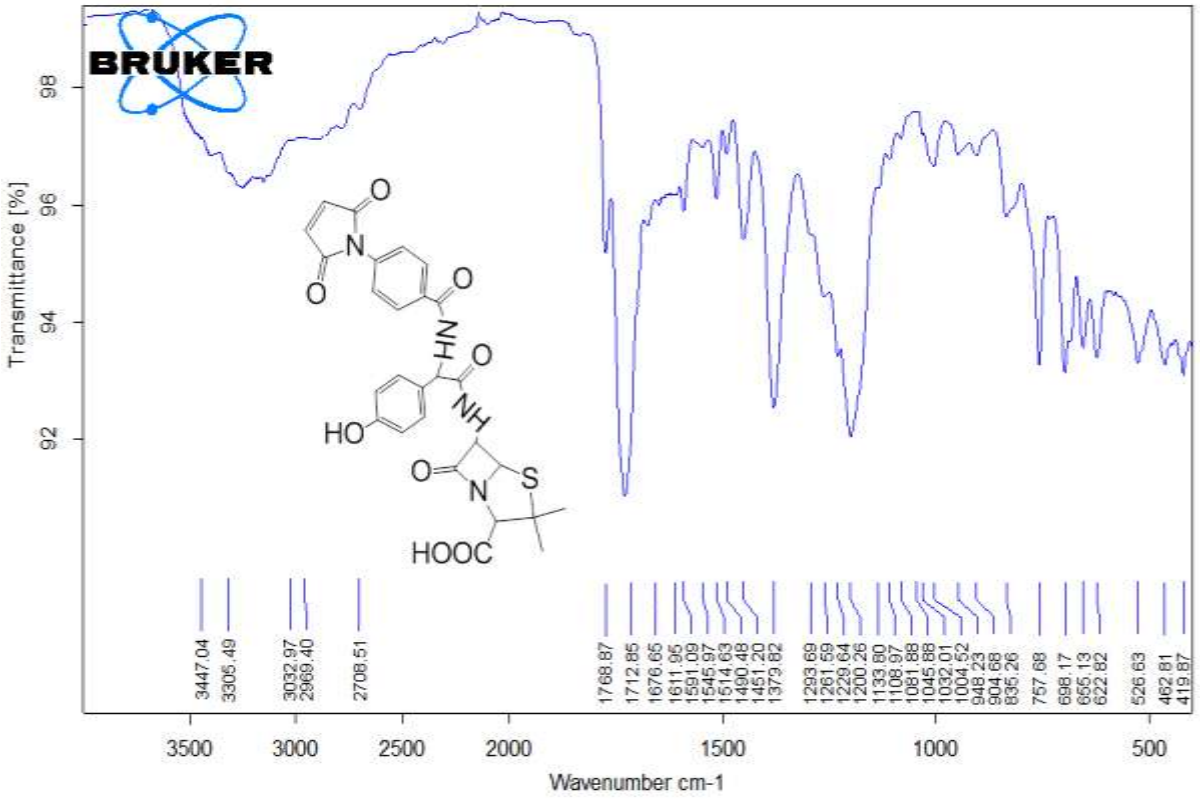

Figure 3.11: FT-IR spectrum of compound [M_4]

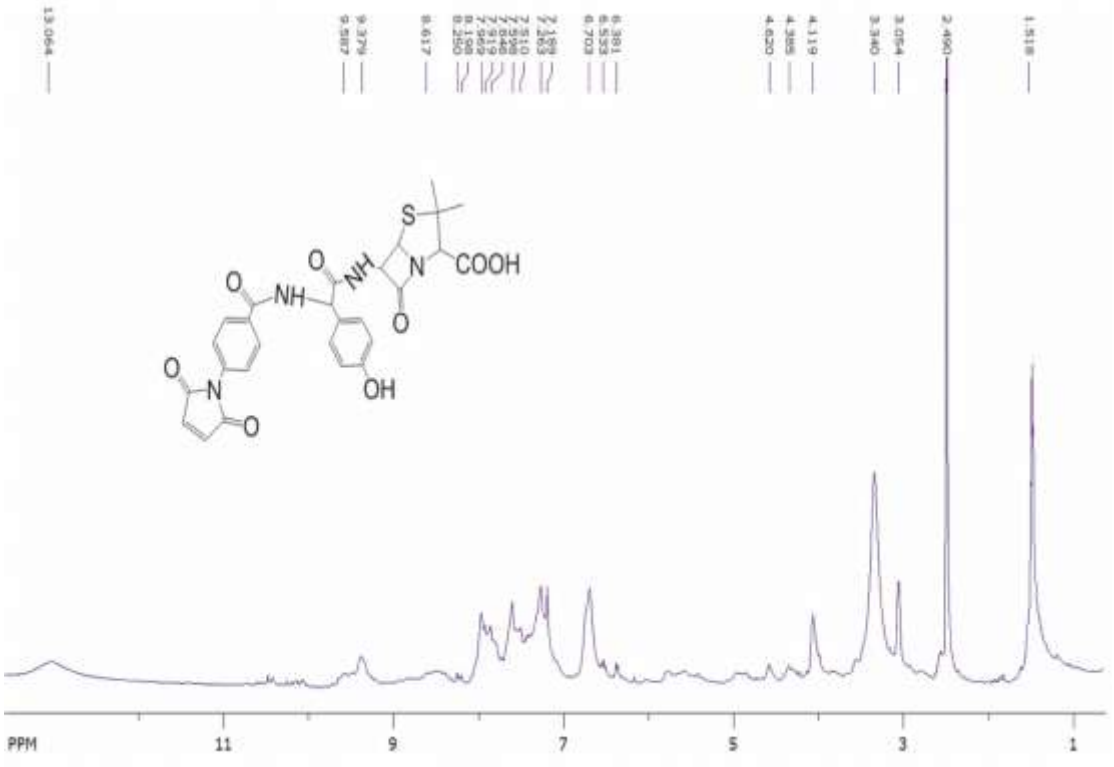

Figure 3.12: ^{1}H-NMR spectrum of compound [M_4]

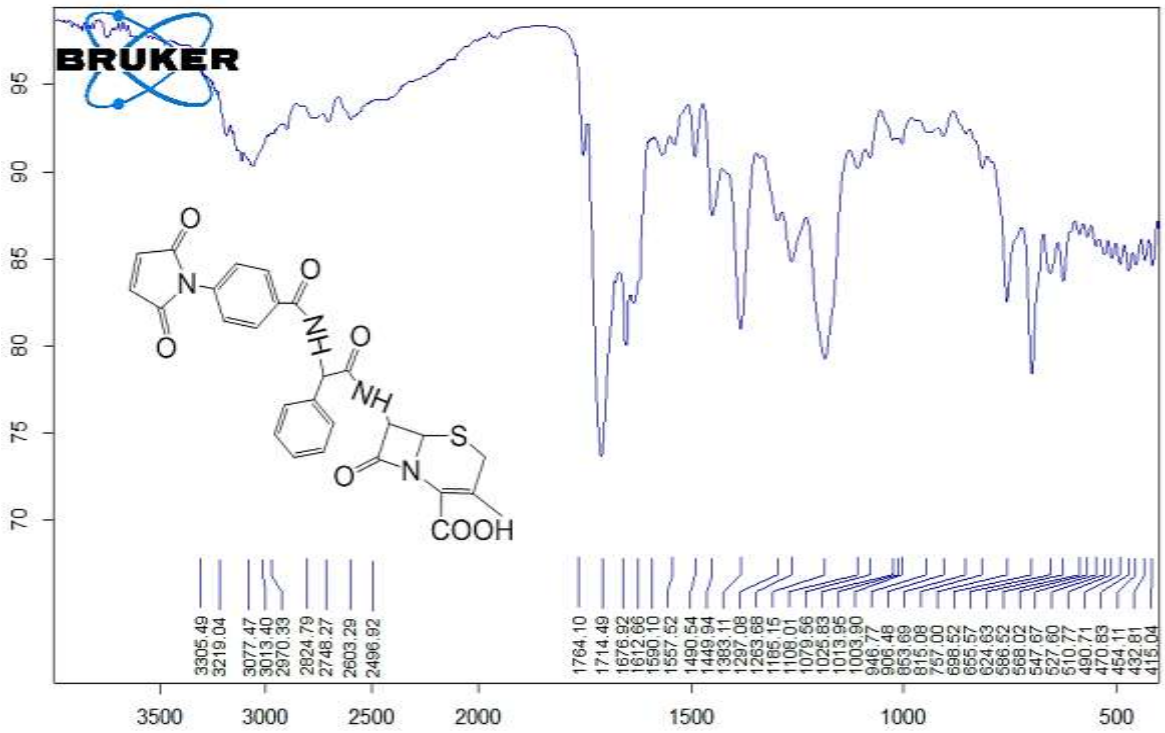

Figure 3.13: FT-IR spectrum of compound [M_5]

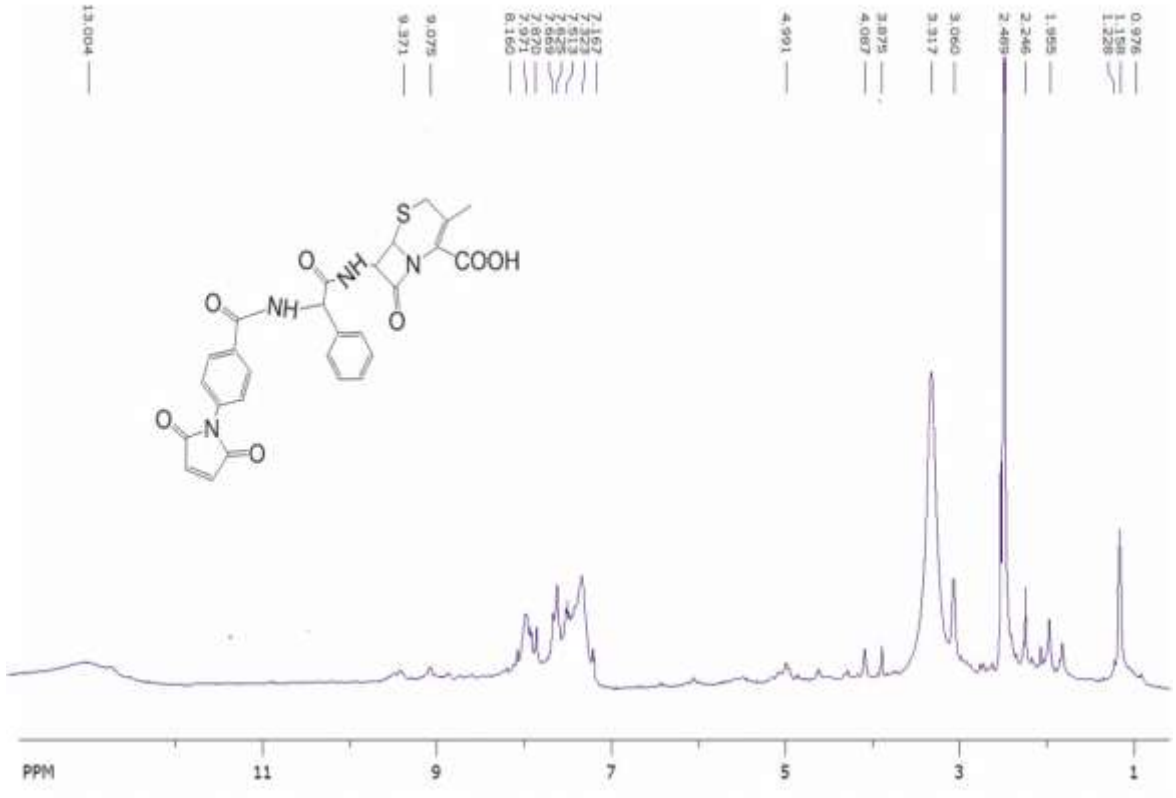

Figure 3.14: ^{1}H-NMR spectrum of compound [M_5]

Synthesis of Compound [M_6]: [M_6] was synthesized by reaction of 3-maleimide benzoyl Chloride [A3] with stirring to solution of ciprofloxacin in dimethyl sulfoxide and triethylamine (NEt_3) was added as catalyst at room temperature, and then heated for (2.5 h.) at 60 ˚C, the final precipitate was recrystallized with acetone with 80% Yield, color: brownish yellow, m.p. = 171-172°C, as shown in equation 3.4.

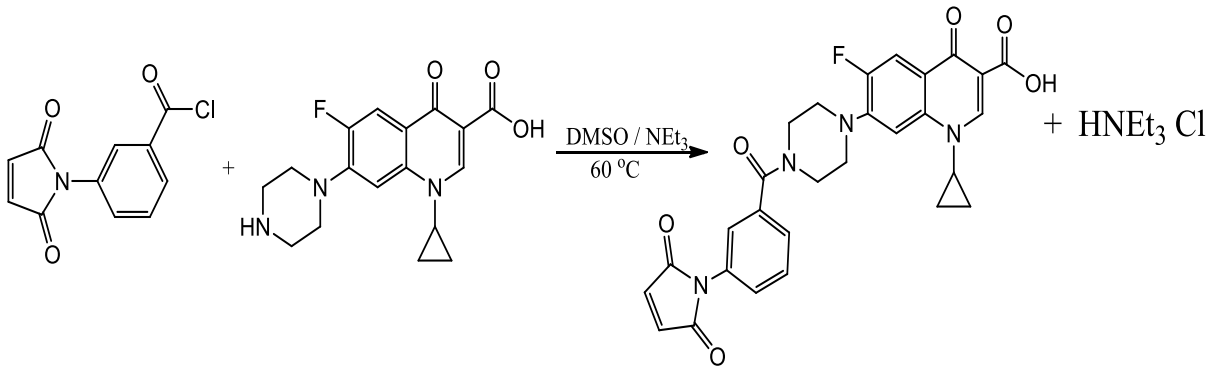

Equation 3-4: Synthesis of compound [M_6]

Characterization of Compound [M_6]: FT-IR (cm^{-1}) spectrum (Figure 3.15) of compound [M_6] show broad band at 3379 belong to hydroxyl group of

carboxylic acid of Ciprofloxacin drug, and (=C-H) of maleimide and aromatic system appeared at 3081 and 3016. Besides this, the spectrum shows the stretching of methylene groups and aliphatic (C-H) at 2970 and 2847, whereas the maleimide carbonyl appeared at 1710, carboxylic acid carbonyl at 1679, and conjugated ketone of quinolinone at 1625 [(112)].

Other bands were appeared at 1550-1452 (C=C, aromatic), 1337 (C-N) and 1260 (C-F).

^{1}HNMR (500 MHz, DMSO-d_6, δ ppm) Figure 3.16: shows appearances the signals of cyclopropyl protons at 1.228 (d, 4H, 2-CH_2-, cyclopropyl ring), 3.046 ppm (m, 1H, cyclopropyl ring), and the signals of piprazine ring at 3.365 and 3.715 ppm. The signals of maleimide (CH=CH), protons appeared at 7.182, 7.448 (s, 1H, Ar-H, quinolinone), 7.990 (s, 1H, Ar-H, quinolinone), 7.544 and 7.629 (d, 2H, benzene), 7.833 and 7.894 (d, 1H, benzene), 8.235 (s, 1H, benzene), 8.628 (s, 1H, vinylic proton) and broad signals at 12.488 attributed to carboxylic acid hydroxyl.

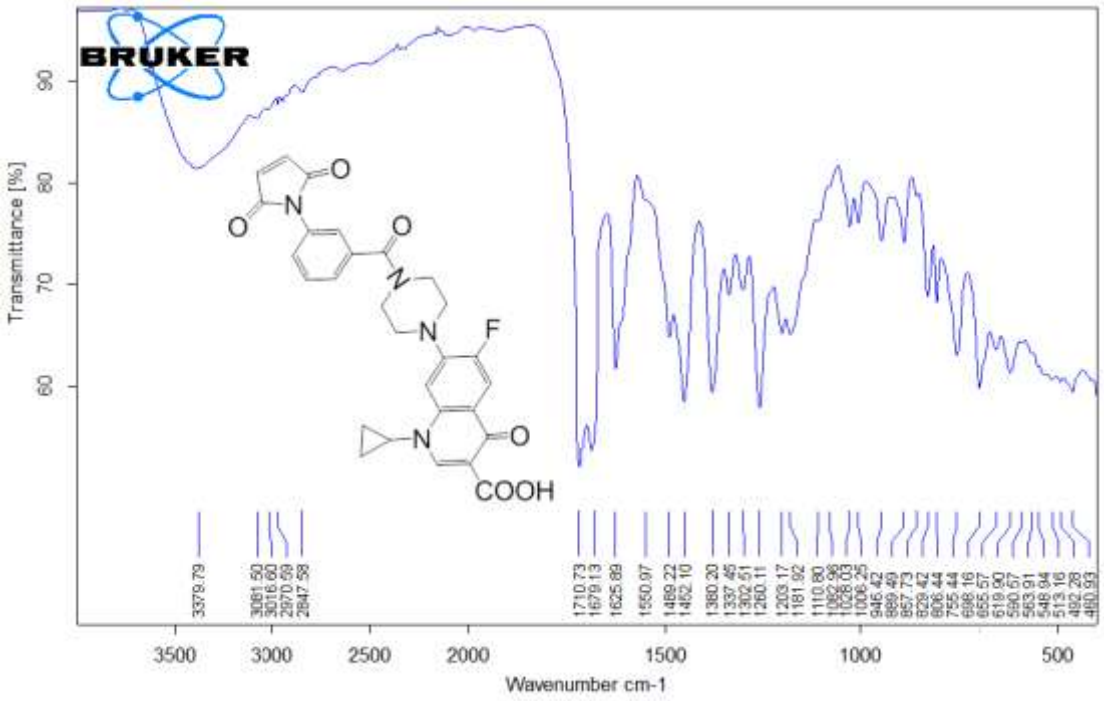

Figure 3.15: FT-IR spectrum of compound [M_6]

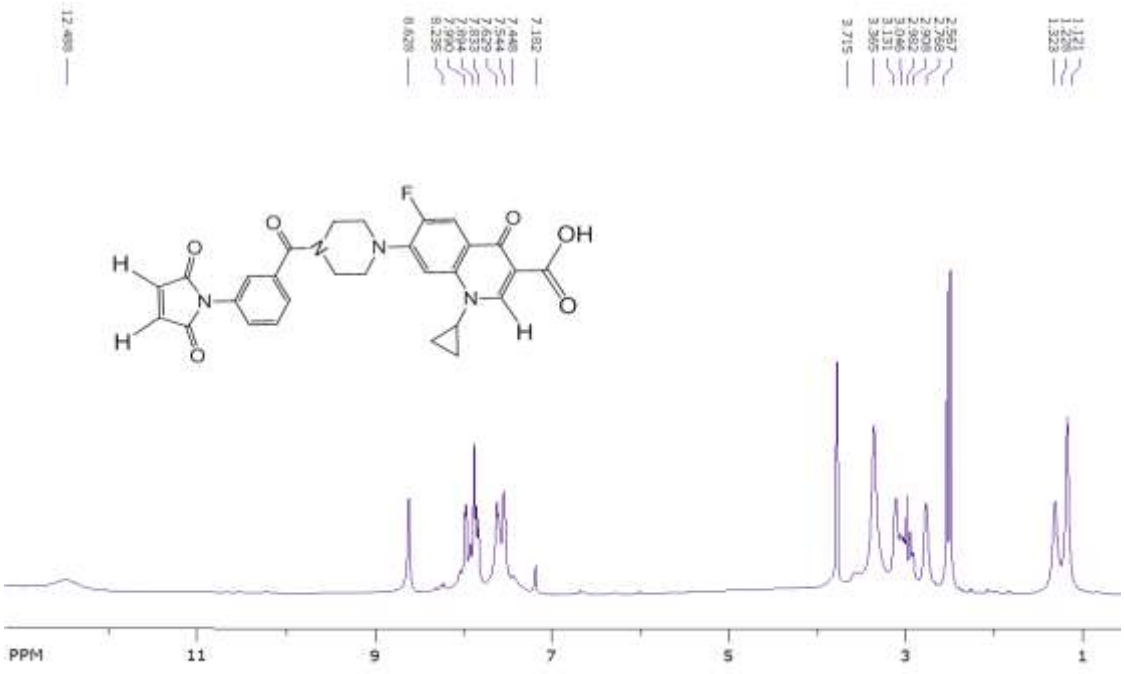

Figure 3.16: ^{1}H-NMR spectrum of compound [M_6]

Synthesis of Compound [M_7]: Compound [M_7] was obtained by amidazation of 3-maleimide benzoyl Chloride [A_3] with stirring to solution of Paracetamol, in ethyl acetate and triethylamine (NEt_3) was added dropwise as catalyst at room temperature, and then heated for (2.5 h.) at 60 ˚C, the reddish brown precipitate was filtered, dried, recrystallized from acetone: ethyl acetate (1:1) with 111-113 °C, 80%Yield, as shown in equation 3.6.

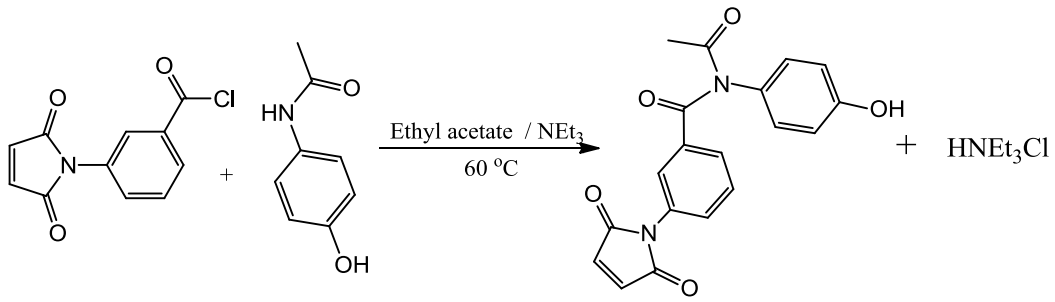

Equation 3-5: Synthesis of compound [M_7]

Characterization of compound [M_7]: The FTIR spectrum (cm^{-1}) of [M_7] as shown in Figure 3.17: Specific phenolic stretching vibration as broad band centered 3292 cm^{-1} and another band at 1711 cm^{-1} can be attributed to C=O Stretching vibration of the maleimide groups.

The bands at 2925 cm^{-1} and 2977 cm^{-1} are assigned to aliphatic C-H stretching vibration of methyl groups. The aromatic C-H stretching vibration is assigned to a band around 3080 cm^{-1}. The bands at 1666 and 1646 cm^{-1} belong to the C=O groups stretching of amide and 1588-1452 cm^{-1} are assigned to an aromatic ring. The absorption around 1376 and 1185 cm^{-1} may be traced to the bending vibrations of (C-N) and (C-O), respectively.

^{1}HNMR (500 MHz, DMSO, δ ppm) spectrum (Figure 3.19) showed the following chemical shifts. Singlet signal at 3.027 ppm belong to methyl group and maleimide (2H) protons signal appeared at 7.200 ppm. The proton of phenol ring appeared as multiplet signals at the range of 7.339 -7.600 ppm, the meta-substituted benzene protons appeared at 7.672-8.127 while the phenolic hydroxyl proton appeared 10.683 ppm.

^{13}C NMR (125 MHz, δ, ppm) spectrum of compound [M_7], (Figure 3.20), showed the flowing signals. The alpha- carbon signal at 27.333 ppm, the two ortho- carbons of phenol ring at 110.402, aromatic carbons at the range of 121.146-135.837 ppm, the maleimide double bond carbon appeared at 143.036, the carbon attached to phenolic -OH appeared at 147.760 (1 C, Ar-C-OH), the N-acetyl carbonyl signal at 160.808 ppm, the signal at 164.979 ppm attributed to maleimide carbonyl, and the signal at 169.795 ppm assigned to the amide carbonyl carbon.

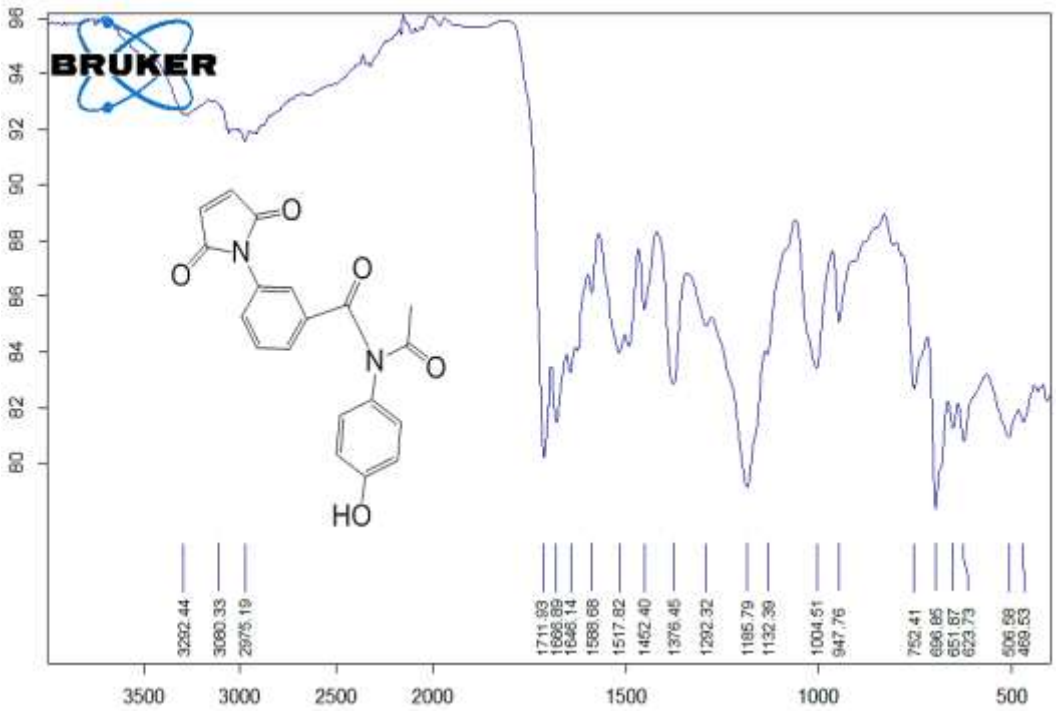

Figure 3.17: FT-IR spectrum of compound [M_7]

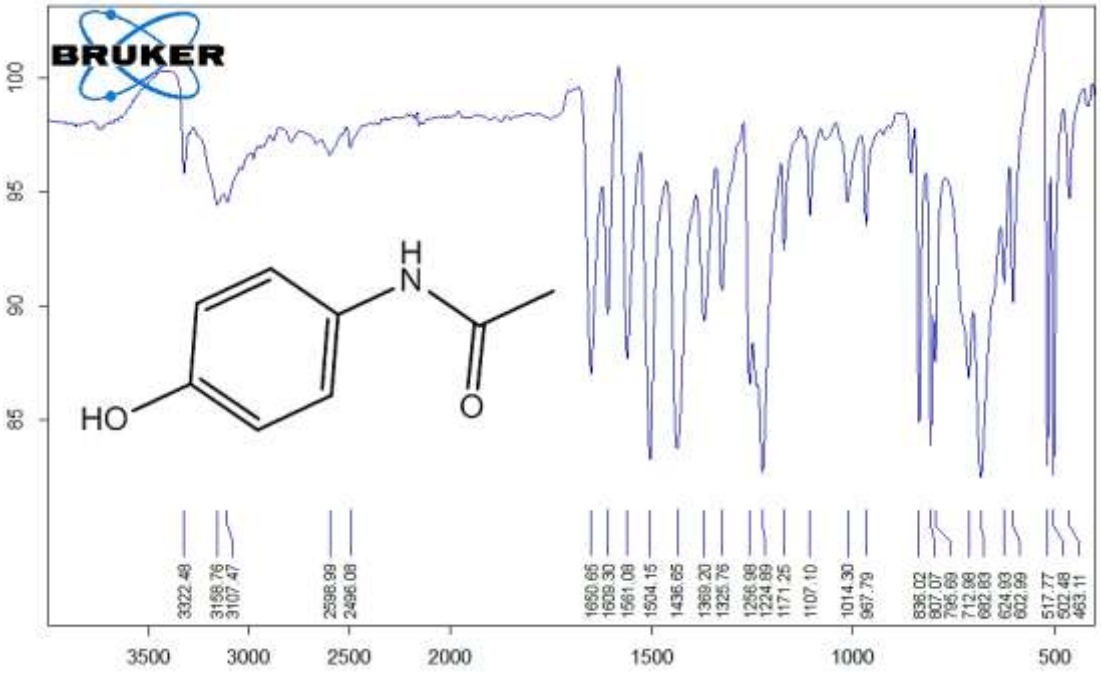

Figure 3.18: FT-IR spectrum of Paracetamol

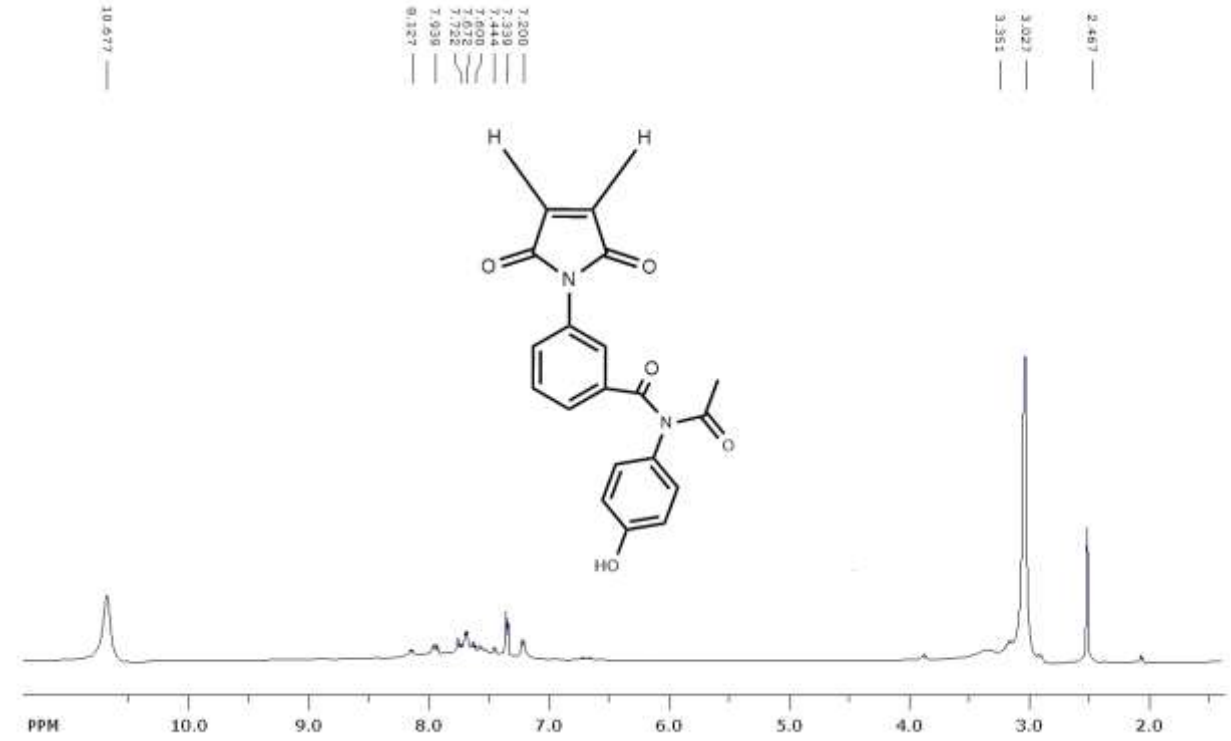

Figure 3.19: ^{1}H-NMR spectrum of compound [M_7]

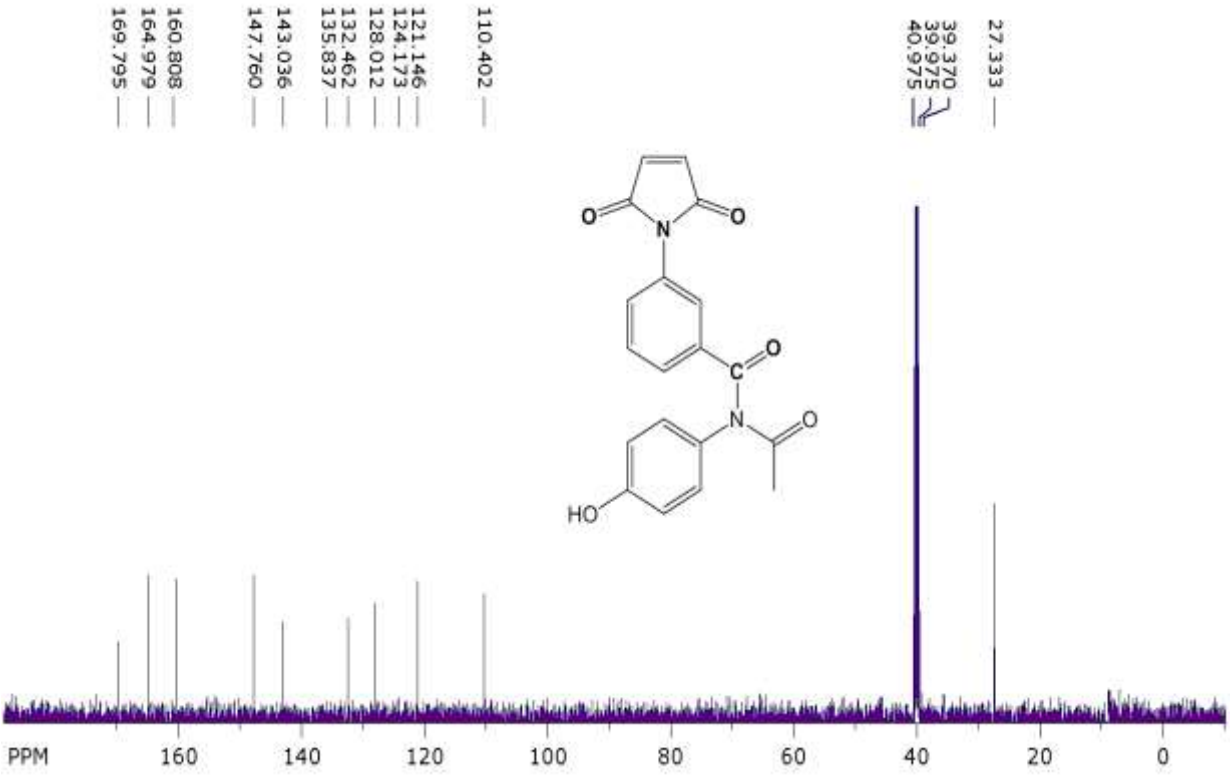

Figure 3.20: ^{13}C-NMR spectrum of compound [M_7]

Synthesis of Compound [M_8]: 3-Maleimide benzoyl Chloride [A_3] was mixed with silver-sulfadiazine drug, in DMSO and triethylamine (NEt_3) was added dropwise as catalyst at room temperature, and then heated for (2.5 h.) at 60 ˚C, the solution was poured crushed ice, left for (30min), was filtered of solution with and dried. The light brown precipitate was recrystallized from Ethanol: water (1:3) with (80%Yield, mp.152 -154 ˚C), as shown in equation 3.7.

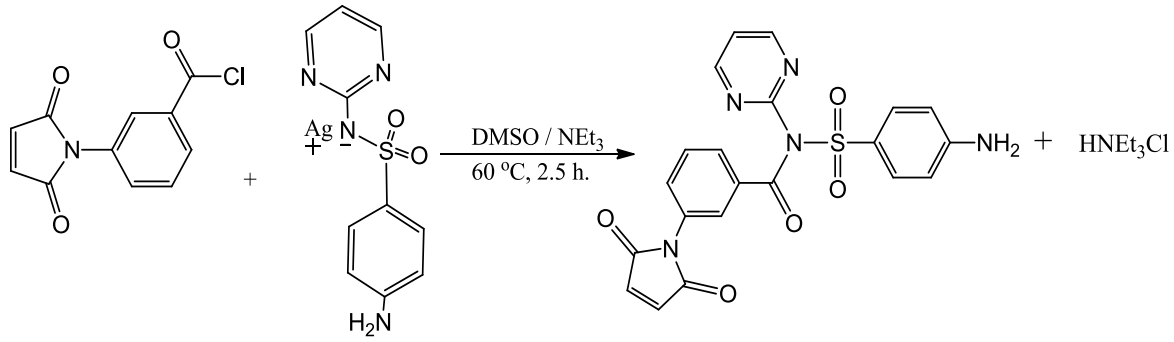

Equation 3-6: Synthesis of compound [M_8]

Characterization of Compound [M_8]: FT-IR spectrum (cm^{-1}) of [M_8] (Figure 3.21), shows the flowing bands. Primary aromatic amine was appeared at 3370 and 3231, aromatic and maleimide (=C-H) at 3084 and 3045, the carbonyl of maleimide stretching and carbonyl of amide centered at 1709 and 1625, respectively. The aromatic (C=C) occurred at the range of 1580-1438, the 1384 band may refer to the (C-N) stretching, while the two bands at 1317 and 1152 attributed to (S=O) stretching, and the band at 568 belong to (R-SO2-N) group. ^{1}HNMR (500 MHz, DMSO, δ ppm), of compound [M_8], (Figure 3.22) showed signals at different chemical shifts as follow. Aniline protons: the primary amino group appeared as somewhat broad singlet signal at 5.987 ppm, the duplet signal at 6.542 ppm belong to the two ortho aromatic protons and the other two aromatic protons appeared as duplet at 7.600 and 7.676 ppm.

Pyrimidine protons: singlet signal at 6.985 ppm belong to forth proton corresponding to the substituted group while the emine like proton (N=C-H) of the pyrimidine ring appeared as triplet signal at 8.462 ppm. The signals of

benzene ring were 7.194, 7.280, 7.493, and 7.994 ppm. The peak at 6.718 ppm belongs to maleimide protons.

^{13}C NMR (125 MHz, δ, ppm) of compound [M_8] (Figure 3.24) showed different chemical shifts for different carbons as follow. The two *o*-position carbons of aniline and C_4 of Pyrimidine appeared at 110.338 and 112.231 ppm, respectively while the other aromatic carbons appeared in the range of 120.178 -142.865 (10 C, Ar-C carbons), the maleimide double bond carbons resonance occur at 143.542 ppm.

The two emine and the site of substitution carbons of pyrimidine ring appeared at 149.980 and 161.010 ppm, whereas signals at 163.575 and 168.177 ppm traced to the maleimide and amide carbonyl carbons.

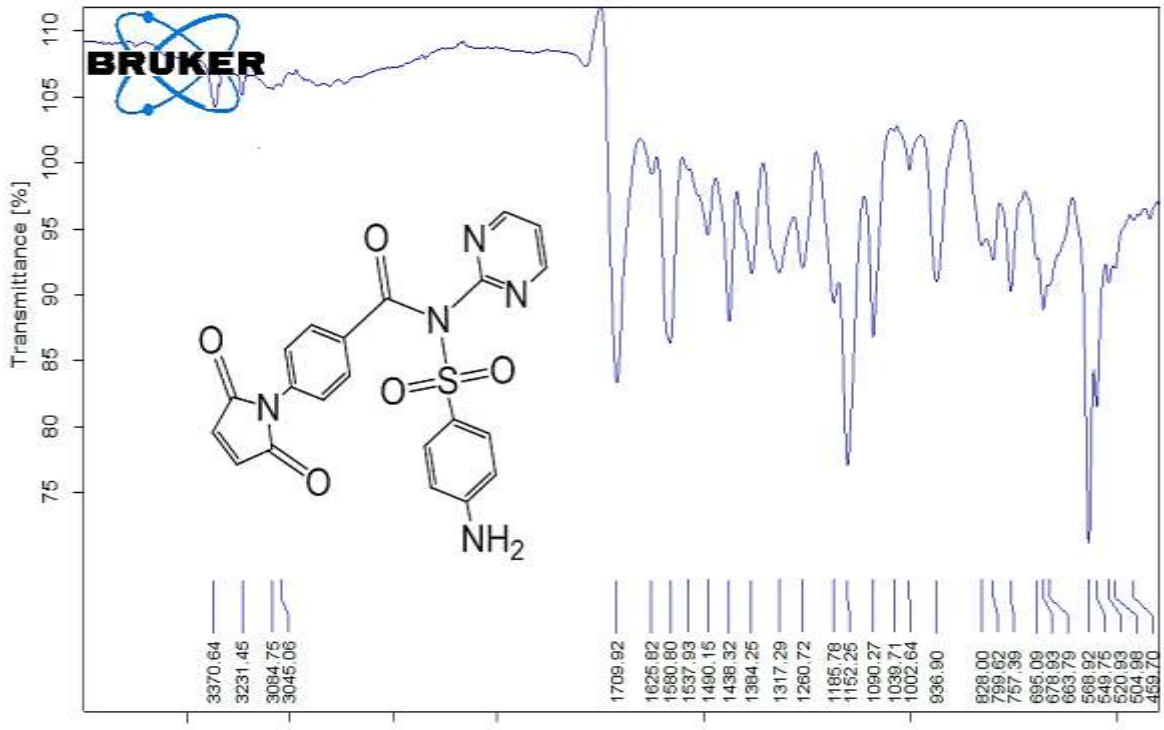

Figure 3.21: FT-IR spectrum of compound [M_8]

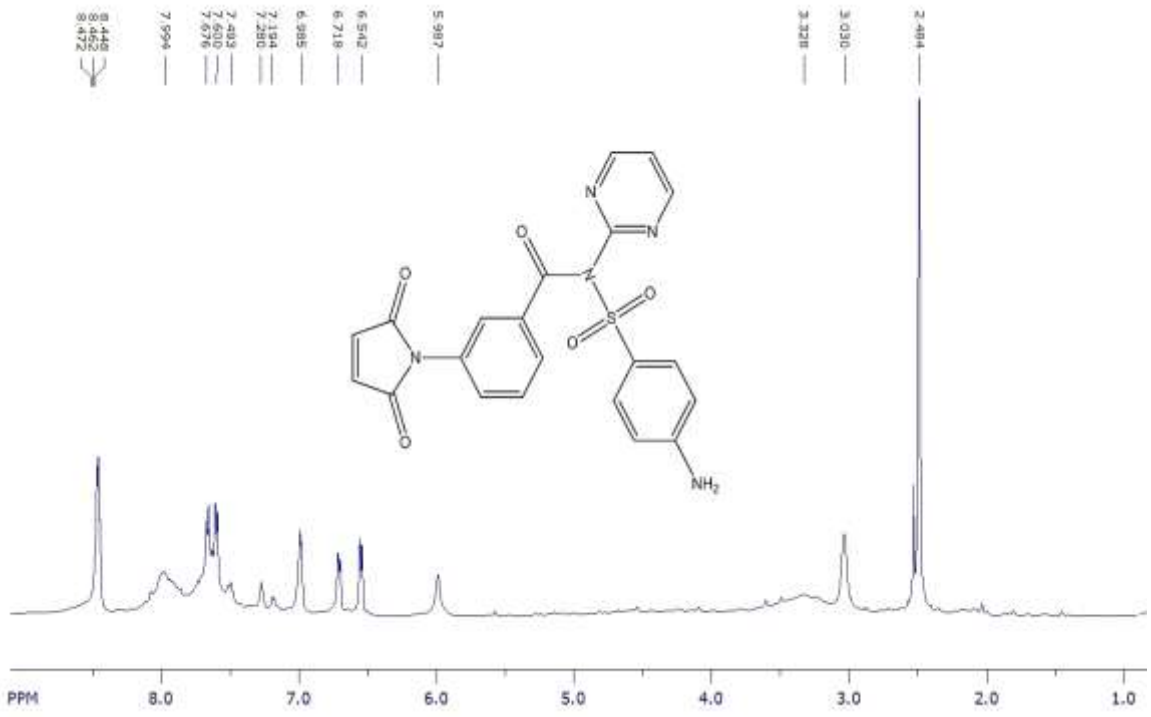

Figure 3.22: ^{1}H-NMR spectrum of compound [M8]

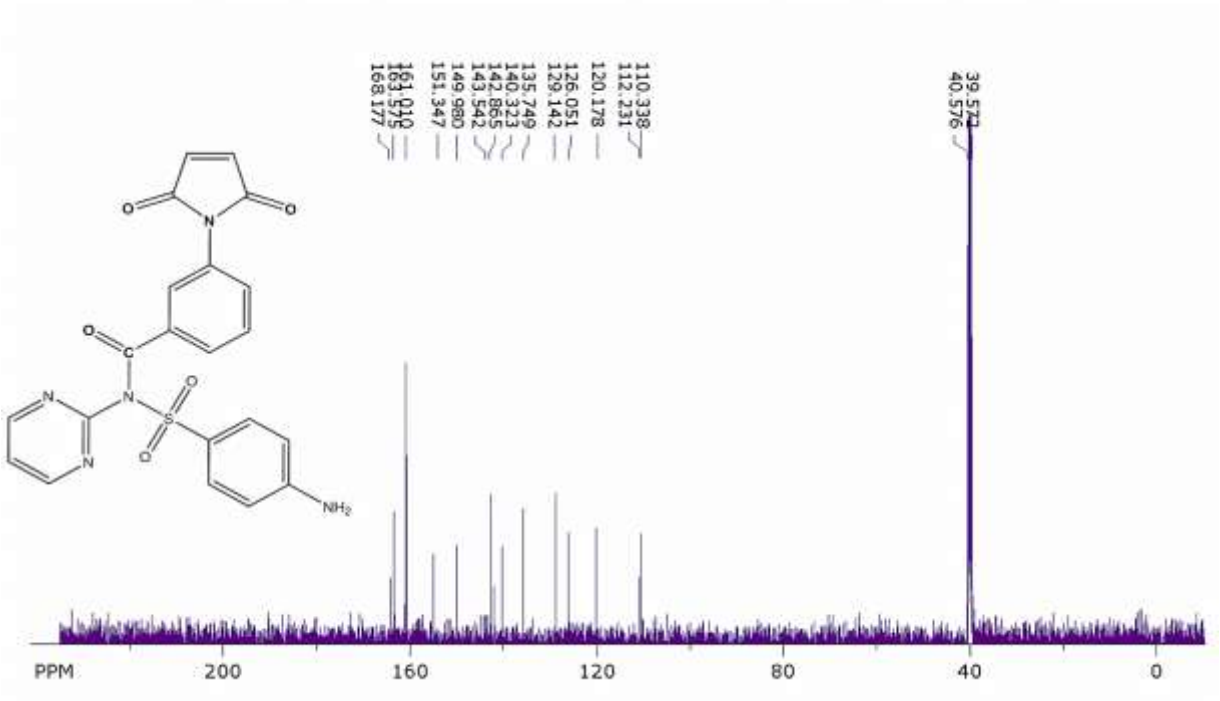

Figure 3.23: ^{13}C-NMR spectrum of compound [M_8]

Synthesis of Compound [M_9]: Synthesis of Compound [M_9]: 3-Maleimide benzoyl Chloride [A_3] was mixed with of Isoniazid drug, in DMSO and triethylamine (NEt_3) was added dropwise as catalyst at room temperature, and then heated for (1 h.) at 60 ˚C, the solution was poured crushed ice, left for

(30min), was filtered of solution and dried. The red precipitate was recrystallized from Ethanol: water (1:3) with (85%Yield, mp.179-181 ˚C), as shown in equation 3.8.

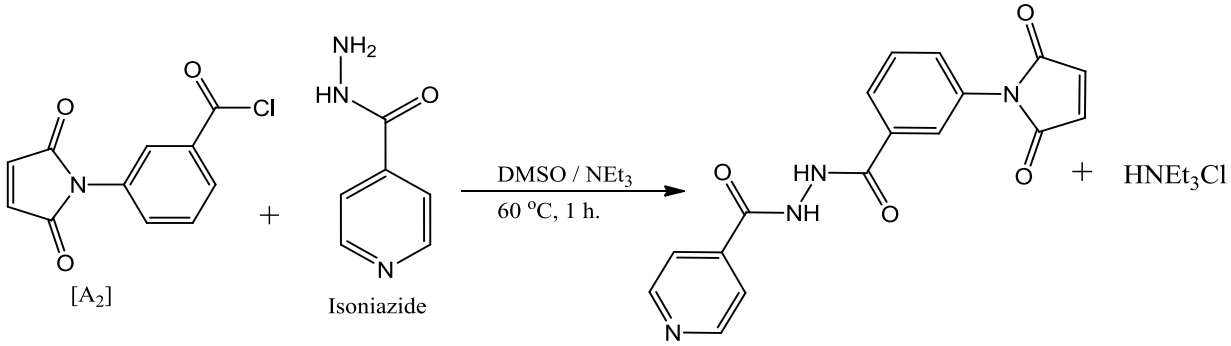

Equation 3-7: Synthesis of compound [M_9]

Characterization of Compound [M_9]: The key characteristic peaks of the FTIR (cm^{-1}) spectrum (Figure 3.24) of the [M_9] monomer are as follows.

No Absorption band for primary amino group of hydrazide (CO-NH-NH_2), and the amide (N-H) groups are observed at 3268 and 3211 cm^{-1}, the aromatic and maleimide (=C-H) appeared at 3055, 3034 cm^{-1} the carbonyl groups of maleimide and amide observed at 1699 and 1655 (C=O, amide) respectively, and the other bands are at 1539-1483 cm^{-1} (C=C, aromatic), and 1398 cm^{-1} (C-N).

In addition to IR, ^{1}H NMR analysis of the [M_9] compound (Figure 3.25) also indicated the proposed chemical structure (Equation 3-7). The appearance of singlet signal at about 6.815 ppm attributed to the maleimide protons and the aromatic protons papered at the range of 7.459-8.744 (m, 8H, Ar-H), and the signal at 10.514 ppm belong to the amide protons.

^{13}C NMR spectrum depicted in (Figure 3.26) shows different signals for different carbons as follow: The signals of aromatic carbons appeared at the range 122.996-140.100 ppm and the maleimide double bond carbons resonate at 143.311 ppm.

The signal at about 153.745 ppm belongs to the maleimide carbonyl carbon atoms while the two signals at 167.147 and 167.401 ppm belong to the two carbons of amide groups.

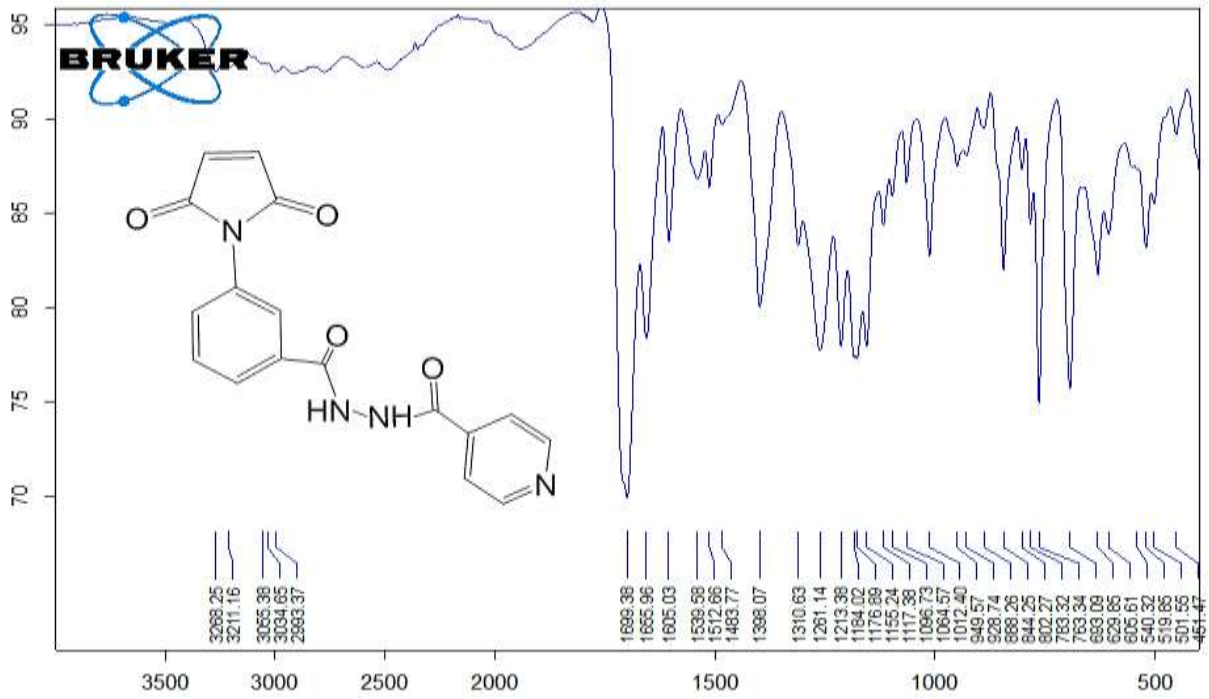

Figure 3.24: FT-IR spectrum of compound [M_9]

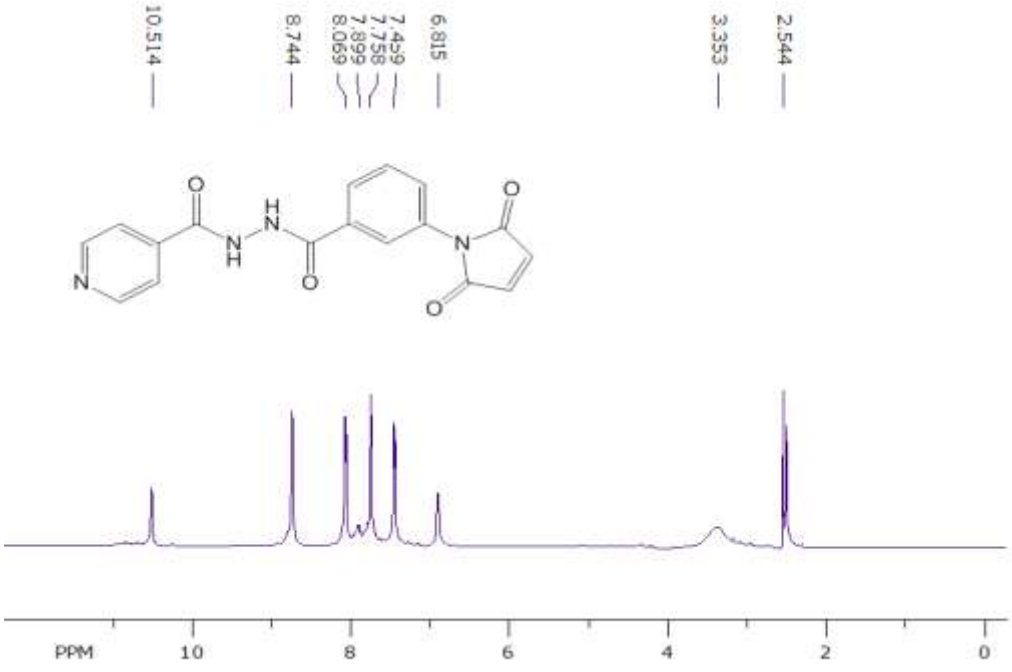

Figure 3.25: ^{1}H-NMR spectrum of compound [M_9]

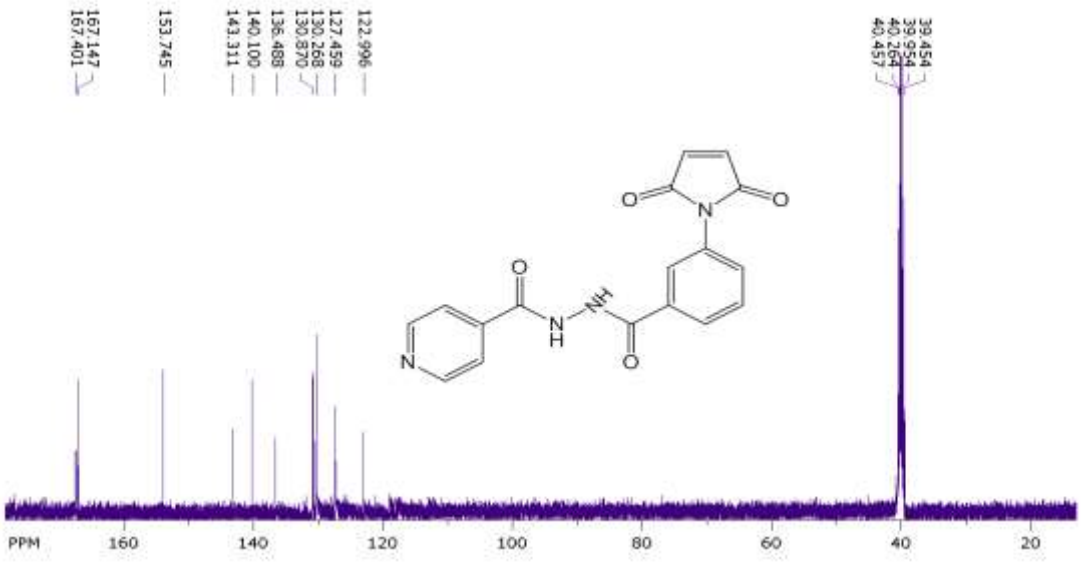

Figure 3.26: ^{13}C-NMR spectrum of compound [M_9]

Synthesis of Compound [M_{10}]: 3-mMaleimide benzoyl Chloride [A_3] was mixed with Carbamazepine drug, in DMSO and 1 triethylamine (NEt_3) was added dropwise as catalyst at room temperature, and then heated for (2.5 h.) at 60 ˚C. The reaction mixture was then cooled down and transferred into the frozen distilled water, left for (30min) until pink precipitate has formed, was filtered of solution and dried. The precipitate was recrystallized from ethyl acetate with (70 %Yield, mp. 109-110 ˚C), as shown in equation 3.8.

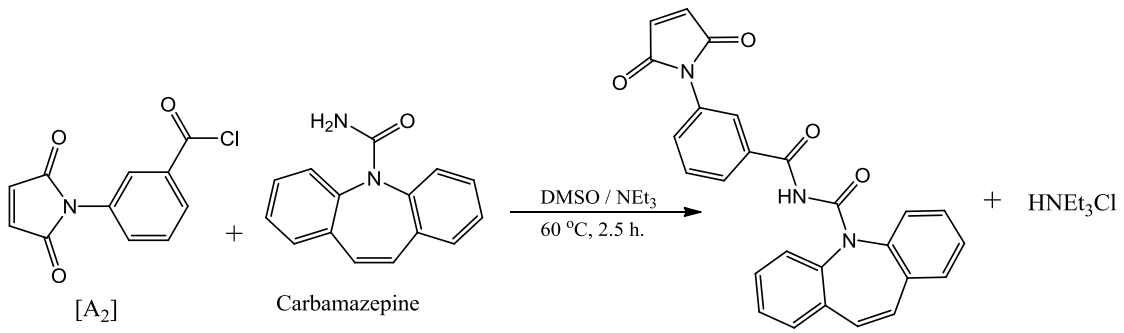

Equation 3-8: Synthesis of compound [M_{10}]

Characterization of Compound [M_{10}]: Figure 3.27 shows infrared spectrum of [M_{10}]. The absorption peaks at 1709 and 1683 cm^{-1} indicate the stretching vibrations of carbonyl groups (C=O) of imide ring and stretching vibration of amide, respectively. Furthermore, the absorption peak at 3150-3022 cm^{-1} indicates stretching vibration of C–H bonding of olefinic groups and aromatic rings and 1593-1460 cm^{-1} assigned to (C=C, aromatic), 1384 (C-N)

stretching. Also, a single peak at 3429 cm^{-1} is observed, which is assigned to the stretching vibration of N-H bond of the acyclic imide. This proves the successful of imidization reaction at the amino group of carbamazepine drug by acyl of maleimide benzoyl chloride (Equation 3-8).

Figure 3.28 shows ^{1}H-NMR spectrum of [M_{10}]. It can be seen that the peak are observed at the chemical shift s of 6.724 and 6.982 ppm belong to the two (-HC=CH-) groups of the maleimide and the seven membered ring. The aromatic protons appeared at the range of 7.161-8.143 ppm and the acyclic imide proton appeared at 10.250 ppm.

The ^{13}CNMR spectrum of compound [M_{10}] (Figure 3.29) shows the following chemical shifts. The aromatic proton showing a range of chemical shifts at about 122.442-135.284 ppm. Furthermore, the peaks with the chemical shift of 141.103 and 143.184 ppm belong to the two (-HC=CH-) groups of the maleimide and the seven membered ring, respectively. The absorption peak at 156.755 ppm assigned to two carbonyl carbons of maleimide ring, while the two peaks at 168.984 and 168.984 ppm belong to the two carbonyl carbons of acyclic imide groups. This confirms the formation of maleimide-drug monomer [M_{10}], as the reaction shown in Equation 3-8.

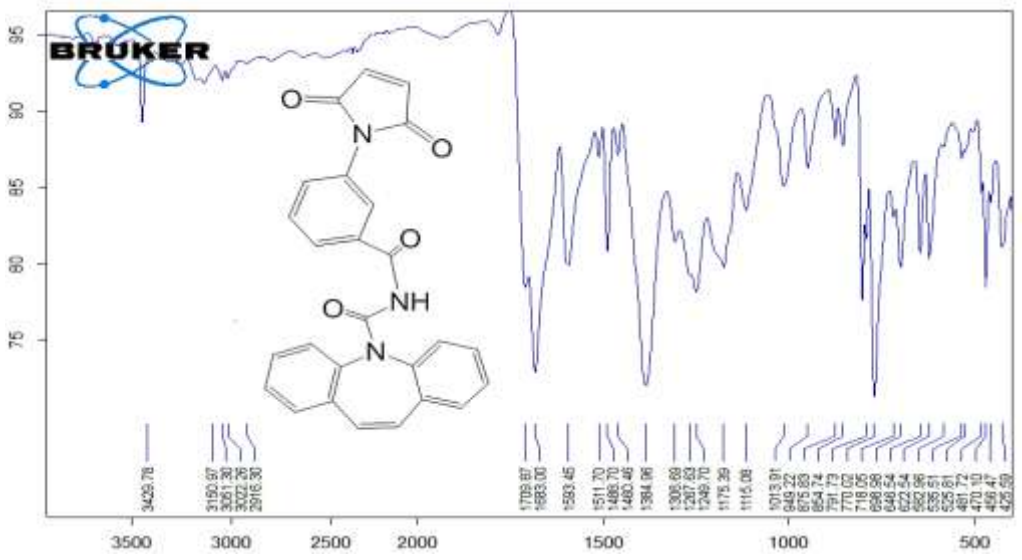

Figure 3.27: FT-IR spectrum of compound [M_{10}]

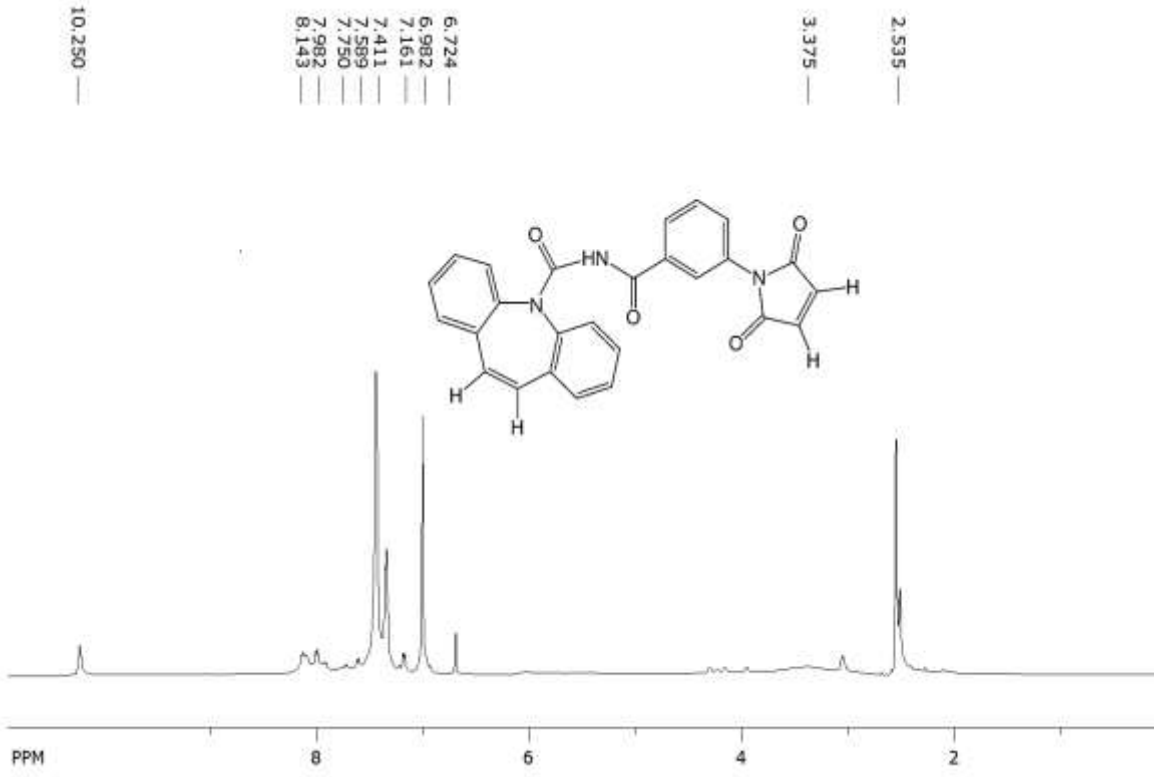

Figure 3.28: ^{1}H-NMR spectrum of compound [M_{10}]

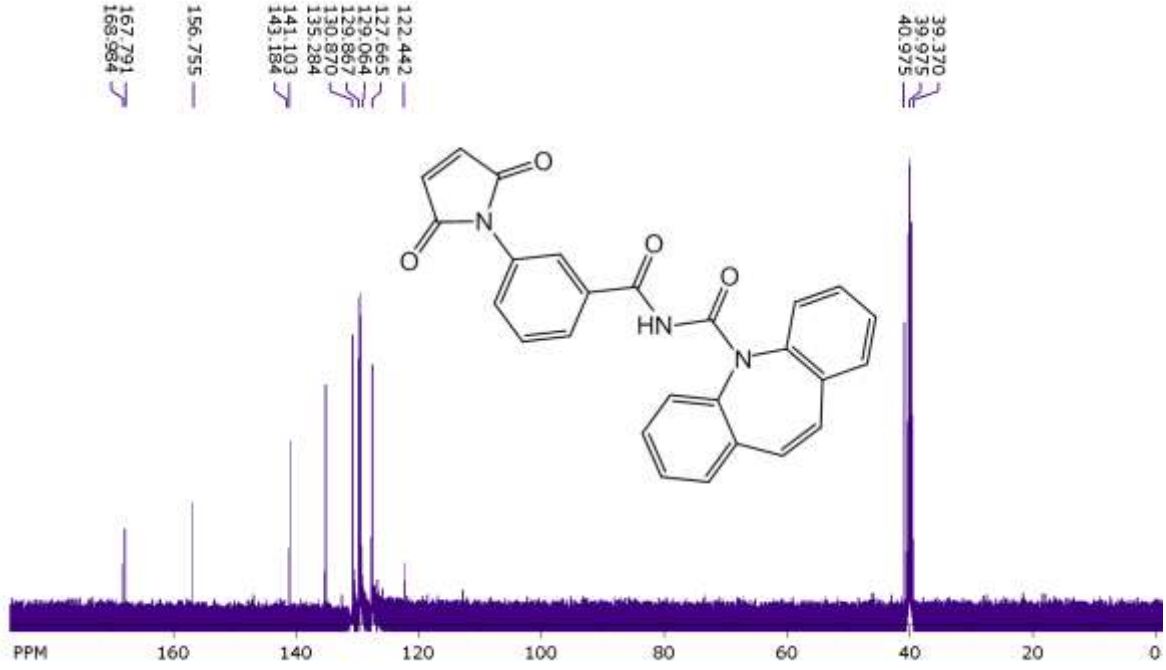

Figure 3.29: ^{13}C-NMR spectrum of compound [M_{10}]

Synthesis of Compound [M_{11}]: 3-Maleimide benzoyl Chloride [A_3] was mixed with Metoclopramide drug, in Benzene and triethylamine (NEt_3) was added dropwise, and then heated for (2 h.) at 60 ˚C with stirring at room temperature until the fuggy smoke has ceased. The formed pale red precipitate

was filtered of solution and dried, recrystallized from acetone: ethyl acetate (1:1) with (75 %Yield, mp. 122-124 ˚C), as shown in equation 3.9.

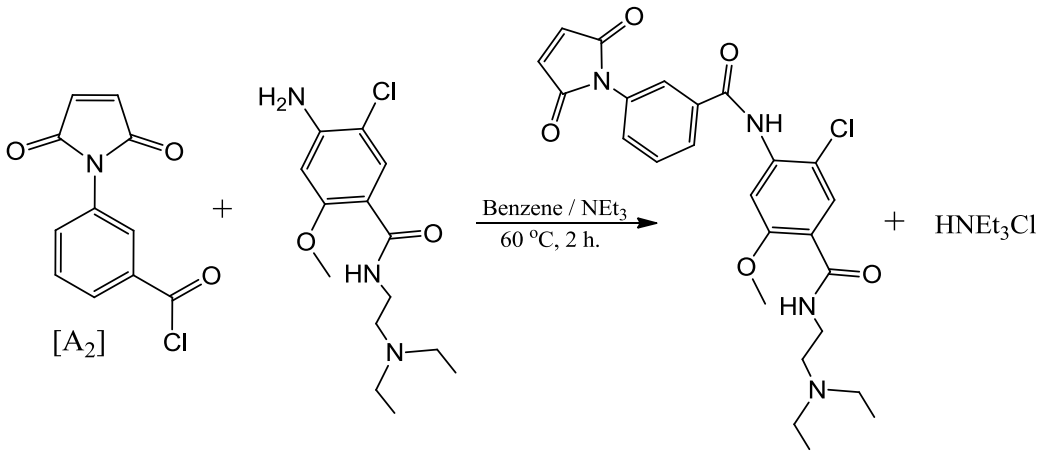

Equation 3-9: Synthesis of compound [M_{11}]

Characterization of Compound [M_{11}]: The FT-IR spectrum (Figure 3.30) of compound [M_{11}] shows different absorption bands as follow. The stretching vibration of (-NH, amide) groups appeared at 3361 and 3272 cm^{-1}, the maleimide and aromatic (=C-H) appeared at 3129 and 3064 cm^{-1}. The stretching vibrations at about 2979-2874 cm^{-1} belong to methyl and methylene groups of the drug, while the carbonyl groups of maleimide and those of the drug appeared at 1714, 1628, and 1590 cm^{-1} respectively. The spectrum also shows another absorption band such as 1508-1443 cm-1 for aromatic ring, 1396 and 1383 cm^{-1} for (C-N) stretching, 1035 cm^{-1} for (C-O) of methoxy group, and 622 cm^{-1} for (C-Cl).

^{1}HNMR spectrum (Figure 3.31) of compound [M_{11}] shows a signal at 1.170 and 2.567 ppm for two terminal N-ethyl groups while the middle ethylene group appeared at 3.592 and 3.817 ppm and singlet signal at 3.918 ppm traced to the methoxy group (s, 3H, -OCH_3).

Maleimide protons appeared at 7.196 (s, 2H, CH=CH), beside to the four aromatic protons of benzene ring at about 7.451-7.969 ppm, while the two protons of aromatic ring of the drug appear at 8.247 and 8.549 ppm and the aryl amide protons (Ar-CO-NH-, amide) occurred at 10.111 and 10.343 ppm. The ^{13}C NMR spectrum of compound [M_{11}] is given in Figure 3.32

shows the following chemical shifts. The two signals at about 17.085 and 34.385 ppm attributed to the two terminal ethyl groups (4 carbons) and the two signals at 53.637 and 56.986 ppm belong to ethylene group (2 carbons).

The signal at 58.196 ppm belongs to carbon of methoxy group and the range of chemical shifts at about 110.010-138.278 ppm belongs to the aromatic carbons and the maleimide double bond carbons appeared at 143.601. The aromatic carbon attached to the methoxy group appeared at 146.485 ppm, while the carbonyl carbons of maleimide ring and two amide carbonyl carbons appeared at 150.255, 162.233 and 168.887 ppm respectively. This confirms the formation of maleimide-drug monomer [M_{11}], as the reaction shown in Equation 3-9.

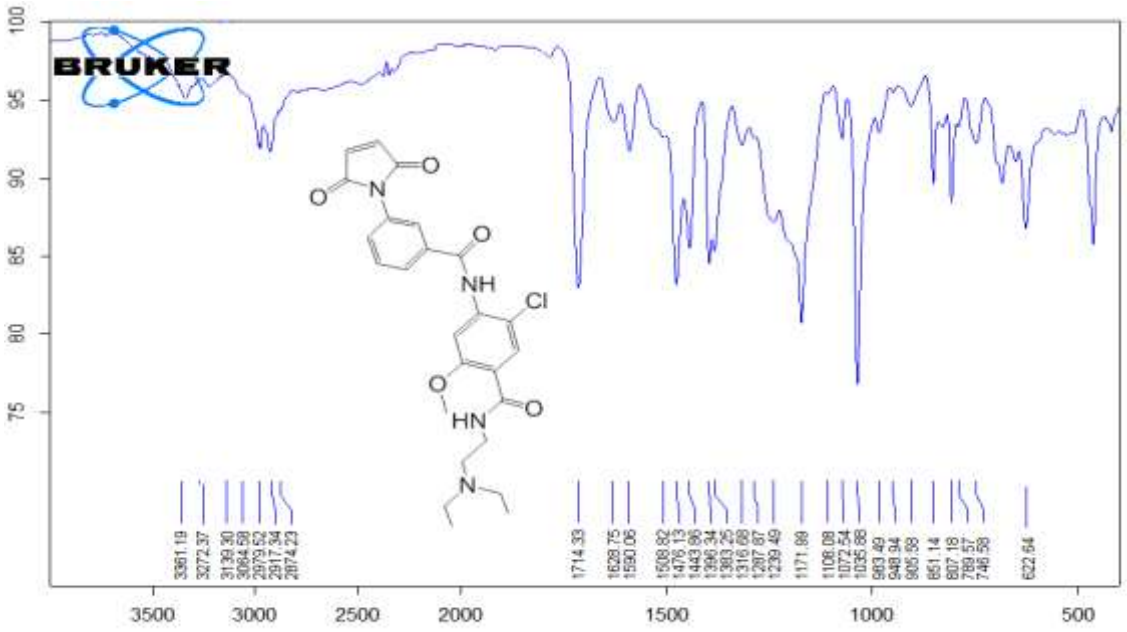

Figure 3.30: FT-IR spectrum of compound [M_{11}]

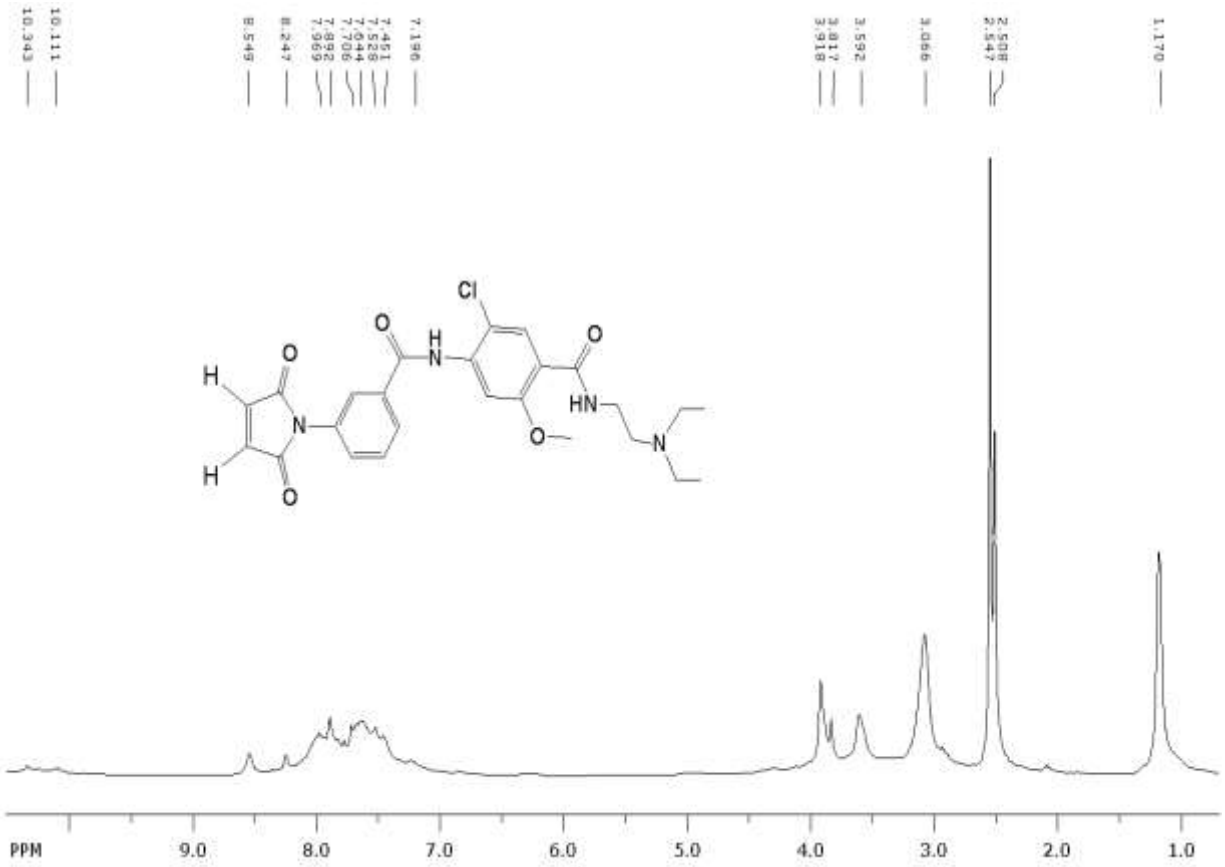

Figure 3.31: ^{1}H-NMR spectrum of compound [M_{11}]

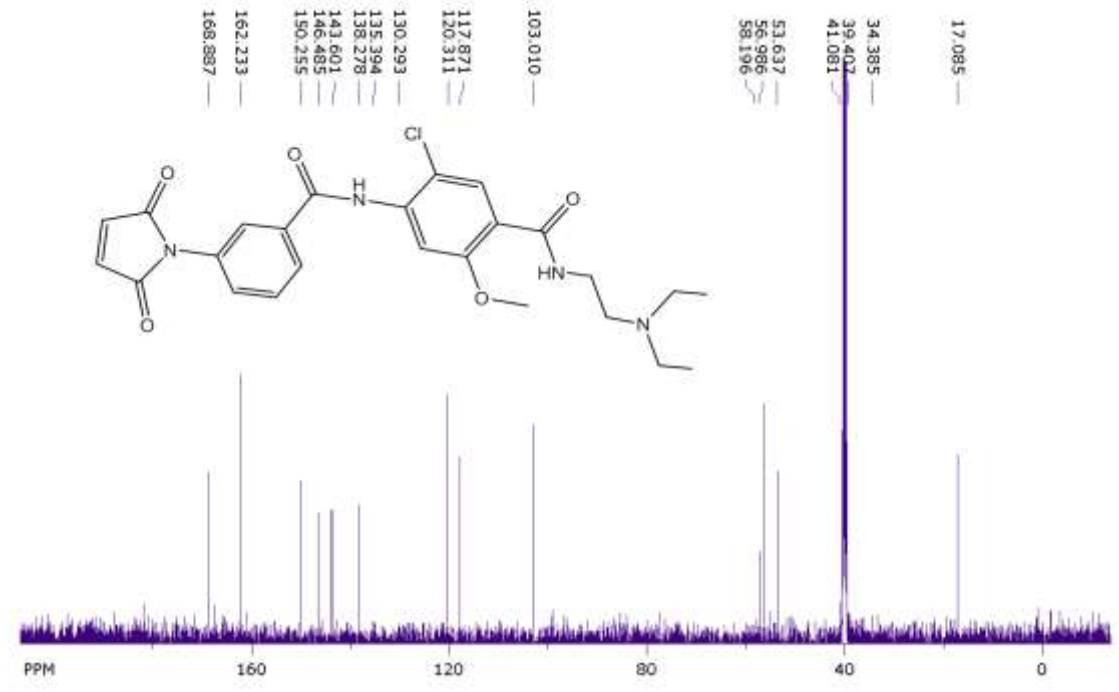

Figure 3.32: ^{13}C-NMR spectrum of compound [M_{11}]

3.4. The physical properties of monomers:

Some physical properties for the monomers such as color, percentage yield, melting point, retention factor, and solubility listed in tables 3.2 and 3.3. In general, all of prepared monomers have very low solubility in water and acidic media but having a good solubility in basic aqueous solution (pH=7.5-8), organic alcohols, acetone, DMF and DMSO, and low solubility in THF, Toluene and Benzene.

Table 3.2: Some of physical properties of prepared monomers

Comp.	Color	Yield (%)	m.p. °C	R_f
A_1	Greenish Yellow	90%	223-224 °C	0.4 1hexane : 3ethylacetate
A_2	Yellow	70%	238-240 °C	0.58 1hexane:3ethylacetate
A_3	Light Yellow	90%	125-127 °C	0.75 1hexane:3ethylacetate
M_1	light Brown	70 %	210- 212°C	0.35 1hexane : 3acetone
M_2	Yellow	80 %	171-172°C	0.44 1hexane : 3acetone
M_3	Brown	75%	142-145°C	0.62 1hexane : 3acetone
M_4	yellow	85%	181- 183°C	0.48 1hexane : 3acetone
M5	Red	75%	177 – 180 °C	0.6 1hexane : 3acetone
M_6	Brownish yellow	80%	171-172°C	0.58 1hexane : 3acetone
M_7	Reddish Brown	80%	111-113 °C	0.46 1hexane : 2 ethylether
M_8	Pink	90%	152 - 154 °C	0.60 1hexane : 3acetone
M_9	Red	85%	189 -191 °C	0.44 1hexane : 3acetone
M_{10}	Pink	70%	109 -110 °C	0.55 1hexane : 3ethylacetat
M_{11}	Red	75%	122- 124 °C	0.42 1hexane : 3ethylacetat

Table 3.3: The solubility of prepared monomers in some solvents

Co.	H_2O	EtOH	$CHCl_3$	Ether	Toluene	DMSO	Hexane	Benzene	Acetone
M1	partial	+	-	-	partial	+	-	partial	+
M2	partial	+	-	-	partial	+	-	partial	**partial**
M3	partial	+	-	-	partial	+	-	partial	+
M4	partial	+	-	-	partial	+	-	-	+
M5	partial	+	-	-	partial	+	-	partial	+
M6	partial	+	-	-	partial	+	-	partial	+
M7	partial	+	partial	-	partial	+	-	+	+
M8	partial	+	Partial	-	partial	+	-	-	+
M9	partial	+	partial	-	partial	+	-	-	+
M10	-	+	+	-	+	+	-	+	**partial**
M11	partial	+	-	-	partial	+	-	partial	+

3.5. The Antibacterial Activity of Maleimide–drug Monomers [M_1-M_{11}]

Maleimides and their related compounds have interesting properties, especially when they can be used as selective inhibitors for monoglyceridelipase [124], and several enzymes containing reactive cysteinyl residues. Furthermore they widely applied for various biological applications like antimicrobial [125], antiprotozoal [126], anti-inflammatory agents [127,128], analgesics [129,130], anti-tumor [131], cytotoxic, DNA binding and apoptotic inducing activity [132]. Moreover, coupling of both maleimide derivatives and some realistic medicines may modify their biological property due to the synergistic effect. The anti-bacterial activity for the synthesized monomers and their loaded drugs were listed in table 3.3 :

Synergistic effects: An effect whereby two chemical substances together have more of an impact than anticipated.

Antagonist effect: is a phenomenon wherein two or more agents in combination have an overall **effect** that is less than their individual **effects**

Table 3. 4: Antibacterial activity of compounds (M_1-M_{11}) at 0.5 mg/mL concentration

Inhibition Zone for *Staph. Coccus* of Maleimide		Inhibition Zone for *Staph. Coccus* of Drug		Inhibition Zone for *E. Coli* of Maleimide	Inhibition Zone for *E. Coli* of Drug
M1	30	Clafuran	20	32	35
M2	30	Ceftriaxone	35	40	20
M3	9	Ampicillin	35	10	26
M4	22	Amoxicillin	35	22	35
M5	32	Cephalexin	30	30	15
M6	30	Ciprofloxacin	35	42	22
M7	20	Paracetamol	13	15	4
M8	25	Sulfadiazine	35	28	9
M9	18	Isoniazid	15	9	15
M10	14	Carbamazepine	0	15	4
M11	18	Metoclopramide	10	14	5
DMSO	0	DMSO	0	0	0

Antibacterial activity against pathogenic strains of *Escherichia coli* and *Staphylococcus aurous* using solution of 0.5 mg from each compound and each loaded drug for comparison in 1 mL of DMSO was carried out using disk-diffusion method [78]. Also, the activity of the DMSO was screened as a negative control which does not show any inhibition for bacterial growth.

The results of antibacterial activity against Gram-positive (*Staphylococcus aurous*) shows synergistic effect for (M_1, M_5, M_7, M_9, M_{10} and M_{11}) compounds were the anti-bacterial activity (inhibition zone) of these compounds are raised comparison to the corresponding loaded drugs. While, antagonist effect for (M_2, M_3, M_4, M_6, M_8) were inhibition zone for these compounds decreased in comparison to the corresponding loaded drugs.

On the other hand most of maleimide derivatives show higher activity against Gram-negative (*E. coli*) than the loaded drugs do, was ten compounds show

synergistic effect (M_2, M_5-M_8, M_{10} and M_{11}), while only four maleimide derivatives (M_1, M_3, M_4 and M_9) showed antagonist effect.

The lipophilic and neutral nature of the maleimide moiety allows it to seamlessly pass through biological membranes [(133)]. Gram negative bacteria's cell walls are made up of one or a few layers of peptidoglycan and a lipid-rich outer membrane [(134)], which explains why they have greater antibacterial activity against *E. coli*.

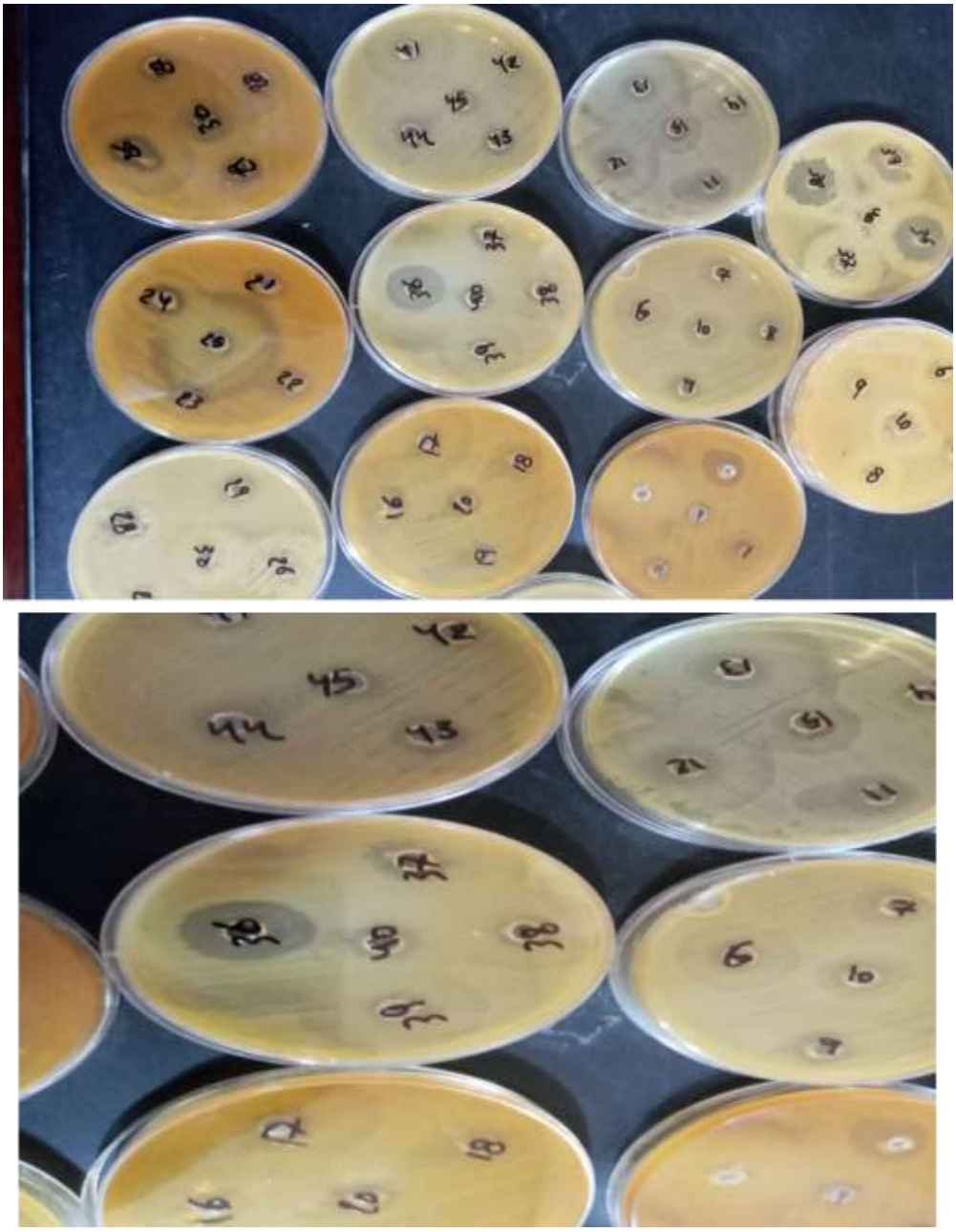

Figure 3. 33: Images of petri-dishes of antibacterial for synthesized monomers.

3.6. Synthesis and Characterization of Homopolymers [PM_1-PM_{11}]

Homopolymerization of maleimide-drug monomers were carried out in toluene solvent by using benzoylperoxid, as free radical initiator, at 90 ºC.

Monomer [$\mathbf{M_1}$-$\mathbf{M_{11}}$] (5.3 mmol) was suspended in 50 mL of toluene in a 100 mL two necks round bottom flask were heated in an oil bath at 90 ºC. To this solution (0.1 g) of benzoyl peroxide was added and the reaction mixture was heated on heating mental at 90 ºC for 10-12 hours under nitrogen flow. At the end of polymerization; the mixture was cooling in ice bath, precipitate was filtered, purified with suitable solvent. Finally dried in an oven at 50 ºC, as shown in equation 3.10.

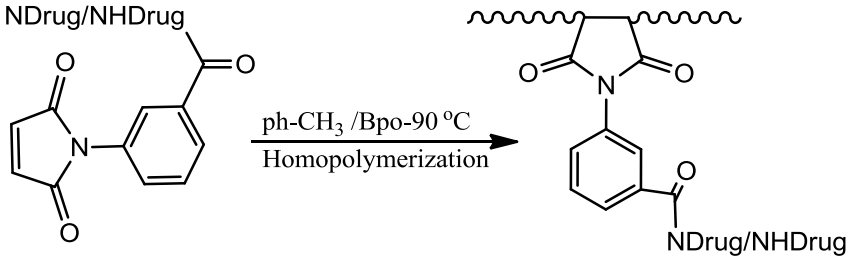

H_2N-Drug / HN-Drug = Clafuran, Ceftriaxone, Ampicillin, Amoxicillin, Cephalexin , Ciprofloxacin, Paracetemol, Silver-Sulfadiazine, Isoniazid, Carbamazepine and Metochlopramiide

Equation 3-10: Synthesis of Synthesis of homopolymers [PM_1-PM_{11}]

Table 3.5: The chemical structure, Color and purification solvents for Homopolymers [PM_1-PM_{11}]

Co.	Chemical Structure	Color	Purification solvents
PM1	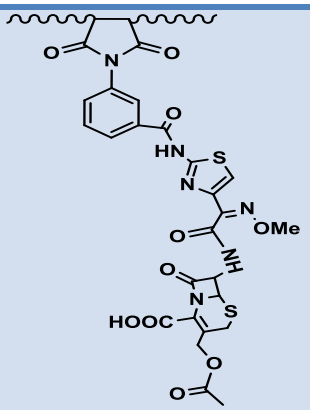	Orange	Washed several times with methanol to remove the un reacted monomer

PM2	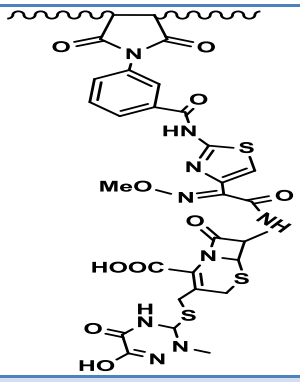	Light Brown	Dissolved in DMF and re-precipitate with water
PM3	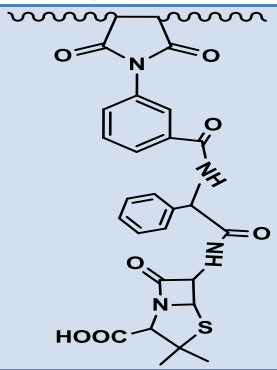	Red	Washed several times with Hot methanol to remove the un reacted monomer
PM4	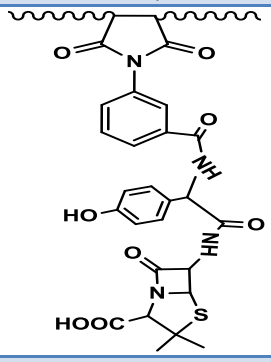	Yellow	Washed several times with methanol to remove the un reacted monomer
PM5	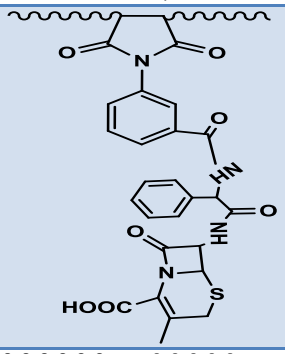	Brown	Dissolved in DMF and Re-precipitate with water
PM6	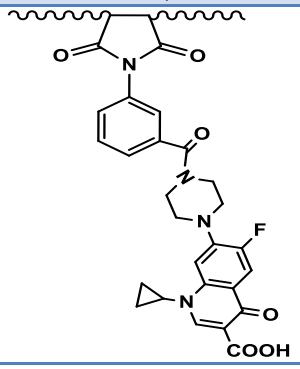	Red	Dissolved in DMF and Re-precipitate with water

PM7	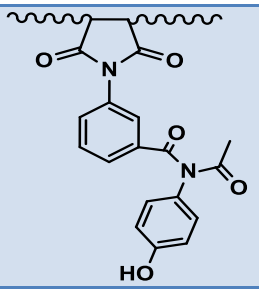	Brownish Red	Washed several times with methanol to remove the un reacted monomer
PM8	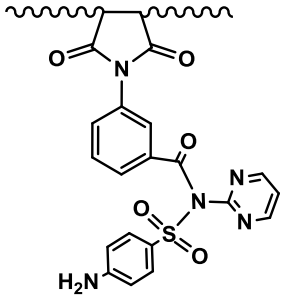	Brown	Washed several times with Acetone to remove the un reacted monomer
PM9	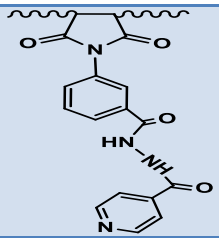	Red	Washed several times with Acetone to remove the un reacted monomer
PM10	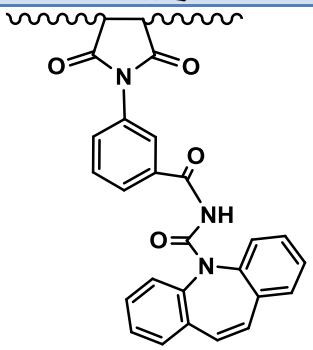	Red	Dioxane only dissolve the polymer
PM11	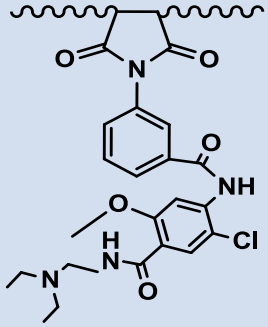	Brownish Red	Ethyl acetate only dissolve the Monomer

The synthesized homopolymers having a very low solubility in water and acidic media but having a good solubility in basic aqueous solution (pH=7.5-8). Solubility properties of prepared polymers in different solvents (H_2O, ethanol, $CHCl_3$, ether, toluene, DMSO, hexane, DMF and acetone) are listed in Table 3.6.

Table 3.6: The solubility of polymers [PM_1-PM_{11}] in different solvents

Polymers	H_2O	EtOH	$CHCl_3$	Toluene	DMSO	Hexane	Pet. ether	Acetone	DMF
PM1	partial	partial	partial	partial	+	-	-	Partial	+
PM2	partial	partial	-	-	+	-	-	Partial	+
PM3	partial	partial	-	partial	+	-	-	Partial	+
PM4	partial	partial	-	partial	+	-	-	Partial	+
PM5	partial	partial	-	partial	+	-	-	Partial	+
PM6	-	partial	-	partial	+	-	-	Partial	+
PM7	-	partial	-	-	+	-	-	Partial	+
PM8	-	partial	Partial	partial	+	-	-	Partial	+
PM9	Partial	Partial	-	-	+	-	-	Partial	+
PM10	-	Partial	-	-	+	-	-	Partial	+
PM11	-	Partial	-		+	-	-	Partial	+

3.6.1. Characterization of Homopolymer [PM1-PM5]:

FT-IR spectra (Figures: 3.34, 3.36, 3.38, 3.40, 3.42) of the Homopolymers [PM_1-PM_5] show strong stretching frequencies for the imide carbonyl groups at 1718-1699 cm^{-1}, and showing a characteristic stretching bands for compounds at 1791-1767 cm^{-1} due to beta lactam carbonyl groups[(132)], the characteristic band at 1751 cm^{-1} for stretching vibration of ester group of drug in [PM_1] Figure 3.42.

The 1H-NMR spectra (Figures: 3.42, 3.44, 3.46, 3.48, 3.50) of these polymers shows appearance of new signals at about (2-2.6) ppm belong to the polyimide (succinimide backbone), and disappearance of the maleimide (HC=CH) protons signals (6.691-7.167 ppm).The beta lactam protons appeared at about 4.053-5.029 ppm(115), the amide (ArCO-NH-) protons appeared at the range 9.363-10.456 ppm and carboxylic protons appeared as broad weak peaks around 12.921-13.010 ppm. This indicates the success of polymerization of these monomer beside that during the polymerization, imide and beta-lactam rings are remained intact.

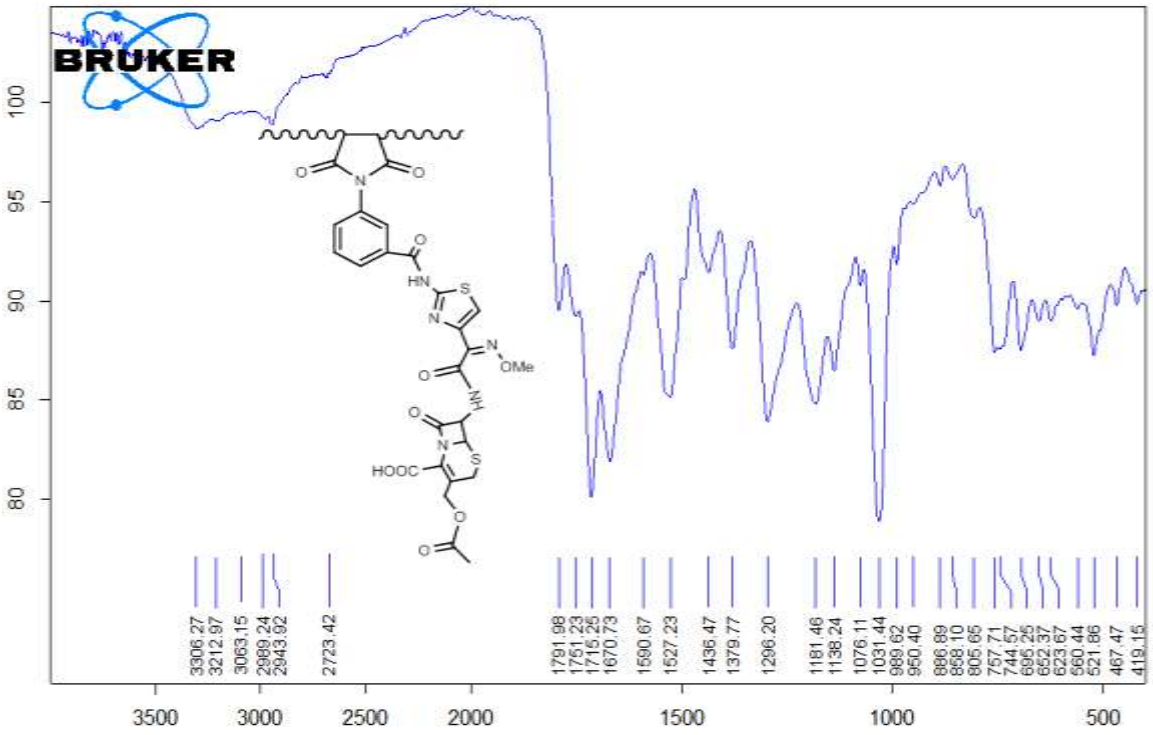

Figure 3.34: FT-IR spectrum of compound [PM_1]

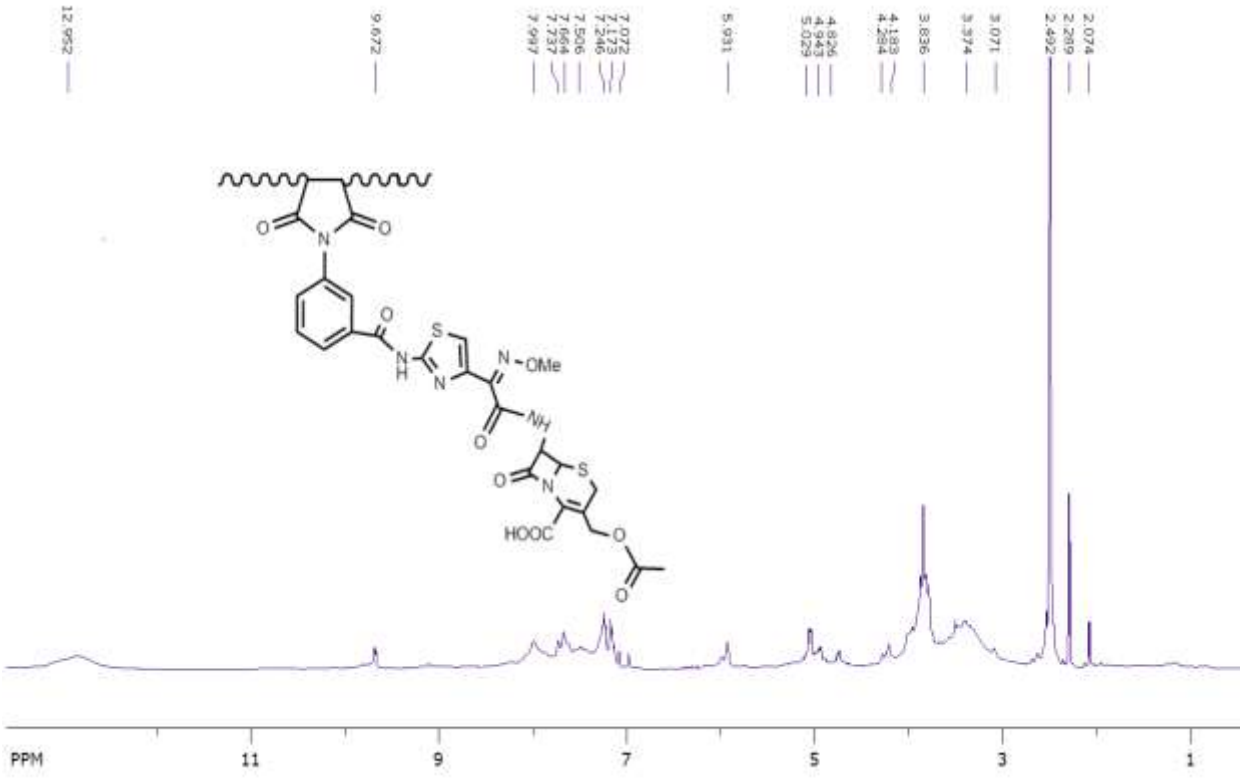

Figure 3.35: ^{1}H-NMR spectrum of compound [PM_1]

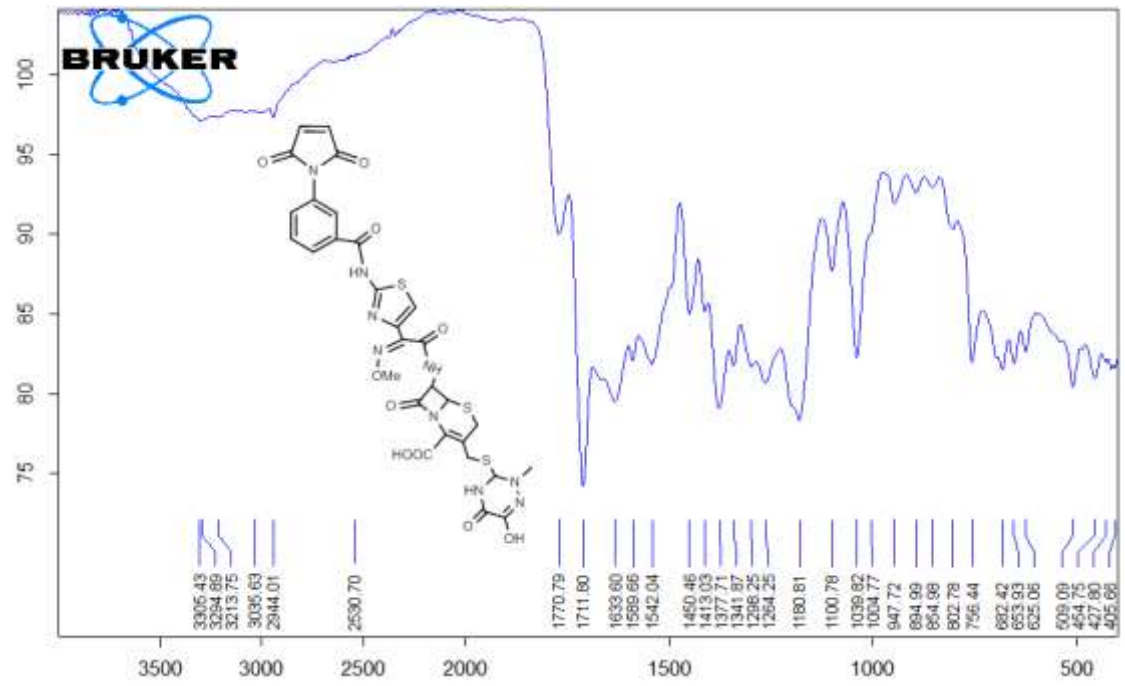

Figure 3.36: FT-IR spectrum of compound [PM_2]

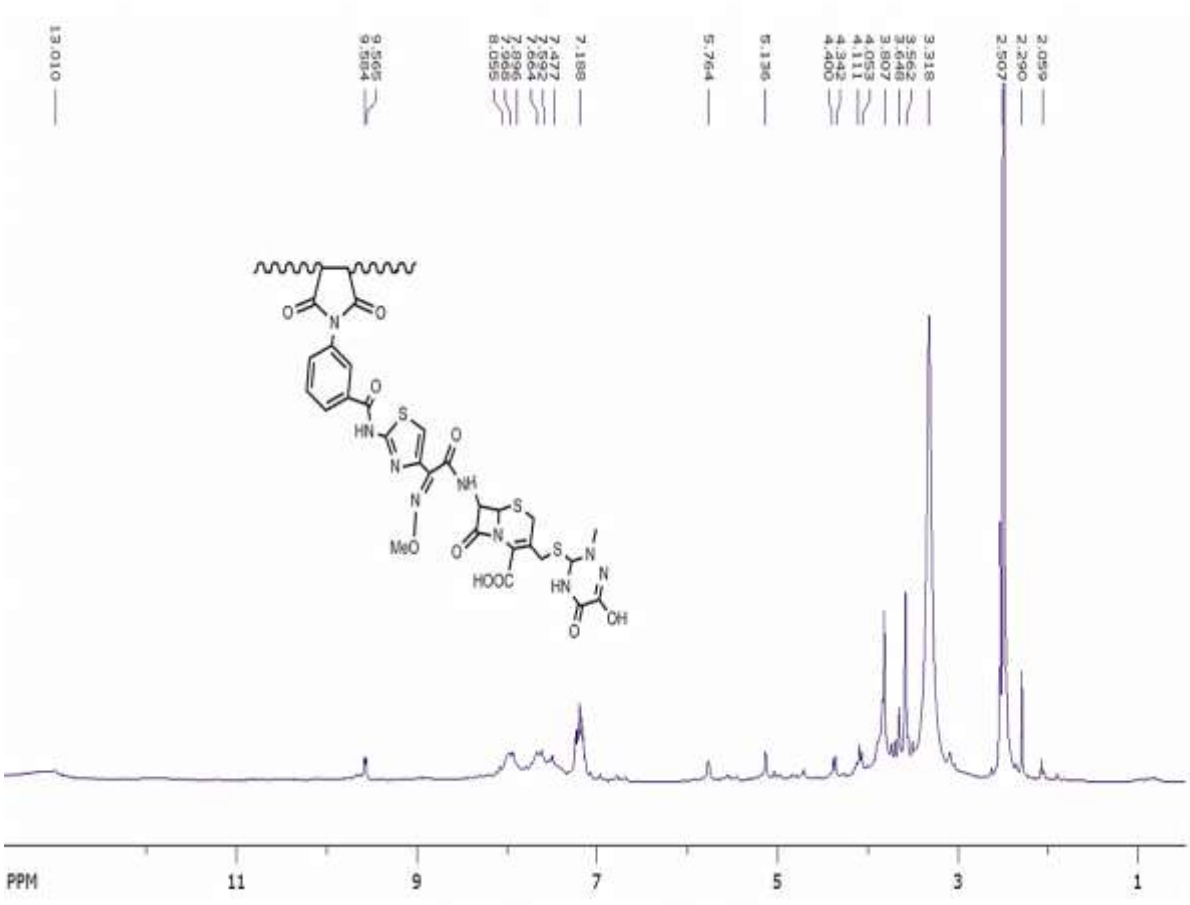

Figure 3.37: ^{1}H-NMR spectrum of compound [PM_2]

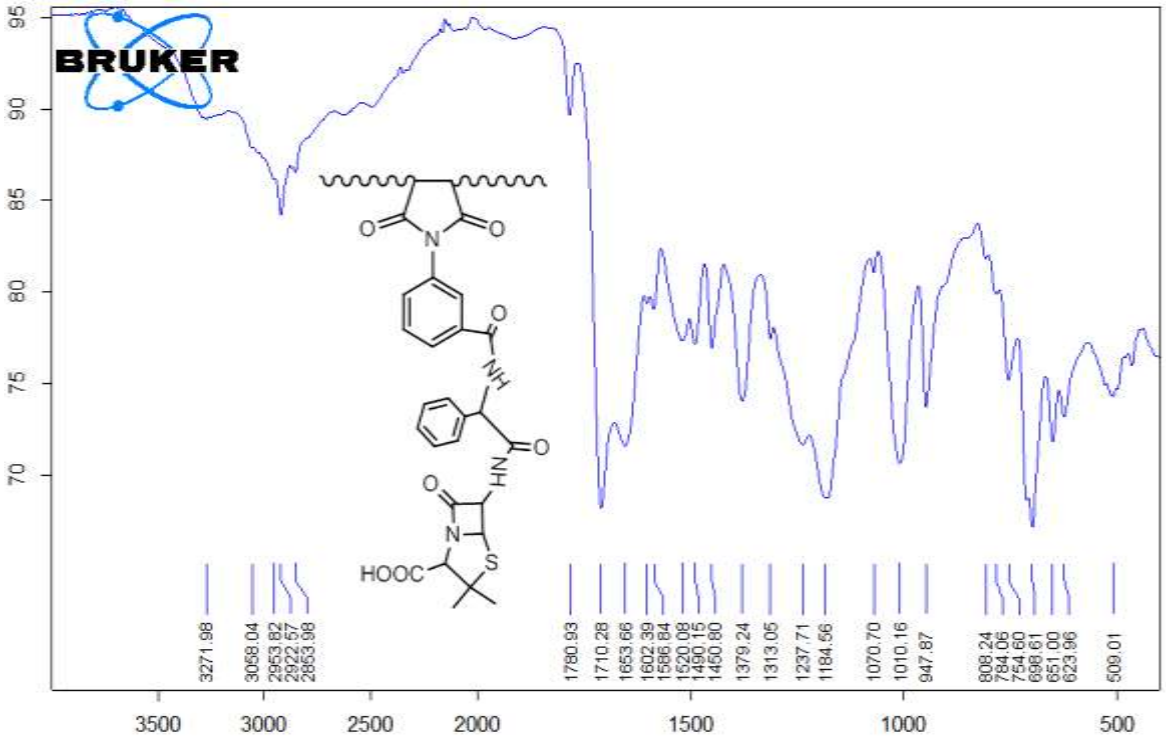

Figure 3.38: FT-IR spectrum of compound [PM_3]

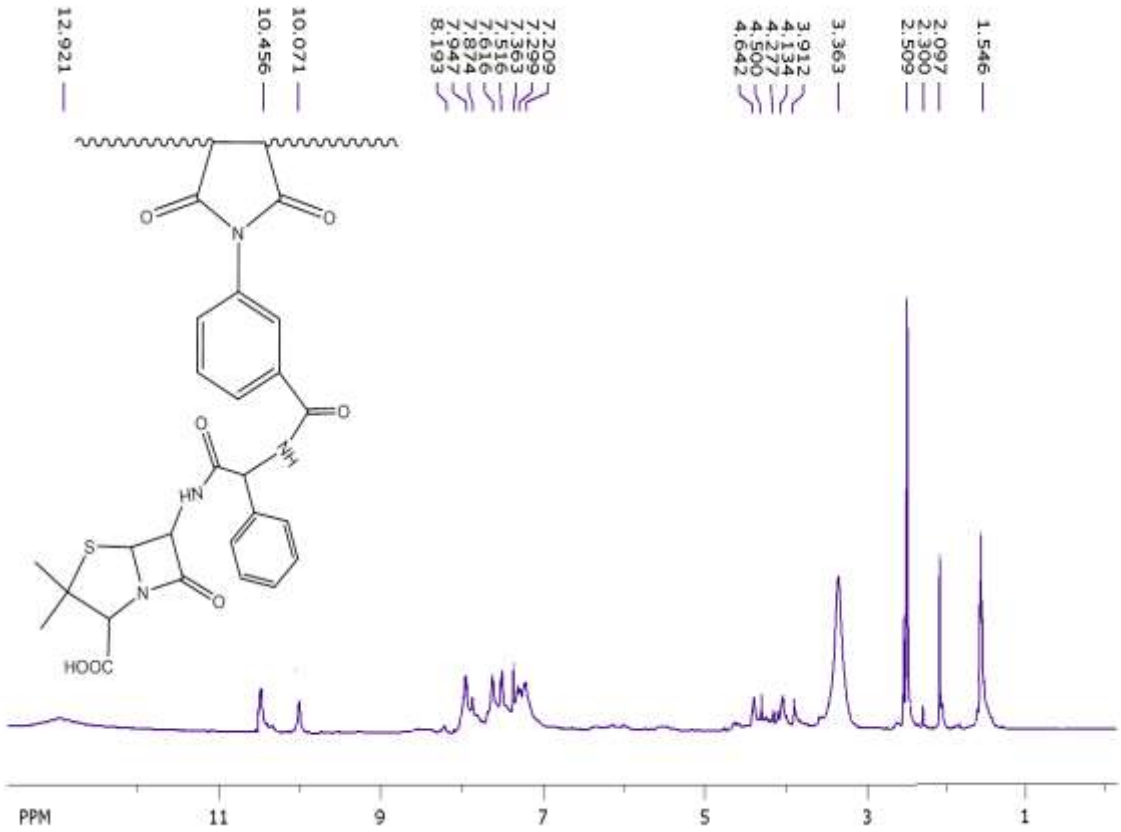

Figure 3. 39: ^{1}H-NMR spectrum of compound [PM_3]

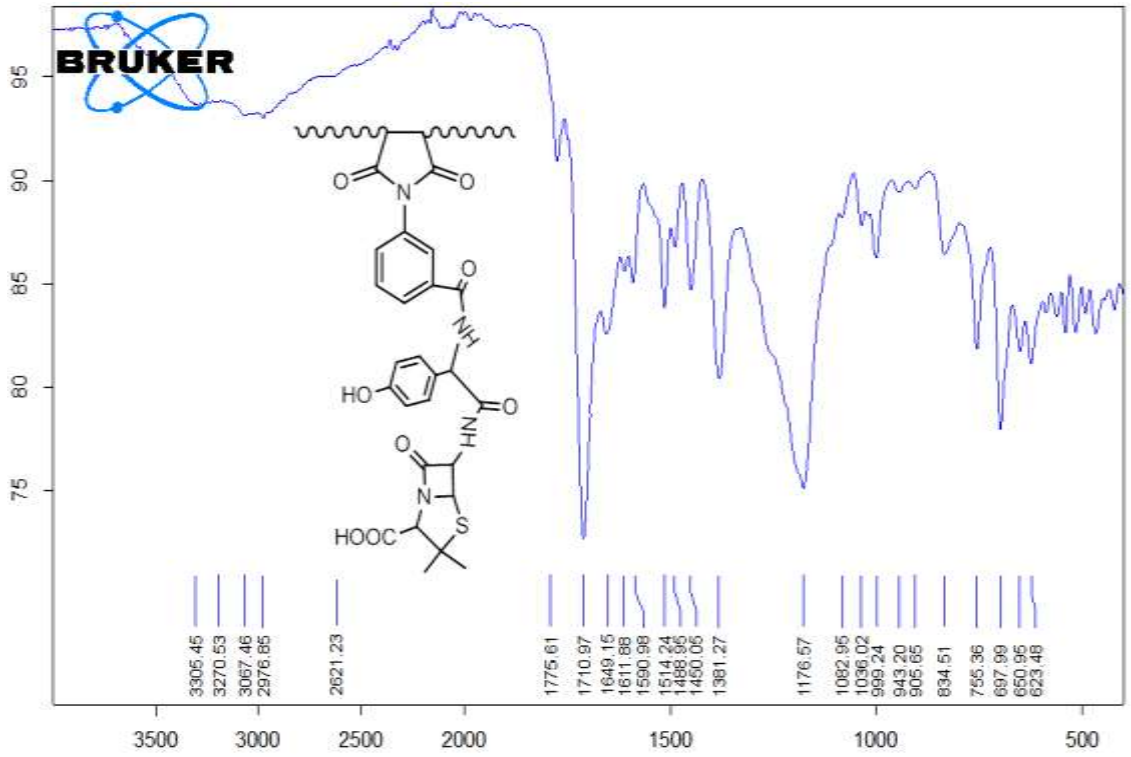

Figure 3.40: FT-IR spectrum of compound [PM_4]

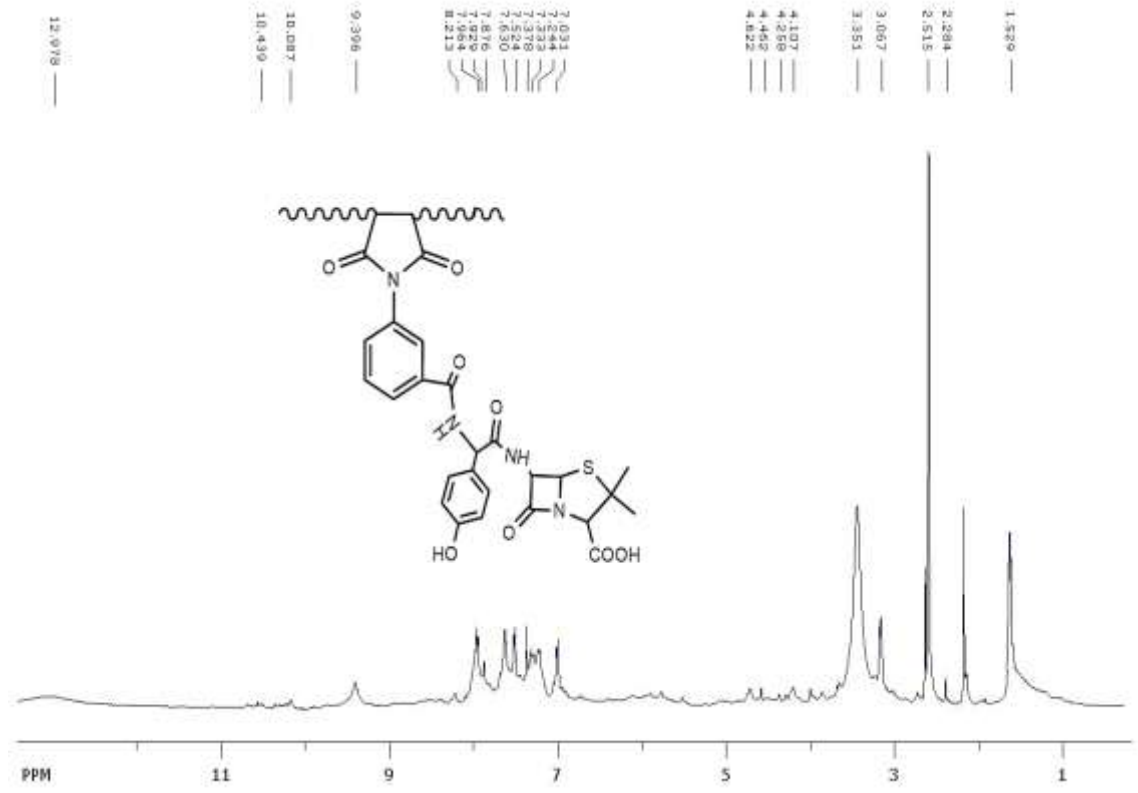

Figure 3.41: ^{1}H-NMR spectrum of compound [PM_4]

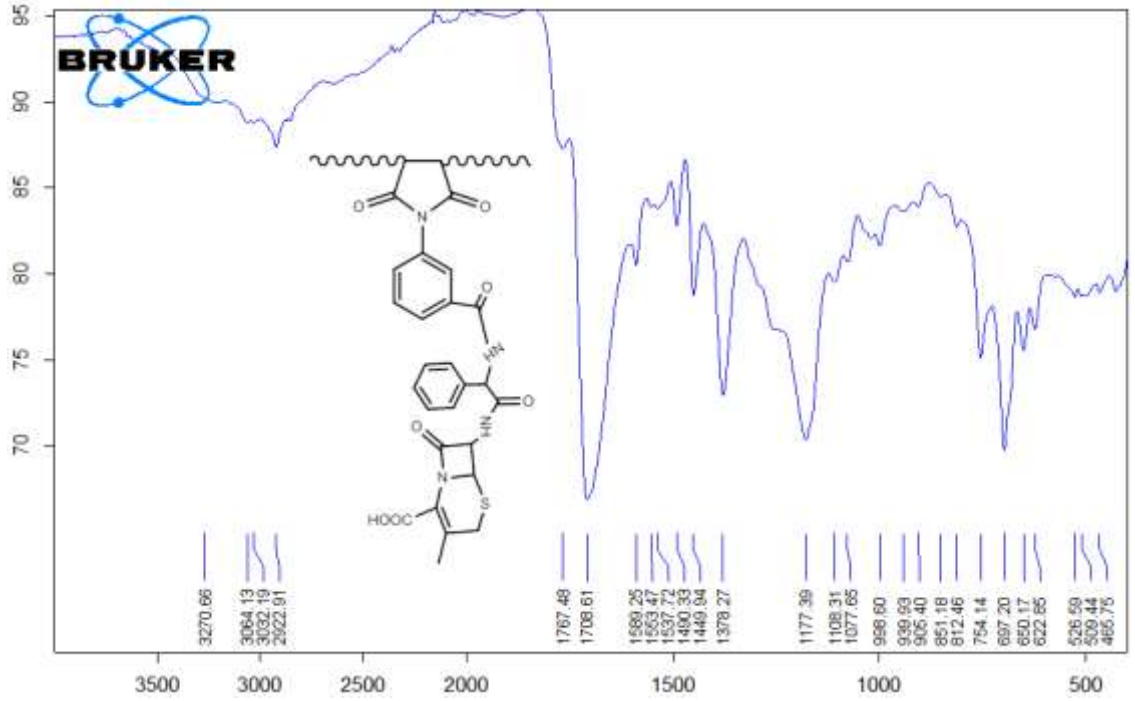

Figure 3.42: FT-IR spectrum of compound [PM_5]

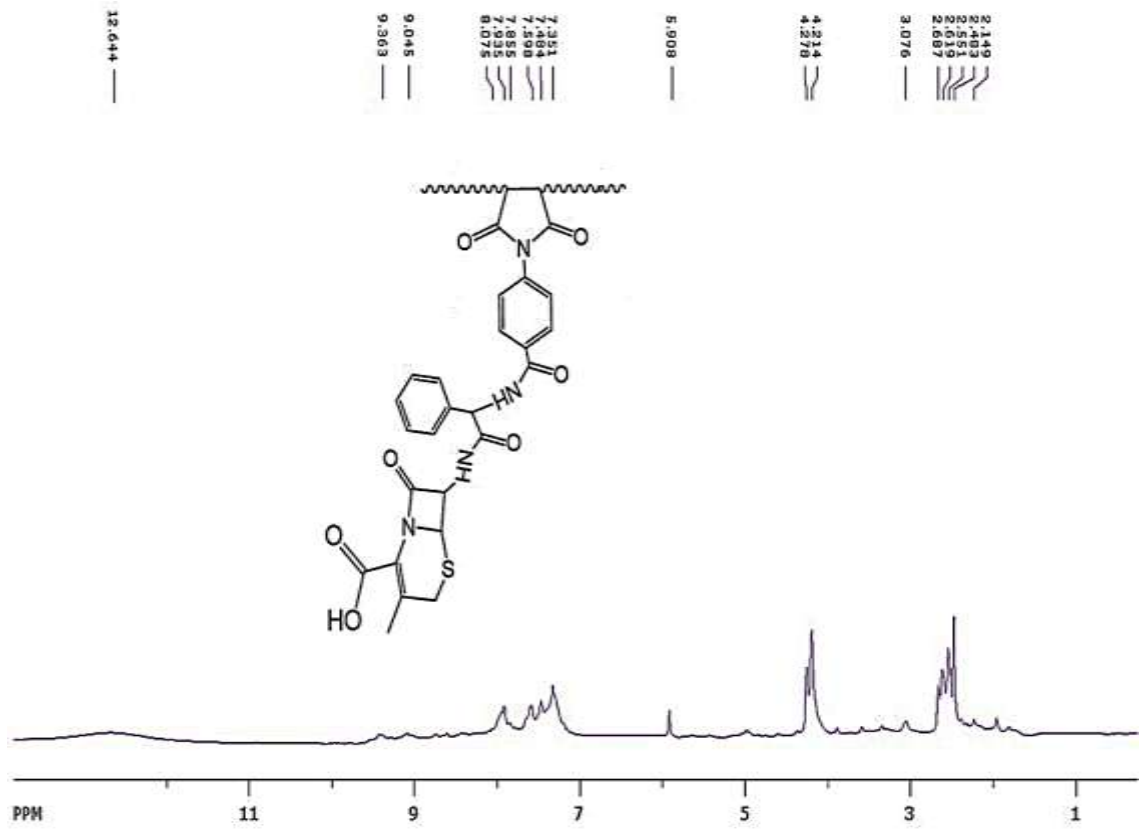

Figure 3.43: ^{1}H-NMR spectrum of compound [PM_5]

3.6.2. Characterization of Homopolymer [PM_6-PM_{11}]

Characterization of Homopolymer [PM_6]: IR spectrum of the **[PM_6]** (Figure 3.45), showed different bands: a band was observed at 3500 cm^{-1} due to (COOH), a band was observed at 3057 and 3024 cm^{-1} due to (=C-H) of aromatic rings, 2918 and 2849 cm^{-1} due to stretching vibrations of the aliphatic groups, a band was observed at 1716 cm^{-1} due to νC=O in imide ring, a band was observed at 1627 cm^{-1} due to (C=C-C=O, Quinolinone) and amid carbonyl. The stretching vibration of aromatic system was observed at 1549-1451 cm^{-1}, the band at 1387 cm^{-1} belong to (C-N) stretching, and the band at 1265 cm^{-1} due to (C-F) stretching vibration.

1H NMR spectrum (Figure 3.46), shows different chemical shifts, a peak at 1.185 ppm belong to the methylene protons of cyclopropyl ring while the single proton of this ring appeared as multiplet signal at 3.064 ppm, two peaks at 2.760 and 2.919 for polysuccinimide protons, the peaks at 3.567 for the protons of piprazine ring, the two protons of the aromatic fused ring appeared at 7.340 and 8.015 ppm, while the aromatic protons of the meta-di-substituted benzene ring appeared at 7.472-7.949 ppm.

The characteristic signal at 8.632 ppm belong to the vinylic proton and two signals for the carboxylic protons, the first appeared as broad signal at 12.952 ppm and the other was highly deshielded and appeared at 15.176 ppm due to the intra-hydrogen bonding as shown in the (Figure 3.44)[136-138].

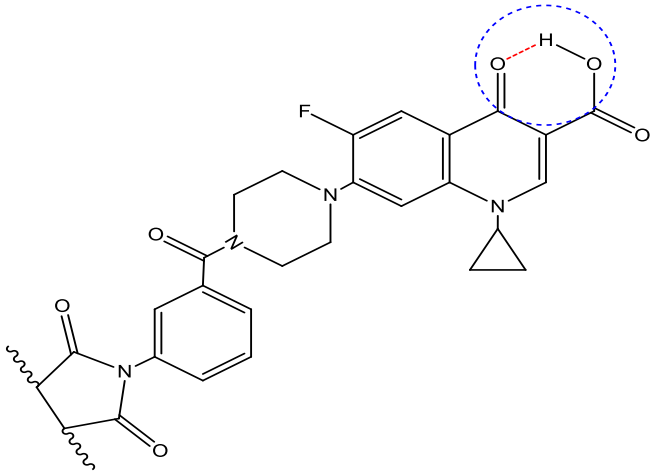

Figure 3.44: Intramolecular hydrogen bond of [PM_6]

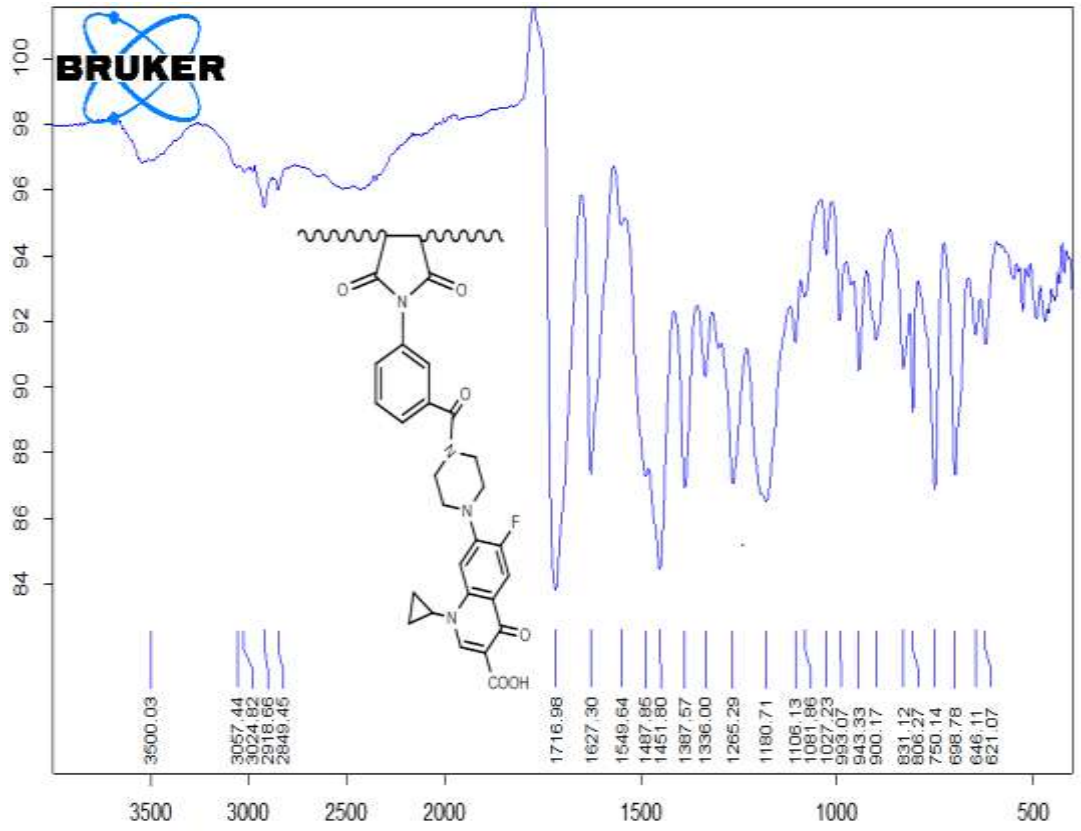

Figure 3.45: FT-IR spectrum of compound [PM_6]

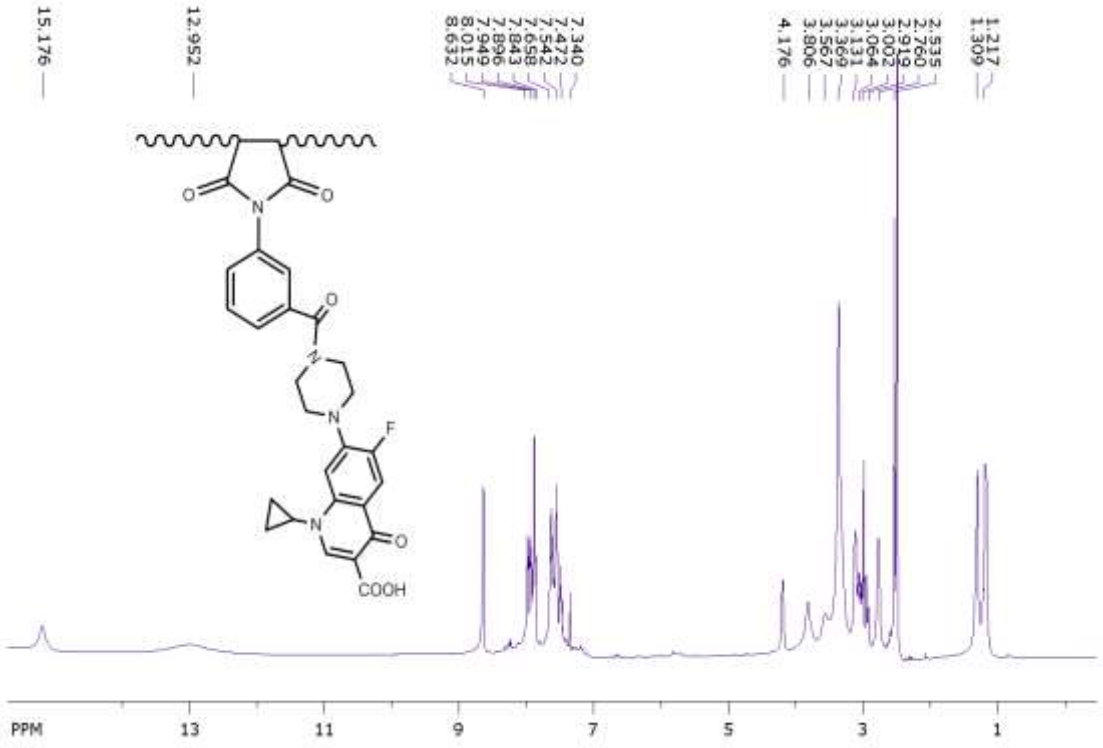

Figure 3.46: ^{1}H-NMR spectrum of compound [PM_6]

Characterization of Homopolymer [PM_7]: FT-IR spectrum of this polymer (Figure 3. 47), shows different vibrational frequencies as follow.

The stretching vibration of the phenolic hydroxyl group occurred at 3322 cm^{-1} (-OH, phenol), the aromatic (=C-H) occurred at 3043 cm^{-1}, the methyl group and aliphatic methine groups of polymer appeared at 2978 and 2945 cm^{-1}, the vibration of maleimide and imide carbonyls appeared at 1711 and 1668 ppm, the bands at the range of 1607-1475 cm^{-1} attributed to the aromatic (C=C), the (C-N) and (C-O) stretching appeared at 1382 and 1234, respectively.

^{1}HNMR spectra (Figure 3.48) show different chemical shifts as follow. The signals at 2.065 and 2.091 ppm belong to the aliphatic protons of the polysuccinimide backbone, the methyl group of the acetyl group appeared at 3.065 ppm, the multiplet signals at the range of 7.237 - 7.499 ppm belong to the aromatic protons of the phenol ring, while the protons of the other aromatic ring appeared at 7.613-7.945 ppm, and the phenolic hydroxyl proton appeared at 9.995 ppm.

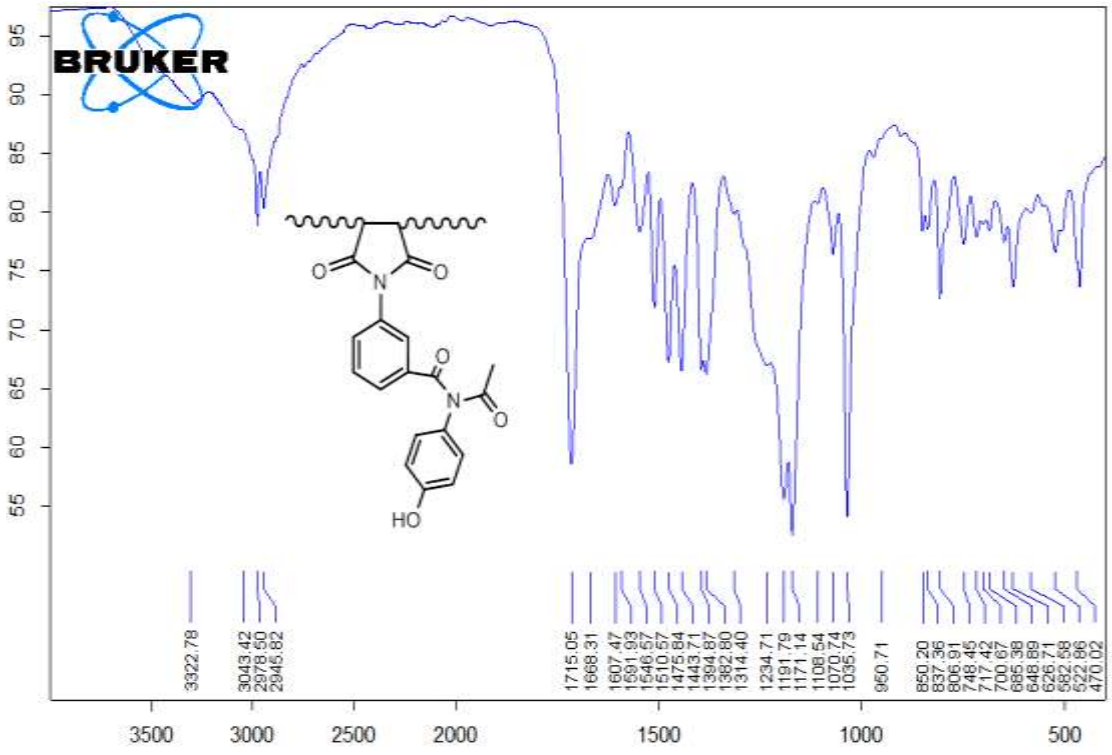

Figure 3.47: FT-IR spectrum of compound [PM_7]

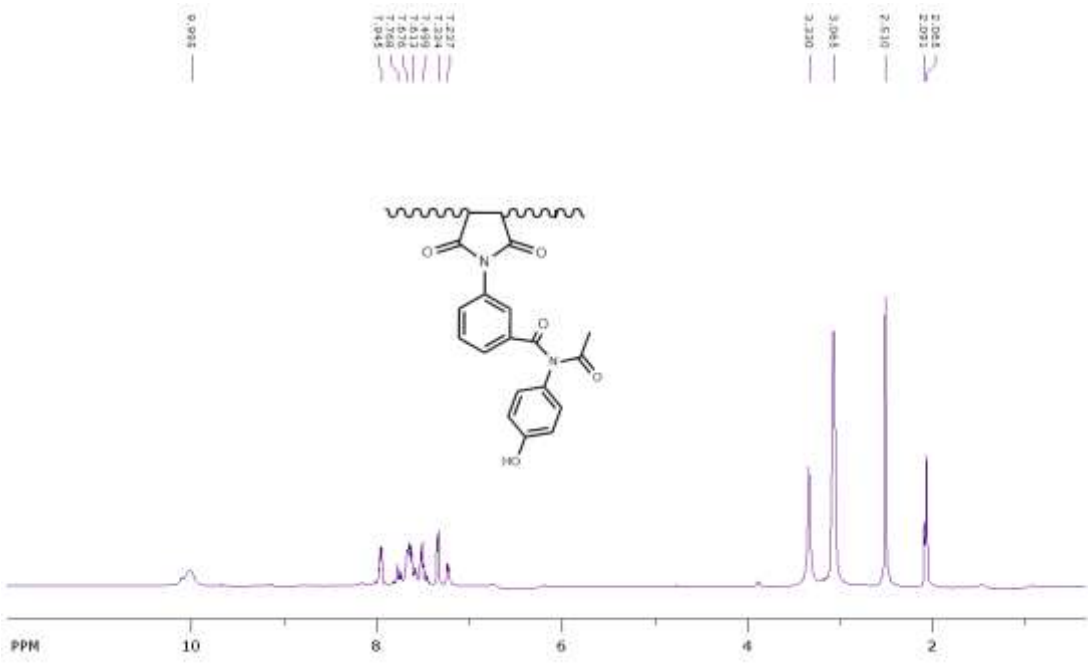

Figure 3.48: ^{1}H-NMR spectrum of compound [PM_7]

Characterization of Homopolymer [PM_8]: The FT-IR spectrum of homopolymer [PM_8], (Figure 3.49) shows the characteristic absorption bands of amino group 3469 and 3376 cm^{-1} and the vibration of (=C-H) of aromatic system appeared at 3084 and 2996 cm^{-1}, the methyl group and aliphatic methine (C-H) groups of polymer appeared at 2934cm^{-1}.

Although characteristic absorption band of imides were observed at 1712 cm^{-1}, and at 1625 cm^{-1} for carbonyl of amide, the aromatic system vibration was observed at 1580-1406 cm^{-1}, the (C-N) stretching appeared at 1381 cm^{-1}, the bands at 1318 cm^{-1} and 1152 cm^{-1} for (O=S=O) stretching, and 568 cm^{-1} due to sulfonamide group vibration (C-SO_2-N).

^{1}HNMR spectrum (Figure 3.50) display a different characteristic chemical shifts that are demonstrate that the success of polymerization of the polymer such as, the two signals at 2.066 and 2.173 ppm for methine protons of the aliphatic polysuccinimide backbone also the disappearing of maleimide's proton signals supports this opinion. The broad signal at 5.454 ppm traced to the amino group protons, the Pyrimidine signals appeared at 6.989 ppm for the single proton at four (or *para*)-position, while the other two

emine like protons appeared doublet signal at higher chemical shift 8.479 ppm (J= 16 Hz), the protons of aniline and the other benzene ring appeared at the range of 7.277 -7.925 ppm.

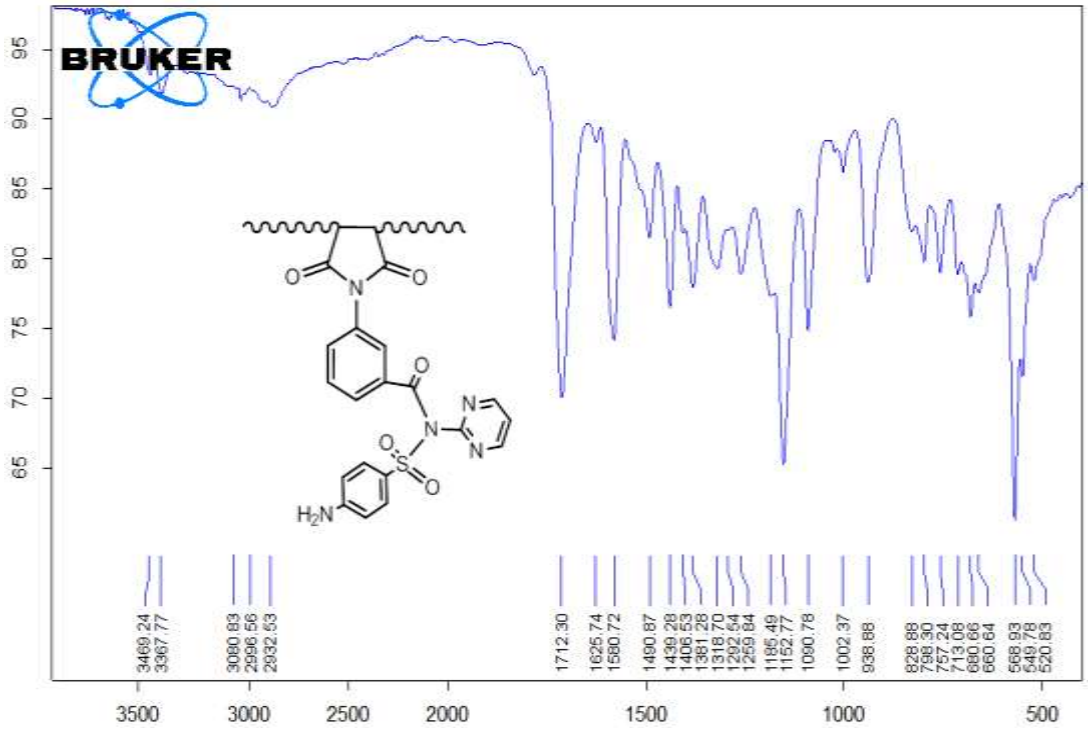

Figure 3.49: FT-IR spectrum of compound [PM_8]

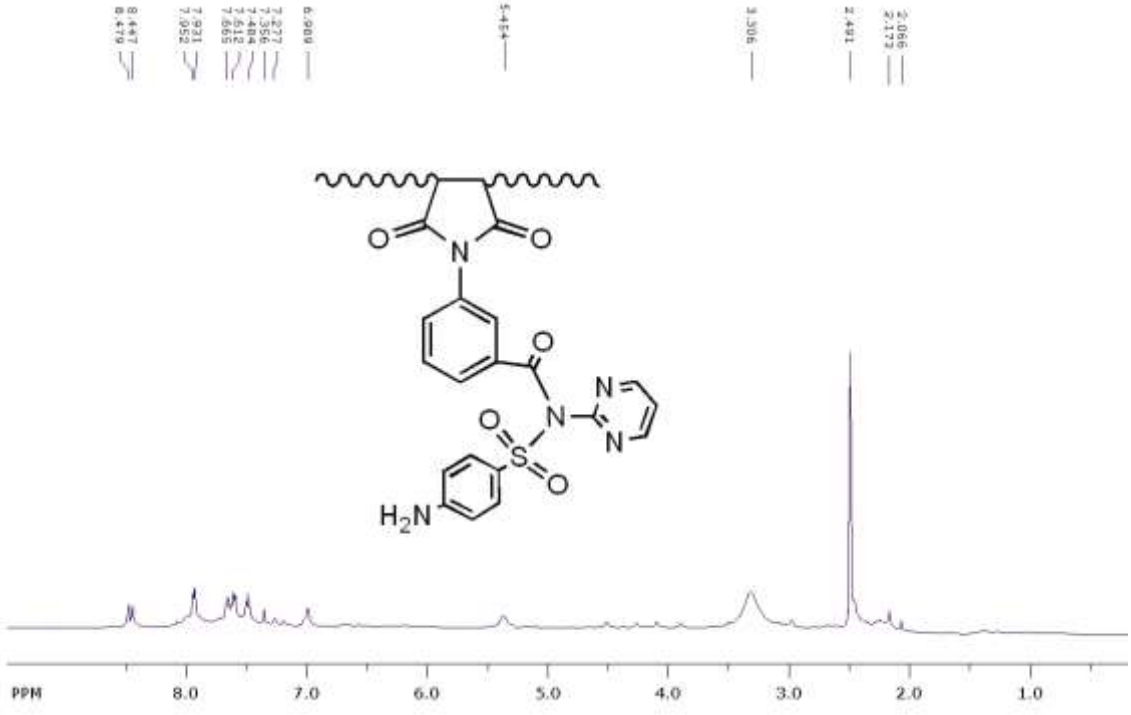

Figure 3.50: ^{1}H-NMR spectrum of compound [PM_8]

Characterization of Homopolymer [PM_9]: The FT-IR spectrum of homopolymer [PM_9], (Figure 3.51) shows the following absorption bands:

The two bands at 3271 and 3213 cm^{-1} belong to the stretching vibration of (-NH) of hydrazide group, the aromatic (=C-H) appeared at 2993 cm^{-1}, 2916 and 2789 cm^{-1} attributed to the (C-H) polyimide backbone stretching.

The carbonyl of imide and of hydrazide appeared at 1703 and 1656 cm^{-1} respectively, while the aromatic double bonds were vibrated at the range of 1605-1483 cm^{-1}, and the (C-N) stretching was observed at 1396 cm^{-1}. ^{1}HNMR spectrum (Figure 3.52) shows two peaks for the aliphatic (C-H) of polysuccinimide protons a singlet at 2.090 ppm and douplet at about 2.841 ppm.

The aromatic protons of benzene ring appeared at the range of 7.443-7.914 ppm while the protons of pyridine ring appeared at the range of 8.016-8.260 ppm, the two signals at 10.341and 10.540 ppm attributed to the hydrazide (-NH) protons.

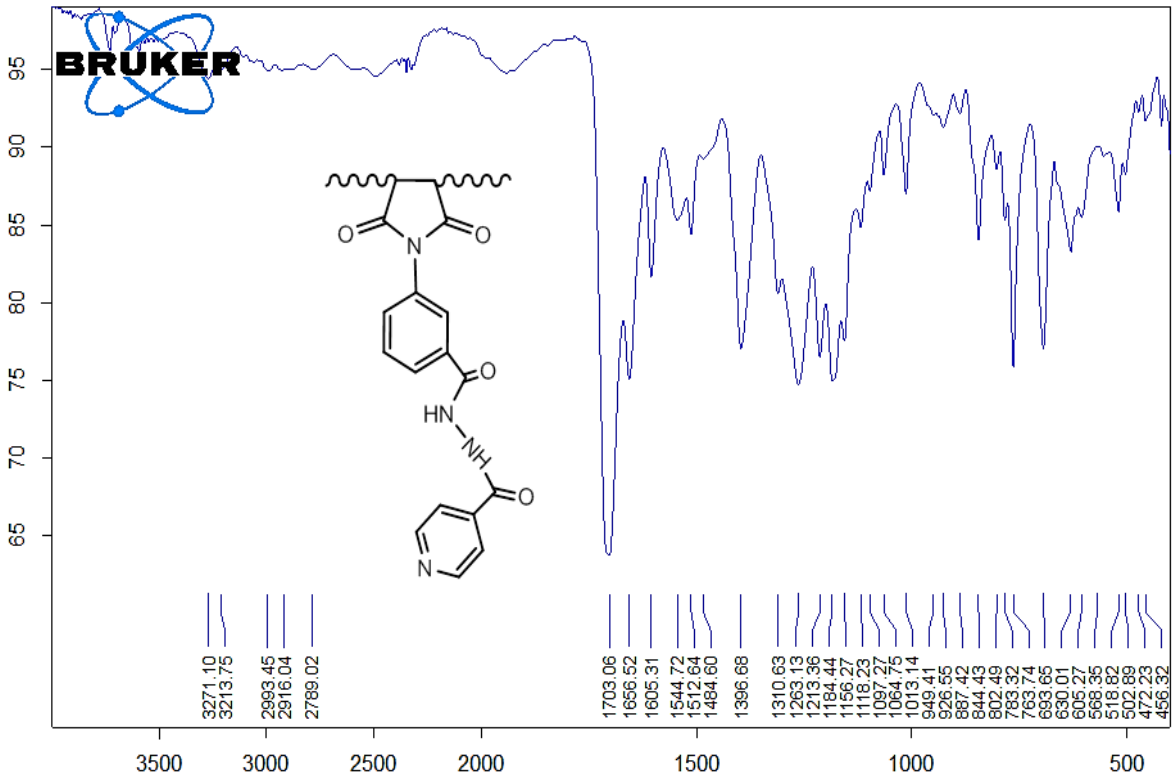

Figure 3.51: FT-IR spectrum of compound [PM_9]

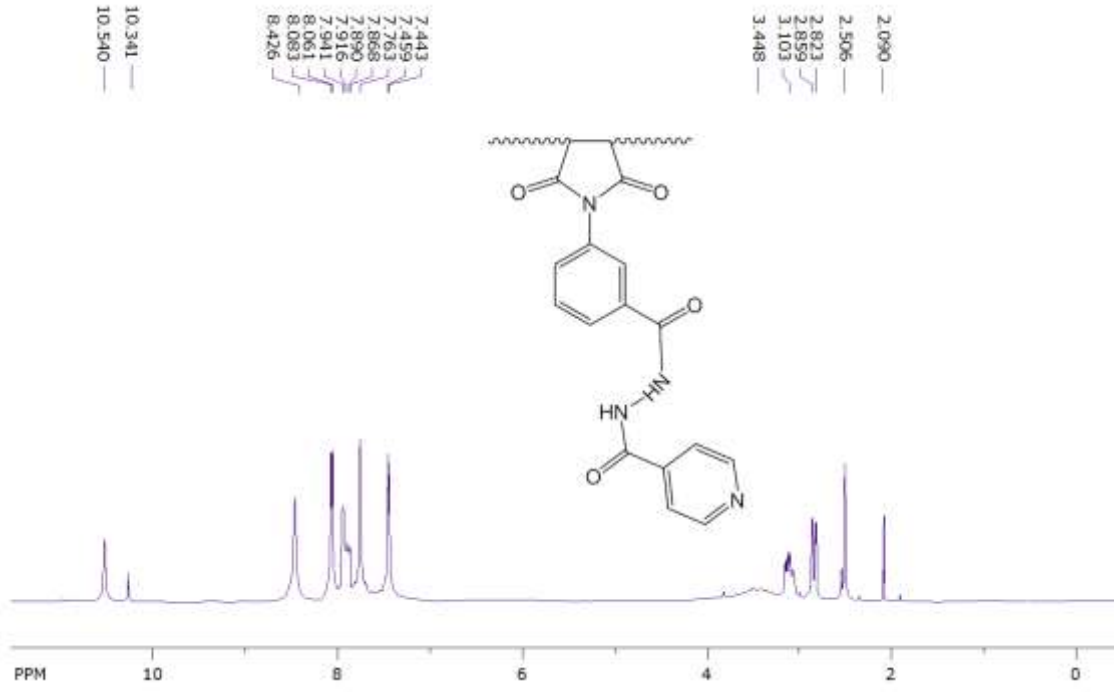

Figure 3.52: ^{1}H-NMR spectrum of compound [PM_9]

Characterization of Homopolymer [PM_{10}]: The FT-IR spectrum (Figure 3.53) for Hetropolymer [PM_{10}] shows the following vibration frequencies.

The -NH stretching of amide groups appeared at 3483 cm^{-1}, the aromatic =C-H vibrations occur at 3052 and 3023, the (C-H) stretching of the aliphatic polyimide backbone take place at 2992 and 2961 cm^{-1}.

Furthermore the double bond region of the spectrum showed some valuable band such as 1710 and 1650 cm^{-1} for carbonyls of maleimide and amide groups, also the range of 1601-1414 cm^{-1} attributed to the vibration of (C=C) of aromatic system and other bands from the finger print region we are picked up the band at 1382 cm^{-1} for (C-N) stretching), and for the (o.o.p =C-H, cis) bending at 802 and 766 cm^{-1}.

^{1}HNMR spectrum (Figure 3.54) of Homopolymer [PM_{10}] shows two peaks for the aliphatic (C-H) of polysuccinimide protons a singlet at 2.075 and 2.288 ppm. The olefinic proton of the seven membered ring appeared at 6.994 ppm while the aromatic protons occurred at the range of 7.164-8.125 ppm, and the imide proton appeared at 10.240 ppm.

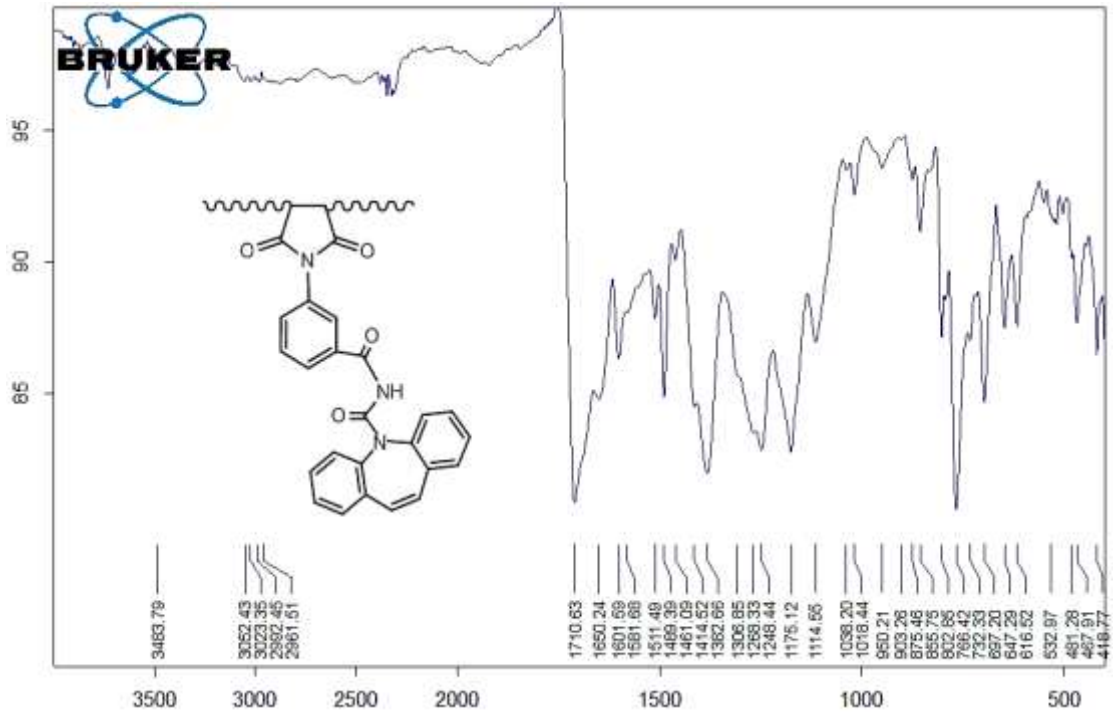

Figure 3.53: FT-IR spectrum of compound [PM_{10}]

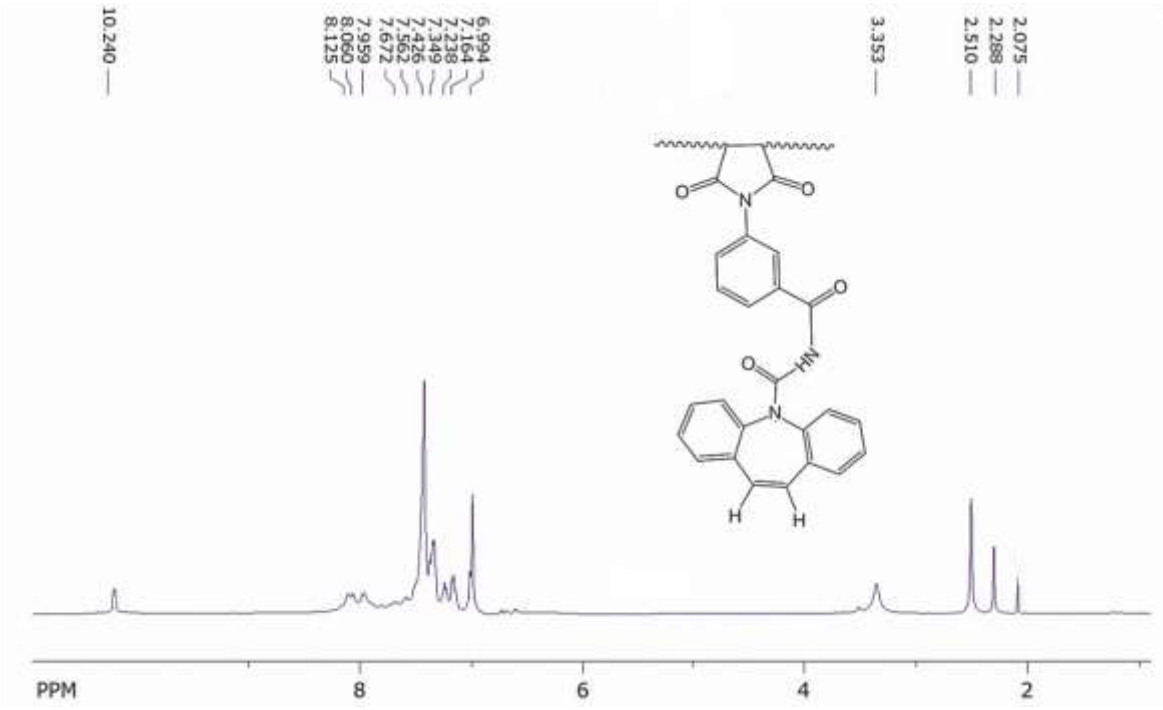

Figure 3.54: 1H-NMR spectrum of compound [PM_{10}]

Characterization of Homopolymer [PM_{11}]: In the FT-IR spectrum (Figure 3.55) for Hetropolymer [PM_{11}] we observed following vibration frequencies.

The (-NH) of amide groups at 3363 and 3232 cm^{-1}, the aromatic (=C-H) at 3004 cm^{-1}, the aliphatic (methyl, methylene and methine of polyimide backbone) groups at 2978-2737 cm^{-1}.

The carbonyl groups of maleimide ring and the amide groups appeared at 1712, 1627 and 1590 cm^{-1}, the aromatic (C=C) occur at 1508-1475 cm^{-1}, the stretching of (C-N) bonds was observed at 1381and 1254 cm^{-1} while the (C-O) stretching of ether group appeared at 1035 cm^{-1} and (C-Cl) stretching appeared at 625 cm^{-1}.

^{1}HNMR (Figure 3.56) shows different chemical shifts as follow: The proton signal of (a) appeared as singlet peak at 1.193 ppm, the polysuccinimide protons signal (i) appeared at 2.074 ppm, the singlet signal at 3.072 ppm belong to the methylene (b) attached to tertiary amine, while the ethylene group appeared as two signals (c) 3.822 and (d) 3.938 ppm, the methoxy protons (e) occur at 3.938 ppm. The range of chemical shift at about 7.491-7.968 ppm attributed to the meta-substituted benzene protons (f), while the two protons (h, g) of the other appeared at 8.358 and 8.647 ppm and the two amide protons (k, l) appeared at 10.153 and 10.409 ppm.

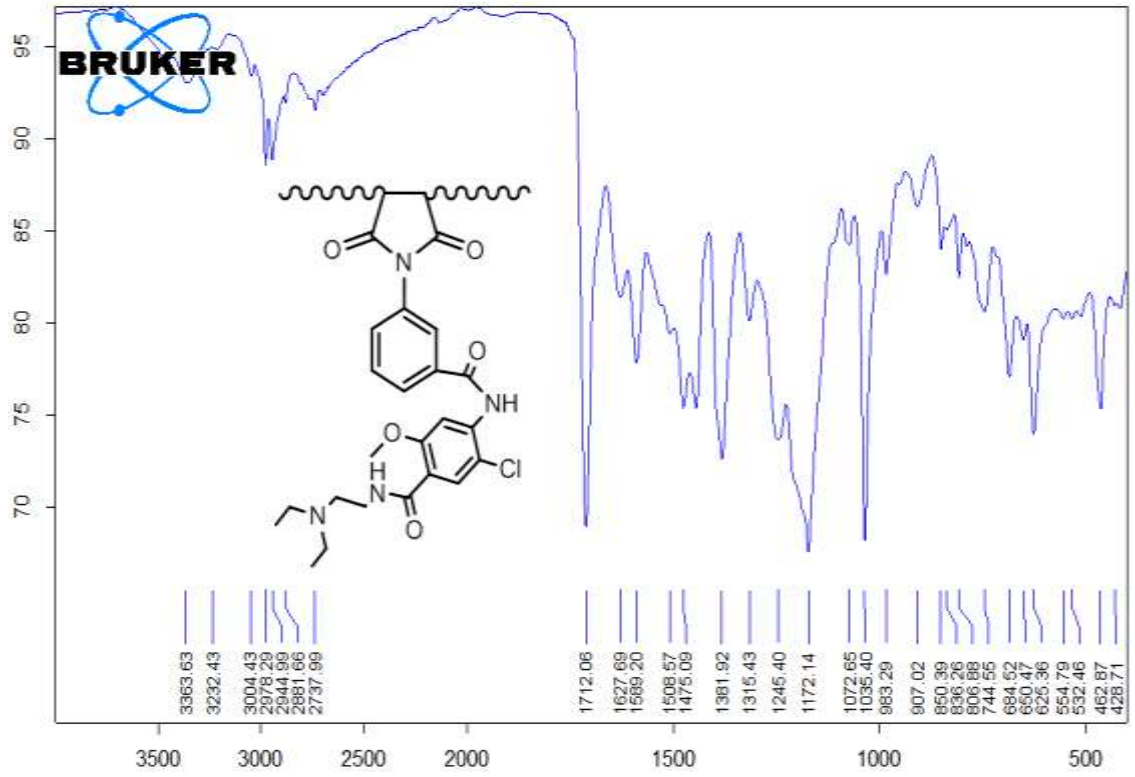

Figure 3.55: FT-IR spectrum of compound [PM_{11}]

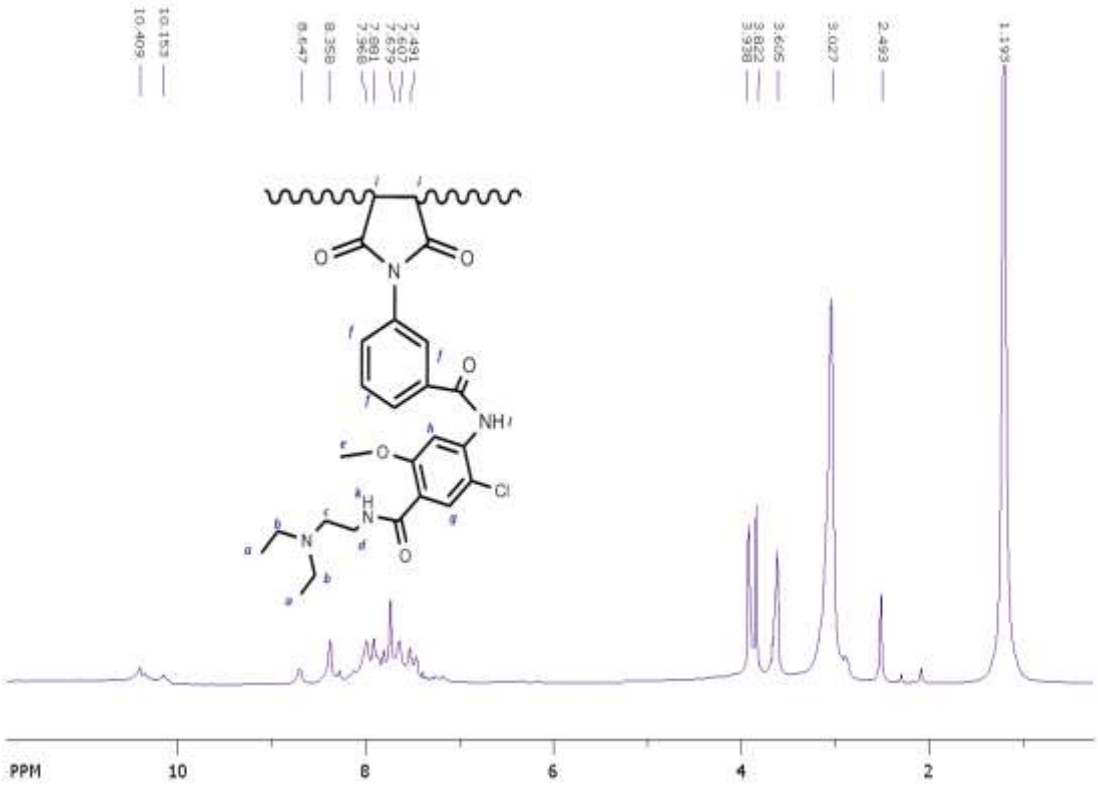

Figure 3.56: ^{1}H-NMR spectrum of compound [PM_{11}]

3.8. Synthesis of Heteropolymers [PM_{12}-PM_{22}]

The Co-polymerization of equimolar amounts of maleimide-drug monomers and acrylic acid were carried out in toluene solvent by using benzoylperoxid, as free radical initiator, at 90 ºC. (3.77 mmol) of Monomers [M_1-M_{11}] and Acrylic acid were suspended in 50 mL of toluene in a 100 mL two necks round bottom flask were heated in an oil bath at 90 ºC. To this solution (0.05 g) of benzoyl peroxide was added and the reaction mixture was heated on heating mental at 90 ºC for 10-12 hours under nitrogen flow and at the end of polymerization; the mixture was cooling in ice path, precipitate was filtered, purified with suitable solvent . Finally dried in an oven at 50 ºC, as shown in equation 3.13 and the chemical structures, purification solvents, and the obtained weight were listed in Table 3.7.

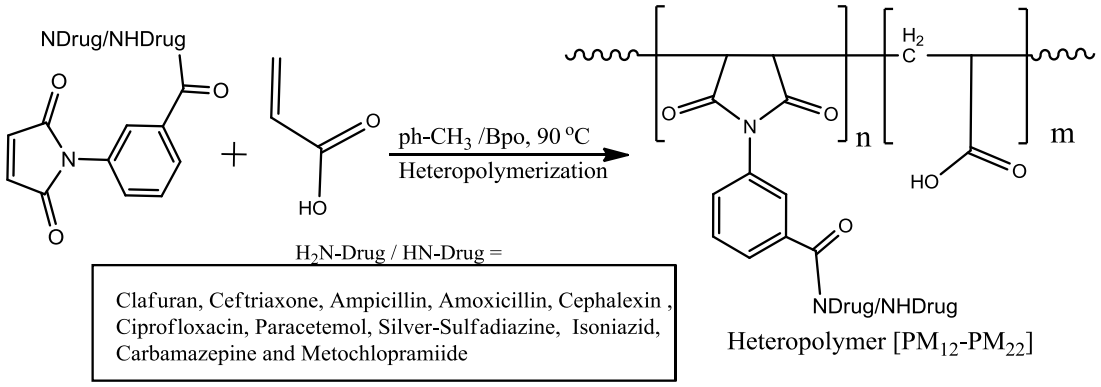

Equation 3-11: Synthesis of Synthesis of Heteropolymers [PM_{12}-PM_{22}]

Table 3.7: The chemical structure, Color and purification solvents for Heteropolymers [PM_{12}-PM_{22}]

Co.	Chemical Structure	Color	Purification solvents
PM12	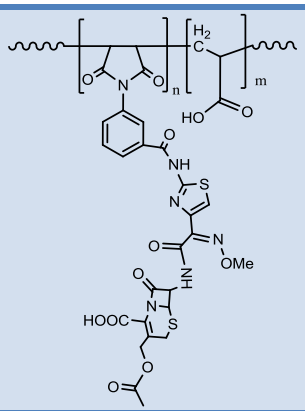	Orange	Dissolving in DMF and Re-precipitate by mixture of water and ethanol 1 : 1
PM13	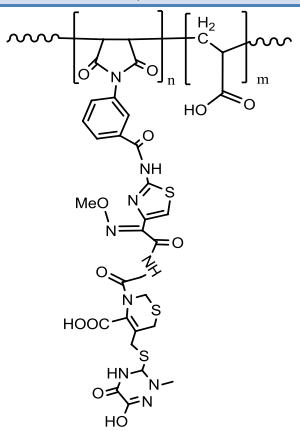	Brown	Dissolved in DMF and re-precipitate with water
PM14	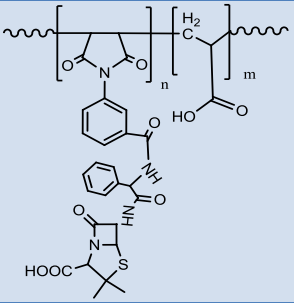	Red	Washed several times with Hot methanol to remove the un reacted monomer

PM15	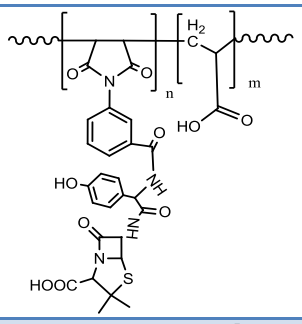	Greenish Yellow	Washed several times with ethanol to remove the un reacted monomer
PM16	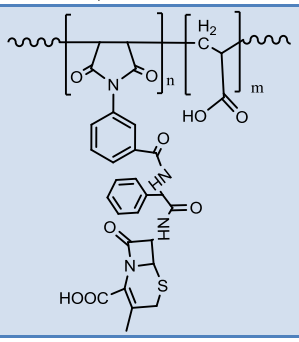	Dark Brown	Dissolved in DMF and Re-precipitate with water
PM17	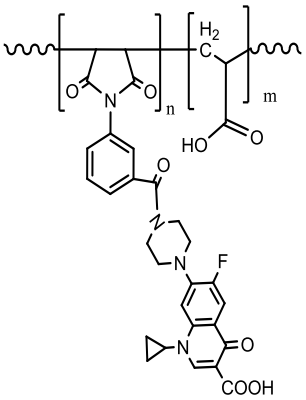	Orange	Dissolved in DMF and Re-precipitate with water
PM18	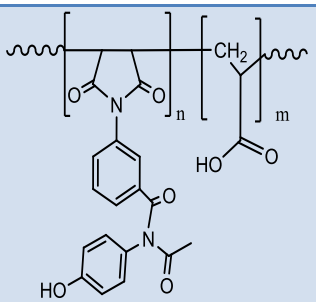	Dark brown	Washed several times with methanol to remove the un reacted monomer
PM19	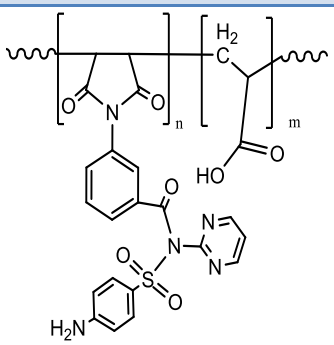	Purple	Washed well with Acetone to remove the un reacted monomer

PM20	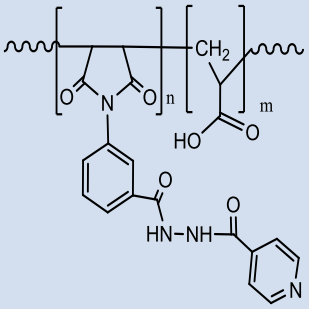	Pink	Washed several times with Acetone to remove the un reacted monomer
PM21	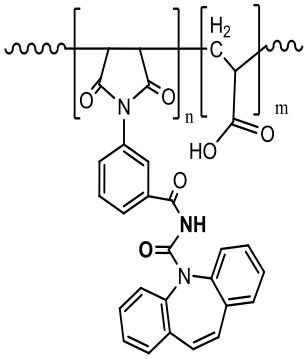	Brown	Dioxane only dissolve the polymer
PM22	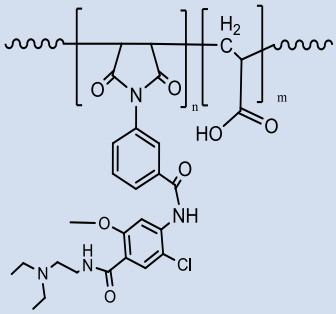	Brownish Red	Ethyl acetate only dissolve the Monomer

Table 3.8: The solubility prepared Heteropolymer in some solvents

Poly.	H_2O	EtOH	$CHCl_3$	Ether	Toluene	DMSO	Hexane	Acetone	DMF
PM12	**partial**	**Partial**	-	-	-	+	-	**partial**	+
PM13	**partial**	+	-	-	-	+	-	+	+
PM14	**partial**	+	-	-	**partial**	+	-	+	+
PM15	**partial**	+	-	-	**partial**	+	-	+	+
PM16	**partial**	**partial**	-	-	-	+	-	**Partial**	+
PM17	**partial**	**partial**	-	-	-	+	-	**partial**	+
PM18	**partial**	**partial**	-	-	-	+	-	**Partial**	+
PM19	**partial**	+	-	-	-	+	-	+	+
PM20	**partial**	**Partial**	-	-	-	+	-	+	+
PM21	**partial**	+	-	-	**partial**	+	-	+	+
PM22	**partial**	**partial**	-	-	-	+	-	**partial**	+

3.9. Characterization of Heteropolymers [PM_{12}-PM_{22}]

Contrary to homopolymers, which does not show the double bond stretching in the FT-IR spectra for their monomers due to the type of symmetry in maleimide ring[118,119], we may can make a conclusion for the successful of Copolymerization with acrylic acid depending on the presence of two characteristic absorption such as carboxylic -OH and the double bond in the spectra, beside to other spectral features in the Heteropolymers spectra will discussed soonly. The FT-IR spectrum of acrylic (Figure 3.57) showing three characteristic band for (C=C), (C=O), and (COOH) at 1635, 17014 and broad band 3200 cm^{-1}, respectively [139]. The vibration of the acrylic acid carbonyl may interfere with the carbonyl of maleimide, as its vibration occurs in a similar range.

The HNMR spectrum of acrylic acid (Figure 3.58) has been reported in literature shows clear peak in the vinylic region. The acrylic acid spectrum consists of three quadruplets centred at 6.42 ppm (*cis*- proton), 6.17 ppm (germinal proton) and 6.01 ppm (trans proton)[137] and carboxylic protons at about 12 ppm. The disappearing f these peaks from IR and NMR spectra of Heteropolymers and showing only carboxylic proton of acrylic acid in some polymer (non-carboxylic drugs maleimide monomers) gave strong evidence for success co-polymerization reaction.

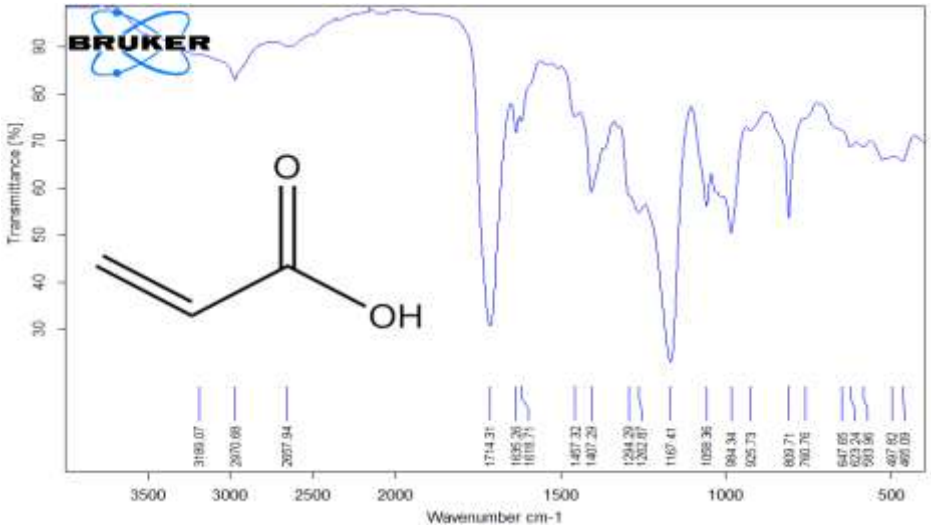

Figure 3.57: FT-IR spectrum of acrylic acid

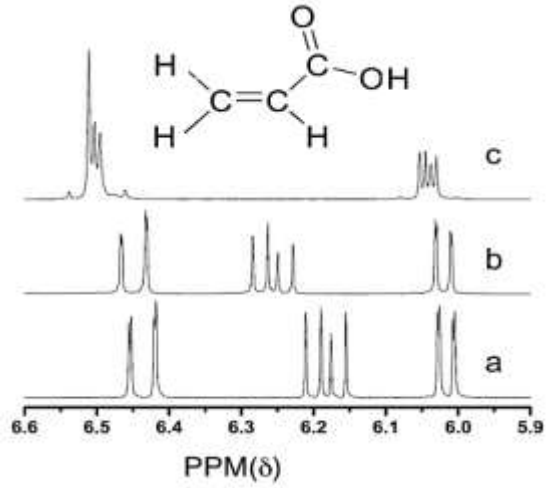

Figure 3.58: ^{1}H-NMR spectra of acrylic acid

Heteropolymer [PM_{12}]: the FT-IR spectrum was displayed in (Figure 3.59); show the following infrared absorption bands.

The broad band within the range of 3500- 2496 cm^{-1} belong to carboxylic acid groups of the Clafuran drug and acrylic acid, 3342 and 3177 cm^{-1} attributed to -NH, amide groups , 3042 cm^{-1} due to =C-H, of aromatic rings, 2978-2838 cm^{-1} (C-H) stretching of methyl, methylene and methine groups, 1786 cm^{-1} traced to the beta-lactam carbonyl, 1749 cm^{-1} carbonyl acetyl ester, 1716 cm^{-1} belong carbonyls of imide ring, 1636 cm^{-1} due to carbonyls of amide groups, 1590 cm^{-1} (C=N-OMe and C=N inside thiazole ring, 1588-1471 cm^{-1} aromatic (C=C) vibrations, 1386 cm^{-1} belong to the (C-N) bond stretching, 1171 (C-O) stretching of ester[111].

^{1}HNMR spectrum (Figure 3.60): the chemical shifts of aliphatic poly succinimide-Co-acrylic acid backbone protons appeared as multiple signals (a, b and c protons) in 2.072, 2.125, 2.621 and 2.682 ppm, the singlet signal at 2.287 ppm belong to the methyl of acetate group (d), 3.751 and 3.828 ppm attributed to methylene groups (e, f), the douplet signal at 4.246 ppm (g, J=22 Hz), the singlet signal at 4.841 belong to the methyl of oxime ether (i), the douplet signal at 5.116 ppm belong to beta lactam proton (h, J= 25 H), 5.926 ppm attributed to the amide of beta-lactam amide(j), while the other amide (O) appeared at 10.676 ppm. The spectrum also showing the aromatic proton

signals at the range of 7.143-7.997 ppm and broad signal at 12.738 ppm for carboxylic (2-OH) groups.

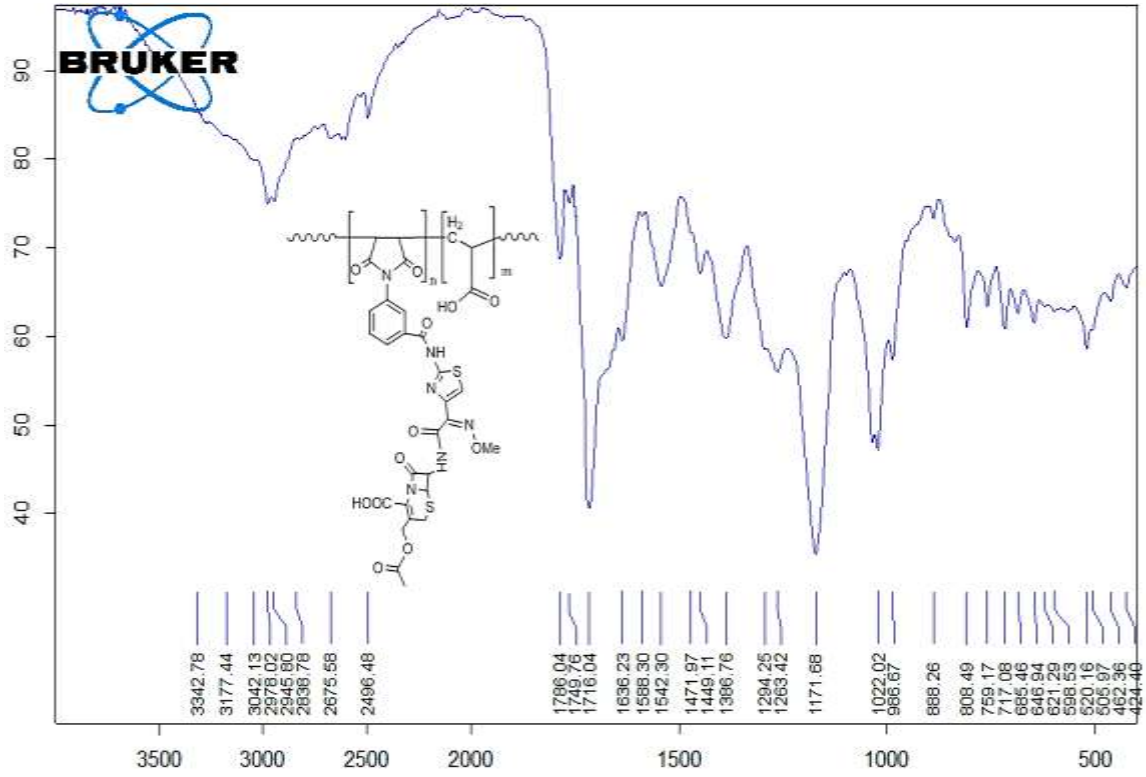

Figure 3.59: FT-IR spectrum of compound [PM_{12}]

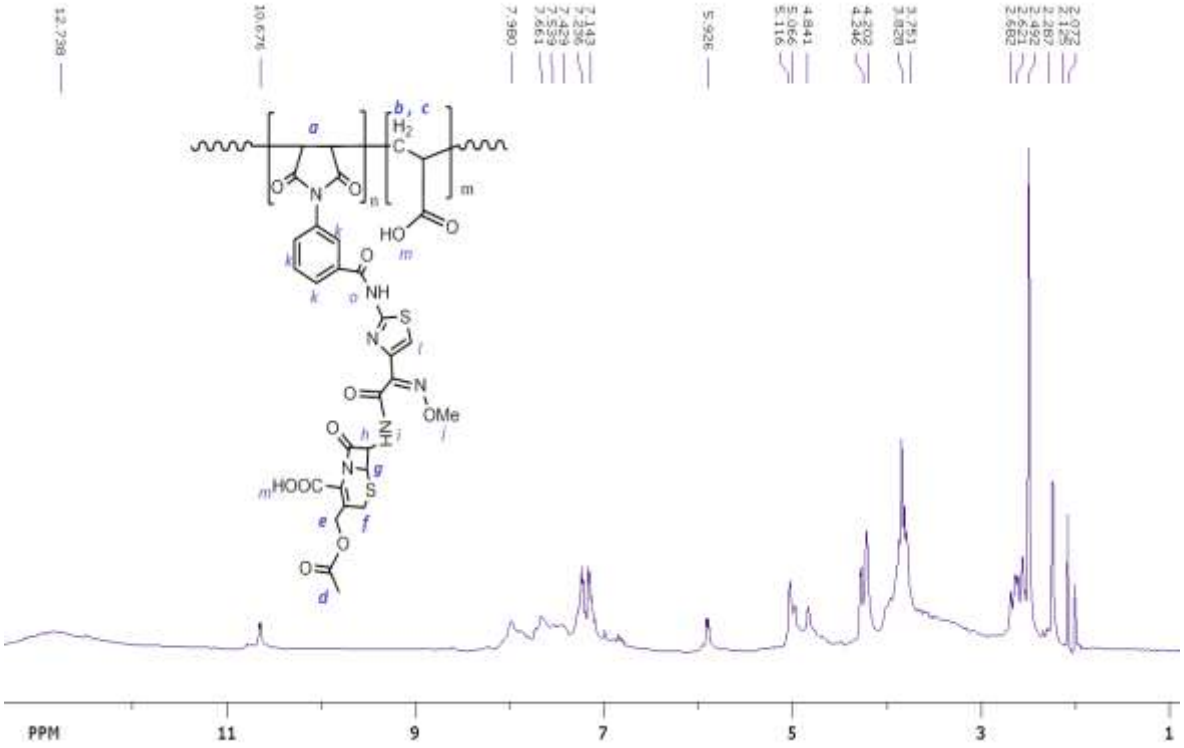

Figure 3.60: ^{1}H-NMR spectrum of Hetropolymer [PM_{12}]

Heteropolymer [PM_{13}]: FT-IR spectrum (Figure 3.61) shows the following absorption band:

The broad band within the range of 3500-2460 cm^{-1} belong to the carboxylic acid groups of the ceftriaxone drug and acrylic acid, the two bands at 3366 and 3196 cm^{-1} belong to the (ArCO-NH-) of amide, the (=C-H) groups of aromatic rings appeared at 3052 cm^{-1}, and the aliphatic stretching of methyl, methine and methylene groups appeared at 2980-2798 cm^{-1}.
Furthermore, the carbonyl groups of beta-lactam, imide, amide and (C=O amide and C=C of the drug) in the spectrum appeared at 1782, 1716 and 1652, and 1637 cm^{-1}, respectively. the imine group of oxime and this inside thiazole ring coupled at 1588 $cm^{-1(106)}$, while the aromatic rings double bonds appeared at the range of 1542-1413 (C=C, aromatic), other bands includes 1377 cm^{-1} (C-N) stretching), 1174 cm^{-1} (C-O) stretching vibration.

The **^{1}HNMR** spectrum (Figure 3.62): included many chemical shifts for different protons as follow. The signals at 1.894, 2.07, 2.278 and 3.069 ppm belong to the polysuccinimide-Co-acrylic acid backbone protons (a, b, c protons), the douplet signal for methylene of thiazine ring (g) at about 3.540 ppm (d, 2H, J = 31 Hz), the signal of methoxy group (k) protons appeared at 3.672 ppm, the beta-lactam douplet signal occur at 4.221 ppm (h, 1H, J = 22 Hz), the triazin proton (p) appeared at 4.693 ppm.

The other doublet signal at about 5.096 ppm (i, 1H, J = 25 Hz) belong to the second beta-lactam proton, the signal at 5.935 ppm may be belongs to the amide group with beta-lactam ring (j), the signal of thiazole ring proton occur at 7.169 ppm, while the other aromatic protons appeared as multiplet signals at the range of 7.243-7.993 ppm (m), the amide proton (o) appeared at 9.562 ppm and the carboxylic acid protons appeared as broad signal at about 12.792 ppm (n).

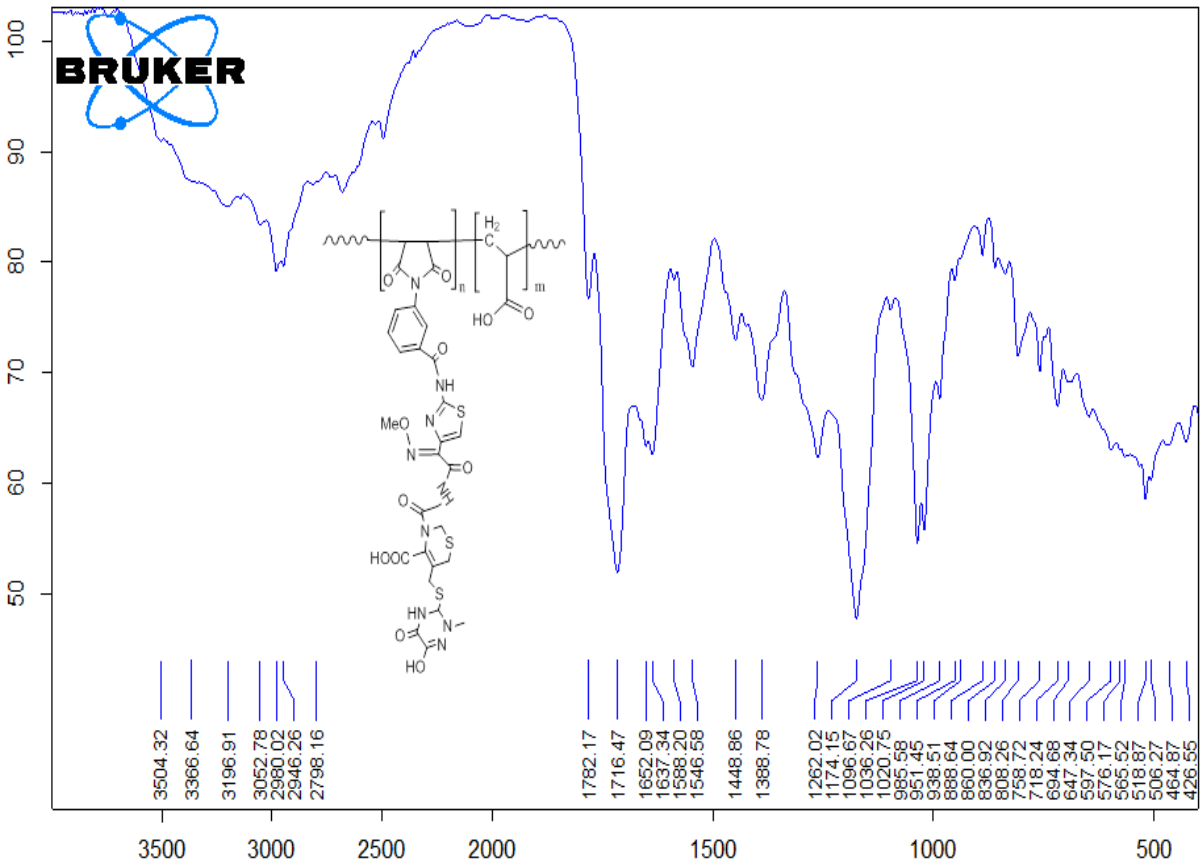

Figure 3.61: FT-IR spectrum of compound [PM_{13}]

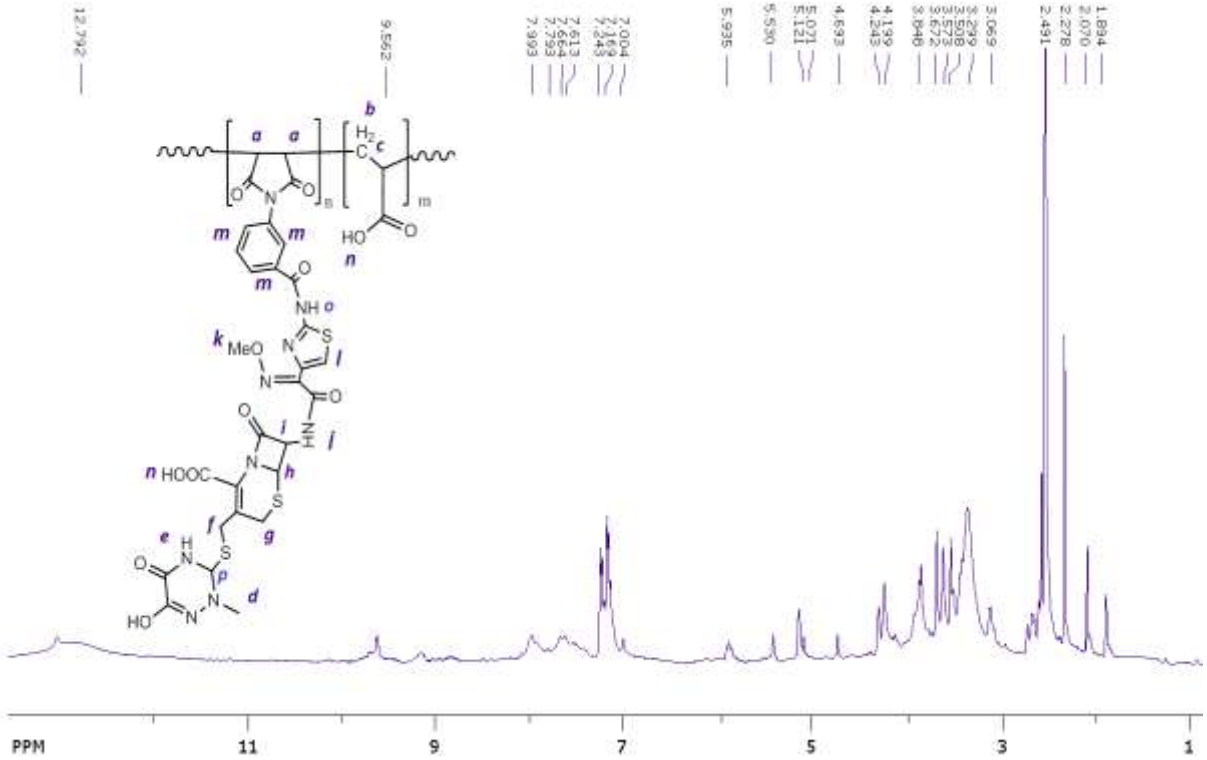

Figure 3.62: ^{1}H-NMR spectrum of compound [PM_{13}]

Heteropolymer [PM_{14}]: FT-IR spectrum (Figure 3.63) shows the following absorption bands; broad band at about ~3500-2250 cm^{-1} for (COOH) group of the Ampicillin drug and acrylic acid, 3292 cm^{-1} (-NH) stretching of amide groups, the aromatic (=C-H) at 3029 cm^{-1}, the aliphatic methyl, methylene and methine groups absorption bands at the range of 2961- 2858 cm^{-1}, characteristic absorption for beta-lactam carbonyl at 1772 cm^{-1}, the carbonyls of maleimide and acrylic acid appeared at 1713 cm^{-1}, amide groups stretching at 1652 cm^{-1}, the absorption bands at the range of 1588-1451 cm^{-1} assigned to (C=C) of aromatic rings, 1381 cm^{-1} for (C-N) vibration.

The ^{1}HNMR spectrum of Heteropolymer [PM_{14}] is showed in (Figure 3.64). The methyl groups signal of the drug appear at 1.538 ppm. the polysuccinimide-Co-acrylic acid backbone protons (-CH-, -CH_2-) appear at 2.083, 2.629 and 2.822 ppm, the beta lactam proton appeared as douplet signal centred 4.226 ppm (f, J = 23 Hz), the signal at 4.353 belong to thiazolidine (e) proton, the signal at 4.620 ppm assigned to the tertiary proton (k). The aromatic protons appear between 7.268 -8.247 ppm, the proton signals of amide appear at 9.379 and 10.587 ppm (h, i), the broad signal centred the chemical shift 12.148 ppm attributed to the carboxylic acid protons of the acrylic acid and drug moiety.

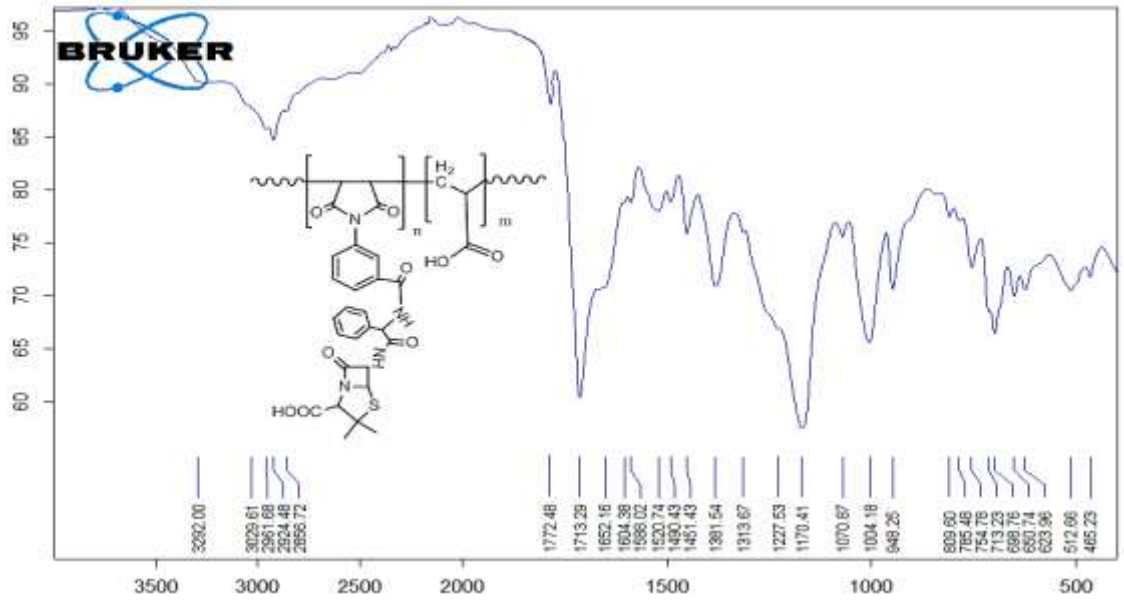

Figure 3.63: FT-IR spectrum of compound [PM_{14}]

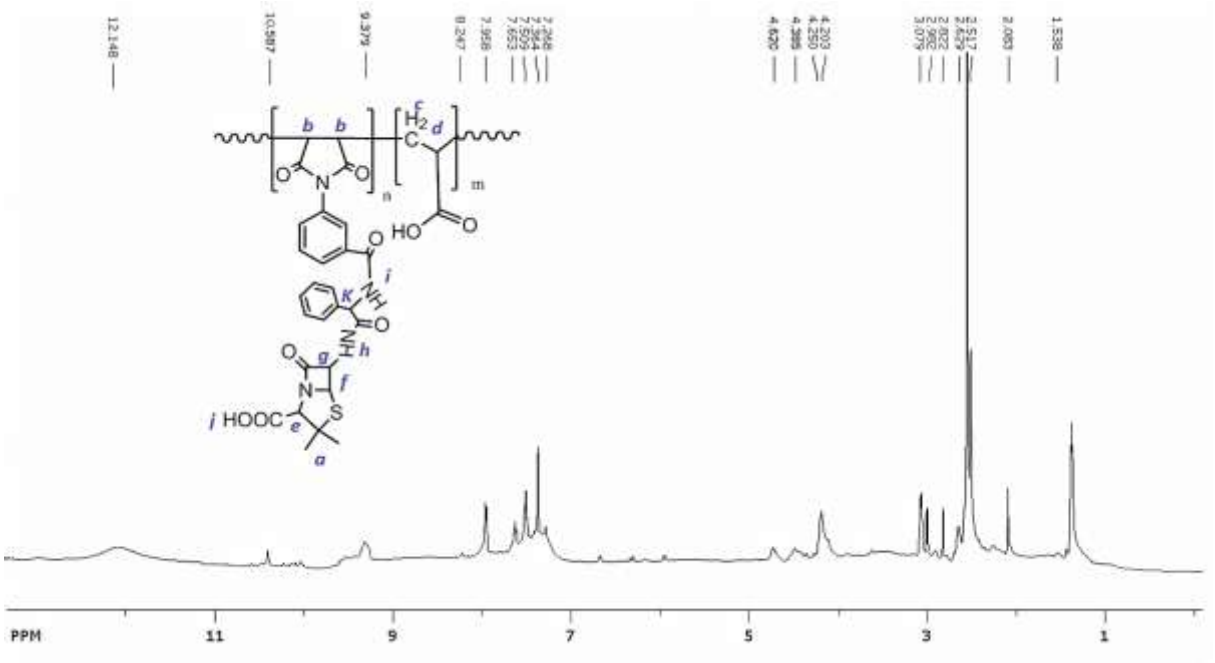

Figure 3.64: ^{1}H-NMR spectrum of compound [PM_{14}]

Heteropolymer [PM_{15}]: FT-IR spectrum (Figure 3.65) shows the following absorption bands; broad band at about ~3500-2250 cm^{-1} for (COOH) group of the Amoxicillin drug and acrylic acid, 3305 cm^{-1} belong to the phenolic O-H of Amoxicillin, 3200 and 3117 cm^{-1} (-NH) stretching of amide groups.

The aromatic (=C-H) at 3068 cm^{-1}, the aliphatic methyl, methylene and methine groups absorption bands at the range of 2974 and 2931 cm^{-1}, characteristic absorption for beta-lactam carbonyl at 1776 cm^{-1}, the carbonyls of maleimide and acrylic acid appeared at 1708 cm^{-1}, it may be overlapped with amide carbonyl groups vibration, the absorption bands at the range of 16012-1451 cm^{-1} assigned to (C=C) of aromatic rings, 1382 cm^{-1} for (C-N) stretching vibration and 1169 cm^{-1} assigned to (C-O) stretching vibration.

The ^{1}HNMR spectrum of Heteropolymer [PM_{15}], (Figure 3.66). The methyl groups signal of the drug appear at 1.539 ppm. The polysuccinimide-Co-acrylic acid backbone protons (-CH-, -CH_2-) appear at 2.060, 2.657 and 2.819 ppm, the signal at 3.956 ppm assigned to the tertiary proton (h). The two beta lactam protons appeared as douplet signals at 4.238 ppm (f, J = 21 Hz), and at 4.624 ppm (J = 23 Hz).

The aromatic protons appear between 7.216-8.201 ppm, the proton signals of amide appear at 9.374 and 10.039 ppm (g, i), the broad signal centred the chemical shift 12.549 ppm attributed to the carboxylic acid protons of the acrylic acid and drug moiety.

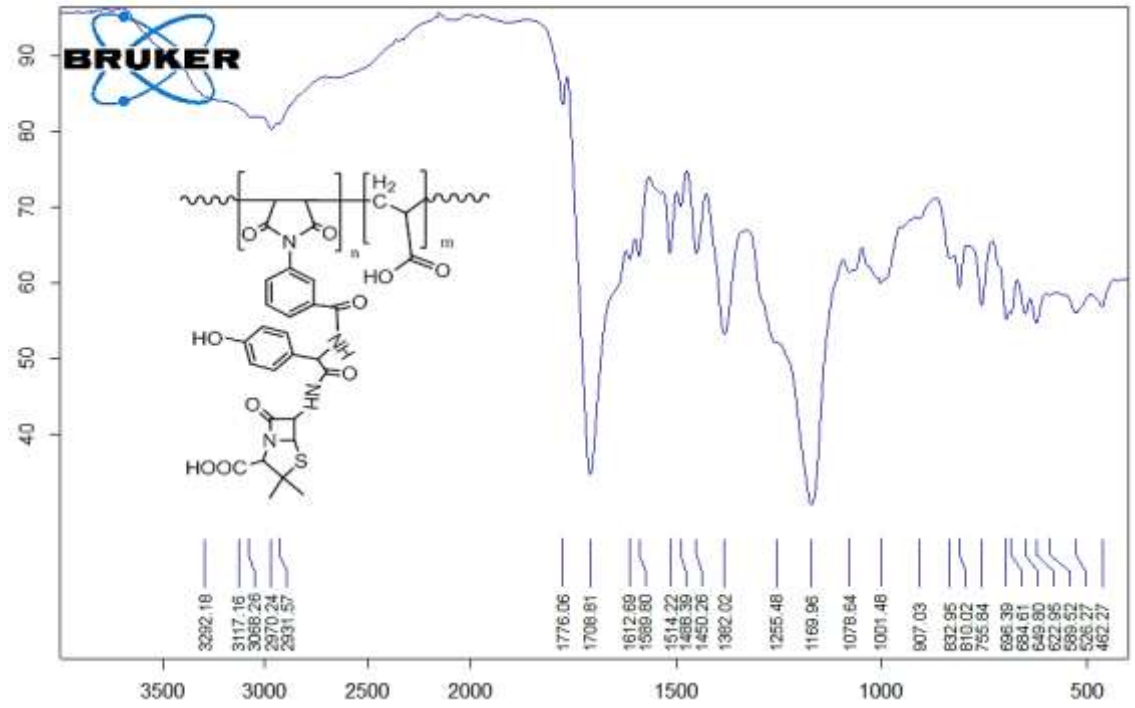

Figure 3.65: FT-IR spectrum of compound [PM_{15}]

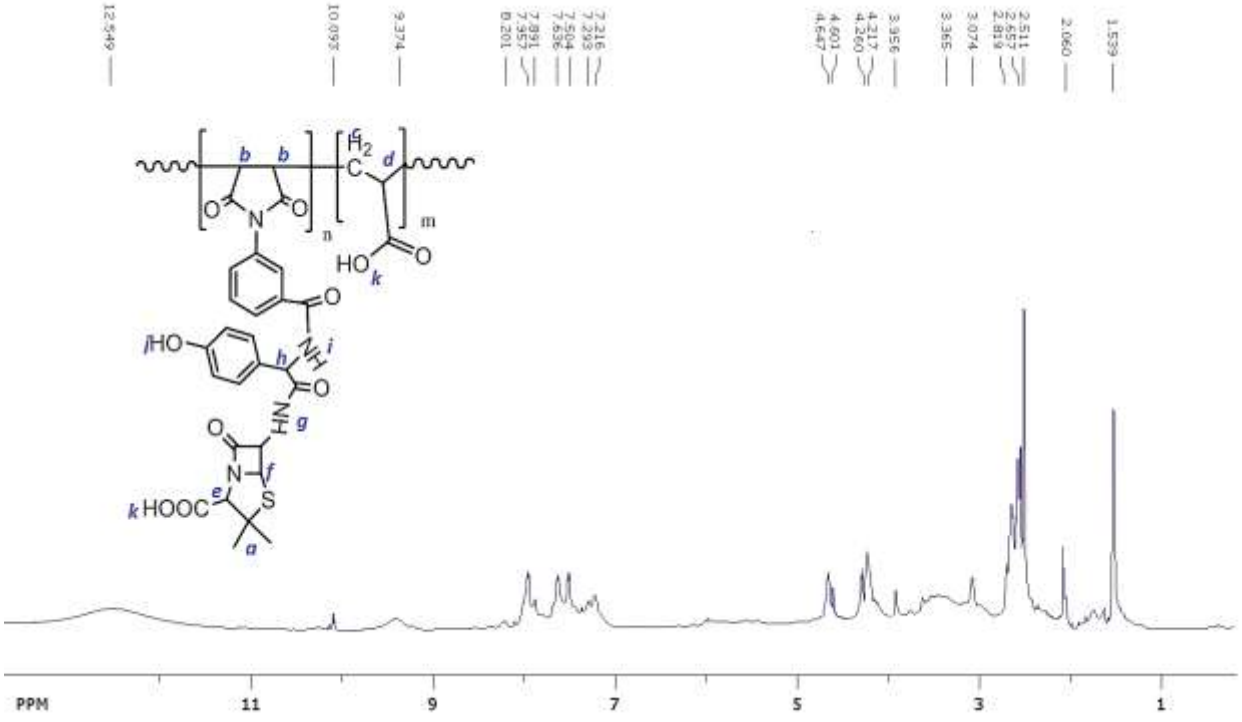

Figure 3.66: ^{1}H-NMR spectrum of compound [PM_{15}]

Heteropolymer [PM_{16}]: FT-IR spectrum (Figure 3.67) shows the following absorption bands:

The broad band within the range of 3500-2400 cm^{-1} belong to the carboxylic acid groups of the drug and acrylic acid, the bands at 3231 cm^{-1} belong to the (ArCO-NH-) of amide, the (=C-H) groups of aromatic rings appeared at 3065 cm^{-1}, and the aliphatic stretching of methyl, methine and methylene groups appeared at 2965 and 2932 cm^{-1}.

Furthermore, the carbonyl groups of beta-lactam in the spectrum appeared at 1762 cm^{-1}, the maleimide carbonyl groups appear at 1716 cm^{-1} may be overlapped with stretching of acrylic acid and amide carbonyls. The aromatic rings double bonds appeared at the range of 1589-1413 (C=C, aromatic), other bands includes 1380 cm^{-1} (C-N) stretching, 1171 cm^{-1} (C-O) stretching vibration.

The **^{1}HNMR** spectrum (Figure 3.68): included many chemical shifts for different protons as follow. The signals at 1.894 ppm assigned to methyl protons (a), the signals at 2.074, 2.238 and 2.626 ppm belong to the polysuccinimide-Co-acrylic acid backbone protons (c, d, e protons), the signal at 3.016 ppm (b protons), the beta-lactam (f, proton) douplet signal occur at 4.342 ppm (1H, J = 23Hz). The other doublet signal at about 5.021 ppm (, 1H, J =25 Hz) belong to the second beta-lactam (g, proton). Aromatic protons appeared as multiplet signals at the range of 7.314-7.984 ppm (m), the amide proton (h) appeared at 9.441 ppm and the carboxylic acid protons appeared as broad signal at about 13.111 ppm belong to the carboxylic acid protons (j).

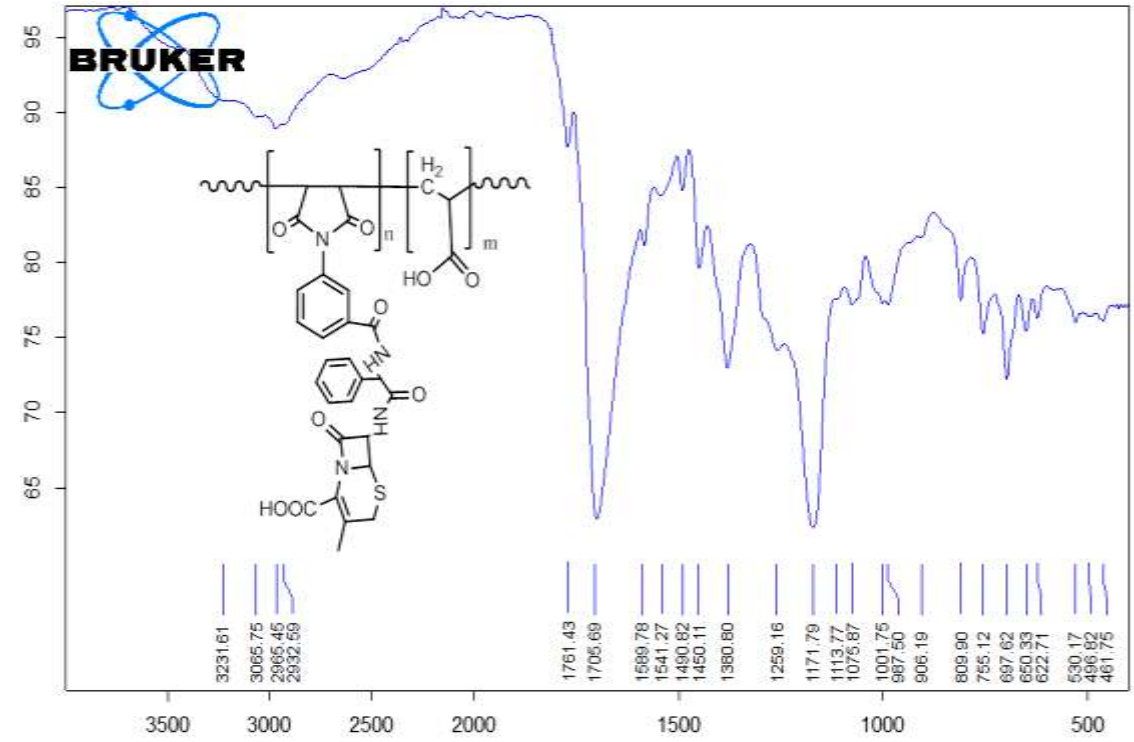

Figure 3.67: FT-IR spectrum of compound [PM_{16}]

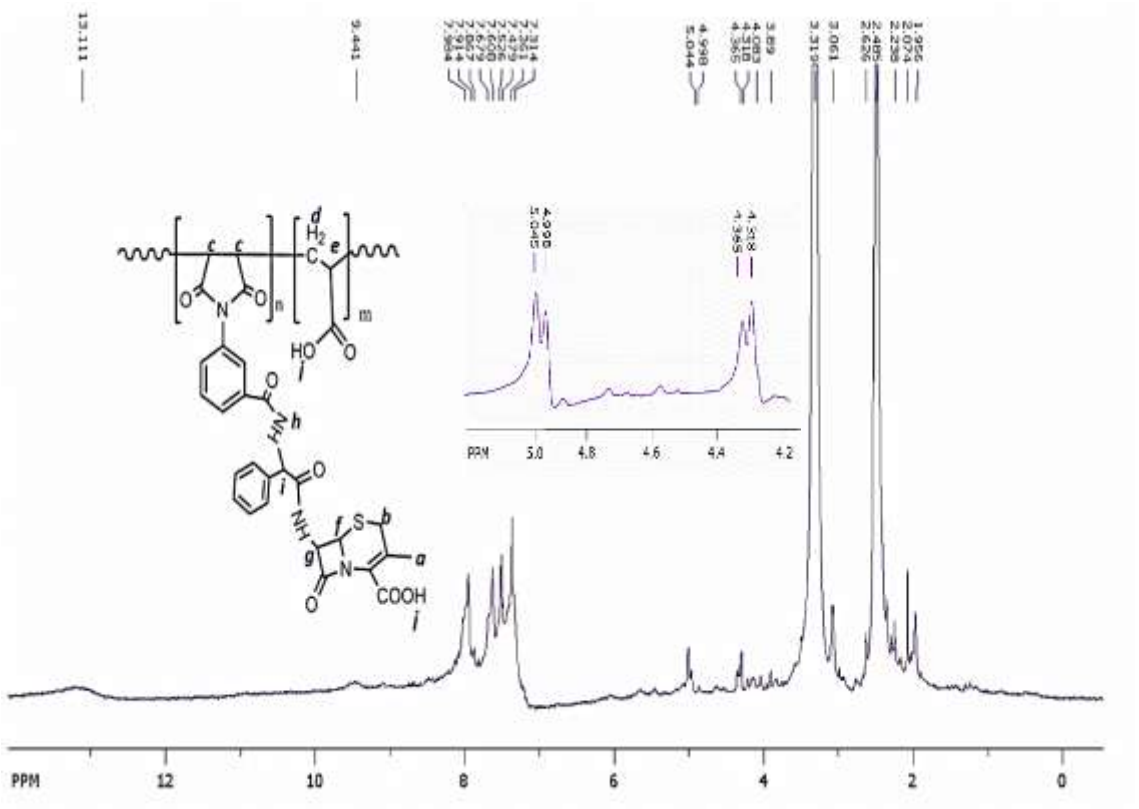

Figure 3.68: ^{1}H-NMR spectrum of compound [PM_{16}]

Heteropolymer [PM_{17}]: The FT-IR analysis of the prepared polymer was demonstrated in (Figure. 3.69). The FT-IR exhibited broad absorption band at 3473-2500 cm^{-1} corresponding to carboxylic acid hydroxyl group of the Ciprofloxacin drug and acrylic acid. The aromatic C-H vibration band occurring at 3063 cm^{-1} and aliphatic C-H vibration bands at 2929 and 2836 cm^{-1} was revealed the presence of different aliphatic hydrogens. The vibration of C=O stretch bands at 1716 cm^{-1}, 1686 cm^{-1}, 1626 cm^{-1}, showed the existence of maleimide, carboxylic acid and amide carbonyls respectively. The frequency of bands occurring at 1543 -1466 cm^{-1}, 1382 cm^{-1} (C-N stretching), 1165 cm^{-1} corresponding to C=C of aromatic rings, C-N and C-F[(109)] stretching vibrations respectively.

^{1}HNMR spectrum of the Heteropolymer [PM_{17}] shows varied peak values with the presence of different protons (Figure 3.70): the triplet signal centered 1.206 ppm belong to methylene (a) of cyclopropyl ring (J = 7 Hz)[(140)], the signals at 2.091, 2.610 and 3.611 ppm indicate the presence of different aliphatic protons for poly succinimide-Co-acrylic acid backbone (c, d, e protons), the quintet signal centered 3.059 ppm attributed to cyclopropyl tertiary (b) proton (J = 7 Hz)[(140)], the six membered piprazine proton appeared at 3.247 and 3.453 ppm (g, f).

The aromatic protons accruing at the range of 7.286-8.056 ppm protons, the signal at 8.462 ppm referred to the vinylic (h) proton. The carboxylic acid protons appeared as to signals (i and k); broad signal at 12.753 ppm for acrylic acid and at 13.573 ppm may be due to the intra-hydrogen bonding in quinolinone ring.

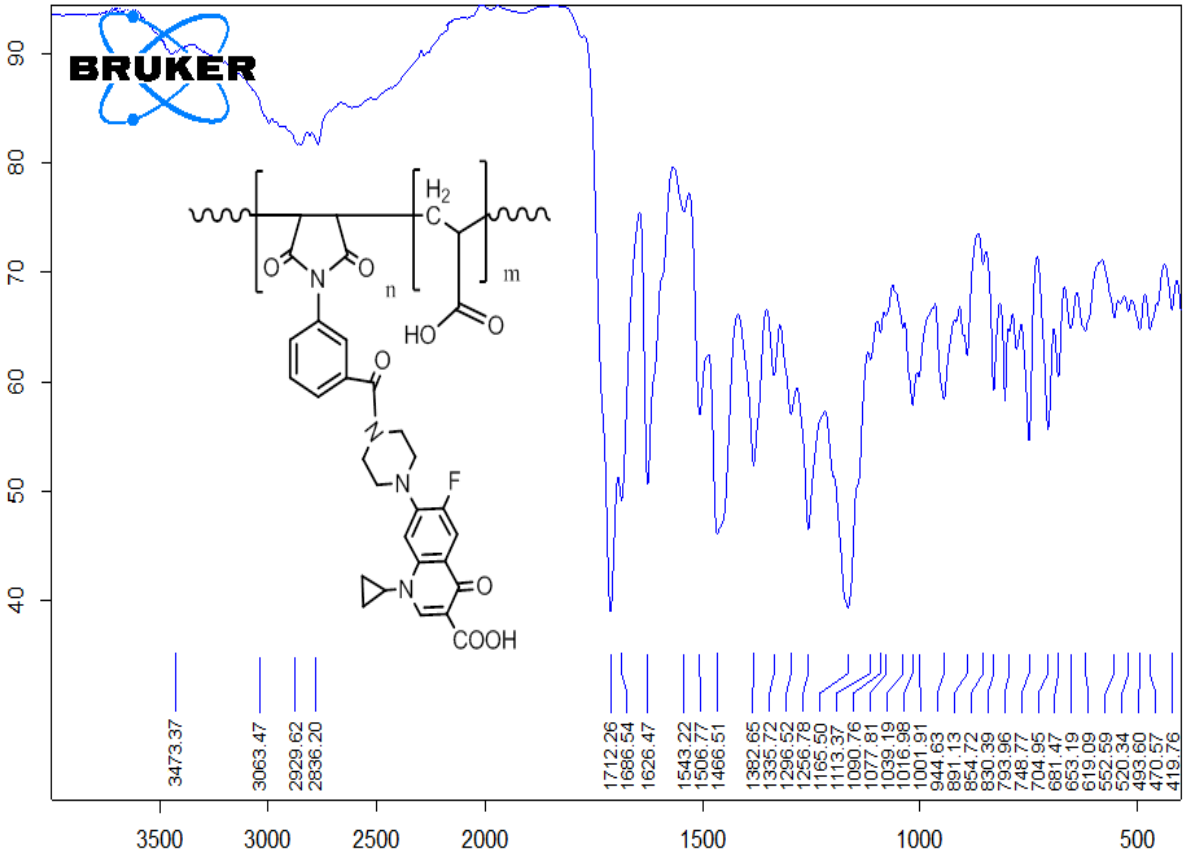

Figure 3.69: FT-IR spectrum of compound [PM_{17}]

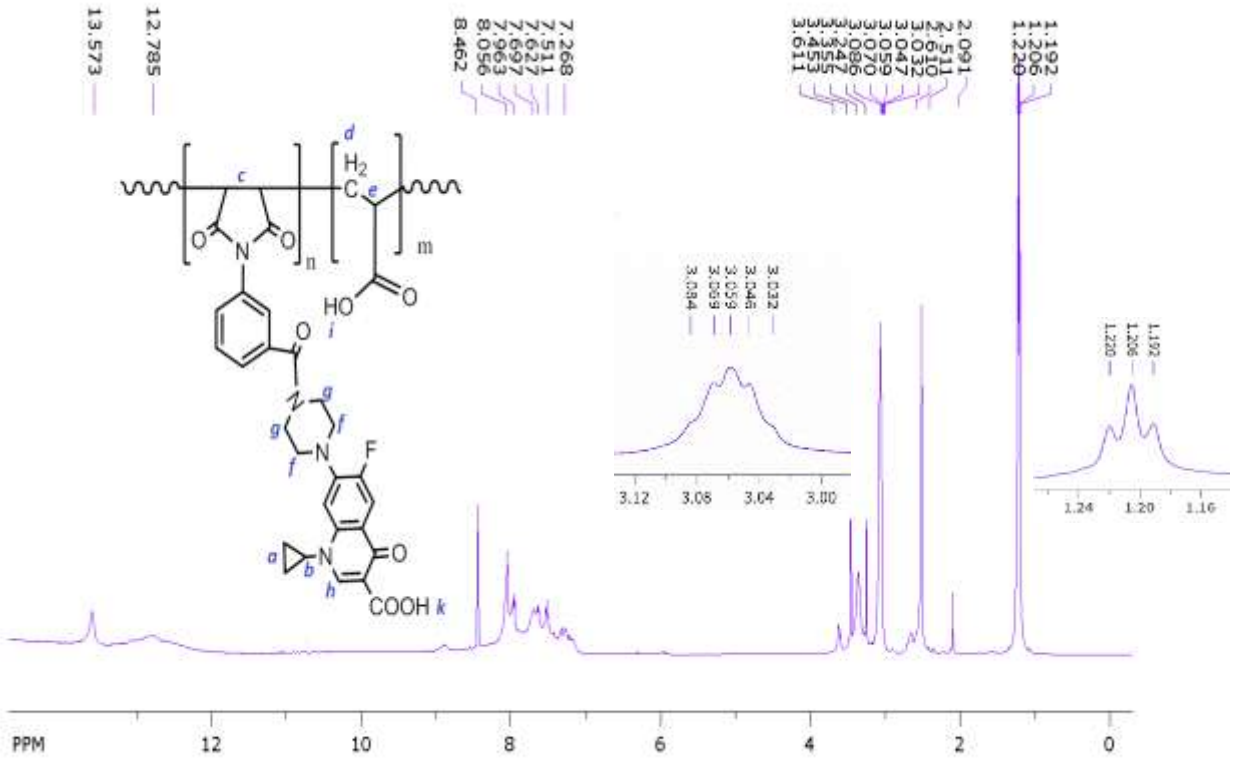

Figure 3.70: ^{1}H-NMR spectrum of compound [PM_{17}]

Heteropolymer [PM_{18}]: FT-IR spectra of heteropolymer [PM_{18}] showed varied peak values with the presence of different functional groups (Figure 3. 71). The broad band between 3400-2496 cm^{-1} belong to carboxylic acid hydroxyl group of acrylic acid, the phenolic –OH occurred at 3303 cm^{-1},

The =C–H stretching vibration band corresponding to aromatic rings showed its occurrence at 3076 cm^{-1}, while the aliphatic C-H bonds occurred at 2978 and 2882 cm^{-1}. The wave number 1718 cm^{-1} was assigned as characteristic absorption of imide and carboxylic acid carbonyls, the C=C of aromatic ring appeared at the range of 1604-1475 cm^{-1}, the C-N bond stretching occurred at 1396 cm^{-1}.

^{1}HNMR chemical shifts of Heteropolymer [PM_{18}] were viewed in (Figure 3.72). The multiple signals at 1.379, 2.060, 2.580, and 2.652 ppm revealed the methylene and methine (b, c, d, e) protons of polysuccinimide-Co-acrylic acid backbone, the singlet signal at 3.065 ppm belongs to the acetyl methyl protons (a). The signals of aromatic protons occur at the range of 7.231-7.997 ppm, the phenolic -OH proton (f) occurred at 8.860 ppm and the acrylic acid proton appeared at 12.634 ppm.

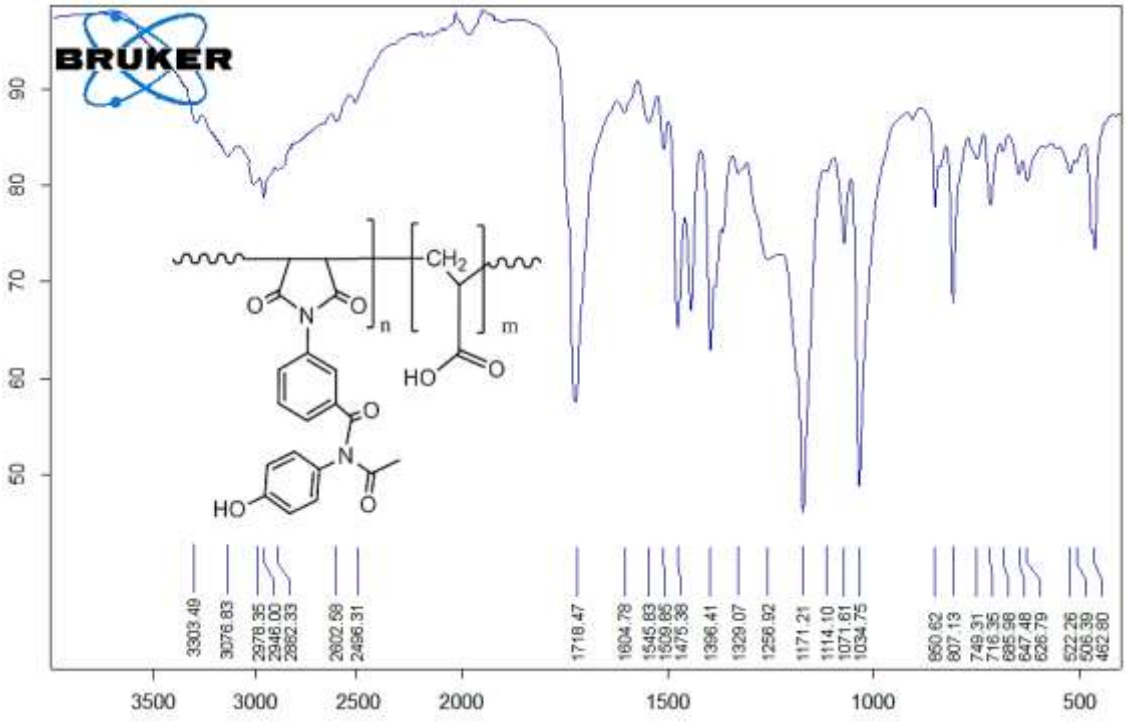

Figure 3.71: FT-IR spectrum of compound [PM_{18}]

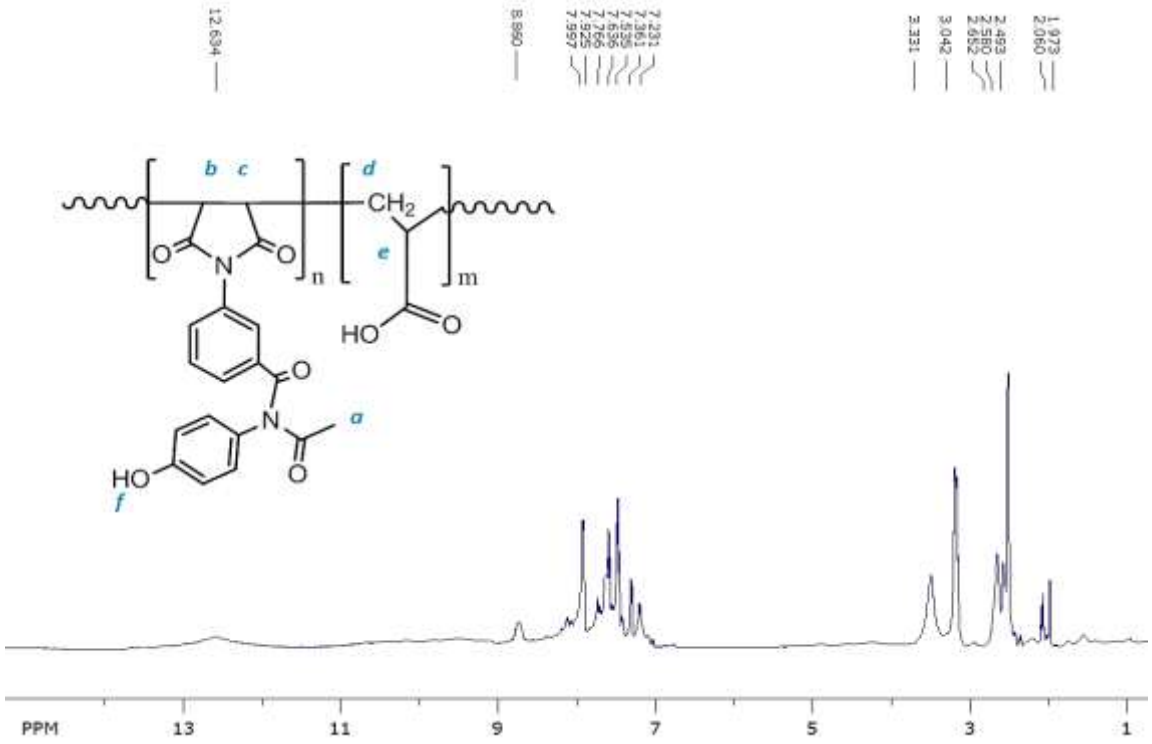

Figure 3.72: ^{1}H-NMR spectrum of compound [PM_{18}]

Heteropolymer [PM_{19}]: The FT-IR peak values for heteropolymer [PM_{19}] were displayed in Figure 3.73. The broad band occurring at 3500-2534 cm^{-1} due to the stretching of acrylic acid O–H, the two bands at 3471 and 3367 cm^{-1} due to the aromatic amino group in the drug structure. The =C–H stretching vibration band corresponding to aromatic rings showed its occurrence at 3080 cm^{-1}, while the aliphatic C-H bonds occurred at 2934, 2873, and 2811 cm^{-1}. The wave numbers 1718 and 1627 cm^{-1}, was assigned as characteristic absorption of carbonyl groups of imide, carboxylic acid and amide respectively. The C=N and C=C of aromatic rings appeared at the range of 1580, 1514 and 1493 cm^{-1}, the C-N bond stretching occurred at 1385 cm^{-1}, 1315 and 1154 cm^{-1} belong to the SO_2 group and the strong band at 569 cm^{-1} may be due to (C-SO_2-N) vibration.

^{1}HNMR spectrum of the Heteropolymer [PM_{19}] showed varied peak values with the presence of different protons (Figure 3.74): the signals at 2.173, 2.278, 2,622 and 2.676 ppm indicate the presence of different aliphatic protons for poly succinimide-Co-acrylic acid backbone (a, b, c, d protons),

the signal centered 5.989 ppm attributed to the amino group protons (e). The aromatic protons accruing at the range of 7.001- 8.066 ppm protons in addition to the signal at 8.473 ppm referred to the imine like protons (g) in the pyrimidine ring. The carboxylic acid protons appeared at 12.574 ppm for acrylic acid.

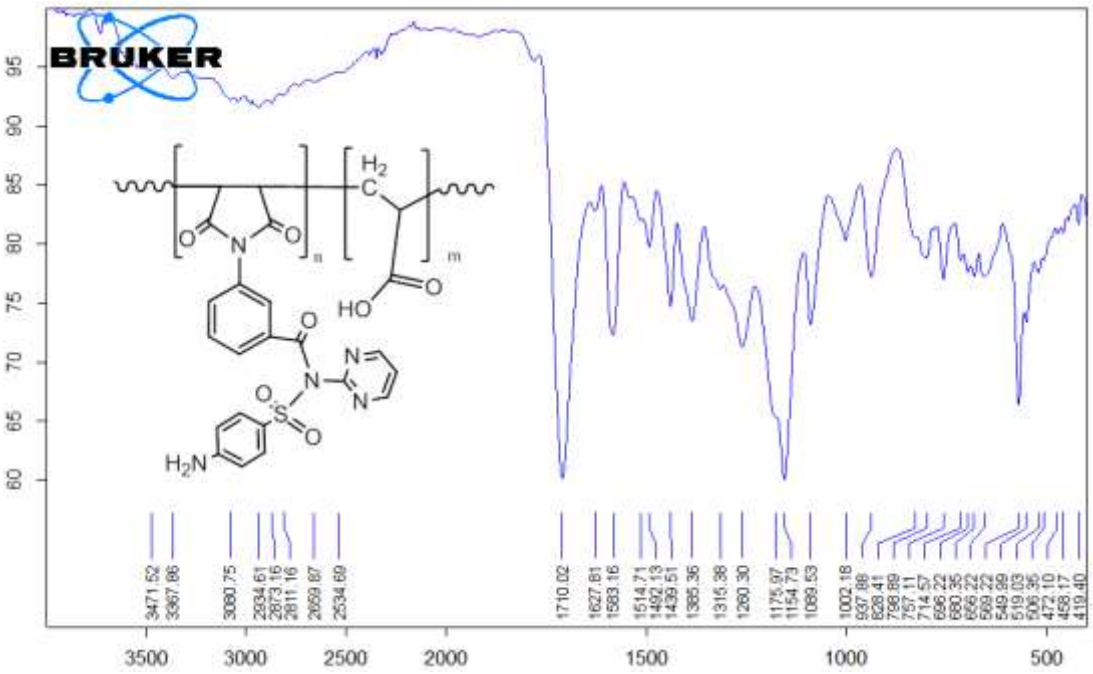

Figure 3.73: FT-IR spectrum of compound [PM_{19}]

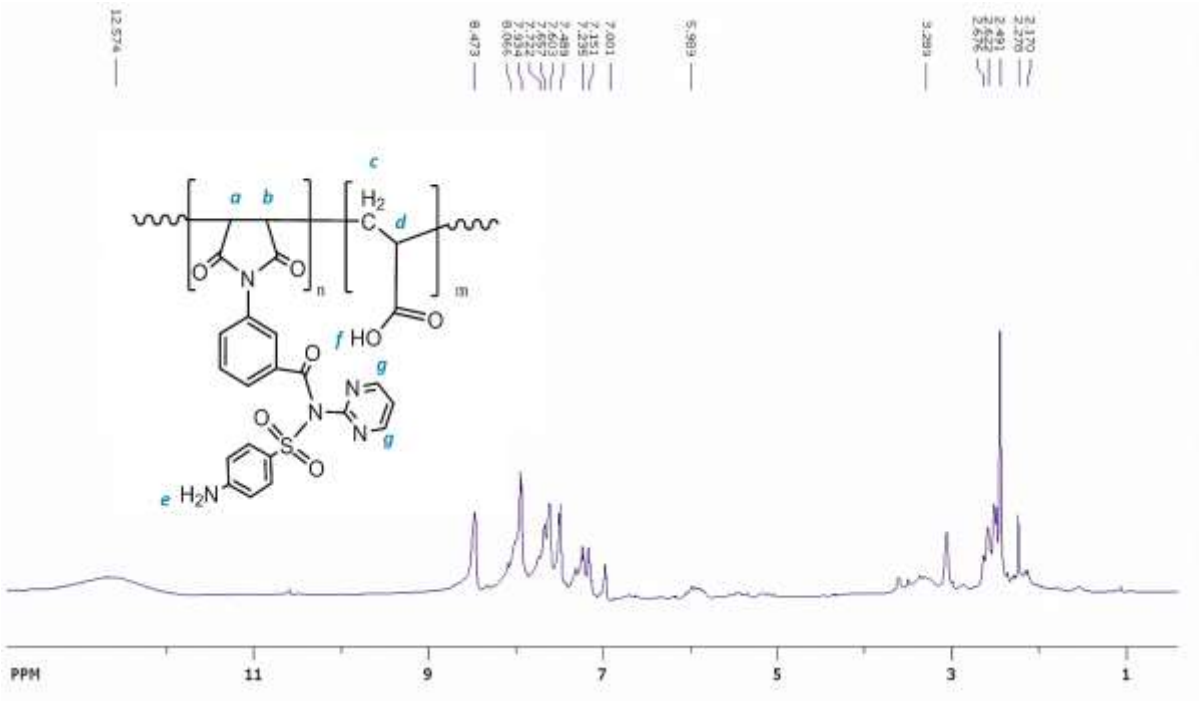

Figure 3.74: ^{1}H-NMR spectrum of compound [PM_{19}]

Heteropolymer [PM_{20}]: The FT-IR analysis result of Heteropolymer [PM20] was demonstrated in Figure 3.75. The FT-IR spectrum exhibited broad absorption band at 3483-2488 cm^{-1} with O–H stretching of acrylic acid. The two weak absorption bands 3269 and 3214 cm^{-1} assigned to -NH stretching of amide groups. The aromatic C-H absorption bands occurred at 3077 and 3059 cm^{-1} and the aliphatic C-H vibration of the polymer backbone appeared at 2992, 2874 and 2774 cm^{-1}.

The wave numbers 1699 cm^{-1}, 1654 cm^{-1} were assigned as characteristic absorption of imide ring (may be overlapped with carboxylic carbonyl) and amide groups. Medium C=C stretching vibrations were located at 1603 cm^{-1}, 1535 cm^{-1} and 1512 cm^{-1} for the aromatic rings and the medium absorption at 1393 cm^{-1} due to C-N stretching.

^{1}HNMR spectrum of the Heteropolymer [PM_{20}] showed varied peak values with the presence of different protons (Figure 3.76): the signals at 2.083, 2.282, 2,643, 2.815 and 2.857 ppm indicate the presence of different aliphatic protons for poly succinimide-Co-acrylic acid backbone (a, b, c, d protons), The aromatic protons accruing at the range of 7.438-8.748 ppm protons in addition to the signal at 8.748 ppm referred to the imine like protons (e) in the pyridine ring. The singlet signal at 10.546 ppm belongs to the N-H proton (f) and broad peak appeared at 12.690 ppm for acrylic acid proton (g).

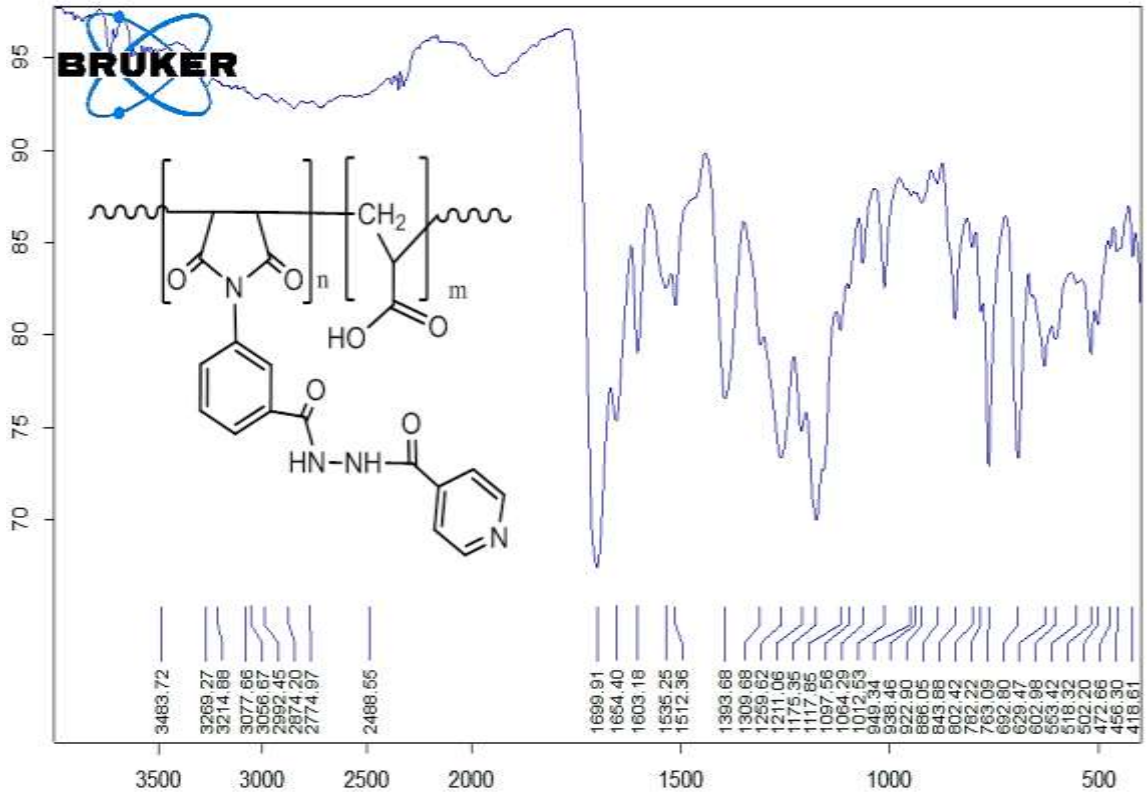

Figure 3.75: FT-IR spectrum of compound [PM_{20}]

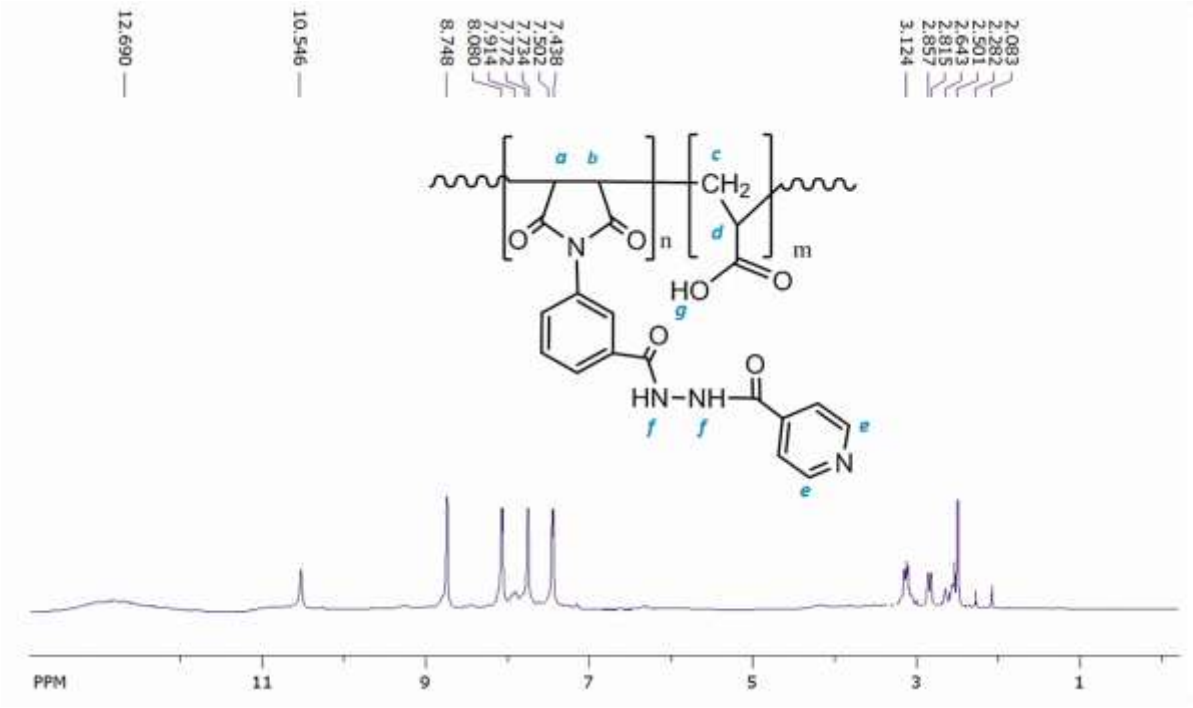

Figure 3.76: ^{1}H-NMR spectrum of compound [PM_{20}]

Heteropolymer [PM_{21}]: FT-IR spectra of heteropolymer [PM_{21}] showed varied peak values with the presence of different functional groups (Figure 3.77). The broad band between 3500-2502 cm^{-1} belong to carboxylic acid

hydroxyl group of acrylic acid, the amide N–H occurred at 3337 cm^{-1}, The =C–H stretching vibration band corresponding to aromatic rings and olefin showed its occurrence at 3064 and 3023 cm^{-1}, while the aliphatic C-H bonds occurred at 2916 and 2883 cm^{-1}. The wave numbers 1708 and 1649 cm^{-1} were assigned as characteristic absorption of imide (overlapped with carboxylic acid carbonyl absorption) and amid carbonyl vibration, the C=C of aromatic ring appeared at the range of 1602-14604 cm^{-1}, the C-N bond stretching occurred at 1381 cm^{-1}.

^{1}HNMR chemical shifts of Heteropolymer [PM_{21}] were viewed in Figure 3.78. The multiple signals at 2.084, 2.299 and 2.690 ppm revealed the methylene and methine (a, b, c, and d) protons of polysuccinimide-Co-acrylic acid backbone. The olefinic protons (h) appeared at 6.993 ppm while aromatic protons accruing at the range of 7.148-8.099 ppm protons in addition to the signal at 10.250 ppm referred to the amide N-H proton (e) in the pyridine ring. The singlet signal at 10.546 ppm belongs to the N-H proton (f) and broad peak appeared at 12.255 ppm for acrylic acid proton (g).

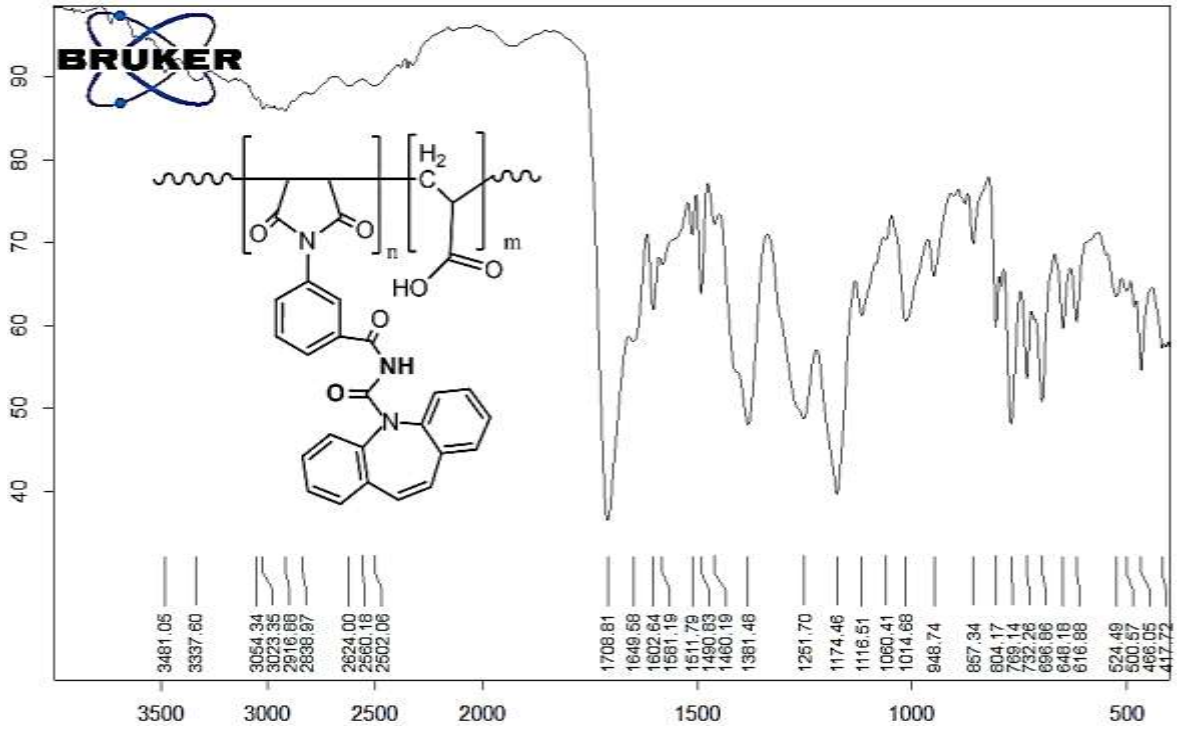

Figure 3.77: FT-IR spectrum of compound [PM_{21}]

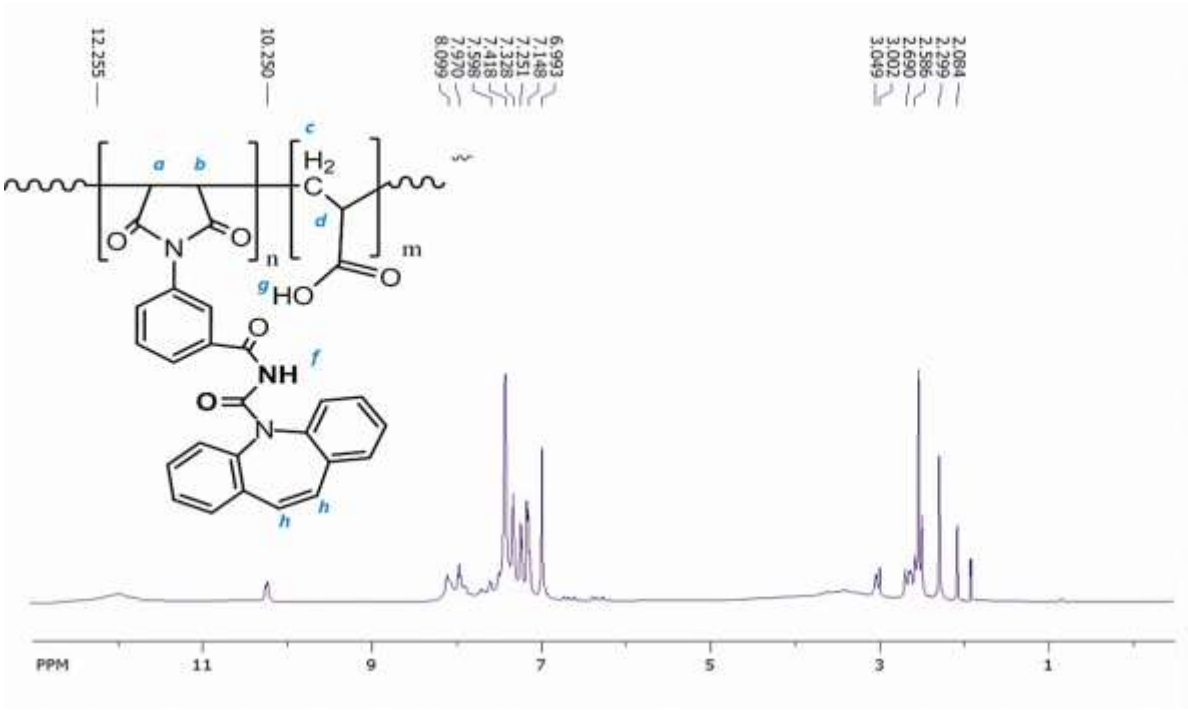

Figure 3.78: ^{1}H-NMR spectrum of compound [PM_{21}]

Heteropolymer [PM_{22}]: FT-IR spectra of heteropolymer [PM_{22}] showed varied peak values with the presence of different functional groups (Figure 3.79). The broad band between 3467-2531 cm^{-1} belong to carboxylic hydroxyl group of acrylic acid, the amide N–H occurred at 3364 cm^{-1}, The =C–H stretching vibration band corresponding to aromatic rings appeared at 3066 cm^{-1}, while the aliphatic C-H bonds occurred at 2979 and 2963 cm^{-1}. The carbonyl groups of imide ring appeared at 1711 cm^{-1} may be overlapped with stretching vibration of acrylic acid carbonyl. The amide carbonyl occurred at 1649 cm^{-1}, C=C bonds of aromatic ring appeared at the range of 1586-1485 cm^{-1}, the C-N bond stretching occurred at 1382 cm^{-1}, and the band at 1180 cm^{-1} belongs to C-O stretching of ether methoxy group, and the band at 625 cm^{-1} due to C-Cl bond stretching).

^{1}HNMR chemical shifts of Heteropolymer [PM_{22}] were viewed in Figure 3.80. Triplet signal centered 1.199 ppm (J= 7 Hz) due to methyl group protons (a), multiple signals at 1.995, 2.091, and 2.348 ppm revealed the methylene and methine (d, e, f, g) protons of polysuccinimide-Co-acrylic acid backbone, quartet signal at about 3.078 ppm (J= 7 Hz) due to methylene (b)

adjacent to methyl groups. The triplet signal at about 3.874 ppm (J= 9 Hz) belongs to ethyl group protons (c), and the methoxy group protons (k) occurred at 4.215 ppm.

The chemical shifts of aromatic protons were accruing between 7.457-8.608 ppm, the two signals at 10.181 and 10.366 ppm referred to the two amide N-H protons (h and i), and the broad singlet signal at 12.086 ppm for acrylic acid proton (j).

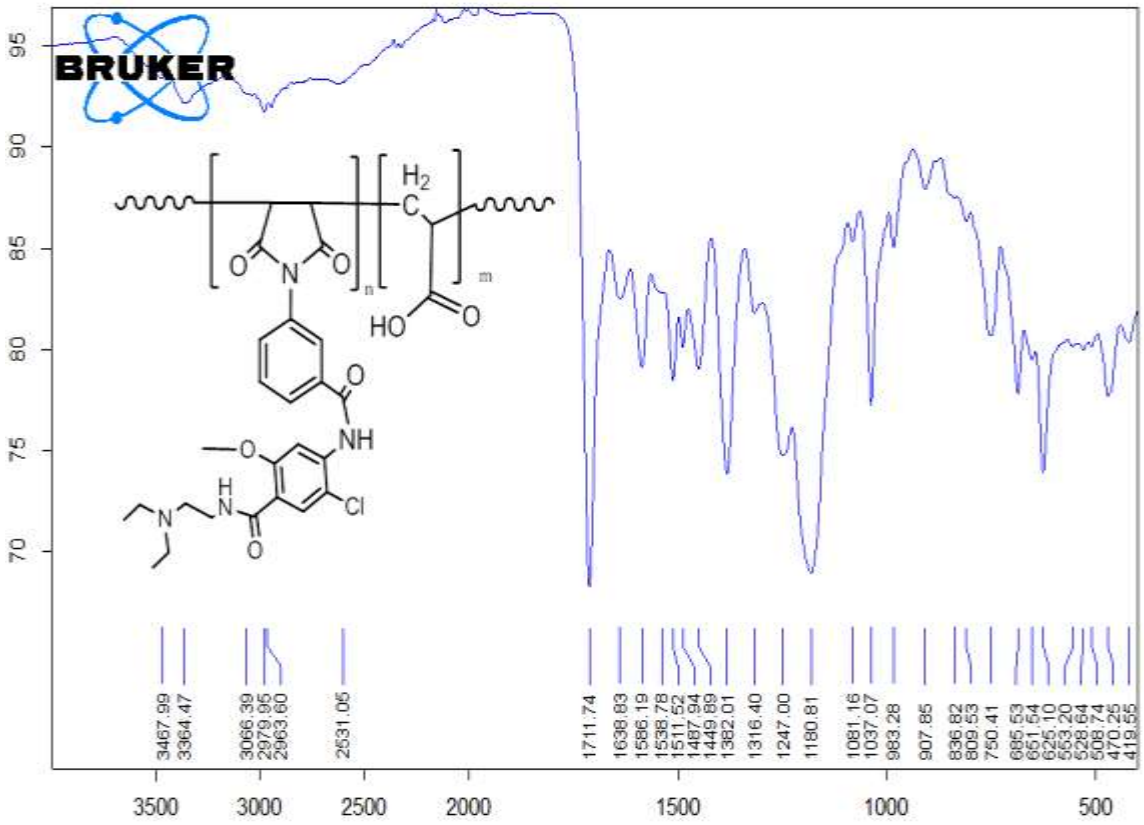

Figure 3.79: FT-IR spectrum of compound [PM_{22}]

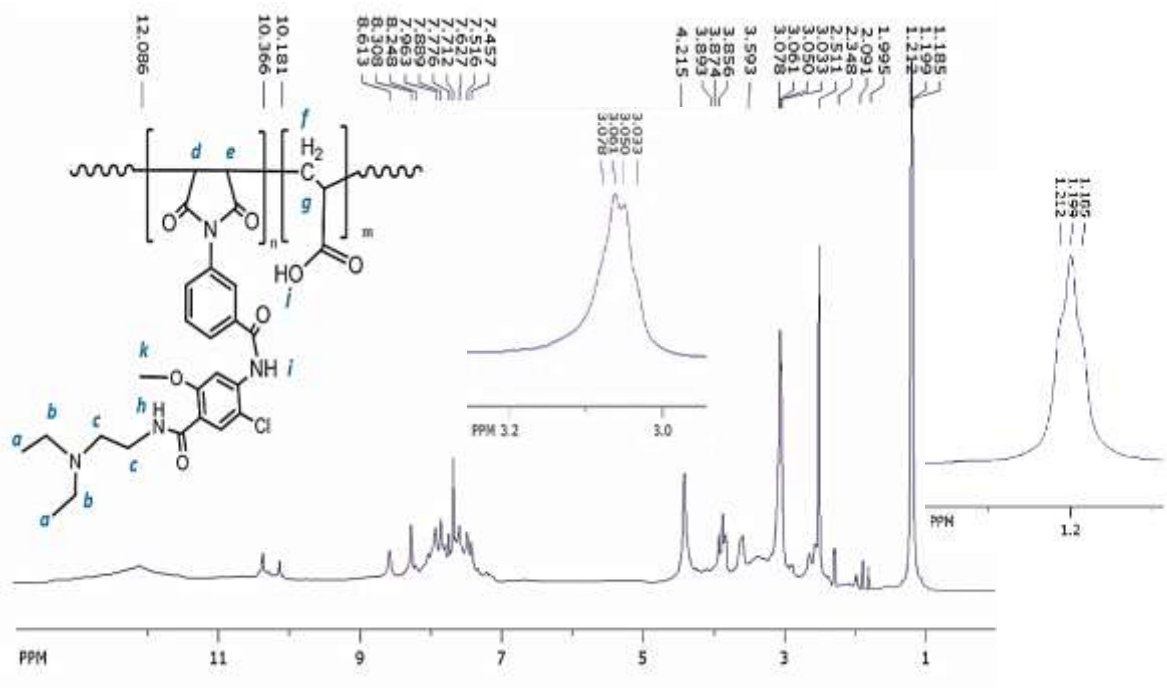

Figure 3.80: ^{1}H-NMR spectrum of compound [PM_{22}]

3.10. Swelling of the Polymers

Hydrogels are chemically cross-linked organic polymer gels. Such gels expand but do not dissolve in excellent solvents, i.e. solvents with polymer affinity. When the excellent solvent is water, the gel is referred to as a hydrogel. Hydrogel can be cross-linked via covalent bonds, as in most synthetic gels, or by Van der Waal's forces and hydrogen bonds[(139)]. Polymerization or copolymerization of hydrophilic monomer(s) can generate homopolymer or co-polymer hydrogels, respectively.

Gravimetric measurements were used to determine dynamic swelling. All polymers showing an acceptable swelling behaviors and does not dissociate until the fifth day, the swilling diagrams were listed in Figures (3. 81-3.84). After this period some polymers start to suspended or dissoluted and sometimes they permeate through the filter paper. Tables (3.10-3.12) represent the swelling ratio of homopolymers at five consecutive hours and days.

Table 3.9: Swelling ratio (%) of Homopolymers [PM1-PM11]

Time	Swelling Ratio %					
	Types of polymers					
Hour	PM1	PM2	PM3	PM4	PM5	PM6
1	2	6	3.4	1	0.4	1.2
2	3.6	7.4	4.2	3.4	6.2	3.8
3	5	8.3	6	4.3	7.4	8.2
4	6.6	9.3	8.4	10.2	8	8.4
5	8.1	10	8.7	10.6	9.9	9.2
Day						
1	9.4	12.2	9.6	12.3	10.2	9.8
2	10.87	12.78	9.21	12.27	12.78	10.62
3	12.19	13.03	10.61	12.75	13.10	11.83
4	12.62	12.79	12.0	13.06	12.14	12.71
5	12.38	12.77	10.6	13.02	12.21	12.55
Time	**Swelling Ratio %**					
	Types of polymers					
Hour	PM7	PM8	PM9	PM10	PM11	
1	3.6	6.2	1.4	0	1	
2	4.2	7.4	3.4	0.6	1.8	
3	6.3	8.2	5.4	3.2	2.4	
4	8	9.4	7	5	3.6	
5	8.6	10.2	7.8	6.1	4.4	
Day						
1	10	12.2	9.4	7.4	6.1	
2	10.6	12.78	10.4	8.2	6.8	
3	12	13.03	10.8	10.4	8	
4	12.2	12.79	11.4	11.6	8.4	
5	11.8	12.77	10	11.2	8.6	

Table 3.10: Swelling ratio (%) of Homopolymers [PM15-PM20]

Time	Swelling Ratio %					
	Types of polymers					
Hour	PM12	PM13	PM14	PM15	PM16	PM17
1	0.6	2	1.4	3.6	0.4	0.8
2	2.2	1.2	2.4	4.1	1.2	1.8
3	4.2	3.6	3.6	6.2	4.2	3.8
4	4.8	4.6	4.2	8.4	5	5
5	6	5.4	6.6	8.7	6.2	7.2
Day						
1	8.2	11	8.4	9.8	7.6	9
2	8.8	12.4	9.6	10.8	8.4	9.6
3	6	12.6	10.8	10.61	10.2	11
4	-	11.8	12	10.61	12.4	12
5	-	12	11.6	10.61	12.6	12

Table 3.11: Swelling ratio (%) of Heteropolymers [PM18-PM22]

Time	Swelling Ratio %				
	Types of polymers				
Hour	PM18	PM19	PM20	PM21	PM22
1	1.4	0	1.6	0	1
2	2.2	2	3.4	0	1.2
3	4.4	4.4	4.3	1	2.2
4	5.8	7	6.2	1.8	3.3
5	8	9	8.6	3.6	4.4
Day					
1	9.8	9.6	10.2	6	7.2
2	10.4	10	12.27	8	8
3	10.6	11	12.45	3.4	9.4
4	9.6	10.4	13.06	3.6	9.2
5	9.2	10	13.02	3.2	9

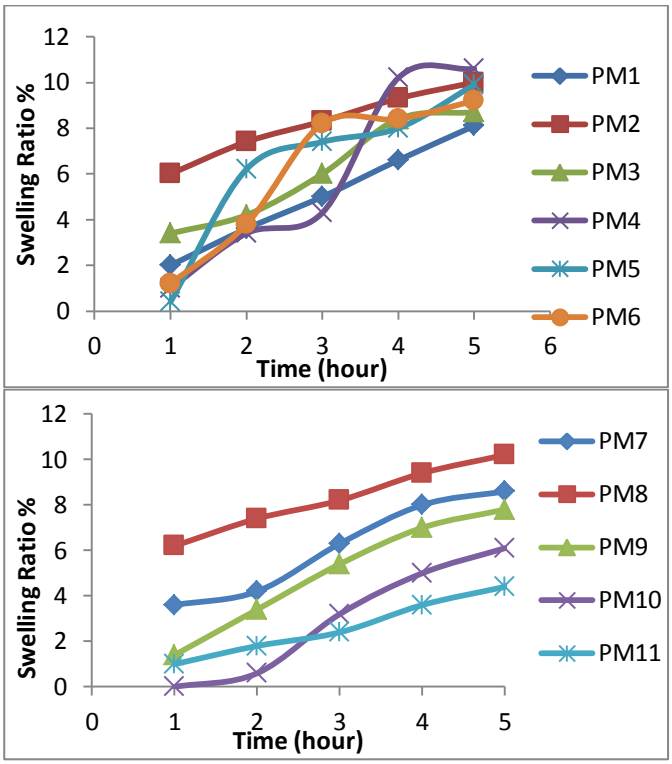

Figure 3.81: Swelling diagram of Homopolymers (PM_1-PM_{11}) in hours

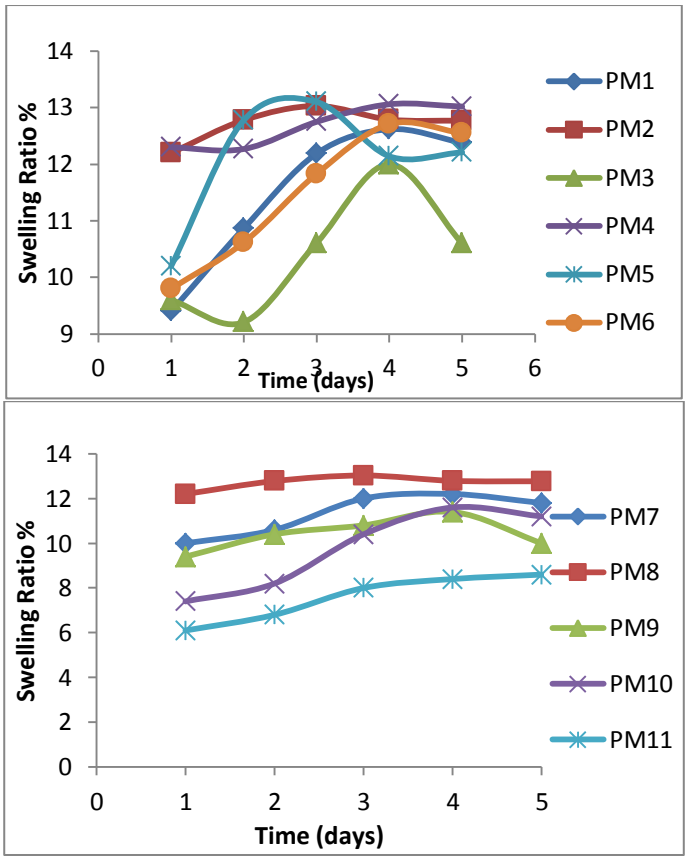

Figure 3-82: Swelling diagram of Homopolymers (PM_1-PM_{11}) in days

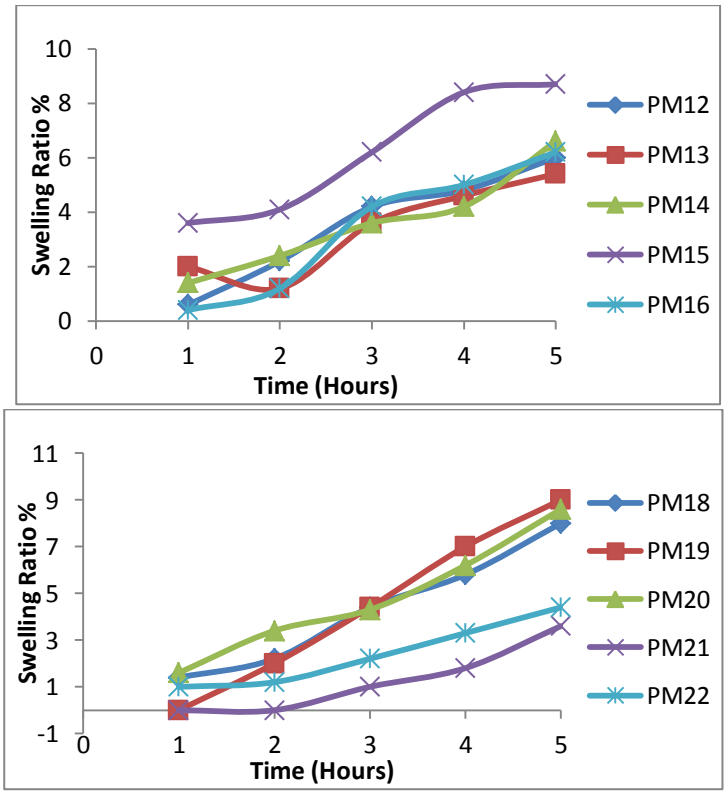

Figure 3-83: Swelling diagram of Homopolymers (PM_{18}-PM_{22}) in Hours

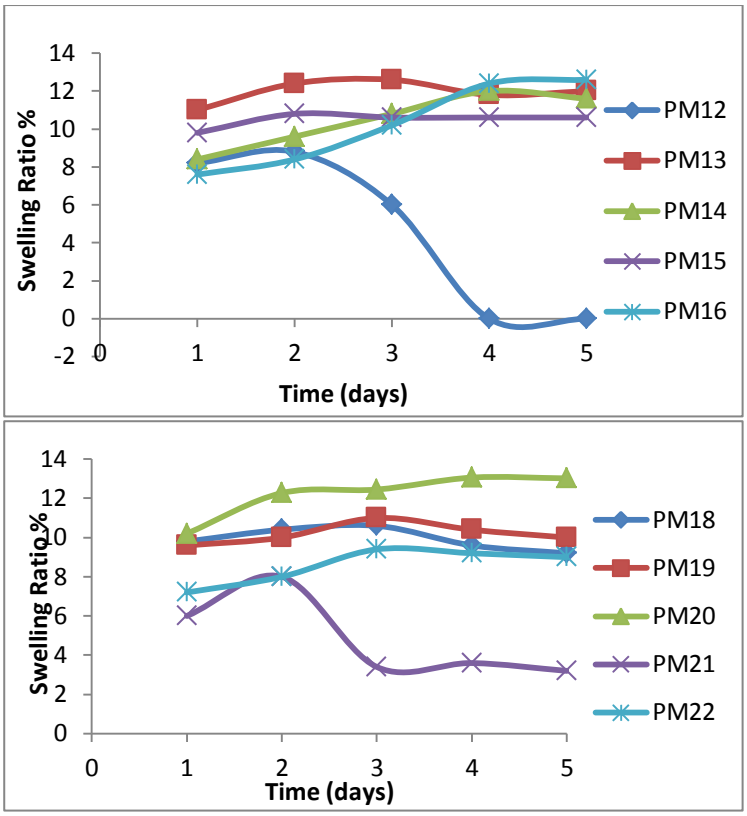

Figure 3-84: Swelling diagram of Homopolymers (PM_{12}-PM_{22}) in days

3.11. Drug Release

When a medication is taken in the usual method, such as by pill or injection, plasma drug levels frequently fluctuate between too high and too low. To keep medication levels in the effective range, scientists have devised a number of drug release optimization methods. The process by which drug solutes migrate from their original position in the polymeric system to the polymer's outer surface and ultimately to the release medium is referred to as "drug release" [(140)]. When plotting the absorption versus time, we get drug release diagrams as in the (Figures 3.85-3.90), as a pharmaceutical unit in the hydrolysis process, the Drug release in the basic environment was faster than the acid.

Table 3.12: Release of drug of the polymers [PM1-PM6] at pH=2

Time	Absorbance of polymers / λmax at pH=2					
Hour	PM1/ 332 nm	PM2/ 314 nm	PM3/ 331 nm	PM4/ 314 nm	PM5/ 306 nm	PM6/ 308 nm
1	0.123	0.95	0.189	0.535	0.09	0.125
2	0.131	1.025	0.211	0.871	0.150	0.421
3	0.145	1.153	0.315	0.902	0.178	0.543
4	0.187	1.254	0.347	1.103	0.190	0.643
5	0.192	1.305	0.362	1.184	0.211	0.669
Day						
1	0.22	1.362	0.561	1.197	0.333	1.19
2	0.324	1.43	0.753	1.271	0.46	1.423
3	0.405	1.524	0.904	1.324	0.618	1.76
4	0.711	1.871	1.54	1.723	1.084	1.897
5	1.147	1.957	1.772	1.876	1.454	2.023
6	1.135	1.95	1.781	1.802	1.469	2.013

Table 3.13: Release of drug of the polymers [PM7-PM11] at pH=2

Time	Absorbance of polymers / λmax at pH=2				
Hour	PM7/ 290 nm	PM8/ 330 nm	PM9/ 306 nm	PM10/ 306 nm	PM11/ 322 nm
1	0.251	0.174	0.118	0.08	0.112
2	0.367	0.641	0.131	0.177	0.217
3	0.551	0.751	0.253	0.258	0.370
4	0.705	0.873	0.547	0.432	0.402
5	1.113	0.984	0.654	0.501	0.482
Day					
1	1.221	1.171	0.702	0.674	0.676
2	1.303	1.237	0.887	0.701	0.835
3	1.426	1.330	1.214	0.796	0.874
4	1.774	1.401	1.142	0.959	1.043
5	2.042	1.421	1.251	1.412	1.376
6	2.112	1.430	1.210	1.401	1.389

Table 3.14: Release of drug of the polymers [PM12-PM17] at pH=2

Time	Absorbance of polymers / λmax pH=2					
Hour	PM12/ 306 nm	PM13/ 316 nm	PM14/ 332 nm	PM15/ 307 nm	PM16/ 306 nm	PM17/ 314 nm
1	0.129	0.154	0.164	0.081	0.187	0.201
2	0.353	0.195	0.192	0.125	0.217	0.231
3	0..521	0.210	0.245	0.162	0.248	0.384
4	0.724	0.423	0.277	0.216	0.279	0.421
5	0.840	0.481	0.340	0.253	0.304	0.478
Day						
1	0.911	0.721	0.410	0.304	0.411	0.617
2	1.132	0.833	0.501	0.379	0.621	0.802
3	1.256	0.911	0.525	0.402	0.713	1.013
4	1.442	1.203	0.537	0.472	0.824	1.222
5	1.731	1.700	0.554	0.511	0.886	1.402
6	1.712	1.703	0.532	0.515	0.804	1.414

Table 3.15: Release of drug of the polymers [PM18-PM22] at pH=2

Time	Absorbance of polymers / λmax pH=2				
Hour	PM18/ 306 nm	PM19/ 290 nm	PM20/ 330 nm	PM21/ 306 nm	PM22/ 322 nm
1	0.098	0.321	0.441	0.522	0.150
2	0.110	0.412	0.484	0.613	0.247
3	0.190	0.548	0.624	0.816	0.387
4	0.211	0.551	0.702	0.898	0.458
5	0.224	0.580	0.761	0.915	0.602
Day					
1	0.233	0.696	1.080	1.414	0.910
2	0.240	0.759	1.245	1.674	1.205
3	0.251	0.904	1.380	1.818	1.562
4	0.262	1.007	1.474	2.160	1.725
5	0.279	1.221	1.552	2.333	1.812
6	0.236	1.212	1.545	2.321	1.802

Table 3.16: Release of drug of the polymers [PM1-PM6] at pH=8

Time	Absorbance of polymers / λmax pH=8					
Hour	PM1/ 332 nm	PM2/ 314nm	PM3/ 331nm	PM4/ 314 nm	PM5/ 306 nm	PM6/ 308 nm
1	0.102	0.311	0.237	0.424	0.126	0.131
2	0.456	0. 510	0.412	0.558	0.282	0.339
3	0.719	0.671	0.590	0.650	0.454	0.495
4	0.806	0.774	0.817	0.780	0.555	0.616
5	0.893	0.912	0.974	0.900	0.711	0.903
Day						
1	0.960	1.153	1.400	1.153	1.007	1.275
2	1.154	1.325	1.632	1.455	1.450	1.414
3	1.410	1.545	1.911	1.874	1.781	1.841
4	1.909	2.021	2.124	2.160	2.252	2.011
5	2.115	2.317	2.500	2.419	2.420	2.160
6	2.010	2.301	2.441	2.300	2.251	2.104

Table 3.17: Release of drug of the polymers [PM7-PM11] at pH=8

Time	Absorbance of polymers / λmax				
Hour	PM7/ 290 nm	PM8/ 330 nm	PM9/ 306 nm	PM10/ 306 nm	PM11/ 322 nm
1	0.178	0.160	0.119	0.055	0.178
2	0.344	0.251	0.470	0.253	0.278
3	0.467	0.547	0.631	0.472	0.471
4	0.6421	0.831	0.803	0.632	0.687
5	0.817	0.917	0.964	0.781	0.921
Day					
1	1.042	1.033	1.210	1.010	1.333
2	1.456	1.114	1.425	1.226	1.687
3	1.727	1.244	1.640	1.422	1.878
4	2.019	1.621	1.959	1.642	2.003
5	2.221	1.861	2.232	1.908	2.547
6	2.210	1.310	2.054	1.876	2.474

Table 3.18: Release of drug of the polymers [PM12-PM17] at pH=8

Time	Absorbance of polymers / λmax pH=8					
Hour	PM12/ 306 nm	PM13/ 316 nm	PM14/ 332 nm	PM15/ 307 nm	PM16/ 306 nm	PM17/ 314 nm
1	0.289	0.191	0.187	0.152	0.160	0.252
2	0.515	0.341	0.307	0.266	0.287	0.408
3	0.640	0.485	0.479	0.302	0.361	0.527
4	0.714	0.681	0.554	0.510	0.497	0.635
5	0.943	0.746	0.639	0.683	0.611	0.706
Day						
1	1.234	1.055	1.017	1.152	1.076	1.001
2	1.512	1.251	1.189	1.354	1.305	1.254
3	1.846	1.780	1.450	1.643	1.678	1.630
4	2.073	2.121	1.852	1.997	1.928	2.086
5	2.321	2.232	2.088	2.461	2.540	2.113
6	2.312	2.204	2. 04	2.450	2.522	2.100

Table 3.19: Release of drug of the polymers [PM18-PM22] at pH=8

Time	Absorbance of polymers / λmax pH=8				
Hour	PM18/ 306 nm	PM19/ 306 nm	PM20/ 330 nm	PM21/ 290 nm	PM22/ 322 nm
1	0.142	0.247	0.184	0.167	0.156
2	0.364	0.387	0.311	0.245	0.161
3	0.536	0.561	0.497	0.414	0.256
4	0.612	0.746	0.637	0.627	0.317
5	0.871	0.903	0.809	0.806	0.375
Day					
1	1. 147	1.204	1.234	1.087	0.711
2	1.386	1.580	1.584	1.520	0.912
3	1.634	1.830	1.836	1.772	1.450
4	1.987	2.206	2.153	2.114	2.063
5	2.402	2.471	2.333	2.407	2.331
6	2.311	2.215	2.371	2.331	2.242

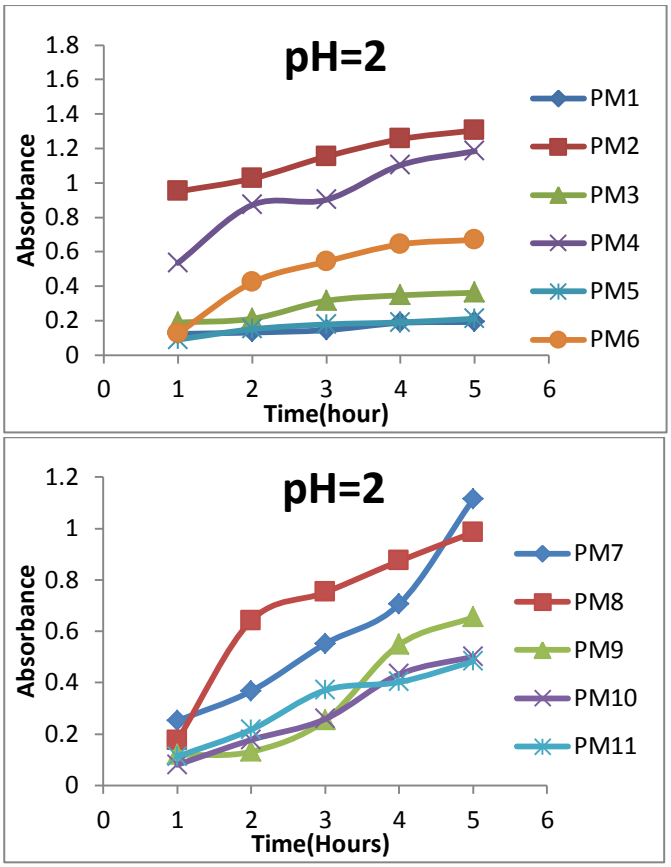

Figure 3-85: The Drug release diagram of homopolymers (PM_1-PM_{11}) in hours

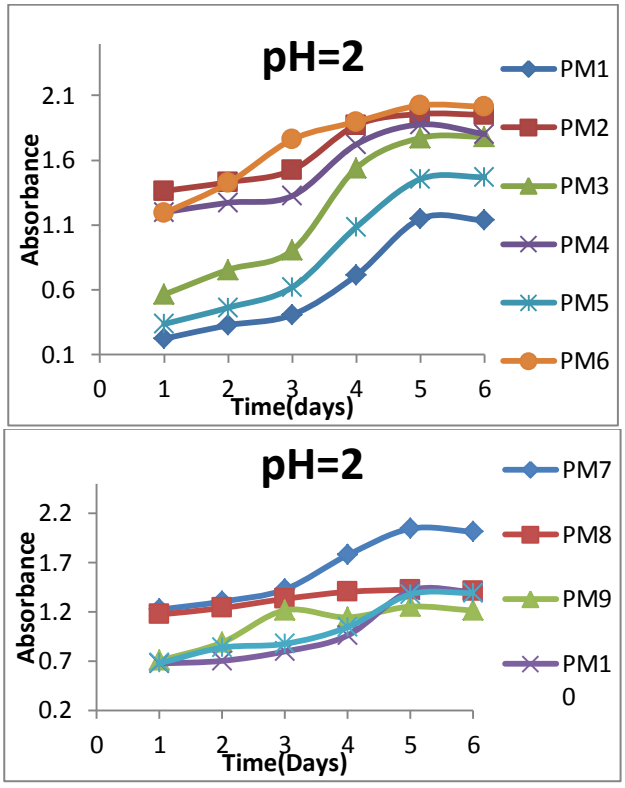

Figure 3-86: The Drug release diagram of homopolymers (PM_1-PM_{11}) in days

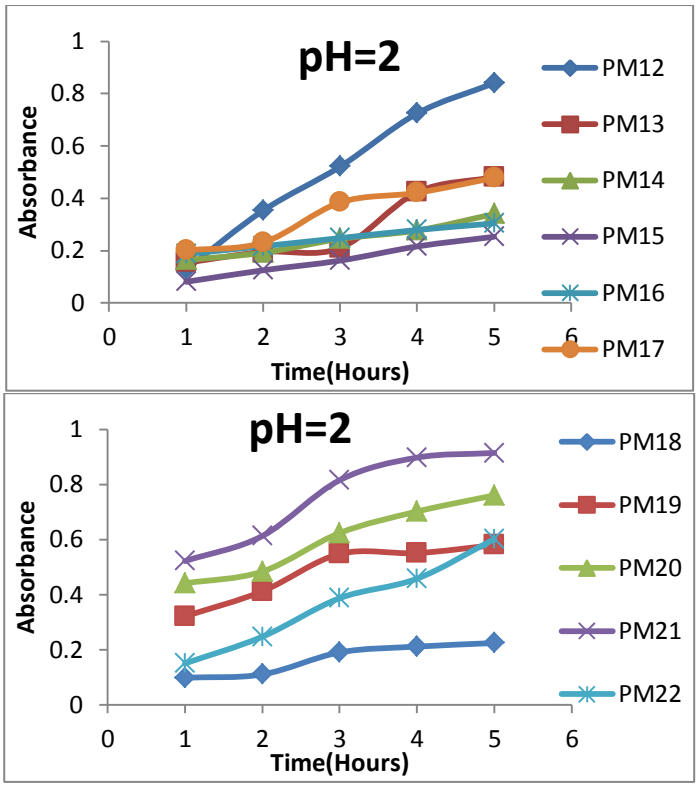

Figure 3-87: Drug release diagram of Heteropolymers (PM_{12}-PM_{22}) in hours

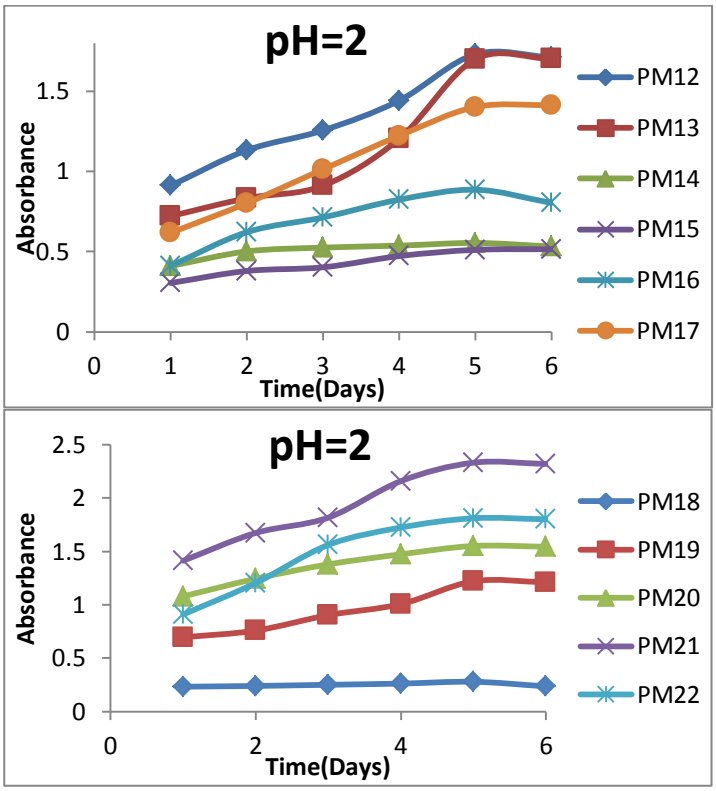

Figure 3-88: The Drug release diagram of Heteropolymers (PM_{12}-PM_{22}) in days

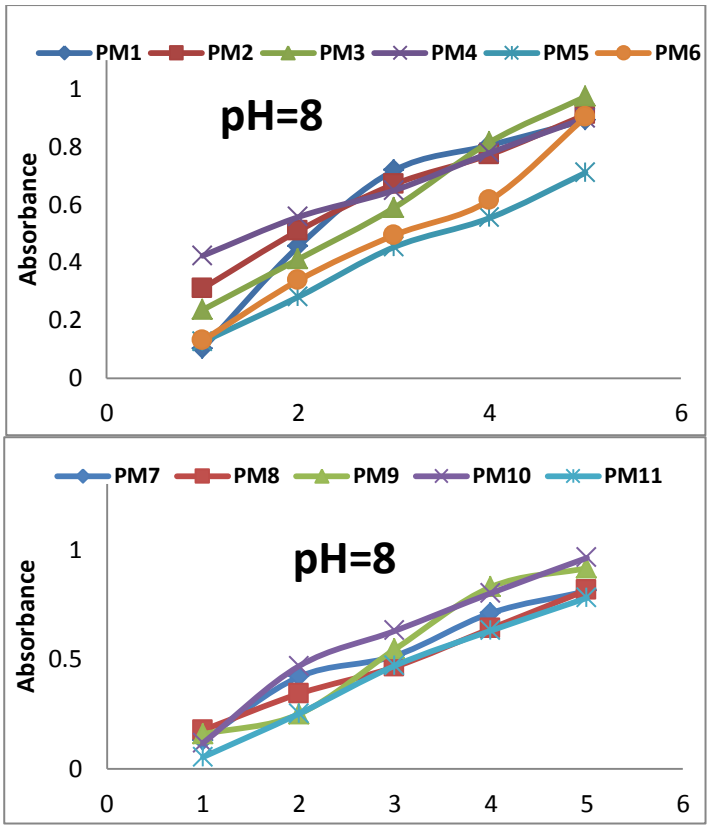

Figure 3-89: The Drug release diagram of homopolymers (PM_1-PM_{11}) in hours

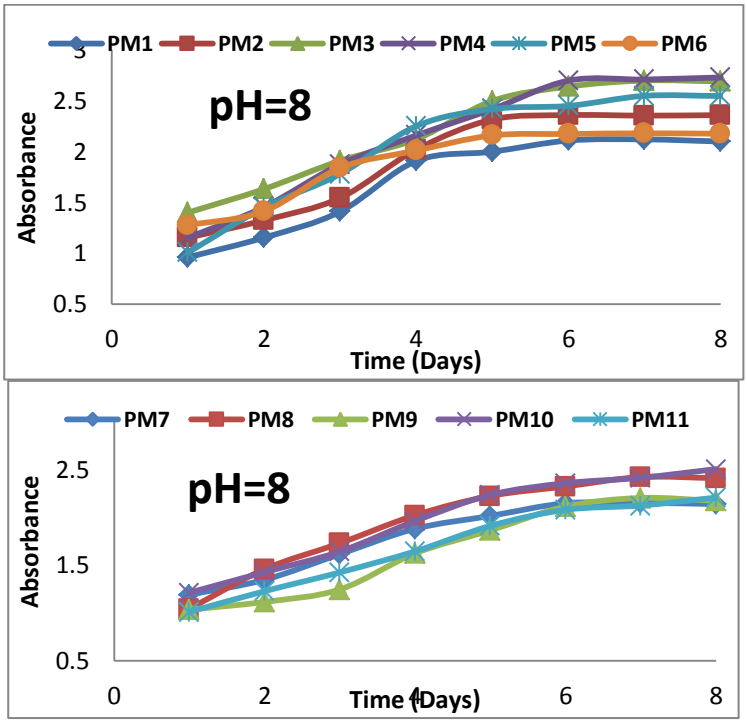

Figure 3-90: The Drug release diagram of homopolymers (PM_1-PM_{13}) in days

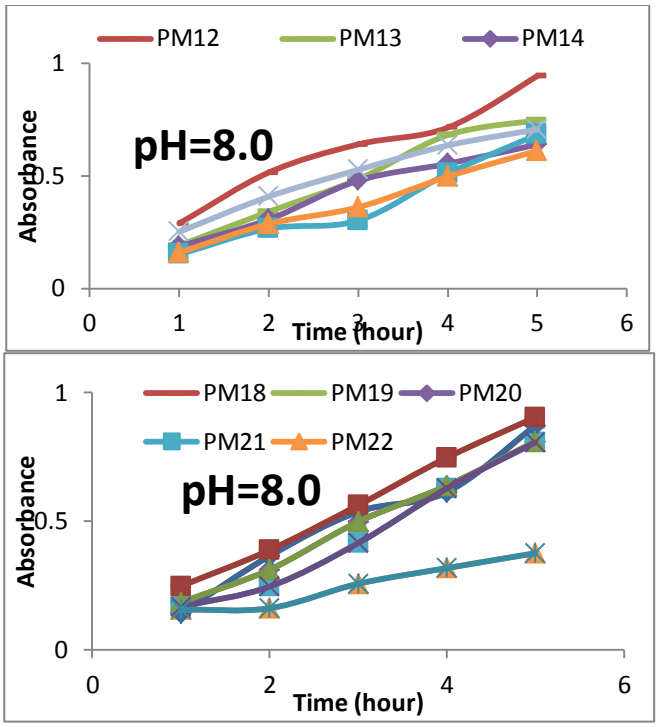

Figure 3.91: The Drug release diagram in Hours for Hetero-polymers (PM_{12}-PM_{22}).

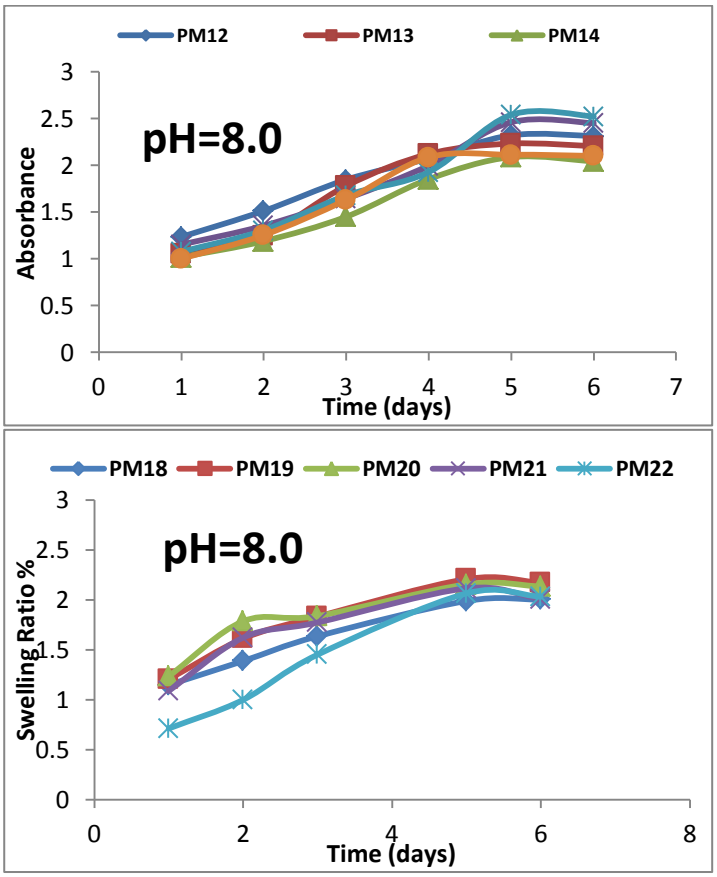

Figure 3.92: The Drug release diagram in days For Hetero-polymers (PM_{12}-PM_{22}).

3.12. Antibacterial Activity of polymers [PM_1-PM_{22}]

Antibacterial activity of the Homopolymers [PM_1-PM_{11}] against pathogenic strains of *Escherichia coli* and *Staphylococcus aurous* using solution of 0.5 mg from each polymer and each loaded drug for comparison in 1 mL of DMSO was carried out using disk-diffusion method, Table 3.2 and 3.3 showed the inhibition zones for [PM_1-PM_{22}] and corresponding drugs.

Table 3. 20: Antibacterial activity of Homopolymers (PM_1-PM_{11}) at 0.5 mg/mL concentration

sample	Inhibition Zone for Staph. Coccus of polymer	Inhibition Zone for E. Coli of polymer	Inhibition Zone for Staph. Coccus of Drug		Inhibition Zone for E. Coli of Drug
PM1	25	20	Clafuran	20	35
PM2	28	32	ceftriaxone	35	20
PM3	0	9	Ampicillin	35	26
PM4	20	12	Amoxicillin	35	35
PM5	12	22	Cephalexin	30	15
PM6	38	40	Ciprofloxacin	35	22
PM7	20	22	Paracetamol	13	4
PM8	22	20	Sulfadiazine	35	9
PM9	12	22	Isoniazid	15	15
PM10	10	20	Carbamazepine	0	4
PM11	15	18	Metoclopramide	10	5
DMSO	0	0	0		0

Table 3. 21: Antibacterial activity of Heteropolymers (PM_{12}-PM_{22}) at 0.5 mg/mL concentration

sample	Inhibition Zone for Staph. Coccus of polymer	Inhibition Zone for *E. Coli of* polymer	Inhibition Zone for *Staph. Coccus of* Drug		Inhibition Zone for E. Coli of Drug
PM12	10	38	Clafuran	20	35
PM13	16	25	ceftriaxone	35	20
PM14	25	10	Ampicillin	35	26
PM15	25	38	Amoxicillin	35	35
PM16	18	22	Cephalexin	30	15
PM17	23	42	Ciprofloxacin	35	22
PM18	25	22	Paracetamol	13	4
PM19	10	18	Sulfadiazine	35	9

PM20	**25**	**30**	**Isoniazid**	**15**	**15**
PM21	**10**	**14**	**Carbamazepine**	**0**	**4**
PM22	**8**	**15**	**Metoclopramide**	**10**	**5**
DMSO	**0**	0	0		0

Most of prepared homopolymer showed lower antibacterial activity toward the tested (*Staph. Coccus*) bacteria (except PM6) than drugs and monomers, the reason may be that the pendent drug molecules are bound in a way that prevents them from sticking to the cell wall.

So, if we study the biological activity after drug release on polymers at different time intervals, we may get strong evidence and may also support the idea of the safety of polymer drugs before drug release.

On the other hand, when we compare the single polymer with the two bacterial strains, the results in (Table 3.7) showed that the activity of some homopolymers towards Gram-negative bacteria is higher than their counterparts.

Most of Heteropolymers showed highest anti-bacterial activities toward *E. Coli* comparison with loaded drugs, exception to PM_{14}.

This effect is thought to be caused by the presence of polyacrylic acid side by side to maleimide-drug in the polymer backbone may lead to lowering in pH over the time. Low pH levels, on the one hand, are known to produce cell stress by altering cytoplasmic pH homeostasis and impairing enzyme and transport system functioning [(144)]. Long-term exposure to acids causes membrane damage, protein denaturation, and DNA depurination [(145)].

3.13. Cytotoxic Activity of Some Polymers

The MTT test is a colorimetric assay used to estimate the vitality or cytotoxicity of cells [(146)]. The vitality of cells present is reflected by the NAD (P) H-dependent cellular oxidoreductase enzyme under specified circumstances [(147-149)]. The tetrazolium dye MTT 3-(4,5-dimethylthiazol-2-yl)-2,5-diphenyltetrazolium bromide, is also reduced by NAD (P) H enzymes to its insoluble formazan, which is purple in color and Because the formazan

is unable to pass cell membranes, it accumulates in healthy cells [148]. This technique is safe, simple to apply, and has higher repeatability, making it a popular choice for cell viability and cytotoxicity testing [151].

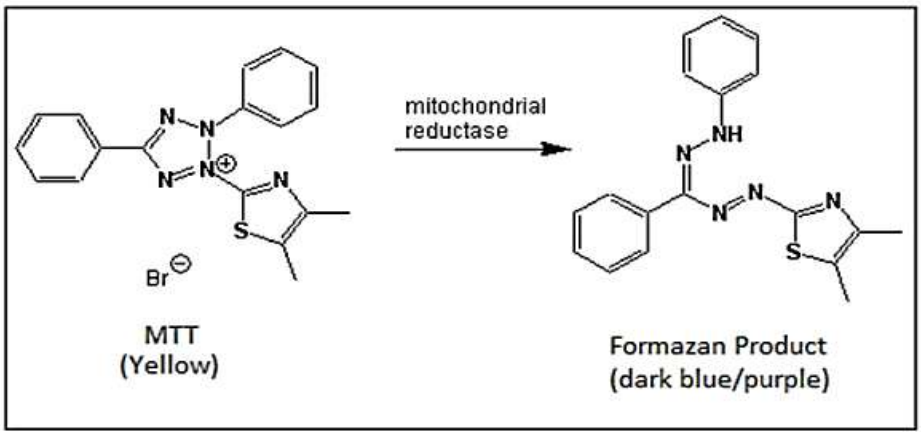

Figure 3.93: Reduction of MTT to formazan

The cytotoxic effects of polymers were evaluated using the MTT assay on human breast cancer cell line (MCF7), and the results were compared to the untreated control [152, 153].

Table 3.22: Cytotoxic effect of [PM_1] in MCF-7 cells

PM1	Concentration (µg/ml)	OD	OD	OD	avg	cell viability
	50	0.128	0.126	0.12	0.124667	31.37583893
	40	0.156	0.149	0.153	0.152667	38.42281879
	30	0.182	0.179	0.167	0.176	44.29530201
	20	0.274	0.218	0.285	0.259	65.18456376
	10	0.381	0.277	0.295	0.317667	79.94966443
	5	0.353	0.3	0.307	0.32	80.53691275
	2.5	0.402	0.349	0.398	0.383	96.39261745
	0	0.422	0.355	0.415	0.397333	100
IC_{50}	31.113					

Table 3.23: Cytotoxic effect of [PM_2] in MCF-7 cells

PM2	Concentration (µg/ml)	OD	OD	OD	avg	cell viability
	50	0.142	0.114	0.108	0.1213333333	29.78723404
	40	0.122	0.141	0.139	0.134	32.89689034
	30	0.21	0.152	0.144	0.1686666667	41.40752864
	20	0.185	0.205	0.168	0.186	45.66284779
	10	0.287	0.271	0.265	0.2743333333	67.34860884
	5	0.309	0.353	0.337	0.333	81.7512275
	2.5	0.396	0.378	0.346	0.3733333333	91.65302782
	0	0.419	0.444	0.359	0.4073333333	100
IC50	26.78					

Table 3.24: Cytotoxic effect of [PM_5] in MCF-7 cells

PM5	Concentration (µg/ml)	OD	OD	OD	avg	cell viability
	50	0.101	0.103	0.124	0.1093333333	24.98095963
	40	0.131	0.119	0.113	0.121	27.64661081
	30	0.145	0.135	0.115	0.1316666667	30.08377761
	20	0.305	0.118	0.172	0.1983333333	45.31607007
	10	0.207	0.217	0.218	0.214	48.8956588
	5	0.29	0.36	0.349	0.333	76.08530084
	2.5	0.378	0.342	0.356	0.3586666667	81.94973343
	0	0.492	0.395	0.426	0.4376666667	100
IC50	20.715					

Table 3.25: Cytotoxic effect of [PM_6] in MCF-7 cells

PM6	Concentration (µg/ml)	OD	OD	OD	avg	cell viability
	50	0.169	0.193	0.179	0.180333	33.5399876
	40	0.257	0.187	0.185	0.209667	38.99566026
	30	0.22	0.202	0.242	0.221333	41.16553007
	20	0.252	0.296	0.232	0.26	48.35709857
	10	0.297	0.297	0.32	0.304667	56.66460012
	5	0.35	0.342	0.367	0.353	65.65406076
	2.5	0.523	0.524	0.452	0.499667	92.93242405
	0	0.559	0.525	0.529	0.537667	100
IC50	22.194					

Table 3.26: Cytotoxic effect of [PM8] in MCF-7 cells

PM8	Concentration (µg/ml)	OD	OD	OD	avg	cell viability
	50	0.135	0.113	0.124	0.124	27.15328467
	40	0.115	0.147	0.134	0.132	28.90510949
	30	0.159	0.164	0.163	0.162	35.47445255
	20	0.274	0.287	0.295	0.2853333333	62.48175182
	10	0.379	0.347	0.354	0.36	78.83211679
	5	0.399	0.391	0.372	0.3873333333	84.81751825
	2.5	0.46	0.4	0.448	0.436	95.47445255
	0	0.378	0.443	0.549	0.4566666667	100
IC50	28.127					

Table 3.27: Cytotoxic effect of [PM_{12}] in MCF-7 cells

PM12	Concentration (µg/ml)	OD	OD	OD	avg	cell viability
	50	0.186	0.171	0.155	0.170666667	36.7816092
	40	0.166	0.18	0.243	0.196333333	42.31321839
	30	0.179	0.2	0.224	0.201	43.31896552
	20	0.377	0.215	0.216	0.269333333	58.04597701
	10	0.347	0.373	0.411	0.377	81.25
	5	0.417	0.484	0.376	0.425666667	91.73850575
	2.5	0.475	0.436	0.427	0.446	96.12068966
	0	0.54	0.414	0.438	0.464	100
IC50	32.338					

Table 3.28: Cytotoxic effect of [PM_{13}] in MCF-7 cells

PM13	Concentration (µg/ml)	OD	OD	OD	avg	cell viability
	50	0.144	0.183	0.149	0.1586666667	32.82758621
	40	0.141	0.188	0.162	0.1636666667	33.86206897
	30	0.167	0.178	0.188	0.1776666667	36.75862069
	20	0.218	0.203	0.245	0.222	45.93103448
	10	0.354	0.308	0.317	0.3263333333	67.51724138
	5	0.475	0.337	0.451	0.421	87.10344828
	2.5	0.437	0.524	0.393	0.4513333333	93.37931034
	0	0.484	0.525	0.441	0.4833333333	100
IC50	27.023					

Table 3.29: Cytotoxic effect of [PM_{16}] in MCF-7 cells

PM16	Concentration (µg/ml)	OD	OD	OD	avg	cell viability
	50	0.108	0.116	0.127	0.117	29.59527825
	40	0.137	0.128	0.128	0.131	33.13659359
	30	0.147	0.175	0.12	0.1473333333	37.26812816
	20	0.19	0.16	0.174	0.1746666667	44.18212479
	10	0.197	0.182	0.166	0.1816666667	45.95278246
	5	0.214	0.198	0.204	0.2053333333	51.93929174
	2.5	0.38	0.38	0.345	0.3683333333	93.1703204
	0	0.356	0.38	0.45	0.3953333333	100
IC50	6.210					

Table 3.30: Cytotoxic effect of [PM_{17}] in MCF-7 cells

PM17	Concentration (µg/ml)	OD	OD	OD	avg	cell viability
	50	0.245	0.261	0.237	0.24766667	53.185397
	40	0.249	0.284	0.277	0.27	57.9813887
	30	0.275	0.267	0.291	0.27766667	59.627773
	20	0.337	0.244	0.315	0.29866667	64.137437
	10	0.344	0.369	0.255	0.32266667	69.291338
	5	0.425	0.426	0.389	0.41333333	88.761632
	2.5	0.458	0.484	0.397	0.4463333	95.848246
	0	0.502	0.447	0.448	0.4656667	100
IC50	57.63					

Table 3.31: Cytotoxic effect of [PM_{19}] in MCF-7 cells

PM19	Concentration (µg/ml)	OD	OD	OD	avg	cell viability
	50	0.136	0.13	0.133	0.133	32.75862069
	40	0.141	0.154	0.152	0.149	36.69950739
	30	0.169	0.167	0.178	0.17133333	42.20032841
	20	0.203	0.28	0.207	0.23	56.65024631
	10	0.312	0.298	0.304	0.30466667	75.0410509
	5	0.394	0.337	0.31	0.347	85.4679803
	2.5	0.398	0.376	0.36	0.378	93.10344828
	0	0.411	0.384	0.423	0.406	100
IC50	**29.957**					

The MTT colorimetric assay was used to evaluate the cytotoxicity of synthesized polymers (PM_1, PM_2, PM_5, PM_6, PM_8, PM_{12}, PM_{13}, PM_{16}, PM_{17} and PM_{19}) against MCF-7 cancer cells, (Tables 3.4-3.12 and Figures 3.94-3.103). The results show that all polymers inhibit the cell growth in a concentration-dependent manner when compared to the control.

Homo-polymer PM5 at a concentration of (50 (µg/ml)) showed the highest degree of inhibition, with 75% of treated cells dying, while at a concentration of 10 (µg/ml), 51% of cells died, and the Inhibitory Concentration value (IC_{50}) was 20.715 (µg/ml) (Fig. 3.96). The degree of cell inhibition at highest concentration (50 (µg/ml)) for PM1 (68%), PM2 (70%), PM6 (66 %), PM8 (72 %), PM12 (63%), PM13 (67 %), PM16 (70 %), PM17 (47 %), and PM19 (67 %), while at a concentration of (5 (µg/ml)) from PM6, 34 % of cells died, which is came in the second ordered after M16 Polymer and the inhibitory concentration value (IC_{50}) was 22.194. The IC_{50} values are listed in the Figures (3. 97 and 3.101).

The Heteropolymer PM_{16} showing highest anti-cancer activity, at a concentration of (50 (µg/ml)) 70% treated cells dying, and this less than that for PM5, but it has the lowest IC_{50} = 6.210 µg/mL and at a concentration of 5 (µg/ml) from PM16, 48 % of cells died.

This is a very significant anti proliferation effect compared to other polymers. The results reveal that all of the prepared polymers were successful

in reducing cancer cell proliferation, suggesting that they could be a useful and promising method for developing an effective drug delivery system for clinical use against breast cancer.

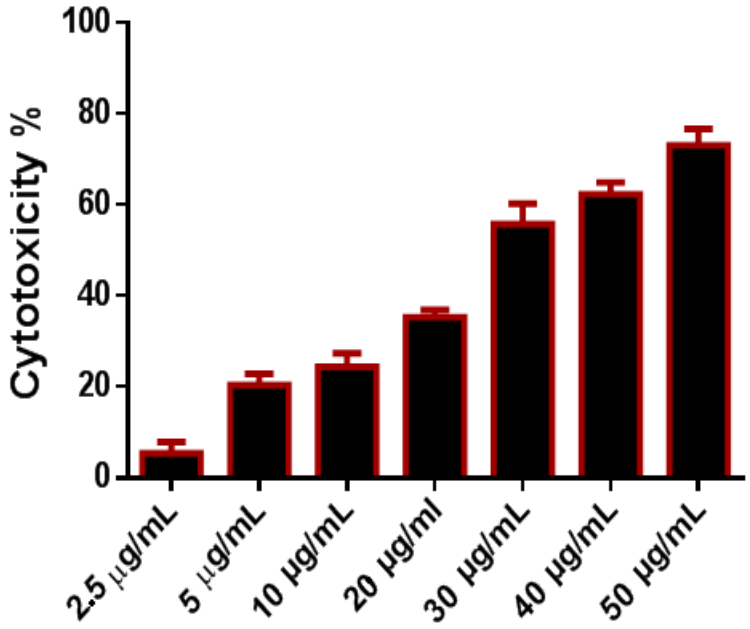

Figure 3.94: Cytotoxic effect of PM1 in MCF-7 cells, IC_{50}= 31.113 (µg/ml)

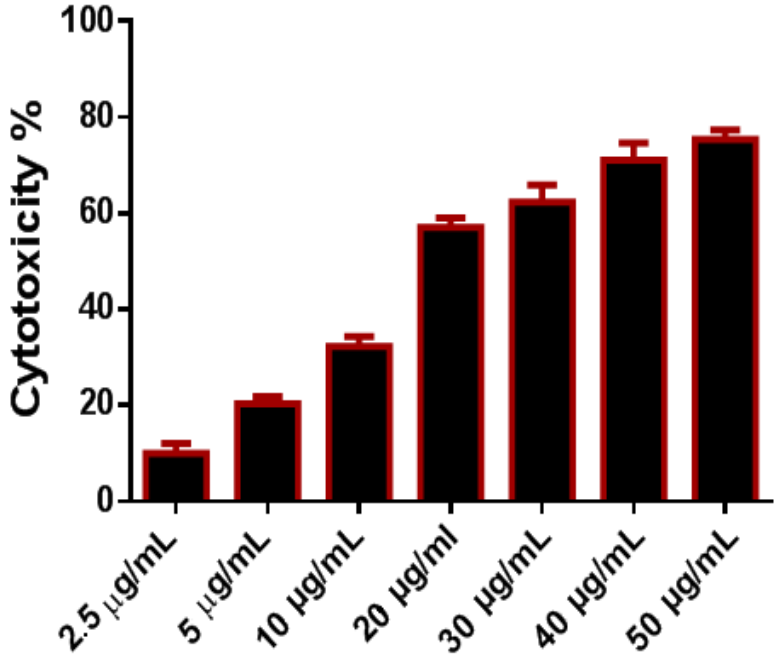

Figure 3.95: Cytotoxic effect of PM_2 in MCF-7 cells, IC_{50}= 26.78 (µg/ml)

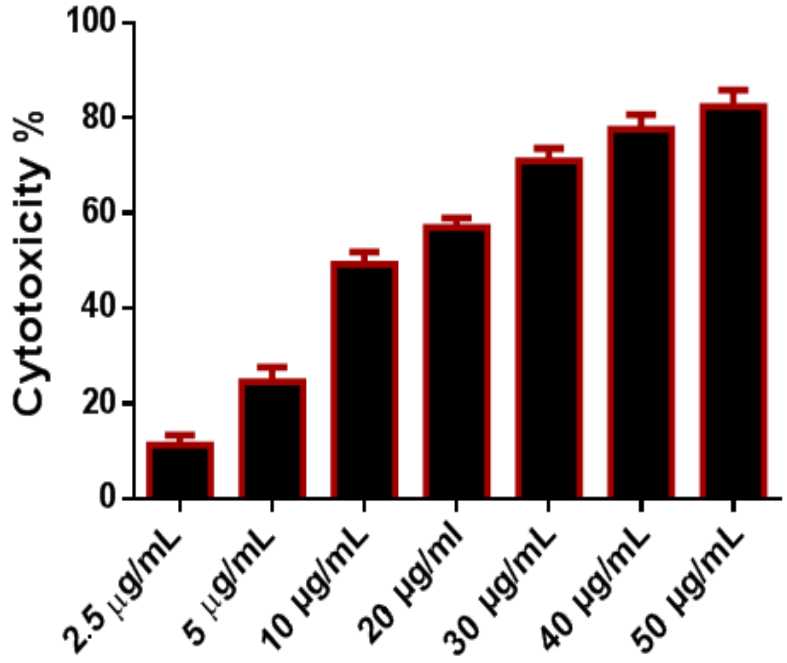

Figure 3.96: Cytotoxic effect of PM_5 in MCF-7 cells, IC_{50} = 20.715 (µg/ml)

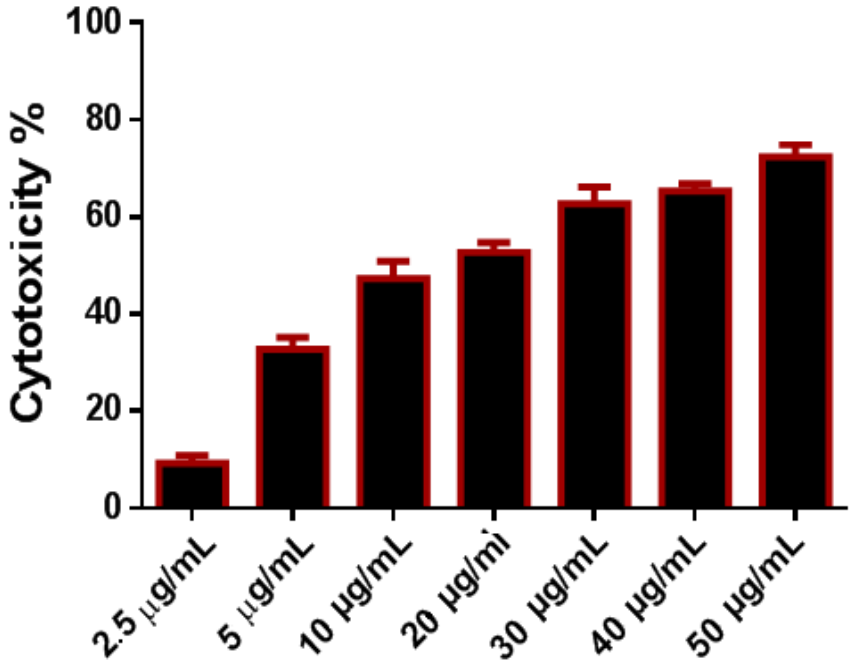

Figure 3.97: Cytotoxic effect of PM6 in MCF-7 cells, IC_{50}= 22.194 (µg/ml)

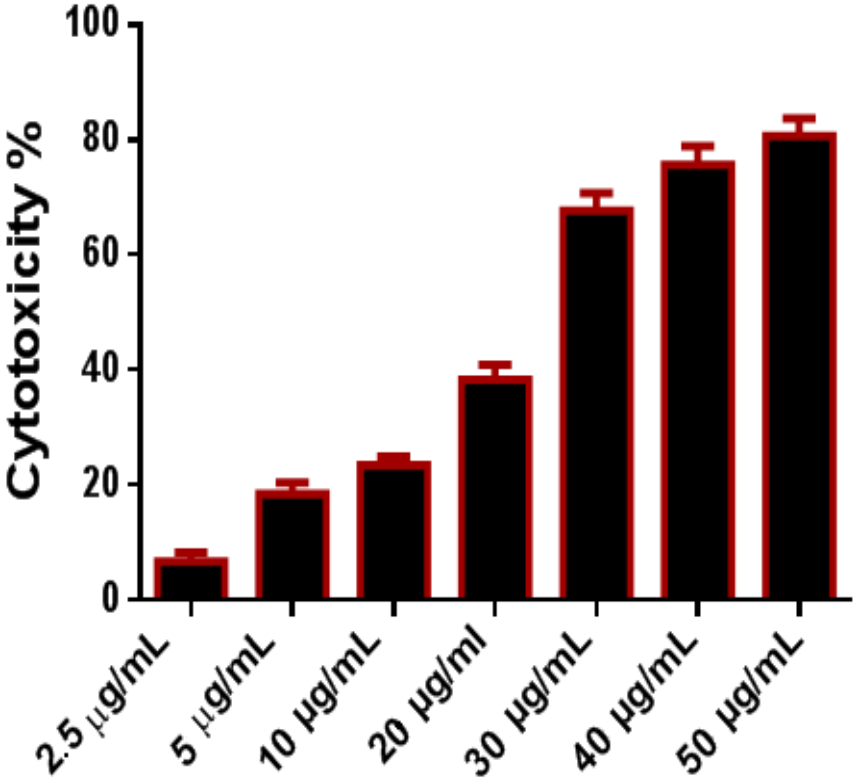

Figure 3.98: Cytotoxic effect of PM_8 in MCF-7 cells, IC_{50}= 28.127 (µg/ml)

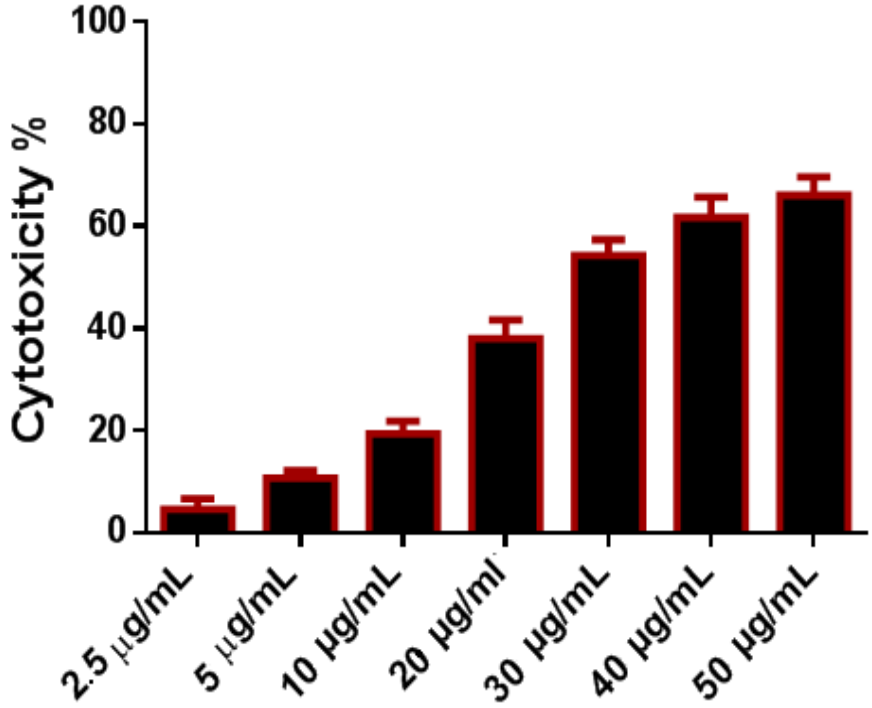

Figure 3.99: Cytotoxic effect of PM_{12} in MCF-7 cells, IC_{50} = 32.338 (µg/ml)

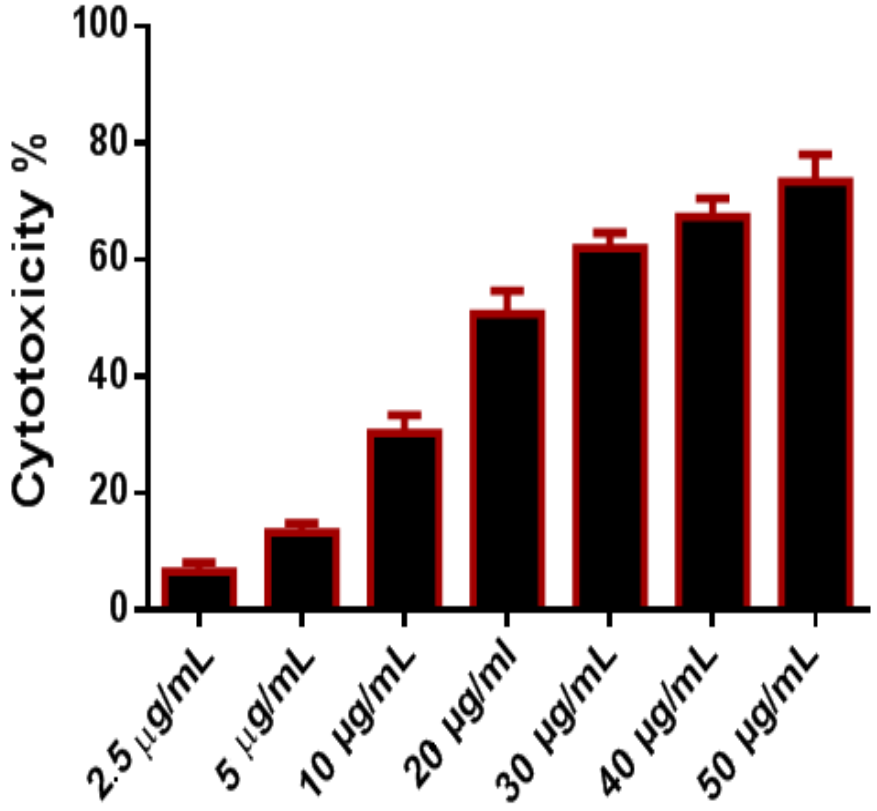

Figure 3.100: Cytotoxic effect of PM_{13} in MCF-7 cells, IC_{50} = 27.023 (µg/ml)

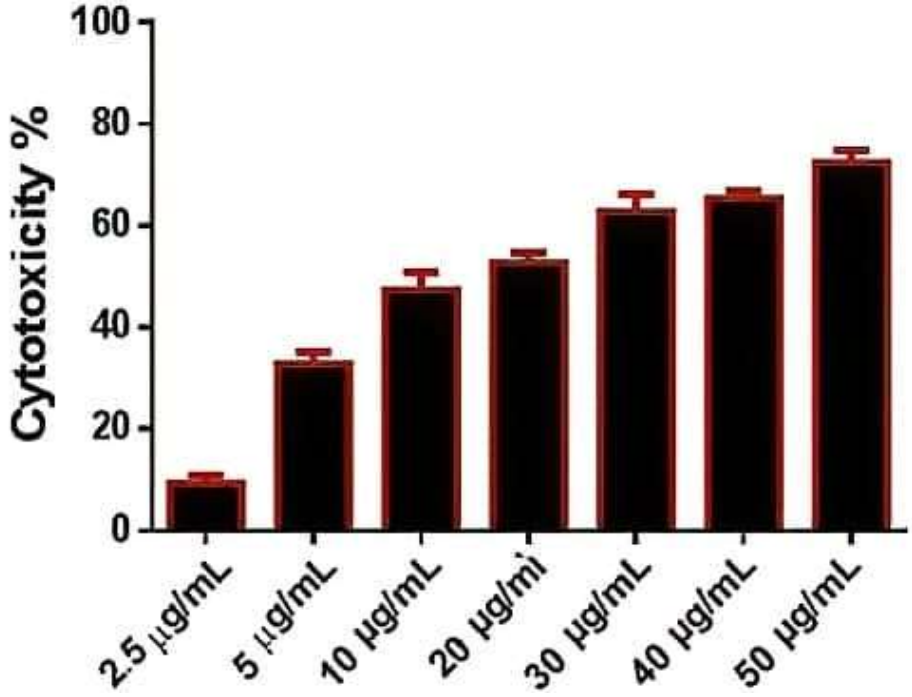

Figure 3.101: Cytotoxic effect of PM_{16} in MCF-7 cells, IC_{50} = 6.210 (µg/ml)

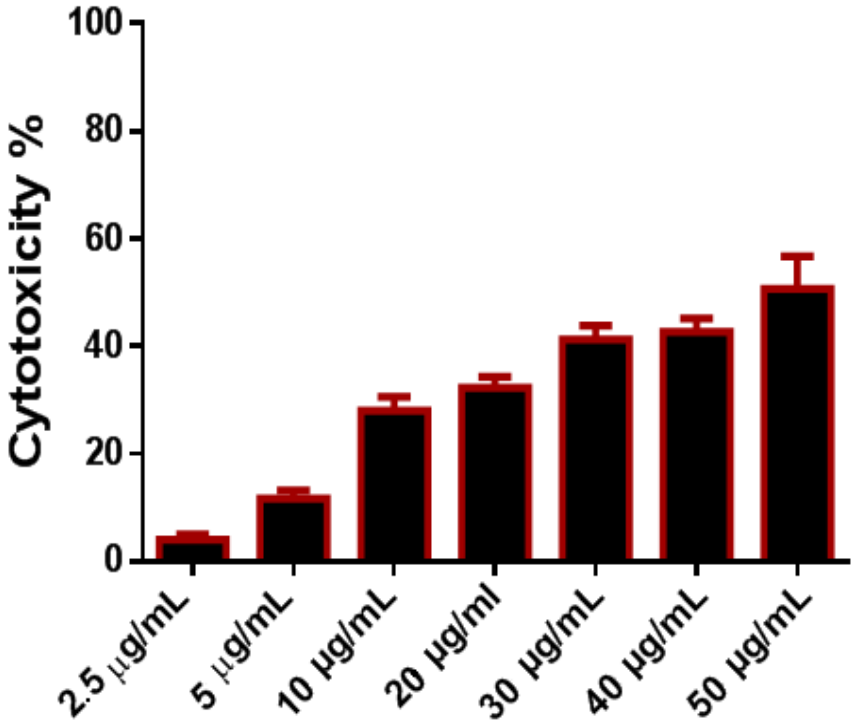

Figure 3.102: Cytotoxic effect of PM_{17} in MCF-7 cells, IC_{50} = 57.63 (µg/ml)

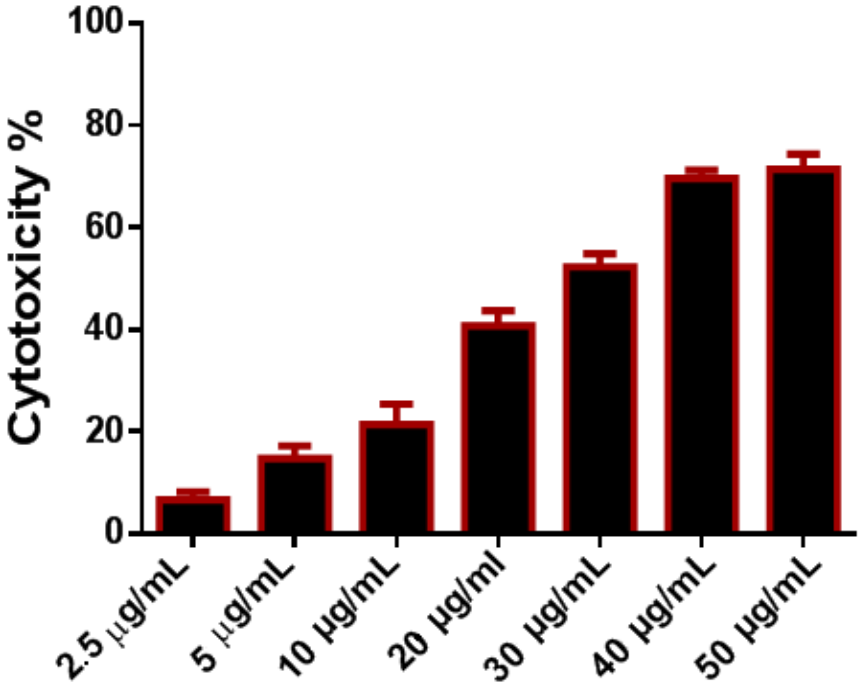

Figure 3.103: Cytotoxic effect of PM_{19} in MCF-7 cells, IC_{50} = 29.957 (µg/ml)

3.14. Molecular Docking Study

A protein found on certain types of cells that binds to a substance called epidermal growth factor. The EGFR protein is involved in cell signaling pathways that control cell division and survival. Sometimes, mutations (changes) in the EGFR gene cause EGFR proteins to be made in higher than normal amounts on some types of cancer cells such as Brest cancer[154]. This causes cancer cells to divide more rapidly. Drugs that block EGFR proteins are being used in the treatment of some types of cancer [155].

The computer drug design largely addresses the technologies of molecular docking used to study the structure and the interactions between medicines and biomolecules. The binding sites in biological molecules and receptors can be determined via molecular docking, which is used to determine the possible binding sites between some prepared homo and hetropolymer and epidermal growth factor receptor (PDB ID: 6D8E, A1 chain) using Molecular Operation environment program (MOE 2019.0102)[156].

3.14.1. Preparation of the ligand

The ligands (**PM2**, **PM12**, **PM6**, **and PM17**) coordinates were built and modeled using the (Chem-BioDraw Ultra 12.0) program. Next, the right atom types (including hybridization states) and right bond types were characterized, hydrogen atoms were added, charges were relegated to each atom, and lastly the structures were vitality limited by utilizing MOE program (MOE 2019.0102). The energies of ligand structures were minimized using the semi empirical AM1 strategy [157] with MOE program.

3.14.2. Selection of protein crystal structures

Crystallographic structures of EGFR with its Ligand (6D8E, A1 chain with FZP ligand for Comparison, Figure 3. 102) are available in the Protein DataBank. In this part, EGFR crystal structure is tested and selected for

docking[158]. The errors of the protein were revised by the structure arrangement process in MOE, isolation the largest and ligand pockets , insertion the tested polymer in these pockets for docking, ligand interaction, calculated total binding energy, H-bond, and Van der Waals (VDW) energies are determined [159].

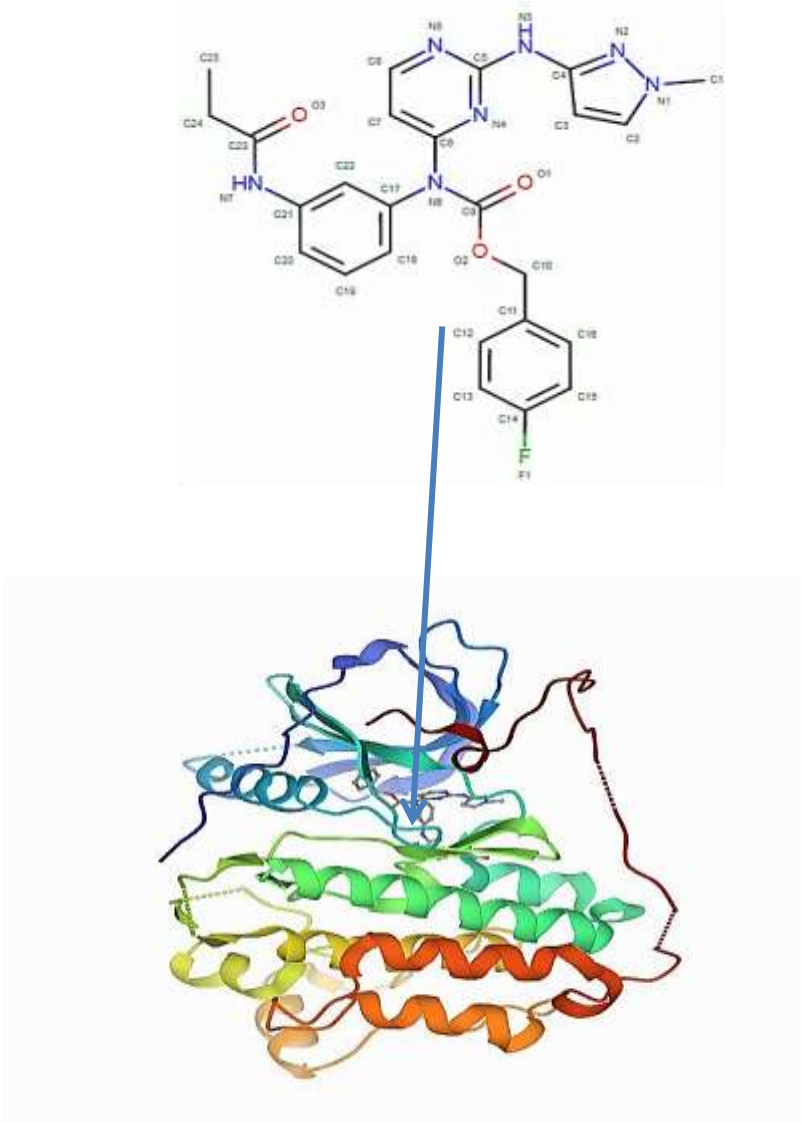

Figure 3.104: Crystal structure of 6D8E-1, Represented by complex of Chain A and FZP original (indicated with blue arrow to the protein center) ligand interaction with the ligand pocket of the EGFR receptor.

From the results obtained from docking reports as shown in Tables 3.9-3.13, compounds **PM_2**, **PM_6**, **PM_{12}**, and **PM_{17}** were the most favorable compounds which meant by its lowest binding energy (Binding energy = -

4.7,-7.7, -13.9 and -9.8 respectively), hydrogen bonding (number of H-bonds = 8, 4, 4, and 7, respectively), and other hydrophobic interactions with the active site of the of EGFR kinase that might be one of the reasons for the good activities shown by these compounds in vitro studies (Figures. 3.103-3.106).

Table 3.32: [PM_2] Protein interaction report

Ligand [PM2]	Interaction	Distance E (kcal/mol)
C 9	MET 766 (A) H-donor	**4.37 -0.5**
C13	MET 766 (A) H-donor	**3.46 -0.6**
C25	ARG 841 (A) H-donor	**3.12 -0.5**
N5	MET 793 (A) H-acceptor	**2.89 -5.1**
ring	LEU 718 (A) pi-H	**4.01 -0.9**
ring	LYS 745 (A) pi-H	**4. 35 -0.8**
O	HIS 805 (A) H-acceptor	**3.00 -9.4**
O	HIS 805 (A) H-acceptor	**3.01 -1.1**
O	HIS 805 (A) Ionic	**2.96 -4.7**
O	TYR 801 (A) H-acceptor	**3.46 -1.2**
O	THR 854 (A) H-acceptor	**2.78 -0.6**

Table 3.33: [PM_6] Protein interaction report

Ligand [PM6]	Interaction	Distance E (kcal/mol)
C13	MET 766 (A) H-donor	**3.46 -0.6**
C25	ARG 841 (A) H-donor	**3.12 -0.5**
N5	MET 793 (A) H-acceptor	**2.89 -5.1**
ring	LEU 718 (A) pi-H	**4.01 -0.9**
ring	LYS 745 (A) pi-H	**4.35 -0.8**
O	LYS 745 (A) H-acceptor	**2.95 -7.7**
ring	LEU 718 (A) pi-H	**4.29 -0.5**
ring	CB LEU 718 (A) pi-H	**4.31 -0.7**
ring	LEU 718 (A) pi-H	**3.76 -0.7**
ring	LYS 745 (A) pi-H	**3.82 -0.7**

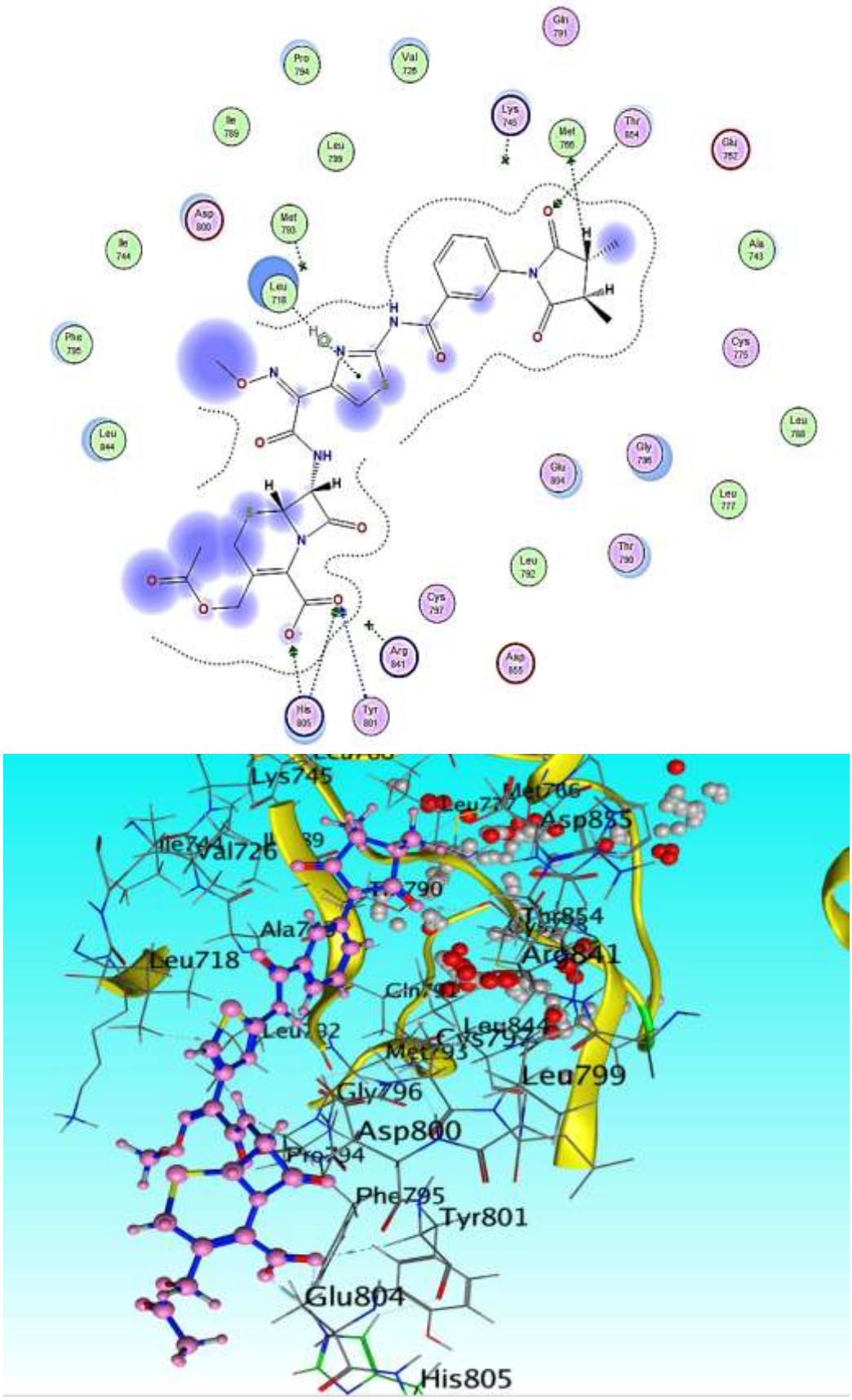

Figure 3.105: [PM_2] ligand interaction with the ligand pocket of the EGFR receptor, 2D and 3D representation.

Table 3.34: [PM_{12}] Protein interaction report

Ligand [PM12]	Interaction	Distance(A) / E (kcal/mol)
C13	MET 766 (A) H-donor	**3.46A / - 0.6**
C25	ARG 841 (A) H-donor	**3.12A / - 0.5**
N5	MET 793 (A) H acceptor	**2.89A / - 5.1**
ring	LEU 718 (A) pi-H	**4.01A / -0.9**
ring	LYS 745 (A) pi-H	**4.35 A -0.8**
O 21	LYS 745 (A) H acceptor	**2.89 A / -13.9**
O 21	LYS 745 (A) Ionic	**2.89 A / -5.3**
ring	VAL 726 (A) pi-H	**4.61A / -0.6**

Table 3.35: [PM_{17}] Protein interaction report

Ligand[PM17]	Interaction	Distance E (kcal/mol)
C13	MET 766 (A) H-donor	**3.46 - 0.6**
C25	ARG 841 (A) H-donor	**3.12 - 0.5**
N5	MET 793 (A) H-acceptor	**2.89 - 5.1**
ring	LEU 718 (A) pi-H	**4.01 -0.9**
ring	LYS 745 (A) pi-H	**4.35 -0.8**
O 22	THR 854 (A) H-acceptor	**2.80 -0.8**
O 21	CYS 775 (A) H-donor	**3.61 -0.9**
O 55	HIS 805 (A) H-acceptor	**2.96 -9.8**
O 55	HIS 805 (A) Ionic	**2.96 -4.7**
O 56	HIS 805 (A) H-acceptor	**3.57 -1.1**
O 56	HIS 805 (A) Ionic	**3.57 -1.6**

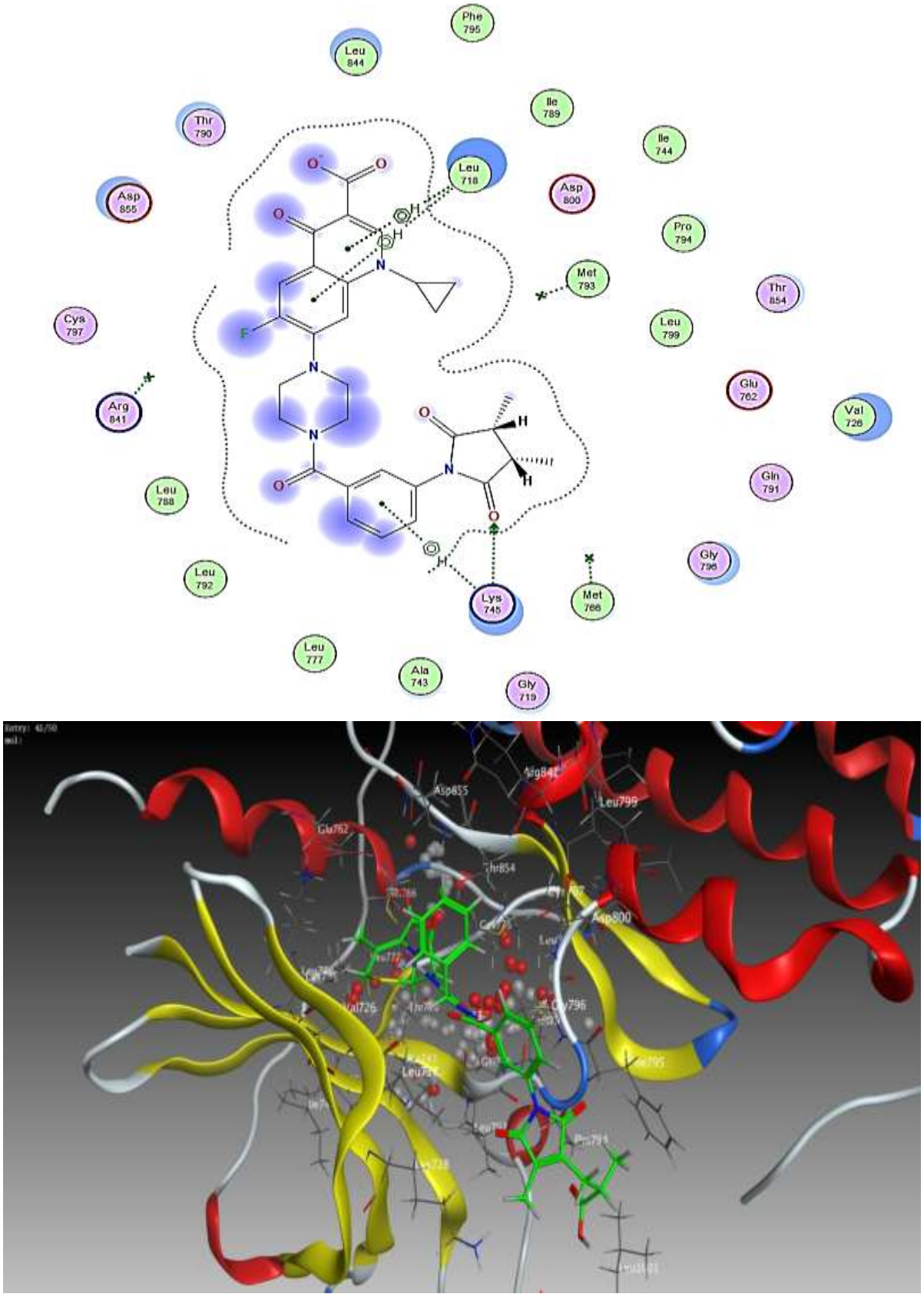

Figure 3.106: [PM_6] ligand interaction with the ligand pocket of the EGFR receptor, 2D and 3D representation.

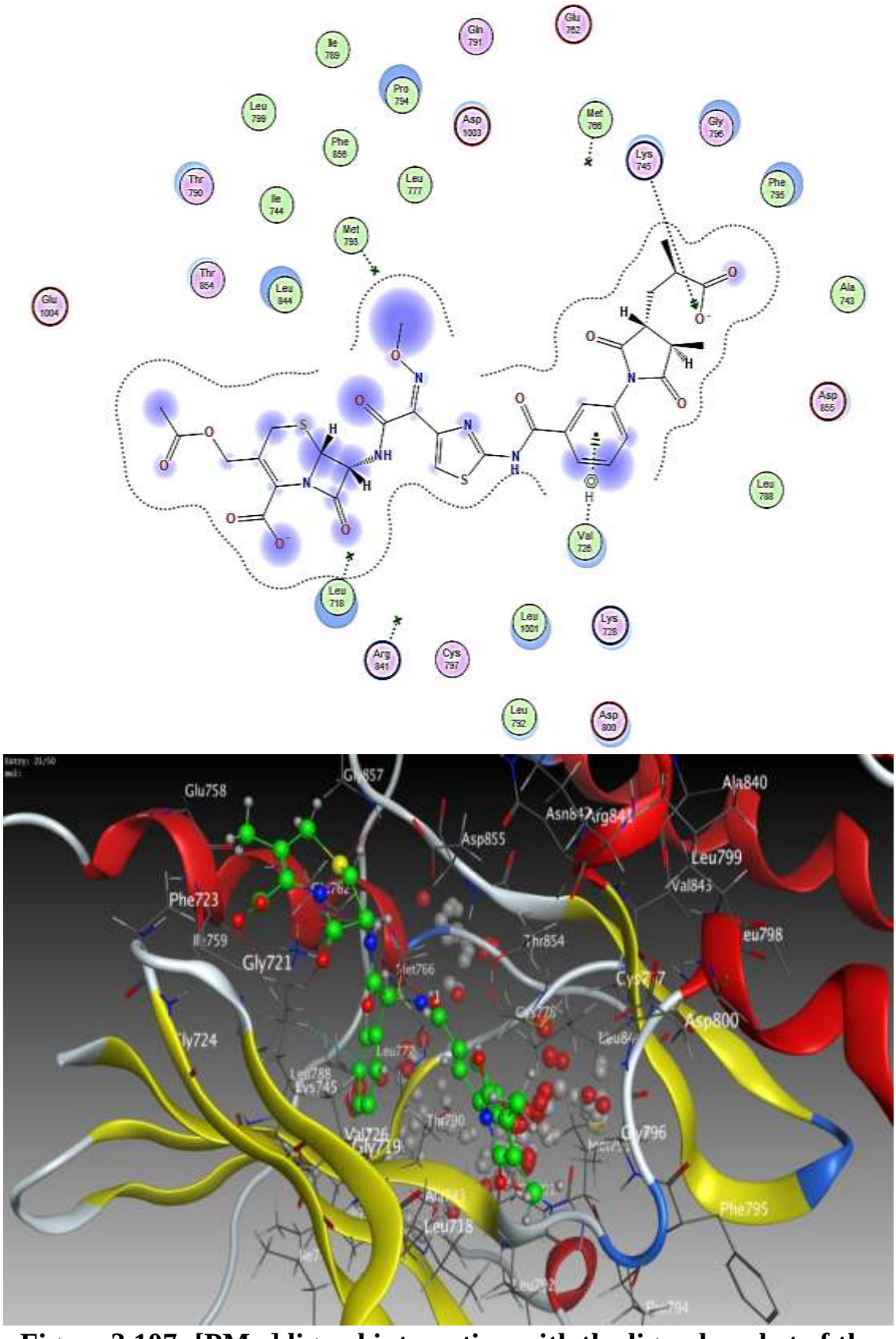

Figure 3.107: [PM_{12}] ligand interaction with the ligand pocket of the EGFR receptor, 2D and 3D representation.

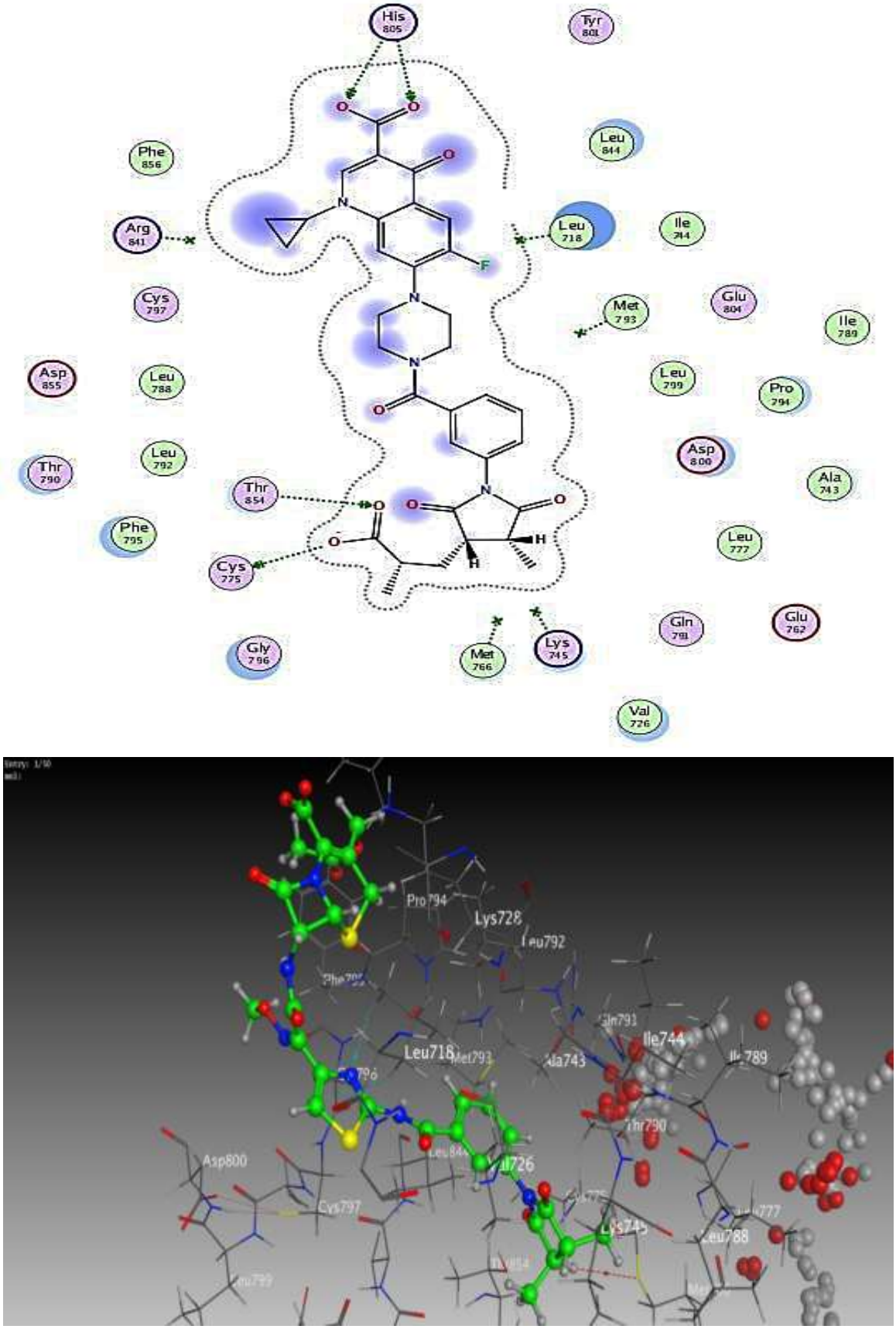

Figure 3.108: [PM_{16}] ligand interaction with the ligand pocket of the EGFR receptor, 2D and 3D representation.

The result of docking in the table 3.13, demonstrate that Heteropolymer [PM_{12}] showed highest poses stability, lowest binding energy and lowest mean square deviation with ligand pocket of EGFR receptor.

Table 3.36: Ligands Poses Energy and Root Mean Square Deviation

Ligand	Score (poses energy)	RMSD
PM2	**-7.4422**	**1.4358**
PM6	**-8.55**	**1.4628**
PM12	**-9.2600**	**1.1973**
PM17	**-8.6112**	**1.8213**

3.15. Conclusions

1. New Maleimide monomers substituted with amino drug molecules were synthesized and characterized.
2. New homopolymers based on maleimide which loaded with medical properties to extend the controlled drug were synthesized and characterized.
3. New Heteropolymers based on maleimide with acrylic acid which loaded with medical properties to extend the controlled drug were synthesized and characterized.
4. All these prepared monomers and polymers were characterized by FT-IR and ^{1}H-NMR, and ^{13}C-NMR techniques and displayed characteristic bands proving the formation of the desired target molecules from the starting material.The physical properties of all prepared monomers and polymers were studied.
5. Synthesized monomers, homopolymers, and copolymers are soluble in DMF, DMSO, and partial in ethanol, diethyl ether, toluene, chloroform, and H_2O.
6. Viscosity measurements in DMF were carried out at different concentrations of homopolymers and copolymers at 30 ^{o}C using an Ostwald viscometer with a capillary diameter of 0.54 mm.
7. In addition, compound PM_{16} showed a promising anti-cancer and anti-inflammatory effect. The active compound could be used as lead compounds for further structural modifications and are also expected to drive new anti-inflammatory drug discovery and may be an appropriate for developing effective drug delivery system to clinical application against breast cancers.
8. The molecular docking study of the selected polymer indicate that there is good affinity toward EGFR ligand pocket and this lead to conclusion of the good anticancer activity of these polymers.

3.16. Recommendations:-

1. Preparation of new derivatives of maleimide utilizing the presence of the double bond as a cyclic addition reaction with appropriate diene or Michael addition reaction with other amino or thiol drugs.
2. Trying to addition of some amino and phenolic drugs drug to the acrylic acid producing acrylic-monomers in ester or amide forms.
3. Study of the thermal properties prepared polymers.
4. Study of the size of polymer particles for the possibility of the presence of polymeric particles with Nano-sizes.
5. Using a new strategy to prepare these polymers, for example, preparing a polymer from maleic anhydride and then adding drugs directly, or the polymerization of maleimide benzoyl chloride and then adding the drugs in order to improve and raise the yield of the product
6. Checking the ability of these types of polymers to form stable complexes with metal ions.
7. Studying the molecular docking of the other polymers with the EGFR largest pocket or with another protein receptor associated with Brest cancer cell, such as HER2.

REFERENCES

References

1. Mancuso R, Amuso R, Armentano B, Grasso G, Rago V, Cappello AR, Galiano F, Figoli A, De Luca G, Hoinkis J, Gabriele B. Chempluschem. 2017;82(10):1235-1244.
2. Baggott J, Denis S E. (1995, January 5). Macromolecules. In NetBiochem.
3. Reece JB, Urry LA, Cain M L, Wasserman S A, Minorsky PV, and Jackson RB., Macromolecules are polymers, built from monomers. In Campbell biology (2011) (10th ed., p. 67). San Francisco, CA: Pearson.
4. Jenkins A, Kratochvil P, Stepto R, Suter U. Pure Appl Chem., 1996;68(12):2287–2311.
5. Berg JM, Tymoczko JL, Stryer L. Biochemistry. 5th edition. New York: W H Freeman; 2002. Available from:
6. Lehninger, AL, Nelson, DL, & Cox MM. (2005). Lehninger principles of biochemistry. New York: W.H. Freeman.
7. Greve H H, Threadingham D . Rubber, 1. Survey. Ullmann's Encyclopedia of Indus trial Chemistry. 2000 ; 31: 579-582.
8. Bshena OES , Synthesis of Permanent Non-Leaching Antimicrobial Polymer Nanofibers. Phd thesis. 2012;147.
9. Ismail R, Ibrahim A, Rusop M, Adnan A. AIP Conf Proc. 2018;1963:1–020009.
10. Molnar C, Gair J., 2015. *Concepts of Biology-1st Canadian Edition*. 1st ed. [ebook] OpenStax College.
11. Dutta J, Tripathi S, Dutta P K, Science F. Food Sci Technol Int., 2012;18 (1):3-34.
12. Tang WJ, Fernandez J, Sohn JJ, Amemiya CT. Biology C. HHS Public Access. 2016;25(7):897-900.
13. Gajera, H P, Patel S V, Golakiya BA. Fundamentals Of Biochemistry

Textbook Student Edition (2008) International Book Distributing Company.
14. Muzzarelli R A A, Muzzarelli C. Chitosan Chemistry: Relevance to the Biomedical Sciences. In: Heinze T. (eds) Polysaccharides I. Advances in Polymer Science, vol 186. Springer, Berlin, Heidelberg.
15. de Queiroz Antonino RSCM, Lia Fook BRP, De Oliveira Lima VA, De Farias Rached R Í, Lima E , Da Silva Lima R J, Peniche Covas CA, et al. Marine Drugs. 2017; 15(5):141-153.
16. Brugnerotto J, Lizardi J, Goycoolea F, Argüelles-Monal W, Desbrieres J, Rinaudo M, .. Polymer 2001, 42, 3569–3580.
17. Dash M, Chiellini F, Ottenbrite RM, Chiellini E. Prog Polym Sci 2011; 36 (8): 981-1014.
18. Agrawal P, Strijkers GJ, Nicolay K. Adv Drug Deliv Rev. 2010;62(1):42-58.
19. Mu A, Fernández-garcía M. prog polym sci 2012;37(2):281–339.
20. Al Ouahabi A, Charles L, Lutz J F. J Am Chem Soc. 2015;137(16):5629–5635.
21. Moldoveanu SC. Analytical Pyrolysis of Synthetic Organic Polymers Chemistry. 2005;25:pp 3-30.
22. Aksakal R, Mertens C, Soete M, Badi N, Prez F Du. Adv. Sci. 2021;8 (6):1–22.
23. Polymers - Types, Classification, Properties, and Uses of Polymers,. IIT JEE Study Material, 2021.
24. D'arcy N. Antimicrobials in plastics: a global review. Plastics, Additives and Compounding, 2001;3(12):12–15.
25. Peili Teo, BIOACTIVE POLYMERS, a*star institute of materials research and engineering.
26. Langer R, Vacanti JP. Tissue engineering. Science. 1993 14;260(5110):920-926.
27. Salgado J, Coutinho OP, Reis RL. Macromol Biosci. 2004;4(8):743–765.
28. Stratton S, Shelke NB, Hoshino K, Rudraiah S, Kumbar SG. Bio act Mater .

2016;1(2):93–108.
29. Gentile P, Chiono V, Carmagnola I, Hatton P V. An Overview. Int J Mol Sci. 2014;15(3):3640-3659.
30. Wang X. micromachines Rev. 2019;10(814):1–25.
31. Warren SM, Fong KD, Nacamuli RP, Fang TD, Longaker MT, Song HM. Biomaterials. 2003;9(1):10-15.
32. Burke JF, Philip L. MULTILAYER MEMBRANE USEFUL AS SYNTHETIC SKIN. US Pat Doc. 1977;(19).
33. Rutnakornpituk M, Ngamdee P, Phinyocheep P. Carbohydr. Polym., 2006; 63(2): 229-237.
34. Parisi O.I., Curcio M., Puoci F. (2015) Polymer Chemistry and Synthetic Polymers. In: Puoci F. (eds) Advanced Polymers in Medicine. Springer, Cham.
35. Witte W. Science. 1998;279(5353):996-997
36. Timofeeva L, Kleshcheva N. Appl Microbiol Biotechnol Synth. 2014;89(3):475–492.
37. Madkour AE, Tew GN. Polym Int . 2008;10(1):6-10.
38. Thamizharasi S, Vasantha J, Reddy BSR. Eur. Polym. J., 2002;38:551-559.
39. Moon W, Kim JC, Chung K, Park E, Kim M, Yoon J. J. Appl. Polym. Sci., 2003;90, 1797-1801.
40. Dizman B, Elasri MO, Mathias L J. J. Appl. Polym. Sci., 2004; 94(2):635-642.
41. Ji J, Zhang W. J Biomed Mater Res A. 2009;88(2):448-453.
42. Kamaruzzaman NF, Tan LP, Hamdan RH, Choong SS, Wong WK, Gibson AJ, Chivu A, Pina MF. Int J Mol Sci., 2019;20(11):2747.
43. Mageed FAR, Kareem MM, Baiati M N. Asian J. Org. Chem., 2019; 31:569-574.
44. Jones DS, Lorimer CP, Mccoy CP, Gorman SP. J Biomed Mater Res B Appl Biomater., 2008;85(2):417-426.

45. Lyon RP, Setter JR, Bovee TD, Doronina SO, Hunter JH, Anderson ME, et al., Nat Biotechnol. 2014;32(10):1059–1062.
46. Aydin Sevinç B, Hanley L. J Biomed Mater Res B Appl Biomater., 2010;94(1):22-31.
47. Xiao Y, Hong H, Matson VZ, Javadi A, Xu W, Yang Y, et al. Theranostics. 2012;2(8):757-768.
48. Wahab A, Favretto ME, Khan GM, Douroumis D. J. Microencapsul., 2012;29(5):479–504.
49. Arun A, Reddy BSR, Rajkumar M. J Bioact Compat Polym., 2003;18(3):219-228.
50. Al-muaikel NS, Al-diab SS, Al-salamah AA, Zaid AMA. J. Applied Polymer Science. 2000;77:740–745.
51. Mohamed NA, El-ghany NAA, Fahmy MM, Perihan A . Int J Poly M Mater., 2018:67(2): 68-77
52. Uppu DSSM, Samaddar S, Hoque J, Konai MM, Krishnamoorthy P, Shome BR, Haldar J. Biomacromolecules 2016; 17 (9):3094-3102.
53. Minoda M, Otsubo T, Yamamoto Y, Zhao J. Polymers (Basel). 2019;11(70):1–14.
54. Yuan Y, Xu S, Cheng X, Cai X, Liu B. AngewChemInt Ed. 2016;55:6457-6461.
55. Gong Y, Tan Y, Liu J, Lu P, Feng C, Yuan WZ, et al. Chem Commun., 2013;49:4009–4011.
56. Goswami KG, Saha B, De P. J Macromol Sci Pure Appl Chem., 2020;57(9):1–9.
57. Bauri K, Saha B, Banerjee A, De P. Polym. Chem., 2020;11: 7293-7315.
58. S Yolles T D, Leafe J H, Woodland FJM. J Pharm Sci., 1975;64(2):348-369.
59. Lohar V, Singhal S, Arora V. Int J Pharm Res., 2012;4(1):15–21.
60. Xiao Y, Hong H, Matson VZ, Javadi A, Xu W, Yang Y, Engle, Jona than W,

Nickles, Robert J, Cai, Weibo S, Douglas A. Theranostics. 2012;2(8):757-768.

61. Uhrich KE, Cannizzaro SM, Langer RS, Shakesheff KM. Chem Rev. 1999;99(1):3181–3198.
62. Theresa M. Allen and Pieter R. Drug Discov., 2004;303(5665):1818–1822.
63. Guo Q, Jiang C. Acta Pharm Sin B., 2020;10(6):979–986.
64. Kakkar A, Traverso G, Farokhzad OC, Weissleder R, Langer R. Nat Rev Chem., 2017;1:1-18.
65. Langer RS, Peppas NA. Biomaterials., 1981;2(4):201-214.
66. Duncan R, Vicent MJ. Adv Drug Deliv Rev., 2013;65(1):60-70.
67. Vasey PA, Kaye SB, Morriso R, Tweves C, Wilson P, Duncan R, Thomson AH, Murray LS, Hilditch TE, Murray T, Burtles S, Fraier D FE and CJ.. Clin Cancer Res. 1999;5:83-94.
68. Blessing T, Kursa M, Holzhauser R, Kircheis R, Wagner E.. Bioconjugate Chem. 2001;12(4):529-537.
69. Saha B, Choudhury N, Bhadran A, Bauri K, De P, . Polym. Chem. 2019, 10, 3306–3317.
70. Koziolová E, Venclíková K, Etrych T. Physiol Res., 2018;67(2):281-292.
71. Jung E, Chung I, Lee N, Park J, Ha C, Cho W., J. Polym. Sci. A Polym. Chem., 2000:38(8):1247-1256.
72. Azad N, Rojanasakul Y. Macromolecular Drug Delivery. In: Biopharmaceutical Drug Design and Development. 2008. p. 293–323.
73. Akbarzadeh A, Rezaei-Sadabady R, Davaran S, Joo SW, Zarghami N, Hanifehpour Y, Samiei M, Kouhi M, Nejati-Koshki K. Nanoscale Res Lett., 2013 ;8(1):102-111.
74. Li T, Takeoka SA. Int. J. Nanomedicine. 2013;8:3855–3866.
75. Harders LR, Eloualid M, Van L, Crommelin DJA, Danhof M, Boer AG. J. Drug. Target., 2004;12(9):569-573.
76. Natfji AA, Osborn HMI, Greco F. Curr Opin Colloid Interface Sci.,

2017;31:51–66.
77. Mohammed IA and Kareem MM. J Phys Conf Ser. 2020;1664(012081).
78. Thakur S, Riyaz B, Patil A, Kaur A, Kapoor B, Mishra V. Biomed Pharmacother., 2018;106(January):1011-1023.
79. Kareem MM, Abbas A L. J Phys Conf Ser. 2019;1294(5).
80. Begam T, Nagpal AK, Singhal R. J Appl Polym Sci. 2003;89(3):779-786.
81. Park H, Guo X, Temenoff JS, Tabata Y, Caplan AI, Kasper FK, et al. Biomacromolecules. 2009;10(3):541–546.
82. Bode C, Kranz H, Fivez A, Siepmann F, Siepmann J. J. Control Release. 2019;306:97–107.
83. J. Singh, "Swelling of polymer gels," Msc thesis, GiIl University Montreal, Quebec Canada, 1993.
84. Abd Al-Aama Z M, AL-Baiati M N. Journal of Global Pharmacy Technology. 2017;12(9):50-56.
85. James M Ritter, Lionel D Lewis TGM and AF. Clinical Pharmacology and Therapeutics. 5 edt. Britain; 2008. pp 1–451.
86. Werner Dubitzky, Olaf Wolkenhauer, Kwang-Hyun Cho HY. Encyclopedia of Systems Biology. 1st ed. Springer; 2013.
87. Lee AA, Yang Q, Bassyouni A, Butler CR, Hou X, Jenkinson S. PNAS. 2019;116(9):3373–8.
88. Kareem S H, Naji A M, Taqi Z J, Jabir M S. J Inorg Organomet Polym., 2020:30: 5009-5023.
89. Al-Shammar A M, Al-Saadi H, Al-Shammari S M, Jabir M S. In AIP Conference Proceedings 2020:2213(1): 020206.
90. Jabir M S, Saleh Y M, Sulaiman G M, Yaseen N Y, Sahib U I, Dewir Y H , et al. Nanomaterials (Basel). 2021;11(2):384.
91. Amritha CA, Kumaravelu P, Chellathai DD. J Clin Diagnostic Res. 2015;9(12):14-26.

92. Aslantürk ÖS, Aslantürk S. In Vitro Cytotoxicity and Cell Viability Assays: Principles, Advantages, and Disadvantages. In: Genotoxicity - A Predictable Risk to Our Actual World. Aydın, Turkey: IntechOpen; 2017. p. 1–18.
93. Khashan K S, Abdulameer F A , Jabir M S, Hadi AA, Sulaiman G M. Adv. Nat. Sci.: Nanosci. Nanotechnol., 2020;11(3):035010.
94. Sameen A M, Jabir M S, Al-Ani M Q. In AIP Conference Proceedings 2020;2213(1):020215.
95. Markossian S, Sittampalam GS, Grossman A, Brimacombe K, Arkin M, Auld D, Arkin M, Auld D, et al. Eli Lilly. 2021. 1–738 p.
96. Kleensang A, Vantangoli MM, Odwin-dacosta S, Andersen ME, Boekelheide K, Bouhifd M. Fornace Jr A J, Li Heng-Hong, Livi C B, Madnick S, Maertens A, Rosenberg M, Yager J D, Zhao L, Hartung T. Sci Rep., 2016;6(28994):1–10.
97. Soule HD, Vazquez J, Long A, Albert S, Brennan M. J. Nat. Cancer Inst., 1973;51(5):1409-1416.
98. Comşa Ş, Cîmpean AM, Raica M. Anticancer Res., 2015;35(3):147-3154.
99. Beyer U, Kriiger M, Schumacher P CU, Klinik FK. Monatshefte fur Chemie., 1997;128:91–102.
100. Sharma N K, Jha K K, Priyanka. Molecular docking: an overview. J. Adv. Sci. Res. 2010,1, 67–72.
101. Seeliger D, de Groot BL. J Comput Aided Mol Des. 2010;24(5):417-422.
102. Shoichet B K, McGovern S L, Wei B, Irwin J J. Curr Opin Chem Biol. 2002;6(4):439-446.
103. Gaina V, Gaina C. High Perform Polym. 2007;19(2):160-174.
104. Kupka T. Spectrochim Acta Part A. 1997;53:2649-2658.
105. Gunasekaran S, Charles J. Asian J Chem. 2008;20(2):1343-1356.
106. Gottlieb HE, Kotlyar V, Nudelman A. J Org Chem., 1997;62(21):7512-7515.
107. Hiarn B L, Boriwal R, Paliwal SN, Regar C, lal M K. J Chem Pharm Res., 2011;3(2):870-877.

108. Al-Omar MA. Profiles Drug Subst Excipients Relat Methodol., 2005 ;31(7):163-178.
109. El-Sakhawy M, Salama A, Kamel S, Tohamy HAS. Cellul Chem Technol., 2018;52(9–10):749–757.
110. Janakiraman N, Johnson M. Rom. J. Biophys., 2015; 25(2):131-140.
111. Ramazani A, Hamidnezhad R , Foroumadi A , Mirzaei SA, Maddahi S HSM. Iran J Parasitol., 2016;11(3):371–376.
112. Brunchi CE, Bercea M, Morariu S. High Perform Polym., 2008;20(3):311–322.
113. Hamidi N, Ihekweazu S, Wiredu A C, Isa O H, Watley K, Rowe C, et al. Adv Chem Eng Sci., 2012;02(04):435–443.
114. Yuan Y, Johnson F, Cabasso I. J Appl Polym Sci., 2009;112(6): 3436-3441.
115. Menges M, Schmidt-Naake G. Angew Makromol Chemie. 1998;258(4535):51-55.
116. Chaudhary J, Purohit S, Jinger S, Chaudhary R. J Sci Ind Res., 2017;76(09):570–4.
117. Hill DJT, Shao LY, Pomery PJ, Whittaker AK. polymer 2001;42:4791–4802.
118. Kolyamshin OA, Rogozhina LG. Russ J Org Chem. 2015;51(6):917–918.
119. Monthly C. Monatshefte fur Chemie. 1997;128:91–102.
120. Aguiar EC, Bosco J, Silva P, Ramos MN. J Mol Struct., 2011;993(1):431–434.
121. Woldbæk T, Klaboe P, Nielsen CJ. J Mol Struct., 1975;27(2):283–301.
122. Olivares B, Martínez F, Rivas L, Calde C, Munita JM, Campodonico PR. Sci Rep., 2018;8(14900):1-12.
123. Bhagare AM, Jayraj S, Gaware M R, Dnyaneshwar D. Lokhande, Anant V, Kardel A D. Bholay ACD. Bioorg Chem., 2020;103(104129).
124. Salewska N, Boros-majewska J, Łącka I, Chylińska K, Sabisz M, Milewska SMJM. J Enzyme Inhib Med Chem., 2012;27(1):117-124.
125. Dürüst Y, Karaku H, Kaiser M, Tasdemir D. Eur J Med Chem.,

2012;48:296–304.

126. Bhagare AM, Aher JS, Gaware MR, Lokhande DD, Kardel A V, Bholay AD, et al. Bioorg Chem., 2020;103(104129).
127. Sabir S, Alhazza MI, Ibrahim AA. Catal Sustain Energy. 2016;2(1):99-115.
128. Mahle F, Guimarães Tda R, Meira AV, Corrêa R, Bella Cruz RC, Bella Cruz A, et al . Eur J Med Chem., 2010;45(11):4761–4768.
129. Panov AA, SimonovAY, Lavrenov S N, Lakatosh SA, Trenin A S. Chem Heterocycl Comp., 2018;54:103–113.
130. Yongxian Fan , Yuele Lu , Xiaolong Chen , Babu Tekwani X-CL and YS. Molecules. 2018;23(11):2878.
131. Akinboye ES, Rogers OC, Isaacs JT. Prostate. 2018;78(9):655–663.
132. Bansode TN, Shelke J V., Dongre VG. Eur J Med., 2009;44(12):5094-5098.
133. Goszczyńska A, Kwiecień H, Fijałkowski K. Med Chem Res., 2015;24(9):3561-3677.
134. Branch SK, Casy AF, Ominde EMA. J Pharm Biomed Anal., 1987;5(2):73–103.
135. Parwe SP, Chaudhari PN, Mohite KK, Selukar BS, Nande SS, Garnaik B. Int. J. Nanomedicine. 2014;9(1):1463-1477.
136. Ruan QF, Zhou XH, Jiang SQ, Yang B, Jin J, Cui H, Zhao ZX. Caesalminaxins O-T. Fitoterapia. 2019;134:50-57.
137. Kowalczuk D, Gładysz A, Pitucha M, Kamiński DM, Barańska A, Drop B. Molecules. 2021;26(5):1442.
138. Umemura J, Hayashi S. Bull Inst Chem. 1974;52(4):585-595.
139. Ramos-Lara F, Lira CA, Ramírez MO, Flores M, Arroyo R, Caldiño U. J. Phys. Condens Matter., 2006;18(34):7951-7959.
140. Pavia DL, Lampman GM, Kriz GS, Vyvyan JR. INTRODUCTION TO SPECTROSCOPY. 5th ed. Bellingham Washington; 2013: p 250.
141. Singh J. Swelling of polymer gels, Msc. thesis, McGiIl University Montreal, Quebec Canada; 1993.

142. Kao YF and WJ. Expert Opin Drug Deliv., 2011;7(4):429-444.
143. Gratzl G, Paulik C, Hild S, Guggenbichler JP, Lackner M. Mater Sci. Eng. C., 2014;38(1):94–100.
144. Foster JW. Nat Rev Microbiol., 2004;2(11):898–907.
145. Handali S, Rezaei M. J. Control . 2020;320:404-411.
146. Alsaedi I I J, Taqi Z J, Abdul Hussien A M, Sulaiman GM, Jabir M S. Res. Express., 2019;6(9): 095413
147. Freedman L, Gibson M, Ethier S, Soule H R, Neve R M, Reid Y A. Nat Methods 2015;12: 493–497.
148. Marx V. Cell-line authentication demystified. Nat Methods. 2014 11(5):483-488.
149. Yu M, Selvaraj SK, Liang-Chu MM, Aghajani S, Busse M, Yuan J, Lee G, Peale F, Klijn C, Bourgon R, Kaminker JS, Neve RM. Nature. 2015;520(7547):307-311.
150. Soule H D, Vazguez J, Long A, Albert S, Brennan M. J Natl Cancer Inst., 1973;51:1409–1416.
151. Comsa S, Cimpean A M, RaicaM. Anticancer Res., 2015;35(6):3147-3154.
152. Jones C, Payne J, Wells D, Delhanty JD, Lakhani SR, Kortenkamp A. Cancer Genet Cytogenet., 2000;117(2):153-158.
153. Nugoli M, Chuchana P, Vendrell J, Orsetti B, Ursule L, Nguyen C, Birnbaum D, Douzery EJ, Cohen P, Theillet C. BMC Cancer. 2003:3:13.
154. Lee HJ, Seo AN, Kim EJ, Jang MH, Kim YJ, Kim JH, et al. Br J Cancer. 2015;112(1):103-111 .
155. Al-gazali HOM, Kzar HH, Wtwt MA, Al-gazally M E.Medico-Legal Updat. 2021;21(1):1367-1373 .
156. Sayed AR, Gomha SM, Abdelrazek FM, Farghaly MS, Hassan SA, Metz P. BMC Chem 2019;13(1):1-13.
157. Dewar MJS, Zoebisch EG, Healey EF, Stewart JJP. J. Am. Chem Soc., 1985;107:3902–3909.

158. Jang J, Son J, Park E, Kosaka T, Saxon JA, De Clercq DJH, et al. Angew Chemie - Int Ed. 2018;57(36):11629-11633 .
159. Verdino A, Zollo F, De Rosa M, Soriente A, Hernández-Martínez MÁ, Marabotti A. BMC Struct Biol., 2018;18(1):1–12.

الخلاصة:

تضمت في هذه الدراسة اربعة مسارات لتحضير وتشخيص ثلاثة وثلاثون مركَّب من مشتقات الماليئيمايد الحاملة لمجموعة دواء ودراسة بعض التطبيقات لها.
في المسار الاول تم تحضير عدد من مونومرات الماليئيمايد (M11-M1) من خلال تفاعل الإضافة للدواء الحاوي على مجموعة امين مع المائيميايد بنزويل كلورايد في مذيب ثنائي مثيل سلفوكسايد (المخطط أ).
وتضمن المسار الثاني بلمرة المونومرات المحضرة من المسار الاول في مذيب التولوين بوجود بيروكسيد البنزويل عند درجة حرارة ٩٠ م° لإنتاج ١١ بوليمر متجانس (PM1- PM11) ومرة اخرى، مع حامض الاكريلك لإنتاج ١١ بوليمرغير متجانس (PM12- PM22) (المخططان ب و ج).
تضمن المسار الثالث دراسة بعض التطبيقات الحيوية كدراسة الفعالية المضادَّة للبكتريا ضد البكتريا الموجبة لصبغة غرام (بكتريا المكورات العنقودية) والبكتريا السالبة لصبغة غرام (بكتريا الاشريكية القولونية) لجميع المركبات.
اظهرعدد من المونومرات والبوليمرات أقطار تثبيط اعلى من الادوية الحرة تجاه (بكتريا المكورات العنقودية) واعطى المونمر (M5) المحمل بدواء السيفالكسين اعلى قطر تثبيط.
في حين اظهرت معظم المونمرات فعالية اعلى تجاه البكتريا السالبة وكان للمونومر (M6) والبوليمر المتجانس (PM6) المحملان بدواء السيبروفلوكساسين اعلى اقطار ثبيط من السيبروفلوكساسين لوحده تجاه كلا النوعين.
اظهر البوليمران غير المتجانسين (PM15) المحملان بدواء الاموكسيسلين قطر تثبيط اعلى تجاه بكتريا (الإيكولاي) من الاموكسيسيلين لوحده و (PM20) المحمل بدواء الايزونيازايد فعالية تجاه كلا النوعين من البكتريا.
تضمن المسار الرابع دراسة أطلاق الدواء (في الوسط الحامضي والقاعدي) والنسب المئوية الانتفاخية والاوزان الجزيئية النسبية بطريقة اللزوجة للبوليمرات المحضرة وكذلك تمت دراسة السمية الخلوية والفعالية المضادة للسرطان لبعض البوليمرات المجانسة وغير المتجانسة تجاه مسار خلايا سرطان الثدي (MCF7) واظهر البوليمر (PM5) تثبيط عالٍ لنمو خلايا سرطان الثدي وسمية خلوية قليلة بينما اعطى البوليمر (PM16) فعالية اعلى لتثبيط نمو الخلايا السرطانية واقل سمية خلوية مما قد يجعله دواء واعدا لعلاج سرطان الثدي.

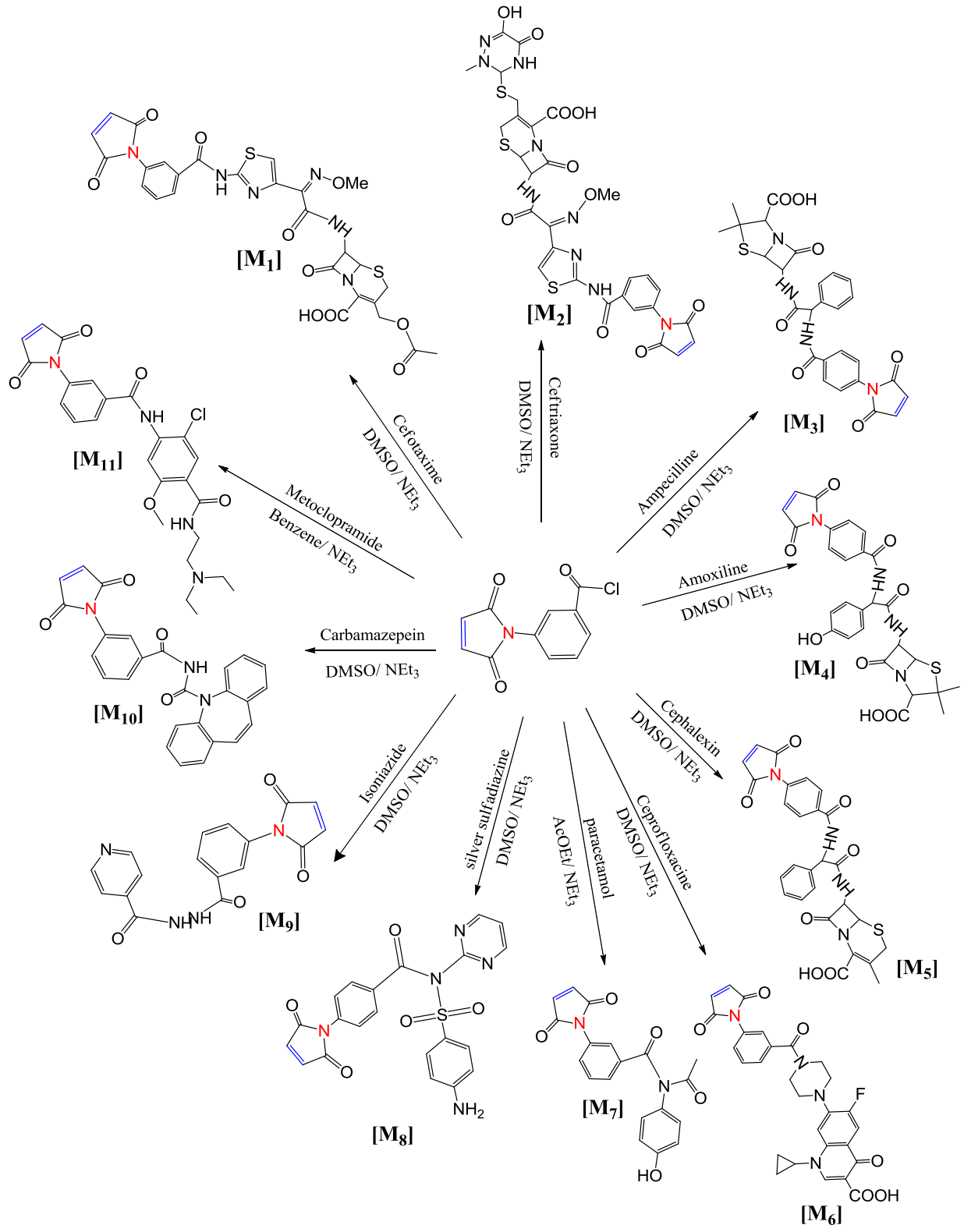

المخطط (أ): تحضير المونومرات (M_1-M_{11})

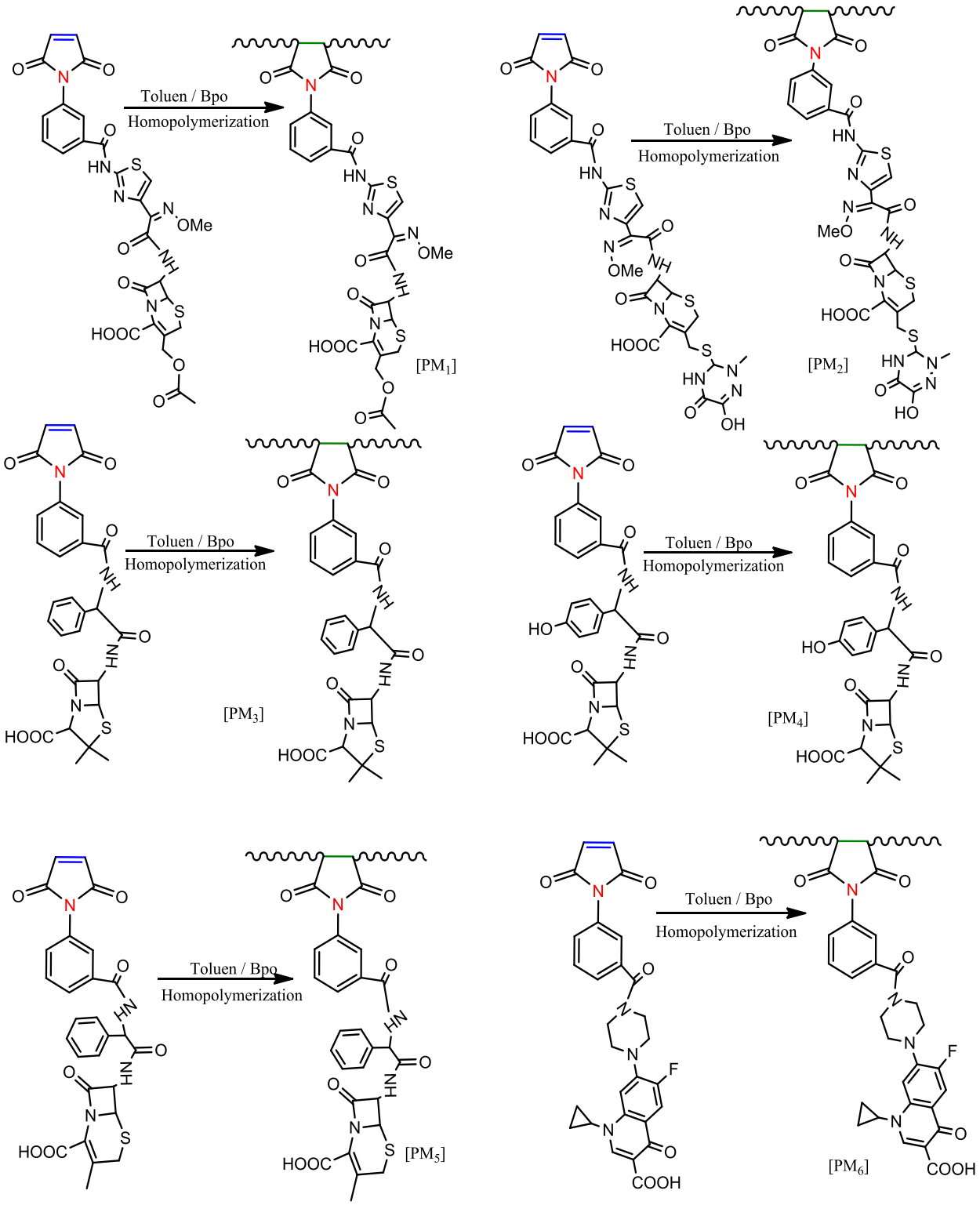
Toluen / Bpo
Homopolymerization
[PM1]
[PM2]
[PM3]
[PM4]
[PM5]
[PM6]

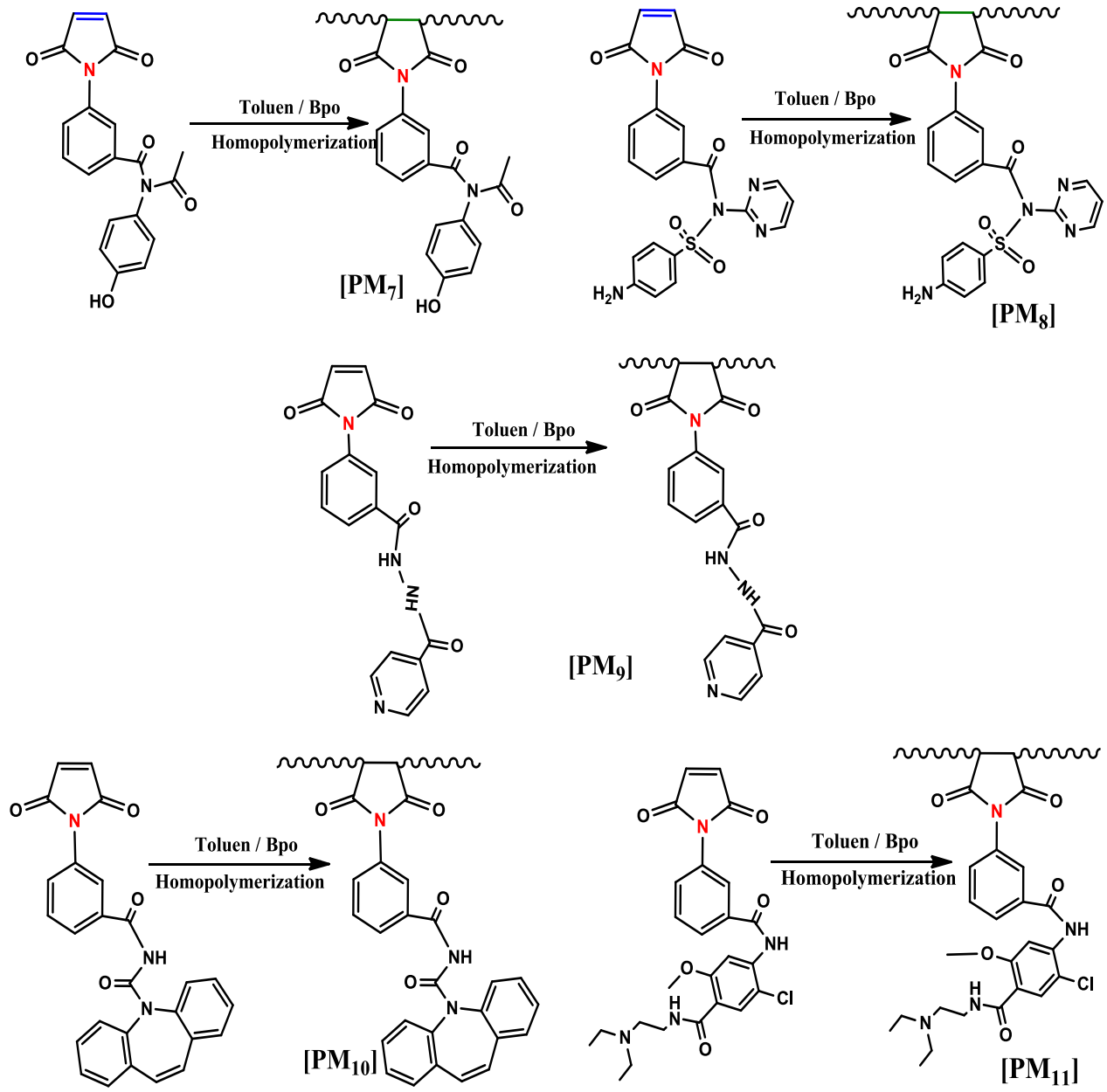

المخطط (ب) : تحضيرالبوليمرات المتجانسة (PM1-PM11)

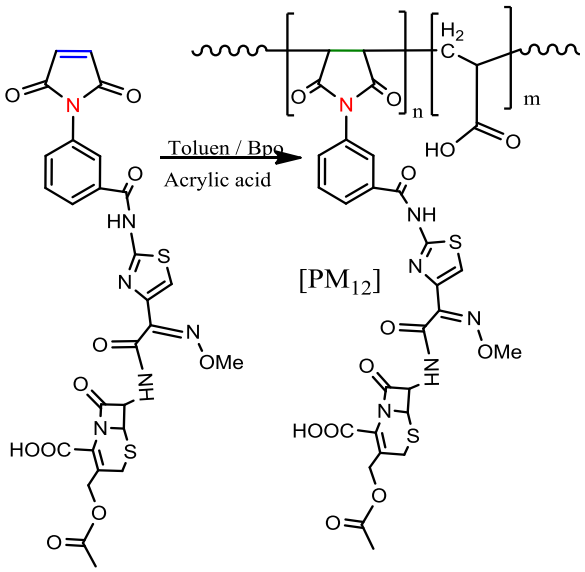

[PM$_{12}$]

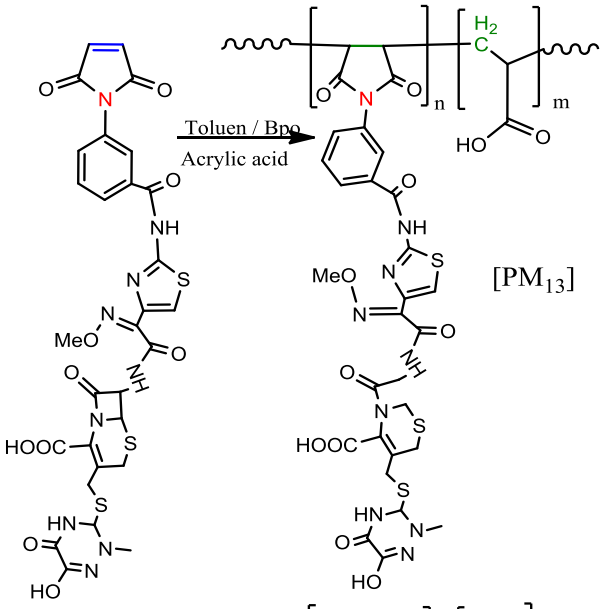

[PM$_{13}$]

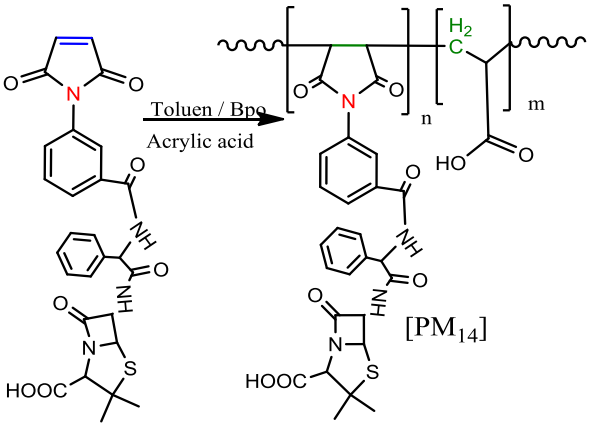

[PM$_{14}$]

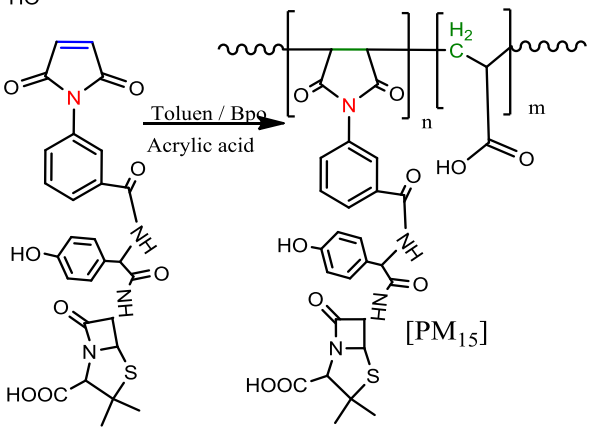

[PM$_{15}$]

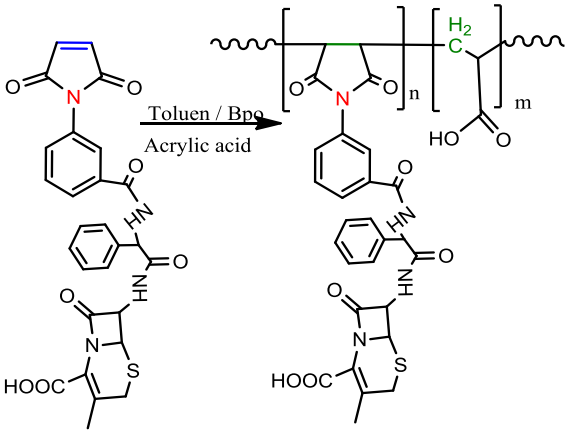

[PM$_{16}$]

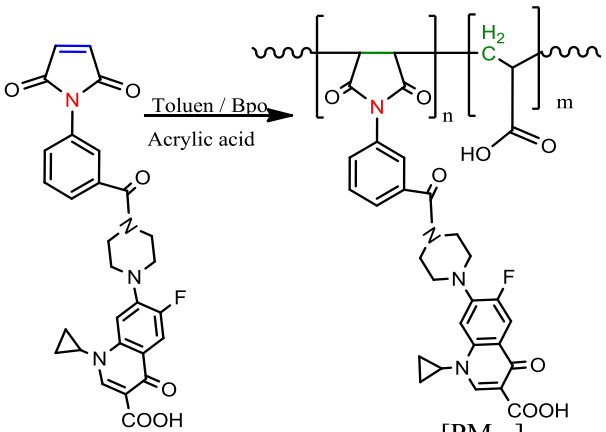

[PM$_{17}$]

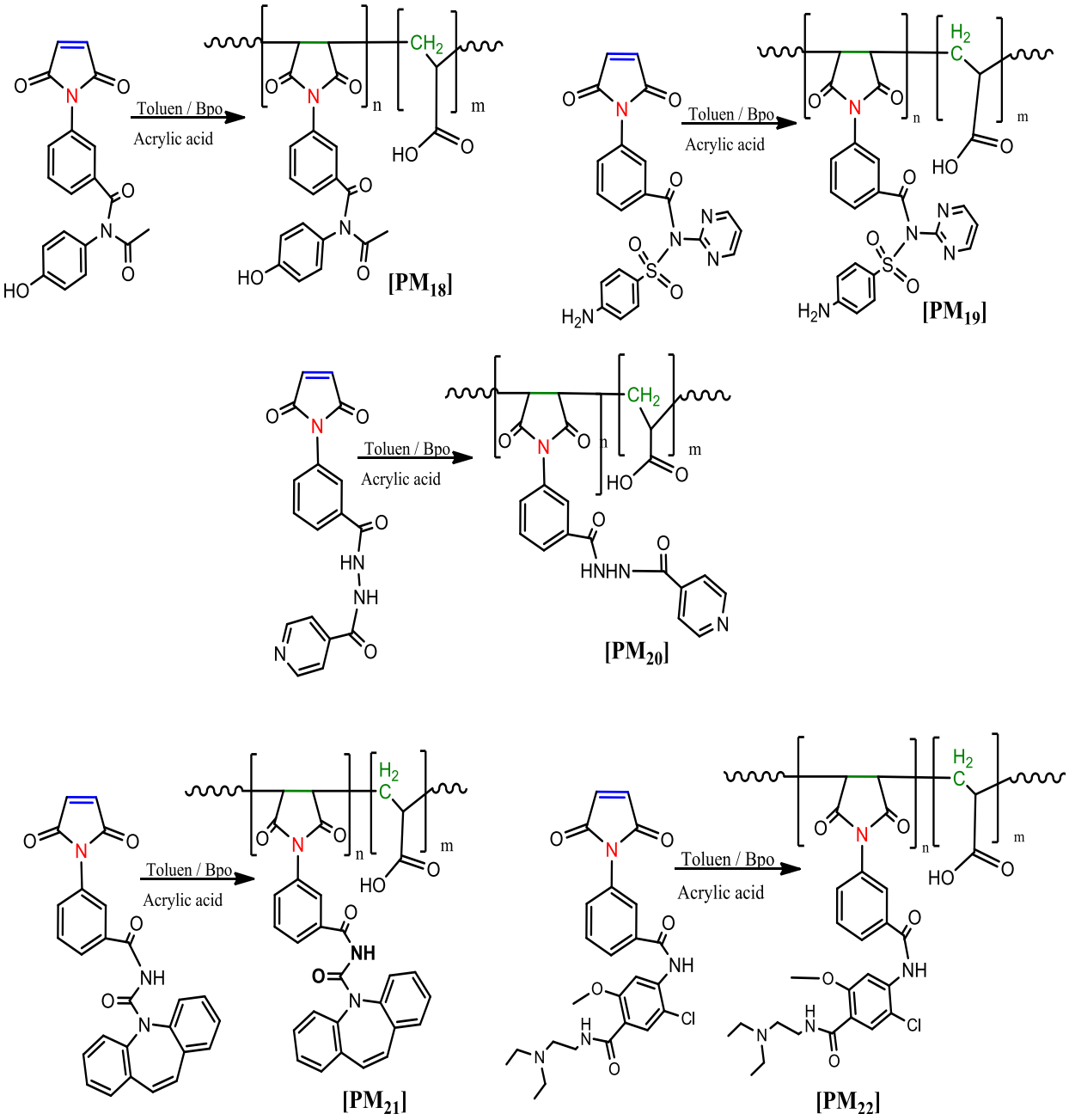

المخطط (ج) : تحضير البوليمرات المتجانسة (PM_{12}-PM_{22})

جمهورية العراق

وزارة التعليم العالي والبحث العلمي

جامعة بابل / كلية العلوم

قسم علوم الكيمياء

تحضير بوليمرات حيوية جديدة من الماليميد ن- المعوض وتطبيقاتها البيولوجية

اطروحة مقدمة

الى مجلس كلية العلوم- جامعة بابل

كجزء من متطلبات نيل درجة الدكتوراه فلسفة في

العلوم/علوم الكيمياء

من قبل

عمار عبد الحسين عواد عبد

بكالوريوس علوم كيمياء / جامعة كربلاء 2011

ماجستير علوم كيمياء / جامعة كربلاء 2014

بأشراف

أ.د.مهند موسى كريم

1443 هجري **2021 ميلادي**